

BỘ GIÁO DỤC VÀ ĐÀO TẠO  
TRƯỜNG ĐẠI HỌC SƯ PHẠM KỸ THUẬT  
THÀNH PHỐ HỒ CHÍ MINH

## DANH MỤC CÔNG TRÌNH CÔNG BỐ

NGHIÊN CỨU SINH: TƯỜNG PHƯỚC THỌ

LUẬN ÁN TIẾN SĨ  
NGÀNH: KỸ THUẬT CƠ KHÍ

TÊN ĐỀ TÀI

NGHIÊN CỨU, PHÂN TÍCH VÀ ĐÁNH GIÁ ẢNH HƯỞNG  
CỦA ĐỘ VĨNG CÁP ĐẾN ĐỘ CHÍNH XÁC VỊ TRÍ CỦA  
CDPR

2024

## DANH MỤC CÔNG TRÌNH CÔNG BỐ

STT	Tác giả	Năm xuất bản	Tên bài báo	Tên tạp chí, hội nghị	ISSN/ ISBN	Ghi chú
<b>I Bài báo quốc tế trong danh mục WoS</b>						
1	<b>Tuong Phuoc Tho,</b> and Nguyen Truong Thinh	11/2021	Analysis and Evaluation of CDPR Cable Sagging Based on ANFIS	Mathematical Problems in Engineering, Volume 2021, Article ID 4776317, 20 pages - ( <i>SCIE - Q3, IF 1.576</i> )	1024123X, 15635147	Chuyên đề 2
2	<b>Tuong Phuoc Tho,</b> and Nguyen Truong Thinh	6/2022	An Overview of Cable-Driven Parallel Robots: Workspace, Tension Distribution, and Cable Sagging	Mathematical Problems in Engineering, Volume 2022, Article ID 2199748, 15 pages - ( <i>SCIE - Q2, IF 1.576</i> )	1024123X, 15635147	CD tổng quan
3	<b>Tuong Phuoc Tho</b> & Nguyen Truong Thinh	10/2023	Evaluating cable tension distributions of CDPR for virtual reality motion simulator	Mechanics Based Design of Structures and Machines - Volume 0, page 1-19 ( <i>SCIE – Q1, IF 3.9</i> )	Print: 1539-7734 Online: 1539-7742	Báo cáo tổng kết
<b>II Bài báo quốc tế trong danh mục Scopus</b>						
4	<b>Tuong Phuoc Tho</b> and Nguyen Truong Thinh,	2/2022	Sagging Cable Analysis and Evaluation of 4-degree-of- freedom Cable Robot Using Adaptive Neural Fuzzy Algorithm	International Journal of Mechanical Engineering and Robotics Research, Vol. 11, No. 2, pp. 73-78, February 2022. ( <i>SCOPUS - Q3, IF 1.012</i> )	2278-0149	Chuyên đề 2
5	<b>Tuong Phuoc Tho</b> and Nguyen Truong Thinh,	7/2022	A Study of Tension Distribution for Control of Planar Cable Driven Parallel Robot Using Quadratic Programming Algorithm	International Journal of Mechanical Engineering and Robotics Research Vol. 11, No. 7, pp 479-485 ( <i>SCOPUS - Q3, IF 1.012</i> )	2278-0149	Chuyên đề 1

STT	Tác giả	Năm xuất bản	Tên bài báo	Tên tạp chí, hội nghị	ISSN/ ISBN	Ghi chú
<b>III</b>	<b>Hội nghị quốc tế có phản biện – có chỉ số ISBN</b>					
6	Xuan, Hoang Tran, <b>Tho Tuong Phuoc</b> , Chien Do Manh, and Nghia Vo Luong Nhon	12/2022	Design and Modeling Camera Cable Robot	Proceedings of the International Conference GTSD2022, pp. 271-281. Cham: Springer International Publishing, 2022	eBook ISBN: 978-3-031- 19694-2	Báo cáo tổng kết
7	Quan, Chu Nhat Minh, <b>Tuong Phuoc Tho</b> , and Nguyen Truong Thinh	12/2022	Implementation of the Racing Game with the Virtual Reality and Cable Suspended Parallel Robot (CSPR)	In 2022 22nd International Conference on Control, Automation and Systems (ICCAS), pp. 288-291. IEEE, 2022	Electronic ISBN:978- 89-93215- 24-3	Báo cáo tổng kết
<b>IV</b>	<b>Bài báo đăng trên tạp chí khoa học chuyên ngành trong nước (Trong danh mục được tính điểm của HBCDGSNN)</b>					
8	Dao, Cong Hoang Kha, <b>Phuoc Tho Tuong</b> , Ngoc Duc Vu, and Minh Nhat Nguyen	8/2023	On Research of Cable Tension Distribution Algorithm for Four Cables-Three DOF Planar Cable-Driven Parallel Robot	Journal of Technical Education Science 78B (2023): 8-17	ISSN: 1859- 1272	Chuyên đề 2
9	<b>Phuoc Tho Tuong</b> , Nguyen Luan Vu Truong	2/2024	Thiết Kế và Tính Toán Hệ Thống Phân Phối Cáp cho CDPR.	Journal of Technical Education Science, 19(SI01), pp.64-71.	ISSN: 1859- 1272	Báo cáo tổng kết

Bài báo số 1 – SCIE Q3 - IF 1.576

Tuong Phuoc Tho, Nguyen Truong Thinh, "Analysis and Evaluation of CDPR Cable Sagging Based on ANFIS", Mathematical Problems in Engineering, vol. 2021, Article ID 4776317, 20 pages, 2021.  
<https://doi.org/10.1155/2021/4776317>

Link: <https://onlinelibrary.wiley.com/doi/10.1155/2021/4776317>



## Research Article

# Analysis and Evaluation of CDPR Cable Sagging Based on ANFIS

Tuong Phuoc Tho  and Nguyen Truong Thinh 

*Department of Mechatronics, Ho Chi Minh City University of Technology and Education, Ho Chi Minh City, Vietnam*

Correspondence should be addressed to Nguyen Truong Thinh; [thinht@hcmute.edu.vn](mailto:thinht@hcmute.edu.vn)

Received 12 August 2021; Accepted 9 November 2021; Published 29 November 2021

Academic Editor: Paolo Boscarol

Copyright © 2021 Tuong Phuoc Tho and Nguyen Truong Thinh. This is an open access article distributed under the Creative Commons Attribution License, which permits unrestricted use, distribution, and reproduction in any medium, provided the original work is properly cited.

The cable sagging problem of cable-driven parallel robots (CDPRs) is very complicated, because several models for calculating cable sag based on the well-known catenary equation have been studied, but time and computational efficiency are a problem to be solved. There is still no simple mathematical model to calculate cable sag by considering all relevant conditions due to the complexity and nonlinearity of the cable sagging model, which involves many dominant variables and their influence on the position accuracy of CDPRs. In this study, we proposed an ANFIS (adaptive neuro-fuzzy inference system) architecture to estimate cable sag for large-sized CDPRs. The ANFIS model can be used to solve nonlinear functions and detect nonlinear factors online in the control system; this characteristic is consistent with the nonlinear model of cable sag. The trained data for ANFIS models were taken from calculation results by Trust-Region-Dogleg algorithm based on two cable tension calculation algorithms as Dual Simplex Algorithm and Force Distribution in Closed Form. Cable sagging data obtained from ANFIS and Trust-Region-Dogleg algorithm are compared and evaluated by statistical factors of evaluations consisting of root-mean-square error, correlation coefficients, and scatter index. The analytical results show that the ANFIS gave computed results with small errors and can be applied to predict cable sagging for any CDPR configuration, with the advantage of fast calculation time and high precision. The results of these models are also applied on a CDPR that contains two redundant actuators.

## 1. Introduction

The study on cable-driven parallel robots is receiving a lot of interest from research institutions [1]. CDPRs have a lot of advantages over traditional serial or parallel robots such as large workspace with a simple structure, high payload, low inertia, easy to transport and install, and low manufacturing cost. A typical CDPR includes a base (fixed) frame (BF) and moving platform (MP) connected and driven by cables and winches. MP is controlled by cable winches, and these cable winches are used as actuators to distribute cables and create a movement for MP; they connect the BF and the MP through anchor points and pulleys. The structure of CDPRs is described in Figure 1. With such transmission characteristics, CDPRs are flexible in performing different tasks in service and industry, especially with applications, and are required to move the heavy objects at a large distance, such as working in a large space [2, 3] or in rehabilitation mechanisms in medicine [4] with high flexibility. Moreover, due to the good

density of dimension and power [1–4], the cost for developing a CDPR is usually less than other robots. CDPRs are usually classified into three types depending on the DOFs and the number of cables. In general, a CDPR with  $m$  DOFs controlled by  $n$  cables was called “underconstrained CDPRs” if  $n$  is less than  $m + 1$ ; “fully constrained CDPRs” if  $n$  is equal  $m + 1$ ; and “redundantly constrained CDPRs” if  $n$  is greater than  $m + 1$ . For underconstrained CDPRs, the poses (orientation and position) of MP depend on its gravity. For the other two groups, the poses of MP depend on variable lengths of driven cables of CDPRs [5]. The main difference between CDPRs and other structures is the cables used for the transmission operating only with positive tension; this is to ensure that the straight line of cables is maintained, thereby ensuring the correctness of the kinematic problem and the rigidity of CDPRs. However, the cable tension characteristic is always positive limiting the application of CDPRs due to the complexity of the controller and the determination of noise errors. The CDPRs are a good choice for applications that

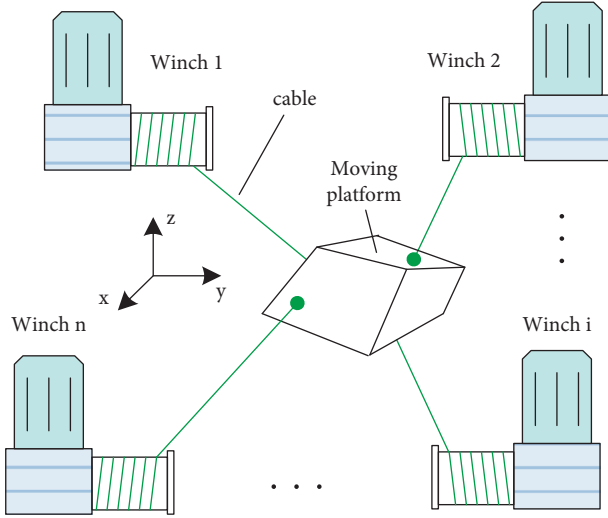


FIGURE 1: Structure of CDPRs.

require moving large objects in a big workspace. However, sagging and vibration of the cables cause reduction in the accuracy of the position controller of MP. Static or quasi-static models are often used to model the kinematic of CDPRs when they are designed to operate at low speed and acceleration. Many studies assumed that cables were massless straight cables [6–8], and this assumption applies to small-sized CDPRs with light loads, but it may not be appropriate for big-sized CDPRs with heavy loads.

Based on the *elastic catenary for computing sag of cables* of Max Irvine [9], the influences of elasticity and cable mass are combined in the computational model. A study of Kozak et al. [10] showed the analysis result of the static model of large-scale CDPRs with the influence of cable mass; due to the sag of cables, static displacement of a uniform elastic cable is also used to calculate the inverse kinematic and the stiffness matrix of the CDPR. This study can be applied not only to determine the workspace with cable sag but also to design large-scale CDPRs. Riehl et al. [11] studied the problem of the effect of cable mass on the model of inverse and forward kinematics of underconstrained CDPRs (the number of DOFs equals the number of driven cables). The inverse and forward kinematics of the large-workspace 3-DOF CDPRs driven by 3 cables were calculated based on the elastic catenary model described by Irvine. This paper showed that for high-load or large-workspace CDPRs, the influence of cable mass on the sag of cables and accuracy of CDPRs is significant. Therefore, it needs to be analyzed when designing and controlling the robot to achieve the desired accuracy. Gouttefarde et al. [12] introduced a new simplified static analysis of CDPRs, with the hypothesis that cables with inelastic properties and negligible mass are used to drive the

CDPR; this cable model is derived from the famous sag cable model, called a catenary equation, with the assumption that the cable sagging is small, but it is necessary to clarify the scope of the effectiveness of the method proposed in the paper to apply to specific robot configurations. Merlet [13] applied the interval analysis algorithm to solve the kinematics problem of CDPRs. Taking into account cable sag in static state, the algorithm was experimented on CDPRs with 8 cables and achieved good results. Gia Luan et al. [14] have developed a new process to generate semistatic and inverse kinetic models for CDPM taking into account cable sag using both analytical and experimental approaches. This model is valid only for CDPR working with low velocity and small acceleration.

In this study, the first two algorithms Minimizing Total Cable Tension [15, 16] and Force Distribution in Closed Form [16, 17] are used to determine cable tension sets of a CDPR. Next, the cable tension sets with corresponding kinematic data are used to calculate cable sags based on Irvine's cable sag model. Finally, the calculation results of the cable sag model will be used to build the ANFIS model to predict cable sags for CDPR, in which the input data are the position and orientation of the MP. The computation result shows that these ANFIS models are suitable to predict the cable sagging of large CDPRs to reduce the time consumption to determine cable sagging in specific cases. The results from these experiments and simulations are presented and analyzed in Section 6.

## 2. Mechanical Structure Analysis

**2.1. Kinematics Problems.** The relationship of the cable lengths (variable joints) and the poses of the moving platform of CDPRs were represented by the kinematics problems. Figure 2 illustrates the structure of the multicable parallel robot. The general structure of the CDPRs is composed of a moving platform and a base frame connected by  $n$  cables through the anchor points  $A_i$  and  $B_i$  ( $i = 1, \dots, n$ ), respectively,  $\mathbf{a}_i$  and  $\mathbf{b}_i$  represents vector  $OA_i$  and  $O_P B_i$  in the B-frame and E-frame. In the general case, the position and orientation of MP are represented by  $(\mathbf{r}, \mathbf{R})$ , where vector  $\mathbf{r}$  represents the positions of origin of E-frame or the  $OO_P$  vector and the rotation matrix  $\mathbf{R}$  represents the orientation of the E-frame in B-frame. The joint variables of the CDPRs are represented by  $l_i$ , which are the length of the driven cables  $i$ . Inverse kinematics of CDPRs can be obtained as follows: [6, 15, 18]

$$l_i = a_i - \mathbf{r} - \mathbf{R}\mathbf{b}_i. \quad (1)$$

Rotation matrix  $\mathbf{R}$  can be obtained based on the roll-pitch-yaw convention as follows:

$$\mathbf{R} = \mathbf{R}_z(\gamma)\mathbf{R}_y(\beta)\mathbf{R}_x(\alpha) = \begin{bmatrix} c\gamma c\beta & c\gamma s\beta s\alpha - s\gamma c\alpha & c\gamma s\beta c\alpha + s\gamma s\alpha \\ s\gamma c\beta & s\gamma s\beta s\alpha + c\gamma c\alpha & s\gamma s\beta c\alpha - c\gamma s\alpha \\ -s\beta & c\beta s\alpha & c\beta c\alpha \end{bmatrix}. \quad (2)$$

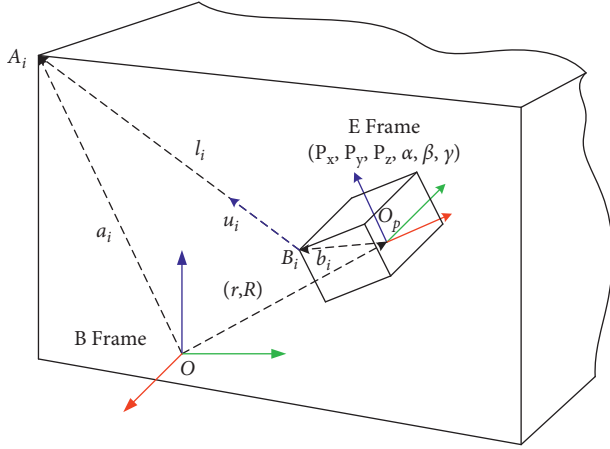


FIGURE 2: Kinematics model of CDPRs.

In equation (2),  $s$  and  $c$  denote the sine and cosine, respectively, and  $\alpha$ ,  $\beta$ , and  $\gamma$  denote rotations around the  $x$ ,  $y$ , and  $z$  axes of the rotation matrix, respectively. By transforming equation (1), we obtained

$$l_i^T l_i = (a_i - \mathbf{r} - \mathbf{R}b_i)^T (a_i - \mathbf{r} - \mathbf{R}b_i). \quad (3)$$

The inverse kinematic for each cable of the CDPR is as follows:

$$|l_i|^2 = |a_i|^2 + |\mathbf{r}|^2 + |\mathbf{R}b_i|^2 - 2a_i(\mathbf{r} + \mathbf{R}b_i). \quad (4)$$

The CDPR velocity kinematics problem shows the relationship between the velocity of MP and the velocities of the driven cables or the angular velocities of the motors.  $\dot{\mathbf{r}} = [\dot{x}, \dot{y}, \dot{z}]^T \in R^3$  represents the linear velocity of tool central point (Op) of MP on B-frame,  $\boldsymbol{\omega} = [\dot{\theta}_x, \dot{\theta}_y, \dot{\theta}_z]^T \in R^3$  is the angular velocity of MP along the three coordinate axes  $x$ ,  $y$ , and  $z$  of B-frame, and  $\mathbf{v} = [\dot{\mathbf{r}} \ \boldsymbol{\omega}]^T \in R^6$  represents the velocity vector of MP and consists of both the angular velocities and linear velocities of MP of CDPR.  $\mathbf{J}$  ( $n \times 6$ ) is the Jacobi matrix of CDPRs. Differentiating (1) concerning time, we obtain inverse velocity kinematic as follows:

$$\dot{\mathbf{l}} = \mathbf{J} \cdot \mathbf{v}, \quad (5)$$

where  $\dot{\mathbf{l}} = [\dot{l}_1 \ \dot{l}_2 \ \dots \ \dot{l}_n]$  are the vector of cable velocities and  $\mathbf{J}$  is the Jacobian matrix, as follows:

$$\mathbf{J} = \begin{bmatrix} u_1 & \dots & u_m \\ b_1 \times u_1 & \dots & b_m \times u_m \end{bmatrix}^T, \quad (6)$$

where  $\mathbf{b}_i$  represents the position vectors of anchor point  $\mathbf{B}_i$  on the MP relative to the origin Op in E-frame and  $\mathbf{u}_i = A_i B_i / \|A_i B_i\|$  is the unit vector of  $i^{\text{th}}$  cables in B-frame.

The angular velocity  $\boldsymbol{\omega} = [\dot{\theta}_x \ \dot{\theta}_y \ \dot{\theta}_z]^T \in R^3$  can be obtained by deriving the rotation angles  $\alpha$ ,  $\beta$ , and  $\gamma$  with the rotation Jacobian matrix  $\mathbf{J}_r$  as follows:

$$\begin{bmatrix} \dot{\theta}_x \\ \dot{\theta}_y \\ \dot{\theta}_z \end{bmatrix} = \begin{bmatrix} c_\gamma c_\beta & -s_\gamma & 0 \\ s_\gamma c_\beta & c_\gamma & 0 \\ -s_\gamma & 0 & 1 \end{bmatrix} \begin{bmatrix} \dot{\alpha} \\ \dot{\beta} \\ \dot{\gamma} \end{bmatrix}. \quad (7)$$

Representing (7) as a matrix

$$\boldsymbol{\omega} = \mathbf{J}_r \boldsymbol{\omega}_r. \quad (8)$$

To satisfy the equilibrium equation of CDPRs, the sum of the acting forces and the cable tensions has to satisfy the following equation:

$$\sum_{i=1}^m \boldsymbol{\tau}_i + \mathbf{F}_p = 0, \quad (9)$$

$$\sum_{i=1}^m (b_i \times \boldsymbol{\tau}_i) + \mathbf{M}_p = 0, \quad (10)$$

where  $\mathbf{F}_p$  and  $\mathbf{M}_p$  are the vectors of the external torques and forces acting on MP, respectively;  $\boldsymbol{\tau}_i$  is the vector of tension forces that each cable acts upon the end effector; and vectors  $\mathbf{b}_i$  represent the positions of anchor point  $\mathbf{B}_i$  on the MP relative to the origin Op in E-frame. From the cable direction shown in Figure 3, with the unit vectors  $\mathbf{u}_i$ , the direction of the forces  $\boldsymbol{\tau}_i$  can be obtained as follows:

$$\boldsymbol{\tau}_i = \tau_i \mathbf{u}_i. \quad (11)$$

From equations (9)–(11), we can have

$$\begin{bmatrix} u_1 & \dots & u_m \\ b_1 \times u_1 & \dots & b_m \times u_m \end{bmatrix} \begin{bmatrix} \tau_1 \\ \vdots \\ \tau_m \end{bmatrix} + \begin{bmatrix} \mathbf{F}_p \\ \mathbf{M}_p \end{bmatrix} = 0. \quad (12)$$

By defining

$$\mathbf{A} = \begin{bmatrix} u_1 & \dots & u_m \\ b_1 \times u_1 & \dots & b_m \times u_m \end{bmatrix}, \quad (13)$$

$$\mathbf{w}_p = \begin{bmatrix} \mathbf{F}_p \\ \mathbf{M}_p \end{bmatrix}, \quad (14)$$

where  $\boldsymbol{\tau} = [\tau_1 \ \tau_2 \ \dots \ \tau_m]$ .

Equation (12) can be rewritten as

$$\mathbf{A} \boldsymbol{\tau} + \mathbf{w}_p = 0, \quad (15)$$

where  $\boldsymbol{\tau}$  is the vector of the cable tensions ( $n \times 1$ );  $\mathbf{A} = \mathbf{J}^T$  is the structure matrix of the CDPRs ( $m \times n$ ); and  $\mathbf{w}_p$  is the vectors of the external wrenches applied on the center of MP ( $m \times 1$ ).

Lagrange equations type 2 or Newton–Euler equations can be used to derive the dynamic model for the CDPRs. The advantage of this form of the equation is that it is easy to solve and reduces calculation time. However, when determining the dynamic model, different methods can be used to simplify the calculation process. In this section, the dynamic model is developed, taking into account the cable models



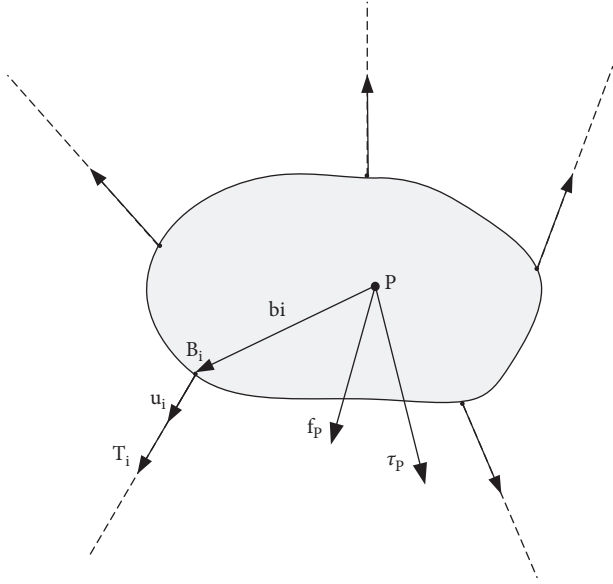


FIGURE 3: Force distribution on the moving platform.

and different subsystems; from [18] and equation (15), the dynamic equation of the CDPR is represented as

$$\mathbf{A}\boldsymbol{\tau} - \mathbf{I}\dot{\mathbf{v}} - \mathbf{C}\mathbf{v} + \mathbf{w}_p + \mathbf{w}_g = 0, \quad (16)$$

where  $\mathbf{I}$  is the inertia matrix of the MP in B-frame,  $\mathbf{C}$  is the Coriolis and centrifugal wrench matrix, and  $\mathbf{w}_g$  is the gravity wrench matrix. In the general case, the centroid of mass  $G$  of MP does not coincide with the origin of the E-frame. Therefore, matrix  $\mathbf{I}$  has the following form:

$$\mathbf{I} = \begin{bmatrix} m_p \mathbf{I}_3 \\ \mathbf{M}\widehat{\mathbf{G}}_p \\ \mathbf{M}\widehat{\mathbf{G}}_p \\ \mathbf{I}_p \end{bmatrix}, \quad (17)$$

where  $m_p$  is the mass of MP,  $\mathbf{I}_3$  ( $3 \times 3$ ) is the identity matrix,  $\mathbf{G}_p = [G_x \ G_y \ G_z]^T$  is the position vector of  $\mathbf{G}_p$  in E-frame, and  $\mathbf{M}\widehat{\mathbf{G}}_p$  is the skew-symmetric matrix associated with the first momentum of MP in E-frame  $\mathbf{M}\widehat{\mathbf{G}}_p$ :

$$\mathbf{M}\widehat{\mathbf{G}}_p = \mathbf{R} \begin{bmatrix} m_p G_x & m_p G_y & m_p G_z \end{bmatrix}^T. \quad (18)$$

Matrix  $\mathbf{I}_p$  is the inertia tensor matrix of MP obtained based on the Huygens–Steiner theorem:

$$\mathbf{I}_p = \mathbf{R}\mathbf{I}_g\mathbf{R}^T - \frac{\mathbf{M}\widehat{\mathbf{G}}_p\mathbf{M}\widehat{\mathbf{G}}_p}{m_p}, \quad (19)$$

where  $\mathbf{I}_g$  is the inertial tensor of MP and  $\mathbf{w}_g$  is the gravity wrench matrix given in the following equation:

$$\mathbf{w}_g = \begin{bmatrix} m_p \mathbf{I}_3 \\ \mathbf{M}\widehat{\mathbf{G}}_p \end{bmatrix} g. \quad (20)$$

The Coriolis and centrifugal wrench  $\mathbf{C}\mathbf{v}$  have the following form:

$$\mathbf{C}\mathbf{v} = \begin{bmatrix} \widehat{\boldsymbol{\omega}}\widehat{\boldsymbol{\omega}}\mathbf{M}\mathbf{G}_p \\ \widehat{\boldsymbol{\omega}}\mathbf{I}_p\widehat{\boldsymbol{\omega}} \end{bmatrix}. \quad (21)$$

Equation (21) represents the relationship between the kinematics, statics, and dynamics of the CDPRs, and this model is used to determine the workspace, tension distribution set, and controller of CDPRs.

The workspace of CDPRs is usually classified into two types: the wrench-feasible workspace (WFW) and the wrench closure workspace (WCW). The wrench-feasible workspace defines a set of poses of the MP, wherein the cable tension set can satisfy  $\mathbf{A}\boldsymbol{\tau} + \mathbf{w}_p = 0$  with the finite external wrench  $\mathbf{w}_p \in \mathbf{f}$  and positive tensions  $\boldsymbol{\tau} > \mathbf{0}$ . The wrench closure workspace defines a set of poses of the MP wherein the cable tensions set can satisfy  $\mathbf{A}\boldsymbol{\tau} + \mathbf{w}_p = 0$  with any external wrench  $\mathbf{w}_p$  and positive tensions  $\boldsymbol{\tau} > \mathbf{0}$ . From equation (15), for each pose of the MB, we have to find the combination of tension forces to balance it with the external forces, which can be obtained by inverting the  $\mathbf{A}^T$  matrix.

$$\boldsymbol{\tau} = -(\mathbf{A}^T)^{-1} \mathbf{w}_p. \quad (22)$$

Because structure matrix  $\mathbf{A}^T$  is not square, Moore-pseudo-inverse matrix can be used to solve equation (15). There are some methods to determine the existence of solutions for an inequality system such as pseudo-inverse matrix, linear programming, and interval analysis. The cable configuration of CDPR with 6 DOFs in this study is shown in Figure 4. The base frame,  $\{B\}$ , is placed at the center of the lower surface of the robot frame. The MP is a rectangular frame connected to the base frame by anchor points  $A_i$  and attaches points  $B_i$ ;  $\mathbf{l}_i$  is the Euclidean norm cable lengths. In all cases  $i=1, \dots, 8$ . This structure has no WCW because there is no set of  $\boldsymbol{\tau}$  to satisfy equilibrium equation (15) with any external wrench. The static workspaces of CDPR are shown in Figure 5 determined by the linear programming algorithm; with this configuration, the external wrench is ignored, as the force has only gravity force caused by the weight of MP with end effector, so the workspace of this CDPR is proportional to the payload (mass of MP). In the same condition, when changing the payload placed on MB, the workspace also changes; the larger the payload, the greater the workspace. Based on this feature, a suitable trajectory can be designed, depending on the mass of the MP.

### 3. Determination of Cable Tension Set: Dual Simplex Algorithm vs Force Distribution in Closed Form

**3.1. Determination of the Cable Tension Set.** The analysis of the tension distribution for the cables of CDPRs was a complex issue in the development of the CDPRs. The problem to be solved is to find the positive tension sets of cables for the poses of the MP satisfying the following force equilibrium equation:

$$\mathbf{A}\boldsymbol{\tau} = -\mathbf{w}_p \text{ with } 0 < \boldsymbol{\tau}_{\min} \leq \boldsymbol{\tau} \leq \boldsymbol{\tau}_{\max}, \quad (23)$$

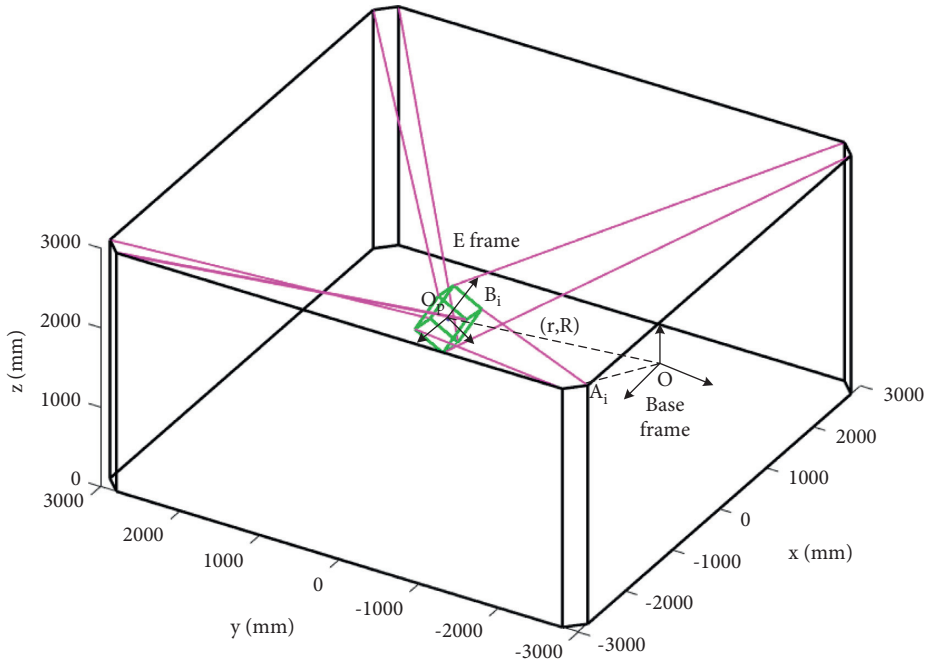


FIGURE 4: Kinematics structure of the CDPR with 6 DOFs and 8 cables.

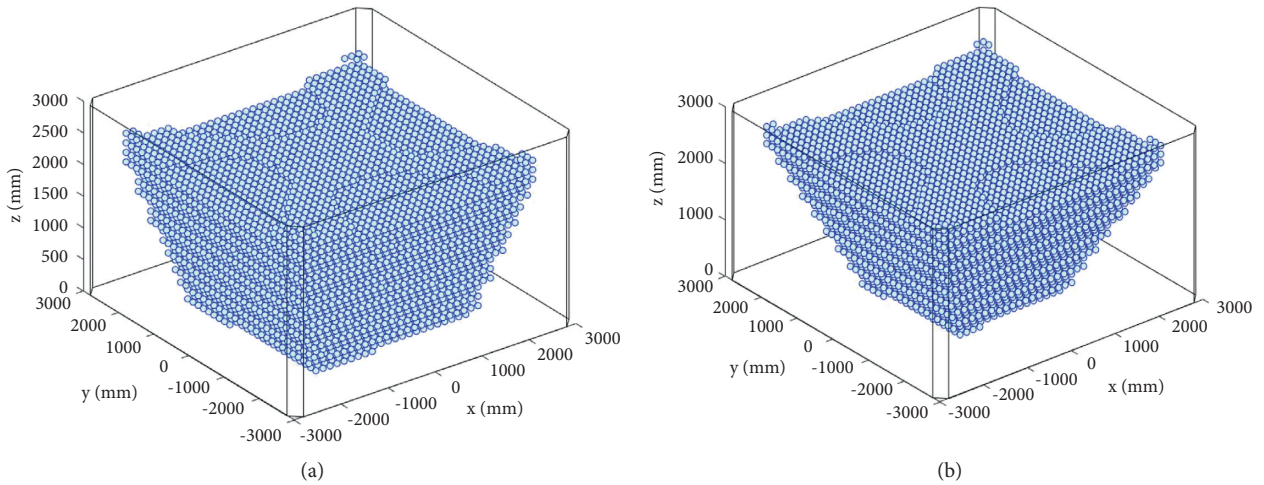


FIGURE 5: The workspace of proposed CDPM ( $[\alpha \beta \gamma] = [0 \ 0 \ 0]$ ; payload = 80 kg and 60 kg).

where  $\mathbf{A}$  ( $m \times n$ ) is the wrench matrix of CDPR;  $\boldsymbol{\tau}$  represents cable tensions vector ( $n \times 1$ );  $\mathbf{w}_p$  ( $m \times 1$ ) is the vectors of the external wrenches applied in the center of mass MP including inertia and gravity;  $\tau_{\min}$  is the lower limit of cable tensions to ensure that the cable is always in tension; and  $\tau_{\max}$  is the upper limit of cable tensions to ensure that the motor or cable is not overloaded. The important issues for calculating the solution of tension distribution of CDPRs are as follows:

- (i) Is there at least one solution  $\boldsymbol{\tau}$  satisfying equation (23) for a given pose? This condition is also used to calculate the workspace of CDPRs.
- (ii) How to determine tension distribution solution so that the sum of the cable tensions is minimal (for example, to reduce power consumption purpose)?

- (iii) How to determine solutions of continuous cable tension distribution along a trajectory (e.g., for force control purposes)?

In this section, the set of cable tensions was obtained by two algorithms: Dual Simplex Algorithm [15] and Force distribution in Closed Form [16, 17]. The results of these methods are used as input for the corresponding cable sag problem. Equilibrium equation (23) was used to define the cable forces  $\tau_i$ . With a feasible position, we can obtain infinite solutions, or there are existing and infinite valid combinations for the tension set. Since the number of cables is more than the number of degrees of freedom, for a position of MP, there are many tension sets satisfying the equilibrium equation. To obtain one desired solution out of these feasible solutions, mathematical techniques are used.

To choose the desired solution from among these possible solutions, mathematical methods will be applied.

**3.2. Dual Simplex Algorithm (DSA).** In the case of finding the tension solutions of the CDPRs satisfying force equilibrium equation (23) with the minimum requirement of the total value of the cable tension set, the problem of finding tension set becomes a linear programming problem [19, 20]. The objective function is minimized described as follows:

$$\mathbf{F} = \mathbf{c}^T \boldsymbol{\tau}. \quad (24)$$

Subject to constraints,

$$\mathbf{A}\boldsymbol{\tau} = -\mathbf{w}_p, \quad (25)$$

$$0 \leq \boldsymbol{\tau}_{\min} \leq \boldsymbol{\tau} \leq \boldsymbol{\tau}_{\max}. \quad (26)$$

The Dual Simplex Algorithm was used to find tension solutions. Problems (24)–(26) were solved as a constrained linear programming problem, where  $\mathbf{c} = [c_1; c_2; \dots; c_n] \in \mathbb{R}^n$  is the cost vector;  $\boldsymbol{\tau} = [\tau_1; \tau_2; \dots; \tau_n]$  is the tension vector of the cables equivalent to variable vector with necessary conditions ( $\boldsymbol{\tau} > \mathbf{0}$ );  $\mathbf{A} \in \mathbb{R}^{m \times n}$  is the structure matrix of CDPRs;  $\mathbf{w}_p = -\mathbf{b} \in \mathbb{R}^m$  is the external force vector; and  $\boldsymbol{\tau}_{\min}$  and  $\boldsymbol{\tau}_{\max}$  are the upper and lower bounds of tension. The calculation procedure and results of this method are presented in [15].

**3.3. Forces Distribution in Closed Form (FDCF).** Minimizing tension sets of Dual Simplex Algorithm has an advantage that minimizes power consumption of the system. This is important for some applications that require long working hours and large payloads such as rapid prototyping, construction 3D printing, and moving large objects along large distances. But, the limitation of this method is the discontinuity of the rope tension along the moving trajectory, which makes it difficult to control the robot. In this section, force distribution in the closed-form method is the noniterative method of computation time suitable for real-time control [16, 17]. In this section, force distribution in closed form for  $p = 2$  was used to distribute the cable tension. The root of this solution is based on dividing the tension vector into  $t$  parts:

$$\boldsymbol{\tau} = \boldsymbol{\tau}_A + \boldsymbol{\tau}_v, \quad (27)$$

where  $\boldsymbol{\tau}_A = (\boldsymbol{\tau}_{\min} + \boldsymbol{\tau}_{\max})/2$  is the average of the lower and upper limit of tension and  $\boldsymbol{\tau}_v$  is a random force vector. Substituting equation (27) into equation (23), we obtain

$$\mathbf{A}(\boldsymbol{\tau}_A + \boldsymbol{\tau}_v) = -\mathbf{w}_p, \quad (28)$$

$$\mathbf{A}\boldsymbol{\tau}_v = -\mathbf{w}_p - \mathbf{A}\boldsymbol{\tau}_A. \quad (29)$$

The tension distribution is continuous along the trajectory of MP if it is close to the vector  $\boldsymbol{\tau}_A$  using a  $p$ -norm with ( $2 \leq p \leq \infty$ ) [5]. To improve the stability of CDPR, the solution is to choose the tensions close to the average value of  $\boldsymbol{\tau}_{\min}$  and  $\boldsymbol{\tau}_{\max}$ . The purpose is to facilitate the control of cable tension that does not approach or exceed the force

limit of the actuator or lower limit of cable tension. The proposed method is to transform the problem from finding the solution of positive tension in the cable to finding the least squares using equation (34). Here, the Euclidean criterion ( $p = 2$ ) was used to define the least-squares solution  $\boldsymbol{\tau}_A$  in equation (29). This can be done by a pseudo-inverse matrix for a matrix with more columns than rows. If  $\mathbf{A}^+$  is pseudo-inverse of  $\mathbf{A}$ , then

$$\mathbf{A}^+ = (\mathbf{A}^T \mathbf{A})^{-1} \mathbf{A}^T. \quad (30)$$

Multiplying both sides of equation (29) by  $\mathbf{A}^+$ , we obtain

$$\boldsymbol{\tau}_v = \mathbf{A}^+(-\mathbf{w}_p - \mathbf{A}\boldsymbol{\tau}_A). \quad (31)$$

Substituting equation (31) into equation (27) yields

$$\boldsymbol{\tau} = \boldsymbol{\tau}_A - \mathbf{A}^+(\mathbf{w}_p + \mathbf{A}\boldsymbol{\tau}_A). \quad (32)$$

The simulations are based on 6-DOF and 8-cable CDPR as shown in Figure 4. The same trajectory is simulated to compare the result of the two proposed force distribution algorithms for computing the tension sets. The MP is to track a square and a circular trajectory in the  $XY$  plane. Figure 6 shows joint motion trajectories for 1000 m square path with  $Z = 1050$  mm divided into 81 node points, and Figure 7 shows joint motion trajectories for 1600 mm-diameter circle path with  $Z = 1000$  m divided into 126 node points. The tension sets of cables were computed, respectively, by Dual Simplex Algorithm (DSA) and Force distribution in Closed Form (FDCF). The eight subplots illustrate the tension profile of each cable along the trajectory. The computation results show that DAS gives the tension set with the sum of cable tensions which is smallest in both trajectories. However, the values of cable tensions tend to approach the lower boundary value and change abruptly at the node points. Meanwhile, FDCF gives more continuous cable tension and there is no sudden change in cable tension profiles, especially with the continuous trajectory of the circle. The cable tension also continues along the moving trajectory, which is convenient for controlling the robot.

## 4. Cable Length Computation with Cable Sagging

For large CDPRs, cable sag significantly affects the accuracy of positioning when calculating the inverse kinematics problem. However, due to the nonlinearity of the cable model, the inverse kinematics of cable robots taking into account cable sag become quite difficult to compute. Assuming that the catenary model is only affected by its gravity, the effects of external forces such as wind or nonuniform mass distribution along the cable are ignored. The cable sag model between two points B and M is shown in Figure 8, where B and M are the attachment points of cables on the base frame and moving platform, respectively,  $L_S$  is the distance between points B and M,  $L$  denotes the length between B and M taking into account sag of the cable,  $g$  is the gravity acceleration,  $\boldsymbol{\tau}$  is the cable tension at point M, and  $\boldsymbol{\tau}_x$  and  $\boldsymbol{\tau}_z$  is the component cable tension of  $\boldsymbol{\tau}$  in the  $x$  and  $z$

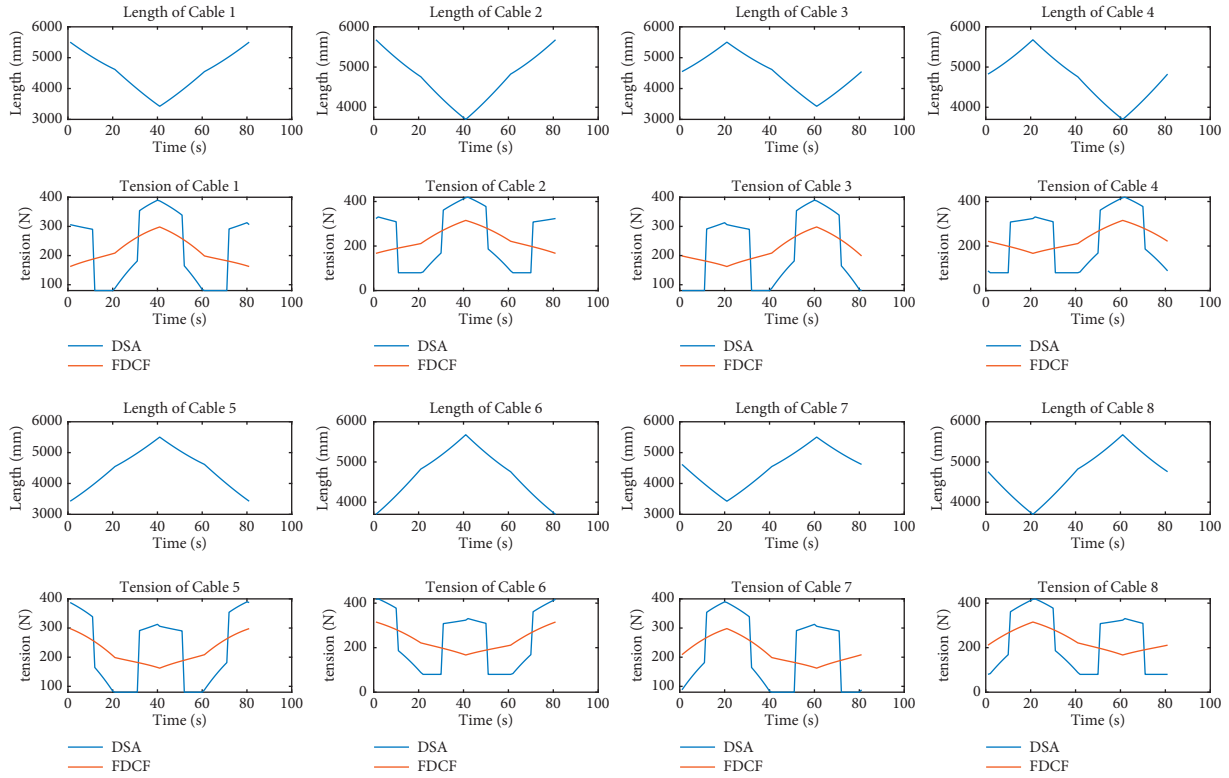


FIGURE 6: Tension of 8 cables of 1600 mm square path DSA vs FDCF, with  $z = 1050$  mm.

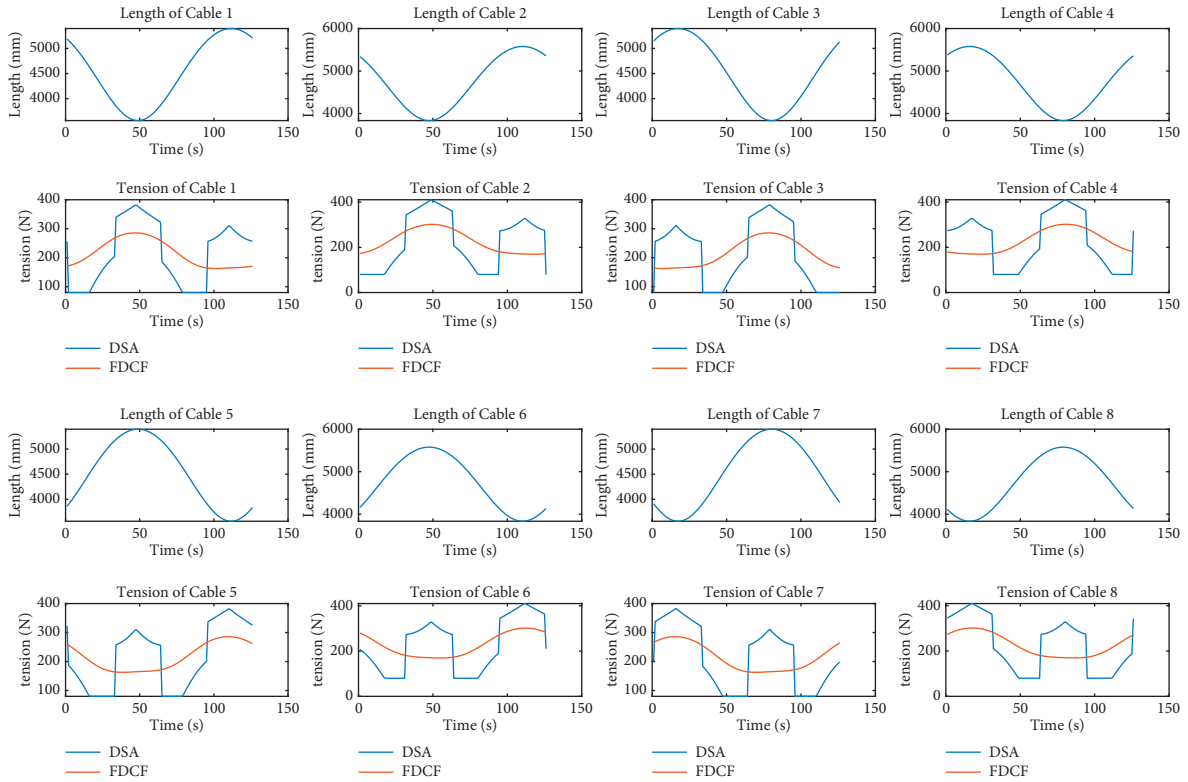


FIGURE 7: Tension of 8 cables of 1600 mm circle path TRDA vs ANFIS, with  $z = 1000$  m and 126 node points.

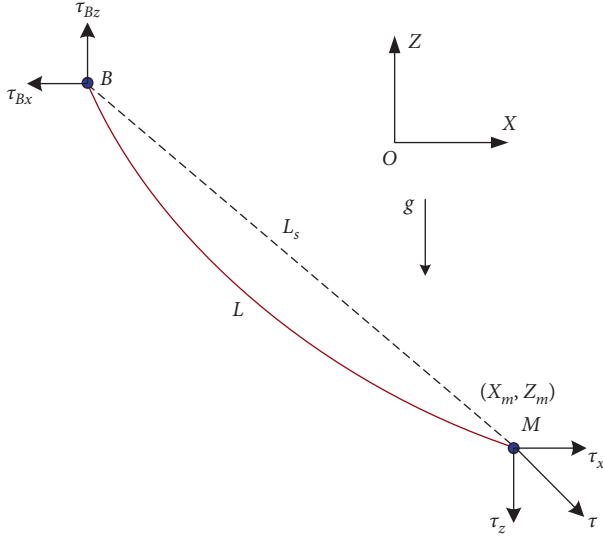


FIGURE 8: The cable sag model between two points.

axes. Similarly,  $\tau_{Bx}$  and  $\tau_{Bz}$  are the component cable tension in the  $x$  and  $z$  axes at point B, and  $(x_m, z_m)$  are the coordinates of M in the XZ frame. Considering a nonstretch cable model as shown in Figure 8, well-known equations of static catenary displacement are simplified as follows [9–15]:

$$x_m = \frac{|\tau_x|}{\rho_L g} \left[ \sinh^{-1} \left( \frac{\tau_z}{\tau_x} \right) - \sinh^{-1} \left( \frac{\tau_z - \rho_L g L}{\tau_x} \right) \right], \quad (33)$$

$$z_m = \frac{1}{\rho_L g} \left[ \sqrt{\tau_x^2 + \tau_z^2} - \sqrt{\tau_x^2 + (\tau_z - \rho_L g L)^2} \right], \quad (34)$$

$$\tau = \sqrt{\tau_x^2 + \tau_z^2}, \quad (35)$$

where  $\rho_L$  denotes the linear density of the cable material and  $g$  is the gravity acceleration.

The sag model in (33)–(35) is a system of equations representing the nonlinear relationship of theoretical cable length, cable tension, sag cable length, and component cable tensions; this is a system of nonlinear equations that can be solved by a numerical method. The Trust-Region-Dogleg algorithm [21] was used to solve this system. Equations (33)–(35) are rewritten as equation (36) with the definition “Given a set of  $n$  nonlinear functions  $\mathbf{F}_i(\mathbf{x})$ , where  $n$  is the number of elements in the vector  $\mathbf{x}$ , the goal of this algorithm is to find a vector  $\mathbf{x}$  that makes all  $\mathbf{F}_i(\mathbf{x}) = \mathbf{0}$ .”

$$F_i = \begin{cases} \frac{|\tau_x|}{\rho_L g} \left[ \sinh^{-1} \left( \frac{\tau_z}{\tau_x} \right) - \sinh^{-1} \left( \frac{\tau_z - \rho_L g L}{\tau_x} \right) \right] - x_m, \\ \frac{1}{\rho_L g} \left[ \sqrt{\tau_x^2 + \tau_z^2} - \sqrt{\tau_x^2 + (\tau_z - \rho_L g L)^2} \right] - z_m, \\ \sqrt{\tau_x^2 + \tau_z^2} - \tau, \end{cases} \quad (36)$$

where  $n = 3$ ,  $\mathbf{x} = [\tau_x \ \tau_z \ L]$ .

For each input condition  $(\tau \ x_m \ z_m)$  in Sections 3 and 4, the Trust-Region-Dogleg algorithm will result in the cable length with sagging and two-component cable tensions  $\mathbf{x} = [\tau_x \ \tau_z \ L]$ . The result of this step is used for training the ANFIS algorithm in the next section for computing the sag of cables in the whole workspace of CDPRs.

## 5. ANFIS

With the rapid development of information technology, soft computing techniques (SCTs) are used to solve many problems in engineering such as geological industry [22, 23], construction [24], mobile robot [25], and industrial robot [26, 27]. Here, the ANFIS structure is one of the useful algorithms of SCT usually used to calculate the kinematics and trajectory planning of the robot. Duka [26] applies ANFIS to calculate the inverse kinematic problem of 3-DOF planar robot; this model was built based on the data obtained from forward kinematics. Narayan et al. [27] developed a method to generate the path for 5-DOF spatial industrial serial robots based on ANFIS. This section describes the application of the ANFIS structure (adaptive neuro-fuzzy inference system) to predict cable sagging based on the reference results of Sections 3 and 4. ANFIS is structured based on the Takagi–Sugeno fuzzy inference system. Roger Jang was one of the first to develop the ANFIS structure. the ANFIS architecture can be used to determine the online nonlinear components in the control system and model nonlinear functions [28]. ANFIS is a combination of FIS (fuzzy inference system) with the learning mechanism of an artificial neural network in determining the membership functions or fuzzy rules from the training data. Therefore, it is possible to generate an ANFIS model from a nonlinear representation of the system based on the ability of ANFIS to learn from training data. In the next section, the ANFIS model is used to define the fuzzy rules and membership functions of the FLC to achieve the desired input-output mappings.

The structure ANFIS consists of five layers [29]; assume that the fuzzy system has  $p$  inputs  $x_i$ ,  $i = 1, \dots, p$ , and let  $O_{l,i}$  be the output symbol of node  $i$  in layer  $l$ , respectively. All nodes in layer 1 are adaptive nodes (square nodes):

$$O_{1,i} = N_i(x_i) \quad \text{for } i = 1, \dots, p. \quad (37)$$

The node functions  $N_1, N_2, \dots, N_k$  have the same role as the membership function  $\mu(x)$  of the fuzzy system, and  $k$  denotes the number of nodes of each input. The membership functions have many different forms, of which the bell-shaped is the typical choice.

All nodes of layer 2 are circle nodes (fixed nodes). The output  $O_{2,i}$  in this layer is a product of AND function for all the output signals of layer 1. Each node output of this layer represents the firing strength of the reasoning rule:

$$O_{2,i} = M_i(x_i) M_j(x_j). \quad (38)$$

Layer 3 also contains fixed nodes, and outputs of this layer will be called normalized firing strengths which are

used to determine the ratio of the  $i^{\text{th}}$  rule's firing strength by summing of all these rules.

$$O_{3,i} = \frac{O_{2,i}}{\sum O_{2,i}}. \quad (39)$$

Layer 4 contains adaptive nodes and is used to perform a Sugeno-type fuzzy system; this class performs the integration of the sum of the input variables  $x_1, x_2, \dots, x_p$  and constant factor  $c_1, c_2, \dots, c_p$ , from the output of IF-THEN rules.

$$O_{4,i} = O_{3,i} \sum_{j=1}^p (P_j x_j + c_j), \quad (40)$$

where  $c_1, c_2, \dots, c_p$  and  $P_1, P_2, \dots, P_p$  are the parameter set of this layer, also called the consequential parameters.

Layer 5 contains a circle node; this single node is used to compute the overall output by summing all input signals, this is the defuzzification step performed by the weighted average method.

$$O_{5,i} = \sum_i O_{4,i}. \quad (41)$$

The above ANFIS model can update parameters by using the gradient descent procedure. Some ANFIS structures have a lot of FIS types, and defuzzification methods can be found in Jang [28]. In this section, the cable sagging is predicted by the first-order Sugeno fuzzy model [29].

According to the calculation results mentioned in Sections 2–4. The cable sagging calculation model is a highly nonlinear model due to the dynamic constraints and equilibrium conditions of the system. The problem of calculating cable sag for cable robots is a multi-input and multi-output system. To solve the problem of calculating cable presented in this work, a parallel ANFIS system is proposed. This system depicted consists of 8 parallel 1-degree-of-freedom layers, where all of them take the Cartesian coordinates of the MP as input. The ANFIS model was developed for inverse kinematics of CDPRs taking into account cable sag illustrated in Figure 9. The position vector of MP ( $R^6$ ) is used as input to ANFIS models, which are nonlinear inputs to calculate cables according to constraints and calculation in Sections 2–4. The Sugeno model with 81 rules and Gaussian membership functions (GMFs) are used to structure ANFIS. In this study, six inputs are presented by 3 GMFs and the membership functions are defined by equation (42). The number of membership functions of each ANFIS was established experimentally.

$$\mu_{Ai}(x; c_i, \sigma_i) = \exp\left(-\frac{1}{2} \left(\frac{x - c_i}{\sigma_i}\right)^2\right), \quad (42)$$

where  $x$  is the input of node  $i$ , the GMFs are defined by two premise parameters ( $c_i, \sigma_i$ );  $c_i$  is the center of GMFs, and  $\sigma_i$  is the width of GMFs. The shape of GMFs depends on the value of these premise parameters with a minimum equal to 0 and a maximum equal to 1.

ANFIS structure phase  $i$  (1, ..., 8) is a multilayer feedforward adaptive network. Layer 1 has 3 input nodes

including the Gaussian transfer functions, and this layer is used to transfer input values to linguistic values, where the input values are the Cartesian coordinates of poses of CDPRs. MP position coordinates and cable sagging are used as ANFIS training data, where 6 coordinates represent MP position role as input and cable sagging role as the corresponding output for ANFIS. The hybrid algorithm is used in the training process to adjust the weights and generate fuzzy rule bases that will stop when the training error is equal to setting up an error or the values of present epochs are over the setup values. The consequence parameters of rule functions are adjustable automatically by the least square method of a hybrid learning algorithm [29].

## 6. Experiments and Discussion

**6.1. Computation.** In this section, experiments are implemented on overconstrained CDPRs and this structure is illustrated in Figure 4. The parameters of the robot are shown in Table 1. To evaluate the effectiveness of the model, the sag of cables  $S$  data generated by TRDA and ANFIS was compared by correlation coefficient (CC).

$$CC = \frac{\sum_{i=1}^n (S_{TRi} - \bar{S}_{TR})(S_{ANi} - \bar{S}_{AN})}{\sqrt{\sum_{i=1}^n (S_{TRi} - \bar{S}_{TR})^2} \sqrt{\sum_{i=1}^n (S_{ANi} - \bar{S}_{AN})^2}}, \quad (43)$$

where  $S_{TRi}$  and  $S_{ANi}$  represent the computed and predicted sag, respectively,  $\bar{S}_{TR}$  and  $\bar{S}_{AN}$  are the average value of computed and predicted sag samples, and  $n$  denotes the number of samples. The higher the CC value, the better the fit of the results from the predictive model to the computational method. For an accurate evaluation, scatter index (SI) and root-mean-square error (RMSE) are also applied with the following equation:

$$SI = \frac{RMSE}{\bar{S}_{TR}}, \quad (44)$$

$$RMSE = \sqrt{\frac{1}{n} \sum_{i=1}^n (S_{TRi} - S_{ANi})^2}. \quad (45)$$

The test data and trained data are obtained by the process in Sections 3 and 4. The sag data of 8 cables are collected in the whole of the feasible workspace of the cable robot with specification in Table 1. More than 8000 poses of MP were obtained by the invert kinematic problem. For each specific position of MP, a set of tensions has been calculated by Dual Simplex Algorithm and Force Distribution in Close Form. The result of invert kinematic and corresponding tensions was used as the inputs of the Trust-Region-Dogleg algorithm to find 8 corresponding lengths of cables taking into account sags of cables. In general, cable sagging is a function that depends on cable length, cable tension, and cable position in space.

Table 2 shows test data and trained data used to calculate statistical measurements; 8420 data samples for training and 1000 data samples for the test were used to analyze the obtained data between TRDA and the ANFIS. Both models were built based on FDCF, and all ANFIS models for 8 cables

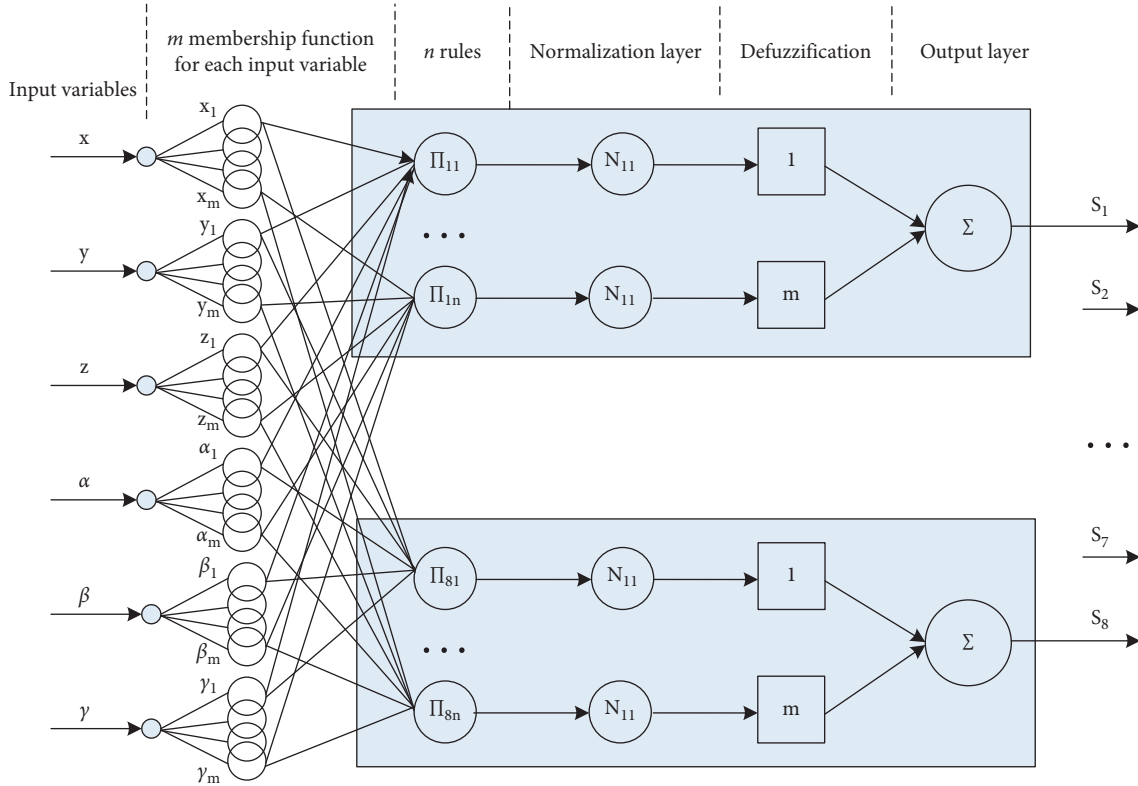


FIGURE 9: Proposed ANFIS architecture for cable sagging prediction.

TABLE 1: Specification of the cable robot.

Specification	
Degree of freedom	6 (3 rotations, 3 prismatic)
Number of cables	8
Fixed frame size (m)	$6 \times 6 \times 3$
End effector size (m)	$0.4 \times 0.4 \times 0.6$
End effector load (kg)	120
Workspace $L \times W \times H$ (m)	$5 \times 5 \times 2.5$
Linear density of cable $\rho_L$ (kg/m)	0.1543
Diameter of cables (mm)	5

TABLE 2: The ANFIS model with correlation coefficients of eight cables.

Cable $i$	Trained data			Test data		
	CCtrain	RMSE	SI	CCtest	RMSE	SI
1	0.9828	0.1348	0.3644	0.9912	0.1203	0.1935
2	0.9866	0.1173	0.3348	0.9948	0.0988	0.1645
3	0.9845	0.1266	0.3417	0.9911	0.1182	0.1905
4	0.9864	0.1132	0.3244	0.9927	0.1138	0.1891
5	0.9834	0.1279	0.3478	0.9908	0.1220	0.1948
6	0.9877	0.1105	0.3176	0.9909	0.1286	0.2132
7	0.9803	0.1403	0.3832	0.9903	0.1276	0.2039
8	0.9829	0.1297	0.3740	0.9922	0.1223	0.2019

show the trained data have CCs higher than 0.9800 and for test data, they are higher than 0.9900. RMSE is less than 0.1403 and 0.1286 for trained data and test data, respectively,

while SI is less than 0.3832 and 0.2132 for trained data and test data. Table 2 and Figures 10 and 11 show that the error of ANFIS models is suitable for predicting sag of cables with all correlation coefficients higher than 0.98.

Next, the trajectories that control the robot to move along the basic paths are calculated by both TRDA and ANFIS methods with 2 methods of calculating cable tension, DSA and FDCF, to evaluate the response and accuracy of the ANFIS model in both cases. Figure 12 shows the trajectory and joint responses of CDPRs for the circle path with radius 1000 (mm) and  $z$  1000 (mm). Figure 13 shows the trajectory and joint responses of CDPRs for the square path with side 1600 (mm) and  $z$  1050 (mm); both of the paths were placed on the XY plane and divided into multiple knot points.

An algorithm performs whether these points are in the workspace of the robot or not (satisfying the equilibrium equation (23)). If the trajectory is possible, these coordinate data will be inserted into the algorithm to find the corresponding cable tension. In the first method, the DSA or FDCF was used to find the set of tension combinations, provided that the tension force must be within the upper and lower limit; the lower limit of the tension is selected based on the equilibrium conditions, ensuring the rigidity and stability of the moving platform. The upper limit of the tensioners is selected based on the motor capacity. The Trust-Region-Dogleg algorithm and ANFIS were used to calculate the cable length, taking into account cable sag. For the second method, only the ANFIS model for DAS or FDCF was used to predict the cable length taking into account the sag of cables.

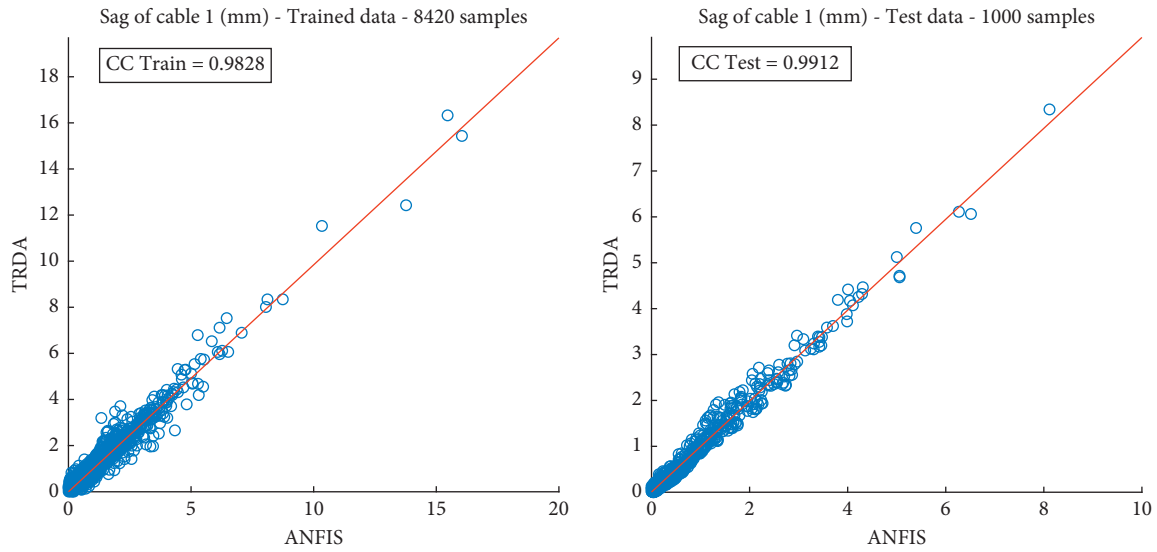


FIGURE 10: Comparison of sag of cable 1 predicted by ANFIS and computed by TRDA.

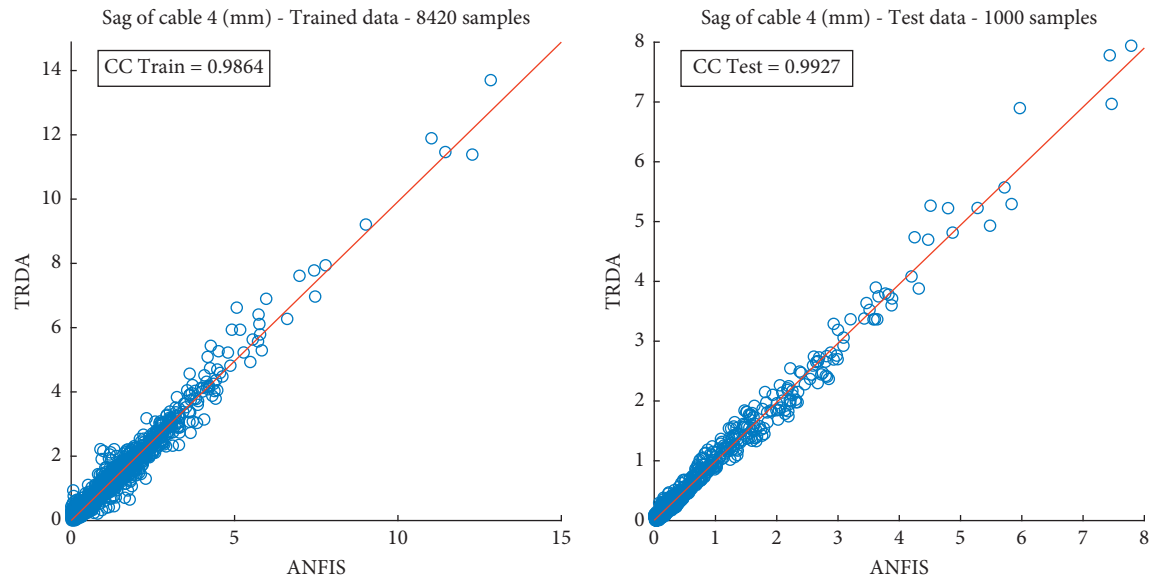


FIGURE 11: Comparison of sag of cable 4 predicted by ANFIS and computed by TRDA.

Figure 14 shows the computation results of the sag of 8 cables when the robot moves along the 2 m-diameter circle path at  $z = 1000$  m. The simulation trajectory is continuous, showing that all the node points are in the WFW. The cable lengths change from 3400 mm to 5700 mm with 126 node points. The sags of cables were computed by two methods, TRDA and ANFIS, based on Dual Simplex Algorithm to minimize the sum of tension forces of CDPRs. The TRDA generated the sag response curve with undulation, while the sag response curve predicted by ANFIS is more continuous. The maximum error is 1.1111 mm according to this trajectory. The largest errors tend to occur where the sag changes abruptly in response to a sudden change in the corresponding tension, while the maximum RMSE is only 0.2521 mm; this shows that the number of large errors is small, occurring only at the points where the cable sag has a

large change. Figure 15 shows the computation results of the sag of 8 cables when the robot moves along the 2 m-diameter circle path at  $z = 1000$  m and with 126 node points; the sags of cables were computed by two methods TRDA and ANFIS based on Force Distribution in Closed Form. Similar to Figure 14, TRDA also generated the sag response curve with undulation but without sudden changes in cable sag values, while the sag response curve predicted by ANFIS is more continuous and both change along the corresponding joint trajectory and tension of cables in Figure 7. The maximum error is only 0.1621 mm according to this trajectory with the maximum RMSE only 0.0668 mm.

The offset length of each cable is inversely proportional to the tension and cable length. Because the cable is inelastic, the offset length is always positive. The longer the cable and the larger the cable weight, the greater the cable. For cable



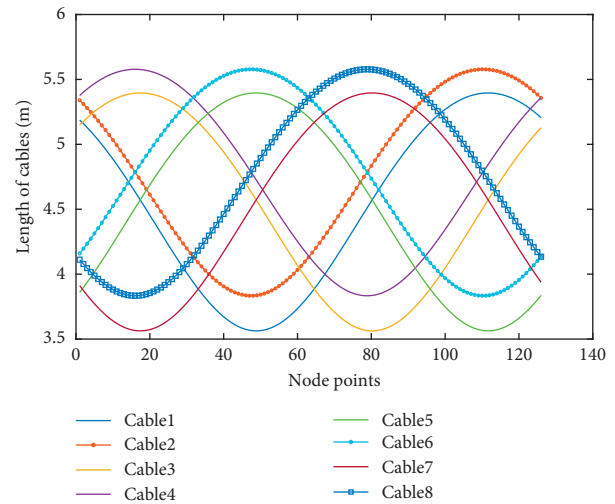
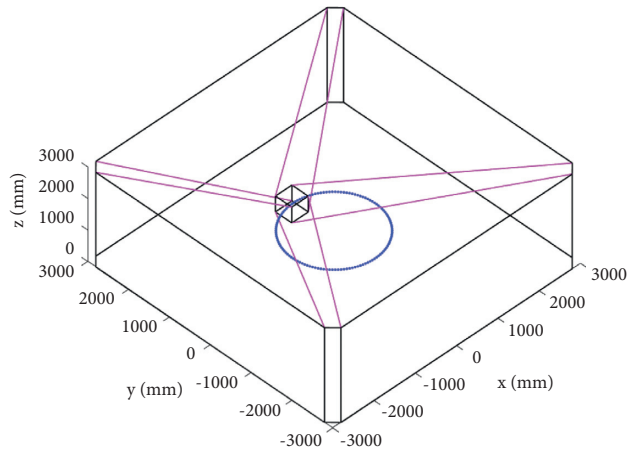


FIGURE 12: Trajectory and joint response of circle path with  $r = 1000$  (mm) and  $z = 1000$  m in XY plane.

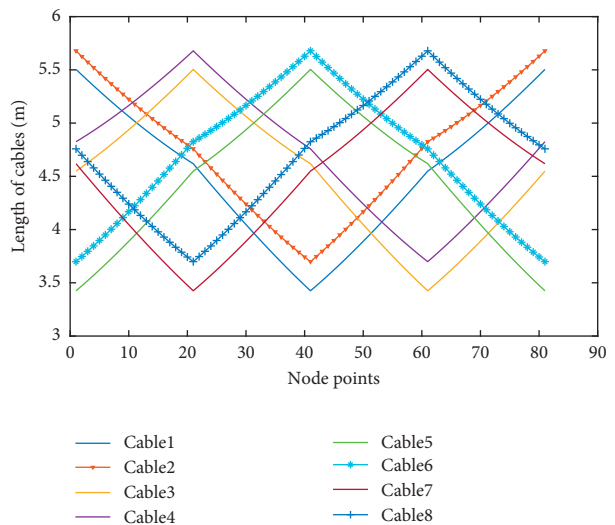
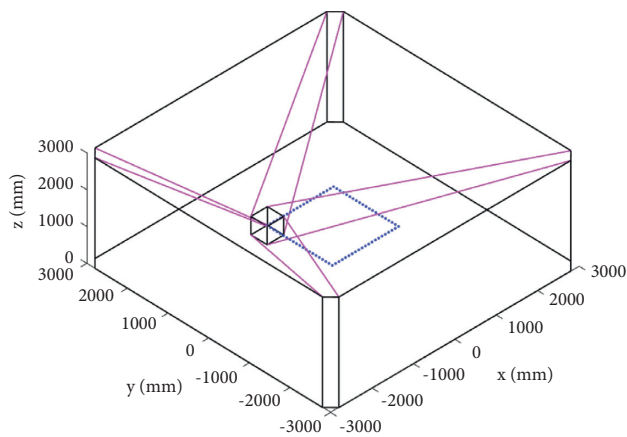


FIGURE 13: Trajectory and the joint response of 1600 mm square path with  $z = 1050$  mm in XY plane.

tension, when the tension is bigger, the cable has more tension, so the smaller the cable. The results of this calculation showed that this calculation method gives suitable results, which can be applied to calculate the control effect for the winch actuators. The tension of all cables is maintained equal to or greater than the lower bound  $\tau_{\min}$  set at 50 N and less than the upper bound  $\tau_{\max}$ , set at 500 N. During this trajectory, the offset lengths range from 0 mm to a maximum of 2 mm. When the cable tension is greater than 300 N, the offset length reaches zero (mm).

Figures 16 and 17 show similar results for the trajectory of the 1600 mm square path with  $z = 1050$  mm. The maximum error and RMSE of 0.9383 mm and 0.2006, respectively, for the ANFIS model based on DSA are much larger than the results calculated by the ANFIS model based on FDCF with max error = 0.1610 mm and RMSE = 0.0548. The calculation results show that the ANFIS model based on the FCDR tension synthesis algorithm gives better accuracy than that of the DSA algorithm with the same computational

trajectory as well as for trained data and test data. The response of the ANFIS is suitable for calculating the trajectory problem for large-sized cable robots, with a faster calculation time than the numerical method. Continuity is guaranteed for controllers designed for different cable robot configurations. In general, the errors in this work depend on the data collection method, because the relationship between the input and the output is highly nonlinear, in which the output reference data are used to build the cable prediction model depending on the method of calculating the cable tension distribution and the coordinates of the MP. The cable tensions corresponding to the positions of the MP must satisfy the constraints of kinematics and dynamics. In this paper, two methods DSA and FCDR are selected to generate the cable tension sets and they give different errors. The ANFIS model gives a better response with FCDR due to the continuity of the cable tensions and the data are taken over the entire workspace of the analyzed robot configuration with a large number of sample coordinates, thus limiting the

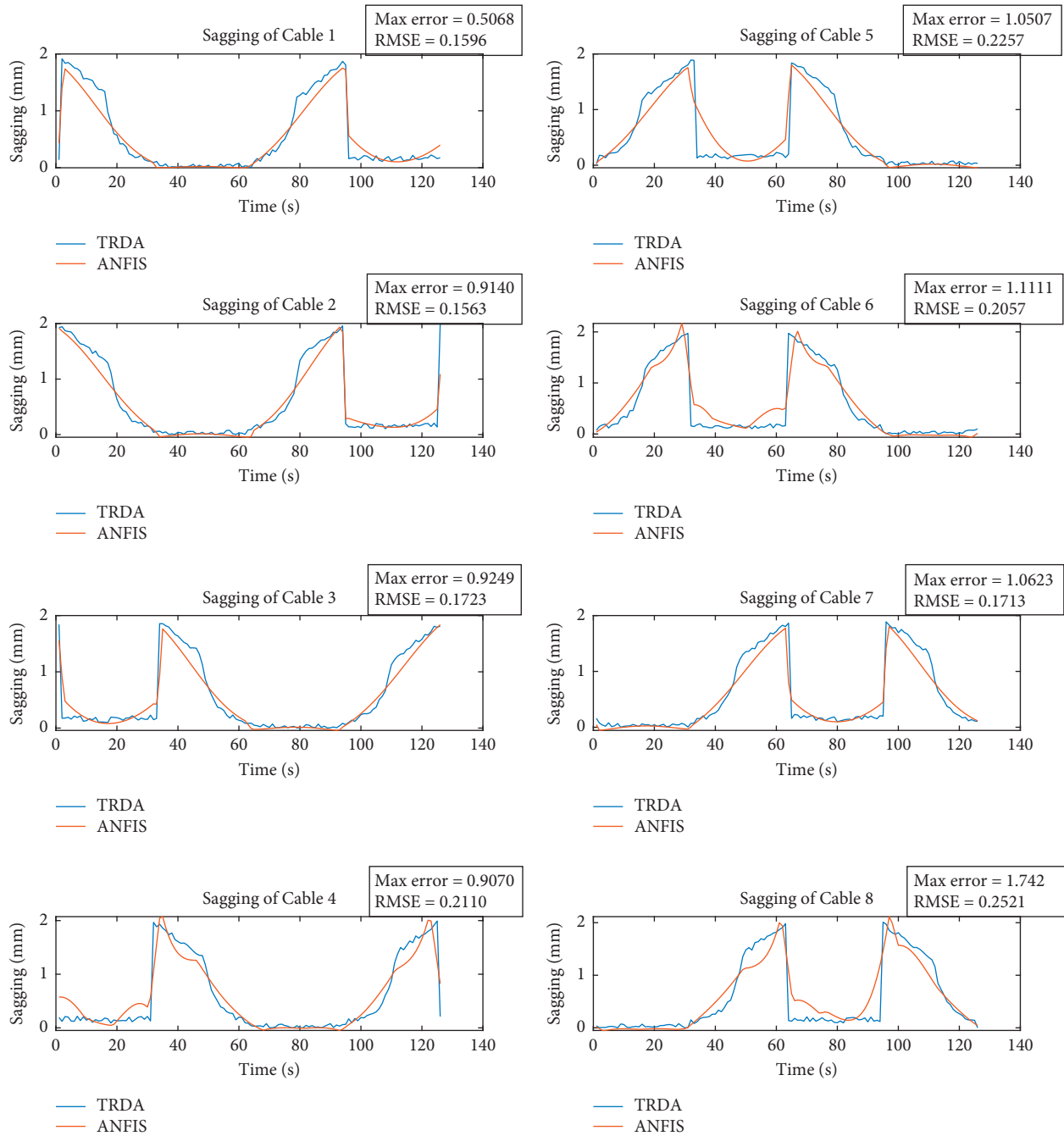


FIGURE 14: Sag of 8 cables of the 1000 m-radius circle path, with  $z = 1000$  m, 126 note points, and minimum tension.

influence of the uncertainty of input data. This has been verified through the calculation results of the ANFIS model for the number of test data being 1000 random samples.

6.2. Experiment. The prototype of CDP and moving platform and parameters are shown in Figure 18 and Table 1. The control system structure [3] has eight similar subcontrollers for controlling eight winches. Each subcontroller contains a set of AC servo motors and feedback sensors controlled by Card PCI-1285-AE 8-Axis DSP-Based Soft Motion Controller through two CIRCUIT

MODULE ADAM 3956 AE boards. Each cable is stored inside the winch and delivered by AC Delta Servo Motor ECMA-C20604RS-400 W. The feedback control data are the length and the tension of each cable obtained using an encoder and a loadcell placed in the winches. The encoder will collect feedback signals for the AC servo controller, while the loadcell provides the tension of the cable and transmits it to PC via the AD converter. The PC acts as a central controller, having the function of calculating and giving control signals to the subcontrollers based on the requested trajectory and feedback signal from the control elements.

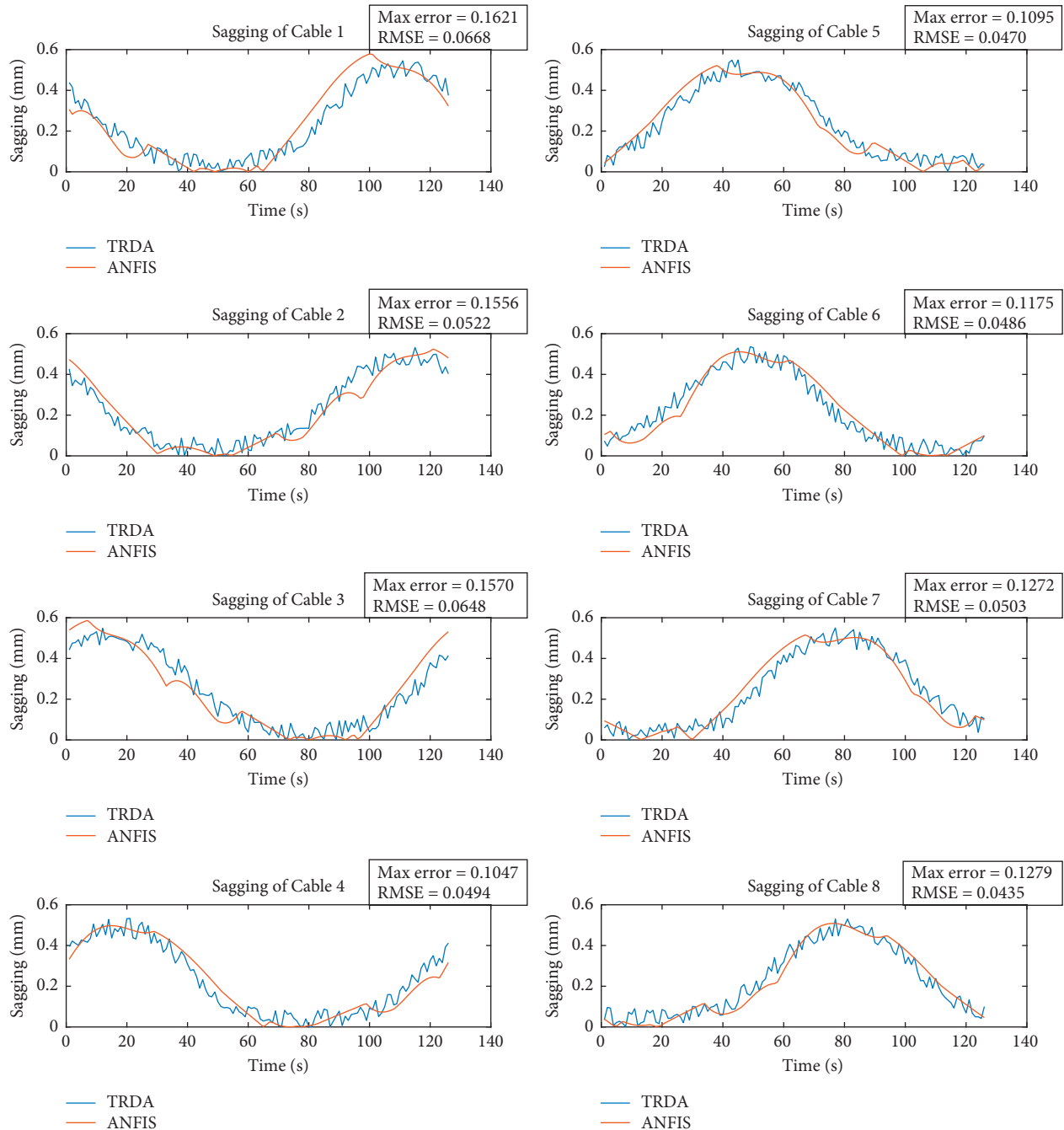


FIGURE 15: Sag of 8 cable of the 1000 m-radius circle path, with  $z = 1000$  m.

The experimental data are measured in a stationary state at the nodal points due to the limitation of the measurement technique. Two fixed cameras were installed on the top and side of CDPR (Figure 18) used to capture the MP position at node points. An image processing program had been developed to determine the actual coordinates of the MP based on the pixel coordinates obtained from the images of the two cameras. This program has been corrected to match the position of the CDPR and the camera.

The set of experimenting positions is taken from wrench-feasible workspace randomly and listed in Table 3. The CDPR is programmed to move through multiple nodes with linear interpolation with the robot control system. This control system consists of two closed-loop controllers. The first controller uses the cable tension and poses MP as reference signals. The second controller is an AC servo driver with a PID position controller; it controls the AC servo motor with an encoder signal feedback. The robot will stop at

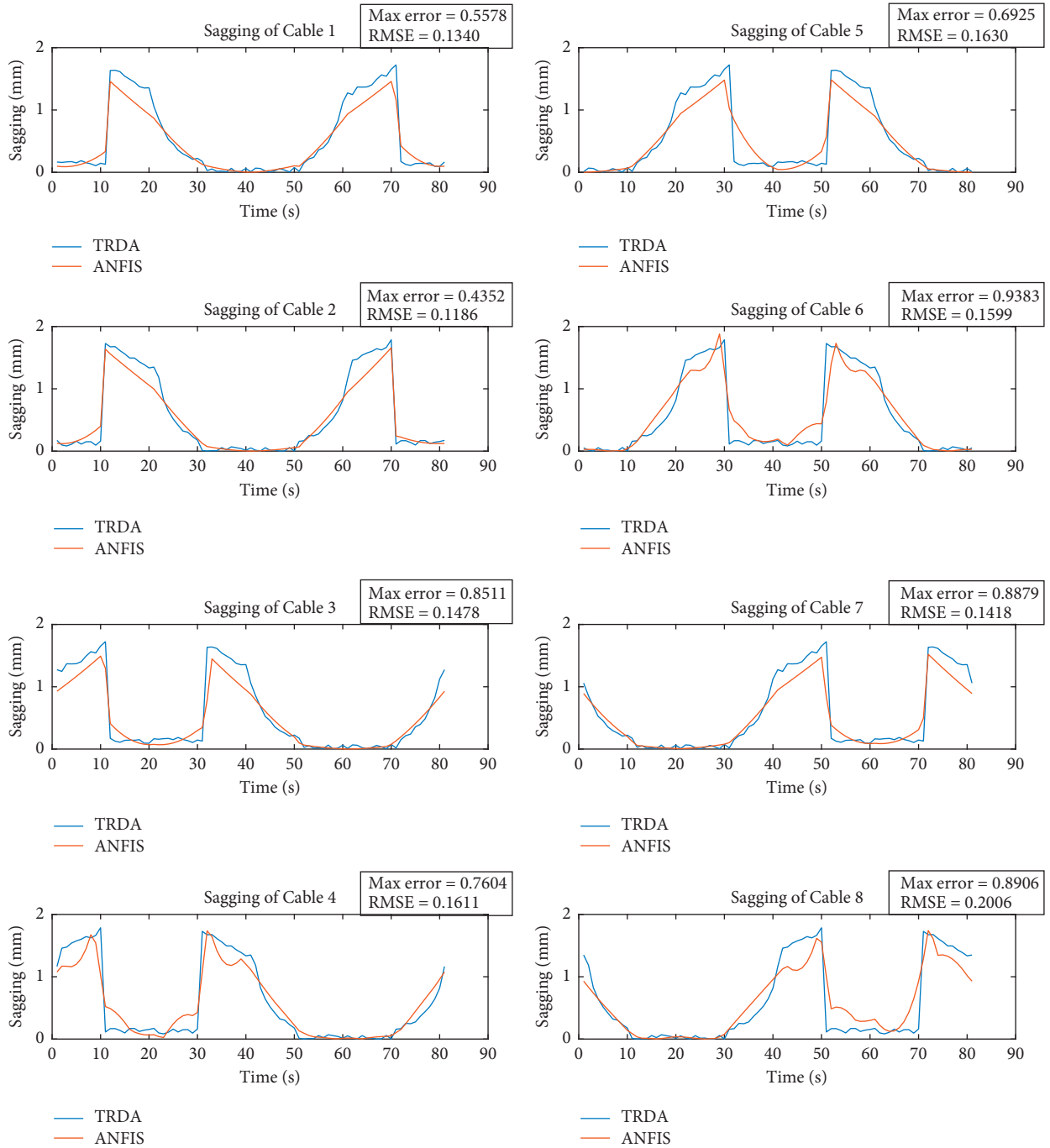


FIGURE 16: Sag of 8 cable of the 1600 mm square path, with  $z = 1050$  m.

11 node points. while measurement and error calculations have done. The experiment results are presented in Table 3, and equation (46) was used to calculate the errors.

$$\begin{aligned}
 & [Ex_i \ Ey_i \ Ez_i \ E\alpha_i \ E\beta_i \ E\gamma_i]^T \\
 & = [x_{Di} \ y_{Di} \ z_{Di} \ \alpha_{Di} \ \beta_{Di} \ \gamma_{Di}]^T \\
 & \quad - [x_{Ai} \ y_{Ai} \ z_{Ai} \ \alpha_{Ai} \ \beta_{Ai} \ \gamma_{Ai}]^T.
 \end{aligned} \tag{46}$$

The converted signal of loadcells for measuring tensions and the signal of encoders for measuring the length of

cables are shown in Figures 19 and 20 when CDPRs are moving along the trajectory. The experiment was completed in about 10 minutes with 100 samples/min. However, the robot had to stop for a period to facilitate measuring the position of the moving platform. The robot will stop at 11 node points (dot-dash lines) for measuring the position of the robot. The robot moves at pose  $P1 = [4 \ 4 \ 404 \ 2.3 \ 0.5 \ 0.9]^T$  and finishes at  $P11 = [-360 \ 40 \ 440 \ 0 \ 0 \ 0]^T$ . The cable tension diagram shows that there are fluctuations with larger amplitude at the time of moving a segment at the dot-dash lines, leading to a jerky phenomenon at the

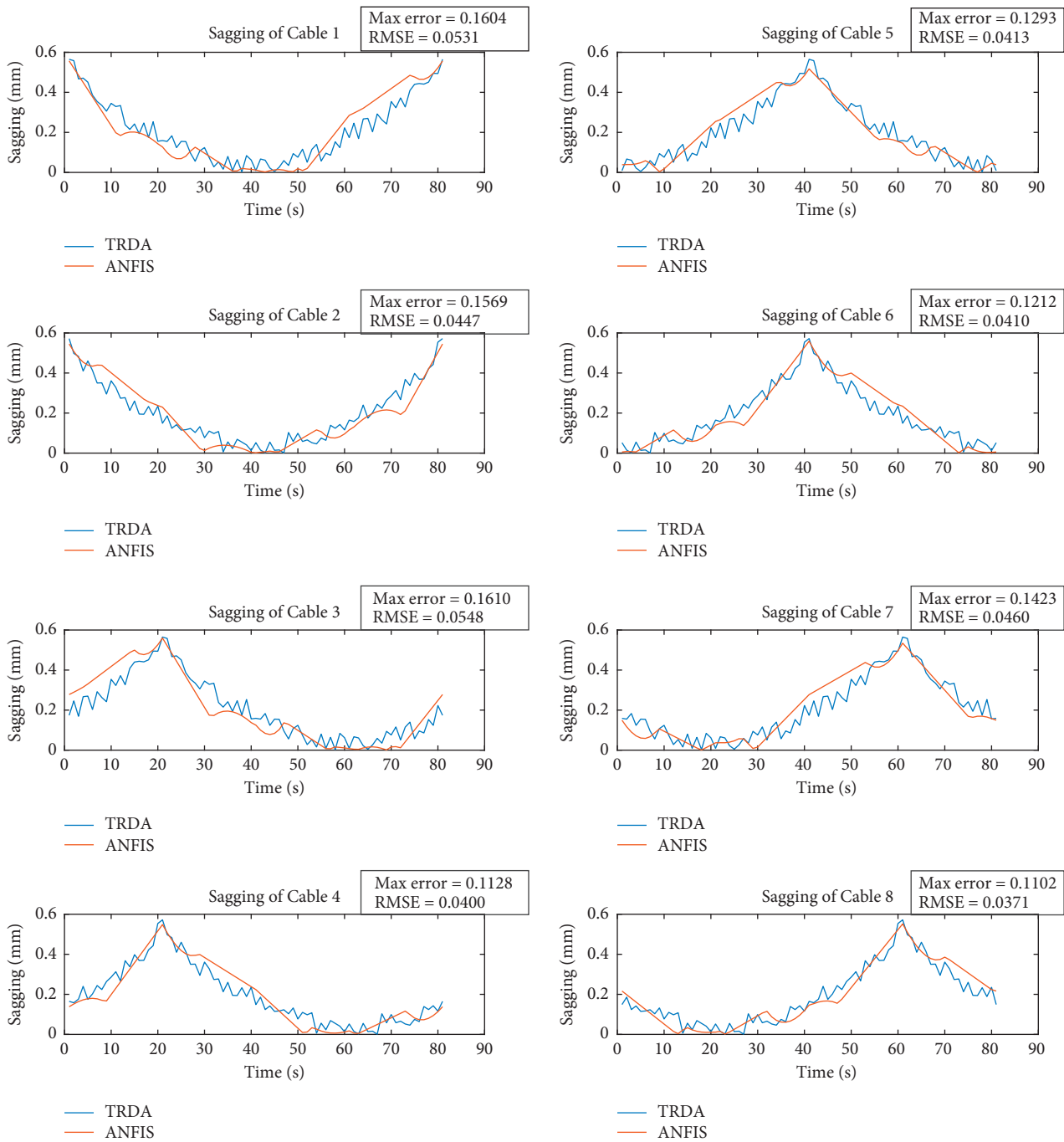


FIGURE 17: Sags of 8 cables of the 1600 mm square path TRDA vs RNN, with  $z = 1050$  m.

beginning. This is due to the overshoot of the PID controller.

Figure 21 shows the node points and moving orientation of the experiment with the size of the nodes representing their error values; the larger the size, the larger the error. The position error of the cable robot can originate from the

following reasons: accuracy of mechanical structure, the large size of the robot, error of control, error of the actuator, error of cable distribution, cable heterogeneity, and especially the error of measurement methods and measuring equipment. Table 3 and Figure 21 also show that the error tends to increase when the MP is at a low position or the

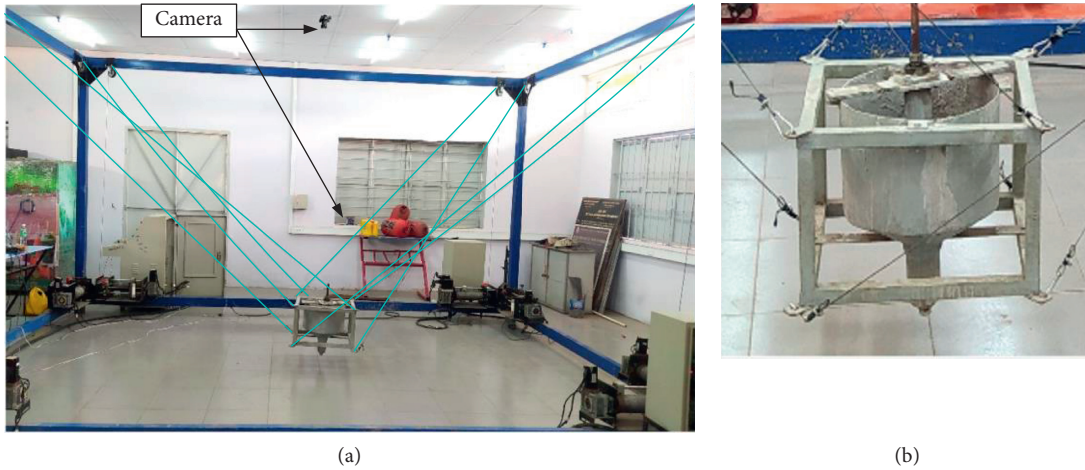


FIGURE 18: CDRP prototype (a); moving platform (b).

TABLE 3: Experiment result of our CDRP with 11 node points.

Pose	Desired positions (mm)	Actual positions (mm)	Errors (mm)
	$(x_{Di}, y_{Di}, z_{Di}, \alpha_{Di}, \beta_{Di}, \gamma_{Di})$	$(x_{Ai}, y_{Ai}, z_{Ai}, \alpha_{Ai}, \beta_{Ai}, \gamma_{Ai})$	$(Ex_i, Ey_i, Ez_i, E\alpha_i, E\beta_i, E\gamma_i)$
P1	(4, 4, 404, 2.3, 0.5, 0.9)	(-8, -9, 413, 8, 6, 7)	(12, 13, -9, -5.7, -5.5, -6.1)
P2	(400, 400, 800, 2.3, 0.5, 0.9)	(348, 390, 812, 7, 7, 9)	(16, 10, 12, -4.7, -6.5, -8.1)
P3	(-200, -100, 1000, 17.2, 17.2, 22.9)	(-208, -107, -1007, 12, 10, 18)	(8, 7, -7, 5.2, 7.2, 4.9)
P4	(-1050, -250, 1055, 5.7, 22.9, 34.4)	(-1042, -241, -1059, 9, 17, 30)	(-8, -9, -2, -3.3, 5.9, 4.4)
P5	(-1155, -1055, 1152, 17.2, 28.7, 45.9)	(-1144, -1065, -1145, 11, 23, 41)	(-11, 10, 7, 6.2, 5.7, 4.9)
P6	(-555, -355, 1552, 34.4, 40.1, 40.1)	(-552, -360, 1549, 33, 43, 43)	(-3, 5, 3, 1.4, -2.9, -2.9)
P7	(45, 345, 1587, 40.1, 28.7, 28.7)	(48, 342, 1586, 39, 30, 32)	(-3, 3, 1, 1.1, -1.3, -3.3)
P8	(268, 866, 1332, 45.9, 17.2, 11.5)	(273, 875, 1335, 48, 22, 14)	(-5, -9, -3, -2.1, -4.8, -2.5)
P9	(673, 365, 707, 28.7, 11.5, 0)	(662, 374, 719, 33, 16, 3)	(11, -9, -12, -4.3, -4.5, -3.0)
P10	(895, 36, 872, 11.5, 5.7, 7.2)	(882, 24, 882, 8, 10, 12)	(13, 12, -10, 3.5, -4.3, 5.2)
P11	(-360, 40, 440, 0, 0, 0)	(-375, 28, 451, 5, 4, 6)	(15, 12, -11, -5.0, -4.0, -6.0)

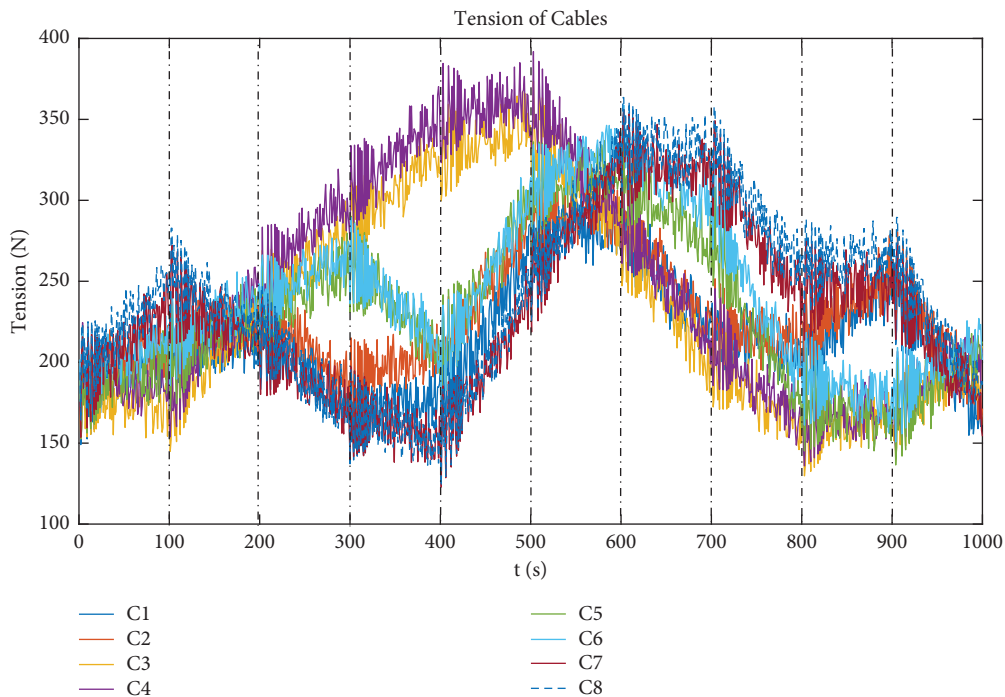


FIGURE 19: Loadcell signal response in the experiment.

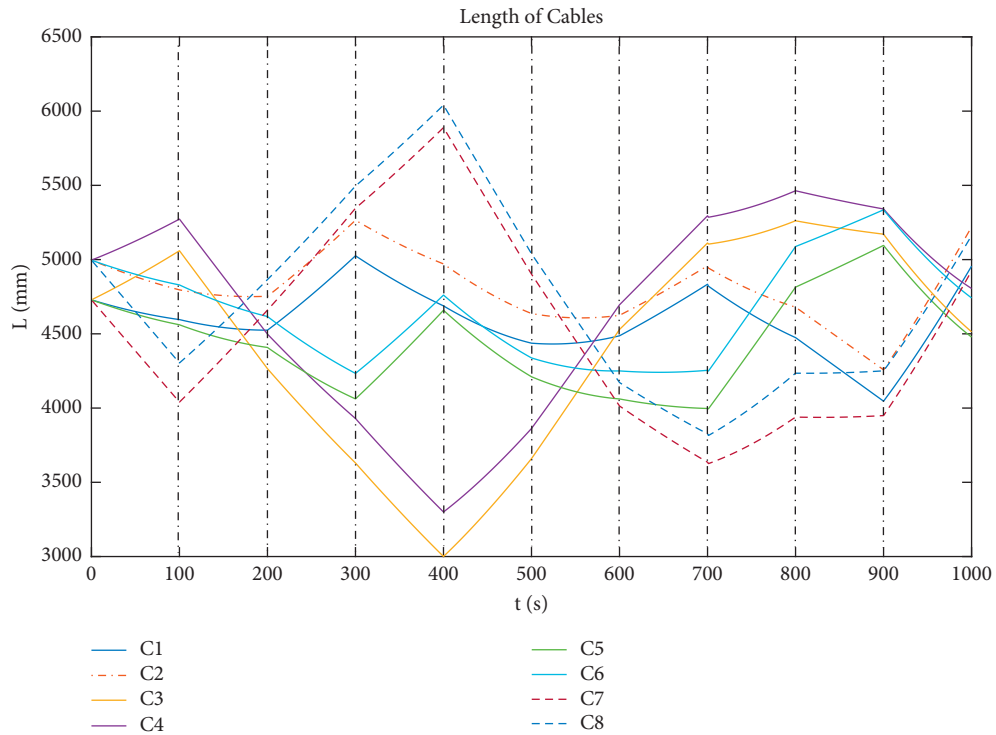


FIGURE 20: Encoder signal in the experiment for measuring the length of the cable.

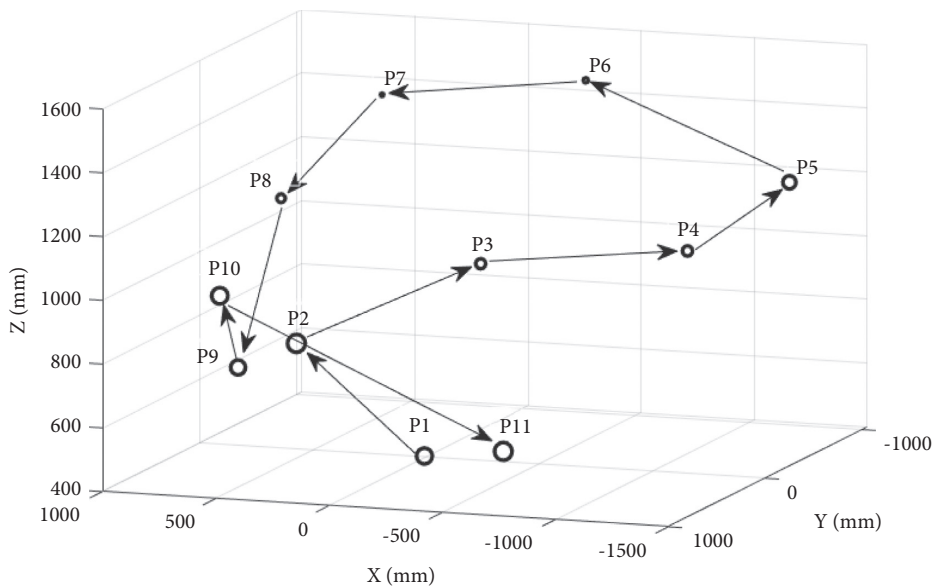


FIGURE 21: Point-to-point paths with 11 node points in the experiment and mean error of positions.

working head approaches the columns of the robot fixed frame. This is because the distribution of cable forces at low positions has a small value, and at corner positions, there is a large difference in cable tension, both of which cause low stability of the moving platform.

### 7. Conclusions

Calculation of cable sag is necessary to improve the accuracy of CDPRs. Numerical methods have been applied to simulate

the problem of finding cable sags, but the computation time is an issue that needs improvement. In this paper, the ANFIS model has been built based on the kinematics problem of a large-sized cable robot to predict cable sag. Parameters affecting cable sag such as kinematic structure, cable tension, and cable tension distribution method are also taken into account when generating the input data for the ANFISs. Eight ANFIS models based on two tension distribution algorithms are constructed to predict the sag of cables. ANFIS models were structured by first-order Sugeno with 81 rules and 3

generalized Gaussian membership functions. ANFIS models are applied to calculate simulations on the trained and test data sets, as well as data from basic moving trajectories. The statistical results consisting of the correlation coefficient, root-mean-square error, and scatter index show that the effectiveness of the approach is appropriate. The ANFIS model can be used to generate sag prediction for CDPRs with fast calculation time and high accuracy, thus making ANFIS an alternative to numerical methods. This calculation procedure can be applied to build ANFIS models that predict cable sags for different CDPR configurations. This procedure builds a model to predict this cable sag based on the coordinates of the MP, so the prediction model depends on the structure of the particular CDPRs as well as the method of calculating the corresponding cable tension distribution. This means that the ANFIS model that predicts cable sag is only applicable to a specific type of CDPRs and a specific tension distribution method. However, according to the sagging model in Section 4, cable sag depends on cable length and cable tension in a local frame, so it is possible to build a common cable sag prediction model for all CDPRs by synchronizing the input data including CDPR configuration and tension distribution method, to obtain the input data for the cable sag calculation model which include the cable coordinates and the cable tension in the respective local axis system. This method has the advantage that it can be applied to any configuration. However, the computation time increases due to the need to solve the CDPR kinematics and cable tension distribution problems. In future works, the ANFIS models in Section 4 are going to be modified and applied to predict cable sag for different CDPRs configurations. Other parameters such as the stiffness matrix and the external wrench are also analyzed to improve the accuracy of CDPRs. The calculated results are going to be compared with existing methods to evaluate the effectiveness of these models.

## Data Availability

Not applicable.

## Conflicts of Interest

The authors declare that there are no conflicts of interest regarding the publication of this paper.

## Acknowledgments

This work was funded by the Ministry of Education and Training of Vietnam, under grant no. B2021-SPK-05, and hosted by Ho Chi Minh City University of Technology and Education, Vietnam.

## References

- [1] S. Qian, B. Zi, W.-W. Shang, and Q.-S. Xu, "A review on cable-driven parallel robots," *Chinese Journal of Mechanical Engineering*, vol. 31, no. 1, pp. 1–11, 2018.
- [2] Q. J. Duan, J. L. Du, B. Y. Duan, and A. F. Tang, "Deployment/retrieval modeling of cable-driven parallel robot," *Mathematical Problems in Engineering*, vol. 2010, Article ID 909527, 10 pages, 2010.
- [3] W. Lv, L. Tao, and Z. Ji, "Sliding mode control of cable-driven redundancy parallel robot with 6 DOF based on cable-length sensor feedback," *Mathematical Problems in Engineering*, vol. 2017, Article ID 1928673, 21 pages, 2017.
- [4] M. Forlani, N. Sancisi, M. Conconi, and V. Parenti-Castelli, "A new test rig for static and dynamic evaluation of knee motion based on a cable-driven parallel manipulator loading system," *Meccanica*, vol. 51, no. 7, pp. 1571–1581, 2016.
- [5] R. Verhoeven, *Analysis of the workspace of tendon-based Stewart platforms*, PhD dissertation, Universität Duisburg-Essen, Duisburg, Germany, 2006.
- [6] S.-R. Oh and S. K. Agrawal, "A reference governor-based controller for a cable robot under input constraints," *IEEE Transactions on Control Systems Technology*, vol. 13, no. 4, pp. 639–645, 2005.
- [7] P. H. Borgstrom, N. P. Borgstrom, M. J. Stealey et al., "Design and implementation of NIMS3D, a 3-D cabled robot for actuated sensing applications," *IEEE Transactions on Robotics*, vol. 25, no. 2, pp. 325–339, 2009.
- [8] G. Abbasnejad and M. Carricato, "Real solutions of the direct geometric-static problem of under-constrained cable-driven parallel robots with 3 cables: a numerical investigation," *Meccanica*, vol. 47, no. 7, pp. 1761–1773, 2012.
- [9] H. Max Irvine, *Cable Structures*, The NTT Press, Birmingham, UK, 1981.
- [10] K. Kozak, Q. Zhou, and J. Wang, "Static analysis of cable-driven manipulators with non-negligible cable mass," *IEEE Transactions on Robotics*, vol. 22, no. 3, pp. 425–433, 2006.
- [11] N. Riehl, M. Gouttefarde, S. Krut, C. Baradat, and F. Pierrot, "Effects of non-negligible cable mass on the static behavior of large workspace cable-driven parallel mechanisms," in *Proceedings of the 2009 IEEE International Conference on Robotics and Automation*, pp. 2193–2198, IEEE, Kobe, Japan, May 2009.
- [12] M. Gouttefarde, J.-F. Collard, N. Riehl, and C. Baradat, "Simplified static analysis of large-dimension parallel cable-driven robots," in *Proceedings of the 2012 IEEE International Conference on Robotics and Automation*, pp. 2299–2305, IEEE, Saint Paul, MN, USA, May 2012.
- [13] J.-P. Merlet, "The kinematics of cable-driven parallel robots with sagging cables: preliminary results," in *Proceedings of the 2015 IEEE International Conference on Robotics and Automation (ICRA)*, pp. 1593–1598, IEEE, Seattle, WA, USA, May 2015.
- [14] P. Gia Luan and N. Truong Thinh, "Empirical quasi-static and inverse kinematics of cable-driven parallel manipulators including presence of sagging," *Applied Sciences*, vol. 10, no. 15, p. 5318, 2020.
- [15] T. P. Tho and N. T. Thinh, "Using a cable-driven parallel robot with applications in 3D concrete printing," *Applied Sciences*, vol. 11, no. 2, p. 563, 2021.
- [16] C. Gosselin and M. Grenier, "On the determination of the force distribution in overconstrained cable-driven parallel mechanisms," *Meccanica*, vol. 46, no. 1, pp. 3–15, 2011.
- [17] A. Pott, T. Bruckmann, and L. Mikelsons, "Closed-form force distribution for parallel wire robots," in *Computational Kinematics*, pp. 25–34, Springer, Berlin, Germany, 2009.
- [18] E. Picard, E. Tahoumi, F. Plestan, S. Caro, and F. Claveau, "A new control scheme of cable-driven parallel robot balancing between sliding mode and linear feedback," *IFAC-Papers-OnLine*, vol. 53, no. 2, pp. 9936–9943, 2020.



- [19] D. Bertsimas and J. N. Tsitsiklis, *Introduction to Linear Optimization*, Athena Scientific, Belmont, MA, USA, 1997.
- [20] K. G. Murty, *Linear Programming*, The University of Michigan, Chichester, UK, 1983.
- [21] Z. Yingliang and X. Chengxian, "A new trust region dogleg method for unconstrained optimization," *Applied Mathematics—A Journal of Chinese Universities*, vol. 15, no. 1, pp. 83–92, 2000.
- [22] R. Mikaeil, S. S. Haghshenas, Y. Ozcelik, and H. H. Gharegheshlagh, "Performance evaluation of adaptive neuro-fuzzy inference system and group method of data handling-type neural network for estimating wear rate of diamond wire saw," *Geotechnical & Geological Engineering*, vol. 36, no. 6, pp. 3779–3791, 2018.
- [23] R. Mikaeil, S. S. Haghshenas, and S. H. Hoseinie, "Rock penetrability classification using artificial bee colony (ABC) algorithm and self-organizing map," *Geotechnical & Geological Engineering*, vol. 36, no. 2, pp. 1309–1318, 2018.
- [24] H. Naderpour and M. Mirrashid, "Moment capacity estimation of spirally reinforced concrete columns using ANFIS," *Complex & Intelligent Systems*, vol. 6, no. 1, pp. 97–107, 2020.
- [25] A. Pandey, A. K. Kashyap, D. R. Parhi, and B. K. Patle, "Autonomous mobile robot navigation between static and dynamic obstacles using multiple ANFIS architecture," *World Journal of Engineering*, vol. 16, no. 2, pp. 275–286, 2019.
- [26] A.-V. Duka, "ANFIS based solution to the inverse kinematics of a 3DOF planar manipulator," *Procedia Technology*, vol. 19, pp. 526–533, 2015.
- [27] J. Narayan, E. Singla, S. Soni, and A. Singla, "Adaptive neuro-fuzzy inference system-based path planning of 5-degrees-of-freedom spatial manipulator for medical applications," *Proceedings of the Institution of Mechanical Engineers-Part H: Journal of Engineering in Medicine*, vol. 232, no. 7, pp. 726–732, 2018.
- [28] J.-S. R. Jang, "ANFIS: adaptive-network-based fuzzy inference system," *IEEE Transactions on Systems, Man, and Cybernetics*, vol. 23, no. 3, pp. 665–685, 1993.
- [29] S. G. Patil, S. Mandal, A. V. Hegde, and S. Alavandar, "Neuro-fuzzy based approach for wave transmission prediction of horizontally interlaced multilayer moored floating pipe breakwater," *Ocean Engineering*, vol. 38, no. 1, pp. 186–196, 2011.

## Bài báo số 2 – SCIE Q3 - IF 1.576

Tuong Phuoc Tho, Nguyen Truong Thinh, "An Overview of Cable-Driven Parallel Robots: Workspace, Tension Distribution, and Cable Sagging", *Mathematical Problems in Engineering*, vol. 2022, Article ID 2199748, 15 pages, 2022. <https://doi.org/10.1155/2022/2199748>

Link: <https://onlinelibrary.wiley.com/doi/10.1155/2022/2199748>



## Review Article

# An Overview of Cable-Driven Parallel Robots: Workspace, Tension Distribution, and Cable Sagging

Tuong Phuoc Tho  and Nguyen Truong Think 

Faculty of Mechanical Engineering, Ho Chi Minh City University of Technology and Education, Ho Chi Minh City, Vietnam

Correspondence should be addressed to Nguyen Truong Think; [thinknt@hcmute.edu.vn](mailto:thinknt@hcmute.edu.vn)

Received 26 December 2021; Revised 8 June 2022; Accepted 28 June 2022; Published 14 July 2022

Academic Editor: Xuping Zhang

Copyright © 2022 Tuong Phuoc Tho and Nguyen Truong Think. This is an open access article distributed under the Creative Commons Attribution License, which permits unrestricted use, distribution, and reproduction in any medium, provided the original work is properly cited.

The researching, designing, calculating, and controlling cable-driven parallel robots (CDPRs) are being promoted in recent years. The researches focus on optimizing the design of CDPRs configuration, computing workspace, calculating cable tension distribution, designing the mechanical structure, and developing controller. However, due to the complexity of the structure and unidirectional characteristic of cable, many computational methods have been applied to solve the above problems. To facilitate the performance of theoretical studies on important issues in the design and control of the CDPRs, a summary of computational methods is needed for important issues related to the functionality and accuracy of CDPRs such as defining the workspace, distributing the cable tensions, and calculating the sagging of the cable. This paper summarizes published studies on CDPRs and focuses on classifying and analyzing methods used to calculate important issues in the process of calculating and designing CDPRs. The efficiency of these calculation methods is also analyzed and evaluated based on the mathematical theories of kinematics and dynamics of CDPRs. The content of this study is an effective reference for studies on important problems in the process of designing and implementing CDPRs, helping researchers shorten the time to review related topics.

## 1. Introduction

Cable-driven parallel robot (CDPR) is a branch of parallel kinetic robot with the moving platform-driven by cables. CDPRs are also known by other names in published studies such as cable-driven parallel manipulators (CDPMs) [1, 2], or simply cable robots (CRs) [3]. As the actuators of CDPRs, cables are usually stored and delivered by sets of winches placed on the fixed frame and connected to the moving platform (MP) via anchor points and guide pulleys. With advantages such as simple structure, large working space, high precision, small volume of the actuator, small inertia force, and low manufacturing cost, CDPRs have been designed and developed for applications requiring large workspace, heavy load capacity, high speed, or for applications that require high flexibility [4, 5]. The world's famous CDPR applications are shown in [4, 6, 7] such as FAST telescope-China with an aperture up to 500 m, SKY-CAM—used to control a camera for recording live sports

matches—with the size of a football field rock and cable-driven parallel robot prototype CoGiRo of dimensions  $15\text{ m} \times 11\text{ m} \times 6\text{ m}$ . CDPRs are usually classified according to their structure, the number of degrees of freedom (DOFs), and the number of cables, where  $m$  is the number of DOFs and  $n$  is the number of drive cables,  $r = n - m$  is the number of redundant cables or the number of degrees of redundant (DORs). The basic configurations of CDPRs include the following [8]:

- (a)  $r < 0$ ,  $m \leq 6$ : incompletely restrained positioning mechanism (IRPM) or underconstrained CDPRs, these types of CDPRs usually only work and reach equilibrium with gravity or a given force, and often cannot work with arbitrary external wrenches.
- (b)  $r = 0$ : kinematically fully constrained CDPRs. The robot is completely limited in terms of kinematics, but the equilibrium equation still depends on gravity or other forces. Therefore, the robot can only work

with a specific set of forces. Due to this property, some studies rank this robot in the same class as IRPM.

- (c)  $r = 1$ : completely restrained positioning mechanisms (CRPM) or fully constrained CDPRs. The certain poses of the MP can be determined entirely through the cables. The limits of the MP movements and the wrenches acting on the MP depend on the cable tension limits.
- (d)  $r > 1$ : redundantly restrained positioning mechanisms (RRPM). The robot is constrained redundancy and wrenches must be distributed by cables. An inverse kinematics result has many corresponding kinematic constraints because the number of kinematic constraints is more than the number of DOFs so the static equilibrium of CDPR can have many solutions.
- (e) If the CDPRs are driven by cables mounted above the MP in the direction of gravity, they are called suspended configuration CDPRs. This configuration relies on the gravity of MP to achieve the equilibrium state [5]. The workspace of the suspended CDPRs is mostly located below the fixed cable anchor points. The above CDPR types are all configurable to operate in a suspended state. The working space of the suspended CDPRs depends greatly on the gravity of the MP, so the payload is one of the important parameters in the design process of the CDPRs with a given workspace. Depending on the design configuration, some CDPRs operate only in the suspended state, some CDPRs can operate in the fully restrained state, or may operate both in the fully restrained state and in the suspended state.

The research on CDPRs mainly focuses on the main contents such as optimizing the structure, determining the working space, developing the cable tension distribution algorithms, studying the models to calculate the sagging of the cable, and designing controller and motion trajectories [9–14]. Huajie Hong et al. [10] compiled CDPR case studies and presented studies on the basic theory and application of several CDPR configurations. The authors systematized and analyzed the studies on the topological architecture of CDPR. The optimal configuration depends on the relationship between the number of DOFs and the number of cables. From the optimized structure of CDPRs, the structure matrix (the transpose of the Jacobian matrix) is built to calculate the tension distribution and dynamic equilibrium. CDPRs have complex structures and constraints because of the unidirectional nature of transmission cables; therefore, the design, calculation, and implementation of an application of CDPRs are challenging. Sen Qian et al. [11] have summarized the development of CDPR and analyzed some recent successful application cases of CDPR. The authors have explored basic CDPR research such as mechanical design, performance analysis, and controller development. Hao Xiong et al. [12] have performed an overview analysis of cable-driven rehabilitation devices.

Many research works proposed methods to solve typical issues of CDPRs, which focus on calculating workspaces, configuring structure, building analytical methods cable tension, calculation of kinematics and dynamics, and calculation of transmission cable sagging, based on many different methods with complex constraints. For an overview of a large number of published CDPRs studies, this paper provides a systematic analysis of the methods used to solve the main issues in the design and development CDPRs. The study is divided into four main sections, the first one shows the kinematic and dynamic of CDPRs including the structure matrix, these are the mathematical model used for determining the main issues of CDPRs; the second analysis the articles that study determining workspace of CDPRs; the third section shows the articles study about tension distribution methods, this section analyzes many solutions built to calculate cable tension for fully of over constrain CDPRs; the fourth section calculates the sagging of cables for large workspace CDPRs.

## 2. Kinematic of CDPRs

The typical configuration of CDPRs (Figure 1) consists of a base frame (BF) with fixed anchor points and guiding pulleys used to guide the cables in different configurations, and the moving platform is connected to the cables via movable anchor points. Cables are stored and delivered by winches usually driven by servo motors so that the speed and position of the cables can be precisely controlled. Normally, cable robots work with large loads, so reduction gearboxes are used to reduce motor speed and increase torque. To facilitate fabrication and installation of cable distributors, winches are usually fixed to the fixed frame. However, there are some configurations where all the winches are placed on the moving platform, and the advantage of this structure is that it is convenient for the transmission of control signals between the motors and the main controller, especially for CDPRs with large workspaces [15, 16].

Figure 2 shows the general kinetics diagram of CDPRs. Where the global reference frame is denoted as B, the other one is the E frame attached to the MP.  $\mathbf{x} = (\mathbf{p}, \mathbf{r}) \in \mathbb{R}^m$  is the vector representing the pose including orientation and position of the E frame in the B frame, and  $m$  is the number of DOFs of CDPRs. According to the vector diagram in Figure 2, the equation for calculating the vector  $l_i$  ( $i = 0 \dots n$ ) corresponding to a configuration of MP can be obtained by the following equation:

$$l_i = \mathbf{a}_i - \mathbf{p} - \mathbf{R}\mathbf{b}_i. \quad (1)$$

The length of cables can be obtained as in (2).

$$|l_i| = \sqrt{[\mathbf{a}_i - \mathbf{p} - \mathbf{R}\mathbf{b}_i][\mathbf{a}_i - \mathbf{p} - \mathbf{R}\mathbf{b}_i]^T}. \quad (2)$$

In the general case, the vector  $\mathbf{p} = [P_x \ P_y \ P_z]^T \in \mathbb{R}^3$  represents the origin  $P$  of the E frame in the B frame, the vector  $\mathbf{r} = [\alpha \ \beta \ \gamma]^T \in \mathbb{R}^3$  represents the rotation angles of the E frame in the B frame (Roll–Pitch–Yaw representation or other orientation representation methods can be used),

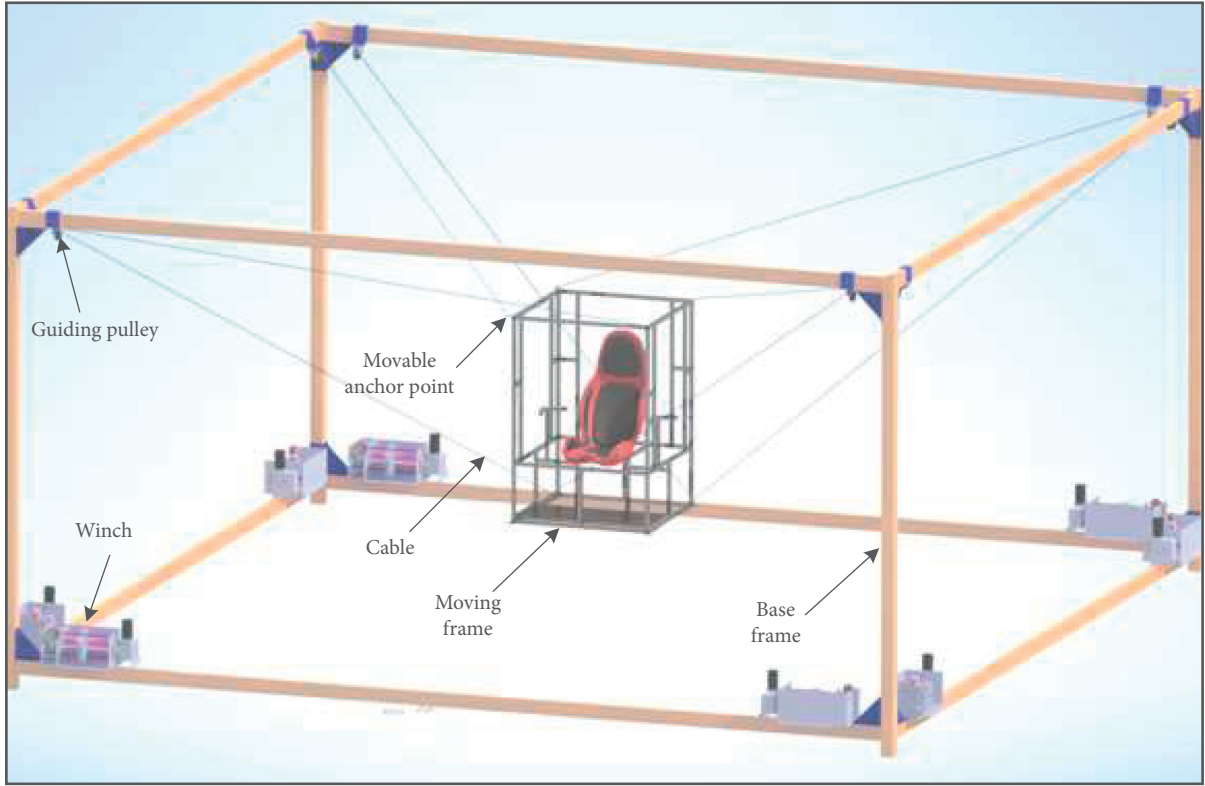


FIGURE 1: A type of configuration of the CDPRs.

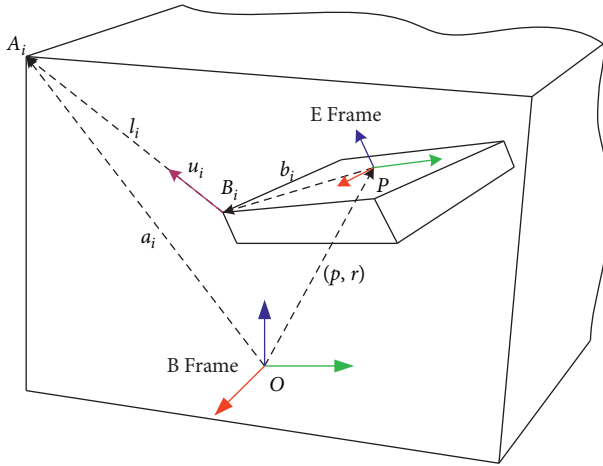


FIGURE 2: General kinematic of CDPRs.

the vector  $\mathbf{a}_i = [A_{ix} \ A_{iy} \ A_{iz}]^T \in \mathbb{R}^3$  is the coordinates of the fixed anchor points  $A_i$  in the  $B$  frame, the vector  $\mathbf{b}_i = [B_{ix} \ B_{iy} \ B_{iz}]^T \in \mathbb{R}^3$  is the coordinates of the movable anchor points  $B_i$  in the  $E$  frame and the unit vector  $u_i$  representing the direction of the cables  $l_i$ . (2) is rewritten as follows:

$$\mathbf{l}_i = \mathbf{a}_i - \mathbf{p} - \mathbf{R}\mathbf{b}_i = \begin{bmatrix} A_{ix} - P_x \\ A_{iy} - P_y \\ A_{iz} - P_z \end{bmatrix} - \mathbf{R} \begin{bmatrix} B_{ix} \\ B_{iy} \\ B_{iz} \end{bmatrix}, \quad (3)$$

where  $R$  is the matrix representing the direction of the  $E$ -axis system in the  $B$ -axis system according to Roll-Pitch-Yaw representation, the RPY consists of the rotation of  $\gamma$  about the  $z$ -axis ( $z$ -axis of the  $E$  frame) called Roll angle, the rotation of  $\beta$  about the  $y$ -axis ( $y$ -axis of the  $E$  frame) called Pitch angle, and the rotation of  $\alpha$  about the  $x$ -axis ( $x$ -axis of the  $E$  frame) called Yaw angle. The  $c$  and  $s$  denote the cosine and sine equation, respectively.

$$\mathbf{R} = \begin{bmatrix} c\beta c\gamma & sas\beta c\gamma - cas\gamma & cas\beta c\gamma + sas\gamma \\ c\beta s\gamma & sas\beta s\gamma + cac\gamma & cas\beta s\gamma - sac\gamma \\ -s\beta & sac\beta & cac\beta \end{bmatrix}. \quad (4)$$

The relationship between the external forces and the cable tensions acting on the MP for a given pose is represented by the equilibrium equation.

$$\mathbf{w} + \mathbf{A}\boldsymbol{\tau} = 0, \quad (5)$$

where  $\boldsymbol{\tau} = [\tau_1 \ \tau_2 \ \dots \ \tau_n]^T \in \mathbb{R}_+^n$  is the positive cable tension vector acting on MP where  $n$  is the number of cables. General structure matrix  $A$  is calculated by the following equation:

$$\mathbf{A} = \begin{bmatrix} \mathbf{u}_1 & \dots & \mathbf{u}_n \\ \mathbf{R} \times \mathbf{u}_1 & \dots & \mathbf{R} \times \mathbf{u}_n \end{bmatrix}. \quad (6)$$

Equations (1), (5), and (6) are important equations in determining the workspace, calculating cable tension, and designing the controller of CDPRs. In the following sections, the parameters defined in this section will be built,

developed, and analyzed to determine the design parameters of CDPRs, including methods of workspace determination, cable tension distribution, and calculation of sagging of cables.

### 3. Workspace and Design

The workspace of the robot is a 2D or 3D space that the robot's end-effector can approach with different position and orientation constraints. This is an important parameter for designing, controlling, and applying the CDPRs. Determining the workspace of parallel robots is more complicated than serial robots because of the complexity of the constraints as well as the unidirectional character of the cables. The workspace of CDPRs is an important parameter in designing the robot structure, calculating the stiffness, as well as controlling the moving trajectory of the MP. With the same case size, CDPR's workspace or moving platform mobility can vary depending on the size and structure of the moving platform, the payload, and the mounting locations of cables on fixed frames and moving platforms. Actuator capacity and load are also important parameters affecting the size of the workspace. The workspace definitions of CDPRs relate to constraints on external forces and limits of cable tensions. Based on the formulas (1–6), the conditions to define the workspace were presented by Veheoven [17–20], mathematical models for workspace calculation are determined based on equilibrium equations, including general workspace, conditions of tension, stiffness, and singularity.

Wrench Closure Workspace (WCW)—Force Closure Workspace (FCW) [21, 22] is defined by the set of poses of the MP where there exists at least one set of cables tension balance to any external force with the upper limit of tension of cable being infinity.

$$\exists \boldsymbol{\tau} \geq 0: \mathbf{A}\boldsymbol{\tau} + \mathbf{w}\mathbf{d} = 0, \quad \forall \mathbf{w}\mathbf{d} \in \mathbf{R}^m. \quad (7)$$

Total Orientation and Constant Orientation Wrench Closure Workspace (TOWCW-COWCW) [23, 24] is defined by the set of poses of the MP (with a set of orientation or one orientation) where there exists at least one set of cables tension balance to any external force with the upper limit of tension of cable being infinity.

Force Feasible Workspace (FFW)—Wrench Feasible Workspace (WFW) [2, 22, 25]: set of poses of the MP in which there exists at least one set of tension cables limited from  $\tau_{\min}$  to  $\tau_{\max}$  equal to a given external force or a given set of external forces:

$$\exists \boldsymbol{\tau} \in [\tau_{\min} \tau_{\max}], \quad \tau_{\min} \geq 0: \mathbf{A}\boldsymbol{\tau} + \mathbf{w}\mathbf{d} = 0, \quad \forall \mathbf{w}\mathbf{d} \in \mathbf{W}. \quad (8)$$

Static Workspace (StW) is the set of poses of the MP for which there exists at least one positive cable tension system balance to the mass and load of MP.

Controllable workspace (CW) [2, 19]—A controllable workspace of postures where forces and torques at the MP can be controlled.

The workspace of CDPRs is a complex geometry due to the constraints of the design parameters. Therefore, it is difficult to determine the workspace of CDPRs

corresponding to changes in key parameters. Due to the unidirectional characteristic of cables that only traction is applied to the moving platform, determining the equilibrium and workspace of CDPRs is a major challenge. The techniques and methods of calculating the workspace used for rigid-link parallel robots or serial manipulators cannot be used for CDPRs. The workspace of CDPRs is a set of poses of the moving platform that satisfies the constraints of geometry, force balance, and structural stiffness with boundary conditions such as force and impact moment, noise, engine power. There are three commonly used methods to define the CDPR workspace. The first method is the pointwise method that considers whether a finite set of discrete points satisfy the constraints of the workspace. The second method is the continuous method with the most commonly used algorithm being interval analysis. The third method is the analytical method that focuses on defining the boundary (geometrical shape) of the workspace, the advantage of this method is that it gives a visual look at the geometry of the workspace. However, this method is only applied individually for each robot configuration.

Structural matrix-based is a commonly used method to determine the workspace of CDPRs. Starting from the equilibrium condition (9), the general solution has the form:

$$\boldsymbol{\tau} = \mathbf{A}^T (\mathbf{A}\mathbf{A}^T)^{-1} \mathbf{w}\mathbf{d} + \mathbf{H}\boldsymbol{\lambda} = \boldsymbol{\tau} + \mathbf{H}\boldsymbol{\lambda}, \quad (9)$$

where  $\boldsymbol{\tau}$  is the minimum norm solution of,  $\mathbf{H}$  (9) is the null space (kernel) of matrix  $\mathbf{A}$ , and  $\boldsymbol{\lambda}$  is an  $n-m$  vector. The constraints for a pose to be included in WCW are  $\text{rank}(\mathbf{A}) = 6$  and  $\exists \tau_n = \mathbf{H}\boldsymbol{\lambda} \in \mathbf{H}: \tau_n > 0$ .

The pointwise method is often applied in determining the workspace of CDPRs. This method is based on considering the discrete points that satisfy the constraints of the poses of the MP to know whether these points belong to the workspace or not. The pointwise method has the advantage that the condition is clear and intuitive, but the accuracy at the boundary depends on the magnitude of the distance of the selected discrete points (resolution), the higher the resolution, the more accurate the results. However, this means increased computation time, especially for CDPRs with large workspace. An important issue of the pointwise workspace determination method is that it is not possible to determine the satisfaction of the points lying between the considered points according to a coordinate procedure such as the random method, radial method, or the equidistant method (Figure 3).

Verhoeven and Hiller [19] suggest a method for defining a controllable workspace based on the pointwise method. This method transforms the force equilibrium equation, then analyzes the rank and kernel of the structural matrix to check the existence of a possible solution for a given combination of forces. However, the study has not considered the moment equilibrium satisfaction for CDPRs with different types of moving platforms such as bars or frames. Verhoeven [20] has proposed a pointwise method to determine the controllable workspace for CDPRs. However, this method is only applicable to a limited number of CDPRs with a simple structure due to the complexity of the

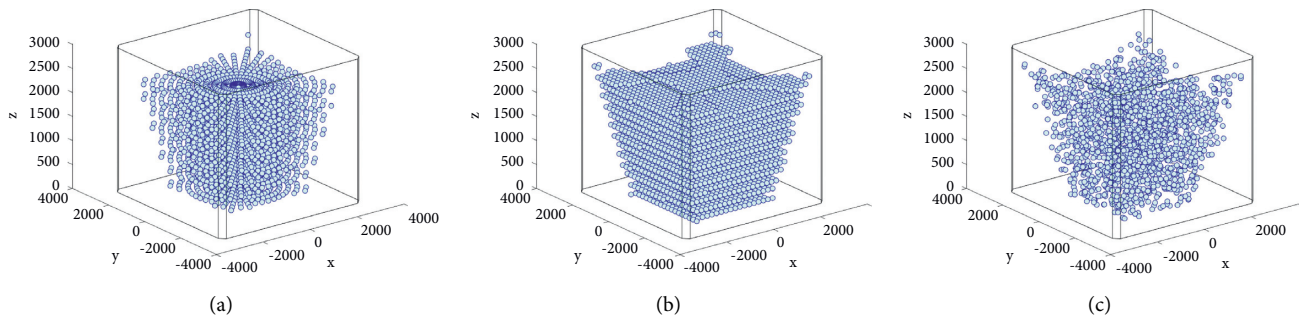


FIGURE 3: Pointwise workspace of suspended configuration CDPR 6 DOFs—8 cables; a-radial space, b-equidistant space, b-random space.

expressions describing the system. Pusey et al. [23] analyzed the workspace of a CDPR 6 DOFs – 6 cables by pointwise method, a performance index was used to evaluate the influence of the robot's structure (size of fixed and moving platforms) on the size of the robot's workspace. These indices depend on the characteristics of the matrix structure. The results apply to the design calculations of CDPR 6 DOFs—6 cables and can be extended to other configurations.

Yang et al. [2] used the tension distribution configuration analysis method to combine the workspace for CDPRs, this method is based on the evaluation of the tension coefficient—the relative tension of the cables—to find the solution of tension distribution corresponds to the optimal workspace, where the determination of the tension coefficient is based on a linear optimization model. Diao and Ma [26] introduce a numerical method to determine FCW. This method checks the condition that a possible solution exists for any external force acting on the MP at a given position of the robot with 6 DOFs and 7 cables. Possible solutions are determined by analyzing the Jacobian matrix to see if there exists at least one all-positive cable tension solution. Lim et al. [27] have developed an algorithm to determine FCW for fully constrained CDPR, based on convex theory, the algorithm checks combinations from the structural matrix of the point under consideration. Ouyang and Shang [28] designed a method to determine the workspace of CDPRs based on the pointwise method. This method determines the satisfaction condition of a pose by computing the null-space of the structure matrix and solving the corresponding system of linear constraint inequalities. Cong Bang Pham et al. [29, 30] used a structure matrix size reduction algorithm based on convex theory to simplify the process of finding the force closure workspace of the fully and over constraint CDPR, the calculation results are applied on a planar-CDPR 3 DOFs—4 cables and a spatial CPDR 6 DOFs—8 Cables.

To increase the accuracy when determining the boundary of the workspace compared to the pointwise method, analytical methods are used to determine the hull of the workspaces. Marc Gouttefarde and Clement Gosselin [21] developed an algorithm to determine the COWCW of 3 DOFs planar CDPR driven by 4 cables. In this paper, the graphical representation is used to illustrate the workspace as a combination of quadratic curves. Gouttefarde et al. [24] have developed an analytical method to determine the

boundary of the Wrench Closure Workspace of CDPRs having fewer DOFs than the cables. This method is based on the linear dependence between columns of the structure matrix to determine the WCW with fixed orientations of the MP, the boundaries of the WCW are defined as a set of cones formed by two redundant cables. The results show that the workspace boundary is composed of conic parts with different shapes. Based on the results of the model analysis in [24], Azizian et al. [31] offer a geometric method used to define the shape of conic sections forming a workspace with a fixed orientation to find the COWCW of planar CDPRs. However, due to the complexity of the calculation formulas, the application of this method to spatial CDPRs needs to be reconsidered. Pott [32, 33] proposed a method to estimate the hull of the translation workspace of CDPRs. This method is based on finding subsets with less dimension such as planes by the analytic method to reduce the computation process, then finding the intersection lines between planes and the workspace to build the hull of workspaces. This method can lead to incomplete estimation of the workspace, and the estimation results depend on the selection of the workspace center. Similar to [32, 33], Perreault et al. [34] have established a method for determining COWCW graphically, which uses lower-dimensional mathematical descriptions such as planes to define the hull of the workspace. The surface shape of the workspace is determined by the combination of curves that intersect the planes and the workspace. Rezazadeh [35] has developed an analytical method for determining the workspace of the multibody CDPR, which builds on the null-space analysis and simplifies the force and moment constraints in the equilibrium equation. Based on [21, 24], Sheng et al. [36] have come up with a general algorithm to find the WCW of spatial CDPRs, this algorithm is based on calculating the kernel of the structural matrix of CDPRs with the Cramer's rule method, thereby giving the satisfied condition of a pose of CPDRs 6 DOFs—7 cables.

Although analytical methods have improved the surface accuracy of the workspace, the volume of the workspace is not completely determined. Therefore, many methods of defining persistent workspaces have been developed to overcome this limitation. To identify continuous workspaces, interval analysis has been studied and applied to different types of CDPRs. This method is based on numerical analysis, in which interval vectors may fully satisfy, partially



satisfy, or not satisfy all the constraints of WFW or WCW. Partial satisfaction interval vectors will be subdivided into intersecting parts and continue testing until the size of the interval vectors is less than a preset threshold. This allows you to define workspaces that ensure continuity within a range and between adjacent intervals. However, the computation of this method is large, especially when the threshold is reduced to increase accuracy as well as smooth the boundary of the workspace. Bruckmann et al. [37] used the interval analysis algorithm to determine the continuous operation space of the CDPR robot. This method can be used to find the optimal configuration of the CDPR with additional criteria such as load, orientation angle, or stiffness of MP. Gouttefarde et al. [38] analyzed the WFW of CDPRs with  $m$  DOFs driven by the number of cables equal to or greater than  $m$ . An interval analysis algorithm is applied to determine WFW with reasonable computation time. Compared with [37], this method shortens the time to determine WFW by using an adding tool to check if the MP coordinates are completely within the feasible region or not. This method reduces the time to separate tension and external wrench. Khalilpour et al. [39] developed a systematic interval method to determine the workspace of planar CDPRs. Based on [38, 39], Loloie et al. [40] studied an interval algorithm based on the fundamental wrench to specify the controllable workspace of both planar and spatial CDPRs. Lamine et al. [41] also established the workspace for CDPRs during the design process based on equilibrium equation calculations with interval analysis, two Planar CDPR 3 DOFs—4 cables and spatial CDPR 6 DOFs—8 cables configurations were analyzed to calculate the minimum size of CDPRs with a given workspace.

Based on the numerical approach, the ray-based method was first studied by Merlet [42] to determine whether the design trajectory is in the workspace of the parallel robot, and this method determines the WCW by solving a combination of univariate polynomial equations. Based on triangulation of workspace hull analysis, Pott [32] developed a method to determine the hull of WFW of CDPR 6 DOFs and one redundant cable. This method defines a sphere with a predicted workspace center and extending in a radial direction. This method has the disadvantage that the result depends on the estimation of the center of the workspace, but it has a simple process and can be applied to the quick determination of the workspace of common robot configurations. Based on the results of [32], Pott and Kraus [43] used the ray-based method of numerical analysis to combine WCW with the fixed orientation of MP. Here, a finite number of rays are used to form the hull of the workspace. Similar to [32, 43], Andreas Pott [33] proposes a workspace calculation scheme that works with the fixed or variable orientation of CDPRs. The triangulation representation allows for quick determination of the volume and boundary of the robot workspace. [44] Darwin Lau et al. proposed a technique that combines numerical and analytical methods to calculate WCW for fully constrained CDPRs configurations. The method used is to reduce the size of the Jacobian matrix to improve the computation time. This method is applied to calculate WCW for CDPR with 6 DOFs and 7

cables. The results show that this method has improved calculation time and accuracy compared to the numerical method. Based on [43, 44], Ghasem Abbasnejad [45] introduces a ray-based method for determining WCWs for different CDPRs configurations, which allow for defining continuum generalized WCWs with any number of cables. This is a general analysis that can be applied to many different types of CDPRs configurations. In which, the two-dimensional representation of the graph can be applied to any number of DOFs of the CDPRs. Zeqing Zhang et al. [46] develop a new method to design trajectories for Spatial CDPRs 6DOFs—7 cables under interference-free (IFC) and wrench-closure (WCC) conditions. Based on the ray-based method, moving platform trajectories including position and orientation are represented as parametric equations with respect to time.

Riechel et al. [25] described the Force Feasible workspace, also known as a useful workspace. This workspace is determined based on the condition that the equilibrium equation is satisfied for a finite set of forces acting in the stationary state. This model is applied to build a workspace for a point-mass CDPR 3 DOFs—3 cables. Cong Bang Pham et al. [1] established a method to optimize the structure of CDPRs based on tension analysis and stiffness matrix. In this study, the connecting points in the fixed frame and moving platform are considered and analyzed to optimize the workspace. A planar CDPR 3 DOFs—4 cables is modeled to calculate the workspace based on structural stiffness parameters and cable tension limits. The results of the workspace calculations are analyzed and used for the design of an algorithm to optimize the robot structure. Giovanni Boschetti and Alberto Trevisani [47] have established a model to evaluate the overall performance of CDPRs with the Wrench Exertion Capability (WEC) performance index. The performance of a CDPR is considered an important parameter in the design and control process; it represents the relationship between the robot structure, the cable tension limits, the force, and torque limit so that the robot can act in a given direction of movement. This model is built based on the linear programming algorithm for the equilibrium equation of CDPRs. Zake et al. [14] introduced the concept of Control Stability Workspace (CSW), where the system stability criterion is an input parameter to determine the CSW. The CSW was significant in designing the controller for the CDPR, which means that for any MP pose in its CSW, the robot controller should be able to guide the MP to that target.

Through articles that have been reviewed, the methods of determining the workspace of CDPRs are studied focusing on the workspace types such as WFW, WCW, COWCW, COWFW, and controllable workspace. In these papers, the analysis method is used to determine the contour of the workspace, this method gives a visual view of the shape of the workspace, but does not determine the volume of the workspace. The disadvantage of this method is that the computational expressions are complex, and it is difficult to combine representation models for different types of CDPRs configurations. Numerical methods include the pointwise method, interval analysis, ray-based method, which are

useful in determining the surface and the volume of workspaces. The pointwise method results in a discontinuous workspace, the accuracy depends on how the coordinates are obtained and the resolution between the points in the workspace. The interval analysis method gives a more general result, ensuring the continuity of the workspace even at the intersections between intervals. However, the surface accuracy of the workspace depends on the threshold of the divisions. The ray-based method is a method that uses the number of rays to determine the surface of the workspace, and this method has better continuity than the pointwise method, but there are still gaps between rays that are not defined. Another problem is that the ray-based method is only applicable to the determination of the workspace for fully constrained CDPRs. However, there is an improvement in computation time compared to interval analysis. Through a summary of relevant research contents, the results of the analysis of the above studies have important implications in choosing suitable options to determine the workspace of CDPRs because each option has its advantages and disadvantages, so researchers need to consider carefully the constraints as well as the computation purposes to select the feasible calculation methods for each specific CDPR configuration. These contents can also help researchers shorten the time to synthesize relevant documents in the research process.

#### 4. Tension Distribution

The calculation of cable tension distribution for CDPRs is very important in the process of calculating, designing, and controlling CDPRs. Cable tension involves important problems such as system equilibrium, workspace determination, actuator and load calculation, system stiffness, trajectory control, and controller design. There are many methods of calculating cable tension that has been studied and applied to the development of CDPRs. This section will analyze the mathematical basis and examine the published calculation methods, thereby giving a more systematic view of this issue.

The linear programming algorithm is often used to find the tension distribution solution with the optimal condition that the sum of the tension forces is minimal. From (5) and (10), the tension distribution for a pose of the MP is the solution of linear programming as follows:

$$\min \text{imize } f(t) = \mathbf{c}^T \boldsymbol{\tau}. \quad (10)$$

With the equality constraints

$$\mathbf{A}\boldsymbol{\tau} = -\mathbf{w}\mathbf{d}, \quad (11)$$

$$\text{Subject to } \boldsymbol{\tau}_{\min} \leq \boldsymbol{\tau} \leq \boldsymbol{\tau}_{\max}.$$

Linear programming (p-norm = 1) is usually solved by Simplex Algorithm or Dual Simplex Algorithm, this algorithm will find the optimal point by detecting the vertices of the polytope constraint. Shiang et al. [48] used linear programming to find tension solutions for the Robotic crane based on its dynamics model. Pham et al. [49] used a linear programming optimization algorithm to calculate the

distribution of cable tension. In this paper, the cable distribution model is reduced to the basic linear optimization form. Agrawal [50] used linear programming to calculate cable tension for planar CDPR, and the calculation results were simulated and compared with other methods. Based on this model, the authors also design a solution to control the robot with negative tension. Similarly, Borgstrom et al. [51] improved the linear programming algorithm to shorten the calculation time of cable tension distribution, and the active-set method is used to determine the optimal solution, the optimal criterion is also the safety tension. This method gives fast computation, but the continuity of cable tension and real-time response need to be further considered. Notash [52] provide an analytical solution to find the minimum cable tension for redundant planar CDPR applications in mechanical engineering.

Similar to linear programming, nonlinear programming was used to calculate the cable tension distribution. Compared with linear programming, this method gives continuous tension distribution results according to the joint trajectory. Quadratic programming (p-norm = 2) [50, 53] has a quadratic objective function, and this method gives continuous root forces because it limits the case those solutions are taken at the vertices of the convex polytope (set of solution). The tension distribution model of quadratic programming has the form:

$$\min \text{imize } f(t) = \mathbf{c}^T (\boldsymbol{\tau} - \boldsymbol{\eta})^2. \quad (12)$$

With the equality constraints

$$\mathbf{A}\boldsymbol{\tau} = -\mathbf{w}\mathbf{d}. \quad (13)$$

Bruckmann et al. [54] introduced methods to define tension solutions for over-constraint CDPRs, including quadratic programming. In this paper, the quadratic objective function is used for better computation time than linear programming. Li et al. [55] used quadratic programming to determine the tension solution for the FAST telescope. In [56], the author used the nonlinear cost function for optimized cable to reduce power consumption. Cote et al. [57] applied quadratic programming to distribute the tension to the cables with the idea of obtaining a second optimal solution by adding a slack variable to the equilibrium equation, which is capable of returning the distribution of tension solution even at positions outside the workspace.

To reduce calculation time and ensure continuity of cable tensions along continuous motion trajectories, the Closed-Form Method is an algorithm developed to calculate cable tension distribution for CDPRs with the number of cables being more than the number of DOFs ( $r > 0$ ). This method converts the problem of finding cable tension into basic numerical equations to shorten the calculation time. This method is suitable for real-time control requirements and minimized objective function is the distance from the solution to a reference vector (usually the mean value of the tension) with p-norm  $\geq 2$ .

Richard Verhoeven [20] established an algorithm called Gradient-based optimization. This algorithm can be applied to different p-norm orders of the objective function, the two

possible solutions with maximum and minimum values are computed for a given  $p$ -norm. The selected solutions will be obtained by linear interpolation between these two values. However, the mathematical model complexity of this method increases when the number of cables is large. Andreas Pott et al. [58] proposed a method called ‘‘Closed-form Force Distribution’’ to determine the tension distribution for CPDRs with more cables than DOFs, this method is based on decomposing the cable tension into two components:

$$\boldsymbol{\tau} = \boldsymbol{\tau}_{\text{av}} + \boldsymbol{\tau}_{\text{ar}}, \quad (14)$$

where  $\tau_{\text{tb}}$  is the mean of  $\tau_{\text{min}}$  and  $\tau_{\text{max}}$  and  $\tau_{\text{ar}}$  is any arbitrary force vector. The tension set  $\boldsymbol{\tau}$  is then calculated according to  $\tau_{\text{tb}}$  and the pseudoinverse of structure matrix. From (5), we can obtain the following:

$$\boldsymbol{\tau} = \boldsymbol{\tau}_{\text{av}} - \mathbf{A}^+ (\mathbf{w} + \mathbf{A}\boldsymbol{\tau}_{\text{av}}). \quad (15)$$

This method gives a result of a continuous tension distribution along the joint trajectory and good execution time is also the advantage of this solution. However, this method may not calculate the cable tension distribution in some cases where a feasible solution exists.

Gosselin and Grenier [59] used specialized optimization for  $p$ -norm to optimize the cable tension distribution for robots with  $m$  DOFs driven by  $n = m + 2$  cables. The goal is to minimize deviations of cable tensions from a given value (within the tension limits), usually the mean of  $\tau_{\text{min}}$  and  $\tau_{\text{max}}$ , and still ensure continuity of solutions. A nonrepetitive algorithm is proposed to perform the calculation of solutions according to the  $P$ -norm, the calculation results are applied to a planar CDPR with 2 DOFs driven by 4 cables, and the solutions are determined according to the  $p$ -norm with the values  $p = 1, 2, 4$ , and  $\infty$ . The results show that the norm  $p = 4$  gives results consistent with the set goals. However, the continuity and real-time constraints have not been covered in this study.

Some works improve the Closed-Form Distribution Algorithm to increase the coverage of WFW, the purpose is to find the distribution of tension at points located in the area where the satisfaction of the constraints has not been determined. Rewrite (11), we have

$$\boldsymbol{\tau} = -\mathbf{A}^+ \mathbf{w} + \mathbf{H}\boldsymbol{\lambda}, \quad (16)$$

where  $\mathbf{A}^+ \in R^{m \times n}$  is the pseudoinvert and  $\mathbf{H} \in R^{m \times r}$  is the kernel of matrix  $\mathbf{A}$ ;  $\boldsymbol{\lambda} (r)$  is an arbitrary scalar vector. The set of cable tension distribution solutions is a convex polyhedron under mapping  $\mathbf{H}$  with hypercube defined by the limits of tensions:

$$\begin{aligned} \boldsymbol{\tau}_{\text{min}} \leq \boldsymbol{\tau} = -\mathbf{A}^+ \mathbf{w} + \mathbf{H}\boldsymbol{\lambda} \leq \boldsymbol{\tau}_{\text{max}}, \\ \boldsymbol{\tau}_{\text{min}} + \mathbf{A}^+ \mathbf{w} \leq \mathbf{H}\boldsymbol{\lambda} \leq \boldsymbol{\tau}_{\text{max}} + \mathbf{A}^+ \mathbf{w}. \end{aligned} \quad (17)$$

Roberts et al. [60] analyzed the statics and the inverse kinematics of the CDPRs based on the kernel analysis of the structural matrix. The static equilibrium of a pose of MP is analyzed based on the kernel properties of the structure matrix for a fully constraint structure. The calculation results

are applied to the planar CDPR to evaluate the effectiveness of the analytical method. Bruckmann et al. [54] proposed a method to calculate the distribution of cable tension online for controlling redundant CDPRs. Based on the kinematic and equilibrium equation of CDPRs, the authors designed two cable tension calculation algorithms for CDPRs with 1 or more redundant cables. Two algorithms gradient-based optimizers and interval analysis are used to calculate cable tension with the requirement of continuous cable tensions along the trajectory of MP. Richard Verhoeven and Manfred Hiller [61] provide a method for determining the cable tension of CDPRs with more than one DORs, this method is based on convex polyhedron analysis of the solution space region for the equilibrium equation. The optimal result is a solution that minimizes the tension of cables but does not guarantee the continuity of the cable tensions along the joint trajectories as the moving platform moves along the given trajectories. Hassan and Khajepou [62] developed an iterative algorithm based on Dykstra’s Algorithm projection to find the tension distribution for a CDPR. This algorithm uses an iterative projection starting from the origin (zero) onto the solution space and back projecting the polyhedron onto the tension limit. The intersection (solution region) will be determined when the distance between the solution space and the polyhedron of the tension limit is zero. The results are applied to calculate the tension for a 3 DOFs robot driven by 3 cables and two redundant limbs to create cable tension with all applied forces.

Based on the geometrical characteristics of the convex polygon that represents the feasible region of cable tension—(17) with  $w = 0$ , Bruckmann et al. [63] proposed a new cable tension calculation algorithm—Safe Force Generation Method—with the requirement that the solutions must be feasible (located in the workspace) and continuous. The algorithm is based on the decomposition of the structural matrix, thereby selecting the solutions located in the safe area (priority to stay away from the boundary values of the cable tension). This allows the MP to be controlled at large speeds and accelerations without the transmission cables slacking. To calculate the real-time cable tensions for a CDPR 3 DOFs—4 cables for moving the camera, Su et al. [64] proposed a nonrepetitive solution based on convex theory, the simulation results show that the obtained cable tensions have a continuous form according to the control trajectory and the calculation time is suitable for real-time control applications. This solution can be modified to apply to other CDPR configurations. However, compute performance metrics and continuity metrics need to be considered for each specific type of configuration. Cui et al. [65] propose a nonrepetitive method to calculate cable tension distribution. This method defines the cable tension feasible region based on Graham’s scanning geometric method applicable to CDPR with 2 DORs. The paper also proposes a method to evaluate the safety of cable tension distribution results. Boumann and Bruckmann [66] develop a method to find solutions to tension distribution when CDPR operates outside the WFW. Based on geometric analysis, the Nearest Corner Method is used to find the closest solutions that satisfy the equilibrium equation based on detecting the

corners of the hypercube composed from the limit of cable tensions. Solution continuity is also considered in the case of robots in the WFW region.

Pott [67] improved the closed-form method to calculate the tension at points in undefined regions for over constraint CDPRs in real-time. Mikelsons et al. [68] designed a non-iterative method to calculate the distribution of cable tension with the optimal condition of safety tension. This method determines the vertices of the feasible convex polytope, then calculates the average value of the vertices found, the tension values are calculated close to the safe value (average of  $\tau_{\min}$  and  $\tau_{\max}$ ), it is also called the Barycentric approach. However, the execution time is an issue to consider when applying this method. Based on Barycentric, Lamaury and Gouttefarde [69] propose a method “Fast Tension Distribution Algorithm” to improve the calculation of cable tension solutions for CDPRs with  $m$  DOFs and the number of cables  $n = m + 2$ . This method is based on determining the feasible convex polygon formed by the intersection between the set of cable tension systems satisfying the constraints in the equilibrium equation and the space bounded by the boundaries of the cable tension. By reducing the number of scanned vertices, the time to determine the feasible convex polygon is improved. The analysis and calculation method of the barycenter of the convex polygon above are applied on a CDPR 6 DOFs—8 cables. The simulation results show that the value of cable tension changes continuously along the design trajectory. Based on the results of [69], Marc Gouttefarde et al. [70] developed a cable tension calculation algorithm called Versatile Tension Distribution Algorithm; the algorithm is applied to CDPRs 6 DOFs driven by 8 cables. With this configuration, the set of possible cable tension solutions is a two-dimensional convex polygon corresponding to 2 DORs. The algorithm is designed based on determining the polygon’s vertices in a clockwise direction or vice versa. Calculation results are verified on two CDPR 6 DOFs—8 cables prototypes in CABLAR and CoGiRo projects. This method is effective with different requirements for determining the optimal tension distribution, as well as for establishing a maximum number of worst-case iterations. Also based on the algorithm of [69], Rasheed et al. [71] designed an algorithm to find the optimal tension distribution for CDPR 6 DOFs—8 cables. This CDPR is reconfigurable since the 4 cable posts are movable with their wheels. Based on [63, 68], Song et al. [72] propose a method called convex analysis to find the optimal configuration for a CDPR 6 DOFs, where the direction of the moving platform is determined in the workspace. Cable mounting configurations are found by comparison and analysis of workspace and flexibility. The authors also propose an algorithm to find real-time cable tension solutions, which is based on calculating the equilibrium equations of a CDPR 6 DOFs driven by 8 cables. The results are compared with two methods, the minimum norm method and the safety tension method, the analysis results show that the tension solutions are continuous and within the limit of the required cable tension, similar to the safety tension method with fast computation time, suitable for real-time applications.

Another method developed based on the closed-form method to calculate the continuous minimum tension along the joint trajectory is the puncture method. This method is based on defining an initial solution in a feasible set, which can be computed using the closed-form method. Then combined with the solution close to the root from the null space of the structure matrix into a straight line, and the minimum solution will be determined on this line because of the linear continuity of the null space. Müller et al. [73] analyzed the results and limitations of the method of minimum tension distribution of the closed-form method, from this result, the author developed an improved puncture method, based on the combination of the improved closed-form method and puncture method. Where the cable tension is distributed continuously and tends to reach the lower limit of the cable tensions, the calculation results show that the improved puncture method gives the results of calculating the cable tension solution in a shorter time with a larger workspace, but the cable tension tends to distribute near the lower limit and has a high amplitude.

Pott [74] provided the analysis method to determine the limits of cable tension for CDPRs. For the maximum tension, the important parameters to be considered are the safety issue, the durability limit of the mechanical structure, the fatigue of the cable during operation, and the capacity of the actuator. Thus, the upper limit force of the transmission cable mainly depends on the mechanical structure and transmission mechanism, which are the main criteria affecting the cost of manufacturing and deploying CDPRs. For the minimum tension, the important criterion to calculate is the cable sagging, especially for the large length cables, the cable tension will be inversely proportional to the cable sagging. The stiffness and elasticity of cable also affect the accuracy of CPDRs, as it affects the operation of the cable distribution mechanism. The vibration of the cables is also analyzed when calculating the lower limit of the cable tension because it is possible to reduce the vibration of the system by increasing the tension in the cables. Notash [75] analyzes the properties of cable tension with the influence of unknown parameters on the structural matrix and the null space of CDPRs, the calculation results are applied to a planar CDPR to evaluate the efficiency of the model. Su et al. [76] propose an iterative method to calculate the cable tension distribution for a large-space camera CDPR3 DOFs—4 cables, the equilibrium equation is built based on the dynamic equation and the sag model of the transmission cable. The iterative algorithm is developed based on the kernel analysis of the structure matrix. The results show that the cable tension changes continuously along the motion trajectory of the CDPRs. Barroso and Saltaren [77] analyze the relationship between the maximum tensions and the external force acting on the MP, the goal is to determine the capacity of the actuator used to design the cable distribution mechanism, thereby determining the workspace of the CDPR based on the null space analysis of the structural matrix. Ueland et al. [78] analyze the problem of determining optimal cable tension distribution for over constraint CDPRs based on studies [58, 70, 77], thereby proposing a new optimal objective function that ensures the

continuity of the cable tension. Hussein et al. [79] provide a solution for determining the minimum value of the upper limits of cable tension for CDPRs with DORs equal to or greater than 1. The constraint condition of this issue is that the cable tension limits must satisfy a required wrench set. This result can be applied to CDPRs that work with large weights and are driven with winches of different structures and capacities. The aim is to optimize the energy consumption and structure of the CDPR.

Through the analysis of the above studies, it is shown that many methods have been developed to calculate the tension distribution for fully and over constraint CDPRs. These methods focus on optimizing solutions according to different goals, such as minimizing tension for applications that require saving energy consumption, safe tension which is convenient for controlling, or maximum tension for increasing the stiffness of the structure. Three methods linear programming, Dykstra, and available wrench set methods give discontinuous tensions according to the joint trajectory, while quadratic programming, nonlinear programming, closed-form, improved closed-form, Barycentric, and puncture methods give continuous tensions following the motion trajectory. In which, closed-form, improved closed-form, Barycentric, puncture methods have fast calculation time, suitable for real-time control requirements. In addition, some methods such as linear programming, Dykstra, and improve-closed-form methods can also be used to determine the workspace according to the pointwise method. Studies [74, 77] also have given a way to determine the limits of cable tension. The lower limit and the upper limit of cable tensions have important significance in designing, determining the structure of the CDPR, calculating the tension distribution, and determining the workspace, and the stiffness of the CDPR.

## 5. Sagging

One of the important problems in the design and development of large CDPRs is determining the sagging of cables, as it directly affects the accuracy of the robot. The general procedure for determining cable sagging of CDPRs is complicated, due to the nonlinearity of the mathematical model. The sagging model of cables is a combination of kinematics, dynamics, cable tension distribution, and cable sagging model. The models for calculating the sagging of cables are mostly based on the catenary equation studied by Irvine [80], where the influence of cable mass, cable elasticity, and cable tension are taken into account in the sagging model.

Based on Irvine's cable sagging equation, Kozak et al. [81] show the results of static model analysis of large-scale CDPR taking into account the mass of cables. Due to cable sagging, the static displacement of uniform elastic cable is also calculated in the postanalysis of the inverse kinematics and CDPR stiffness. This result can be used for the calculation of workspaces with sagging cables or the design process of large CDPRs. Korayem et al. [82] analyzed the kinematics and determined the workspace of the large CDPR taking into account the sagging of the elastic cable. Nicolas

et al. [83] researched the influence of cable mass on the kinematics of CDPRs (the number of DOFs is equal to the number of cables). The forward and inverse kinematics of a large-size suspended CDPR with 3 DOFs-3 cables are calculated based on the elastic cable model of Irvine. The results show that the influence of cable mass on the sagging of cables and the accuracy of CDPR is significant when CDPRs operate with large workspaces or heavy payloads. Based on these results, the authors determined a large CDPR workspace that takes into account cable sagging [84].

FAST telescope is a famous project for the application of giant CDPR. Related to this project, Yao et al. [7] set up a complete model for CDPR 6 cables taking into account the mass and elasticity of the transmission cables, the model is set up as a simple structured equation, and the computation time is faster than catenary equation model. However, the accuracy of this model is not high and a calibrated model is needed to meet the required accuracy. This model is tested on a miniature version of FAST with an accuracy of less than 2 mm. Hui [85] calculated the inverse kinematics of the real version of FAST and planned the orientation of the cabin according to the given trajectory. The study shows that the orientation of the cabin depends on the position of the cabin and the sagging of the cables.

Based on the parabolic cable profile equation of Irvine [80], the sagging model of the large inelastic transmission cable is considered a parabolic curve. Gouttefarde et al. [86] proposed a new simplified static analysis of the CDPRs assuming that a cable with negligible mass and inelastic properties is used to drive the CDPRs. Based on the catenary equation (80), this cable sagging model is developed which assumes that the sagging of the cable is small. The model is simplified by linearizing the relationship between the two projections of the cable tension projected onto the analyzed axis system. This model cannot be applied to under-constrained CDPRs and elastic cables. Also based on the Irvine cable sagging model, Gouttefarde et al. [87] calculated cable sagging with the influence of guide pulley diameter. Nguyen et al. [6, 88] calculated the invert kinematic taking to account cable sagging for reconfigurable CDPRs, the paper proposes a simple cable sagging model and analyzes the remaining problems of this model. Dallej et al. [89] build a vision machine feedback controller. Where the cameras are designed to respond to the position and orientation of the MP to the controller, these data are used to directly correct the robot's inverse kinematics with cable sagging. The article only stops at evaluating simulation results, not experimenting on the CDPR prototype. Sridhar [90] built and simulated a transmission cable compensation model for suspended CDPR in large outdoor spaces. This paper compares the straight-line cable model and the sagging cable model, thereby evaluating the relationship between the cable tension optimization and the error of the cable length calculation model.

Merlet [91–98] studied the inverse kinematic and forward kinematic, calculating cable sagging with different influencing parameters. In [91, 92], the forward kinematics for CDPRs were solved based on interval analysis taking into account the elasticity and mass of the cables, the cable sag

model is considered in static equilibrium. The results are tested on CDPR 6 DOFs—8 cables and give several interesting results. Besides, inverse kinematics for CDPR—6 DOFs—6 cables with cable sagging expressed as catenary equations was developed in [93], and interval analysis is also used to set up an algorithm to calculate the inverse kinematics of this robot. However, the relationship between the limit of MP and the workspace has not been clearly defined. In [94], the author analyzed the workspace of CDPRs for both straight cables and sagging cables. In the case of sagging cables, the boundary of the workspace is not clearly defined. The direct kinematic of CDPR in the case of cable sags [95] was calculated by sensors. The important properties of the static-elastic model based on Irvin's cable sag equation were analyzed, and this result can be used to calculate the CDPR kinematics taking into account the sagging of cables [96]. In this study, a new form of the Irvin equation has been established that can reduce the calculation time of forward and inverse kinematics by interval analysis. Besides, the singularity of CDPR taking into account the sagging of the cables was analyzed, and the results show that CDPR's singularity tends to appear near the edge of the workspace [97]. Calculation results only identify individual singularities, not yet identified singularities for both inverse and forward kinematic. In [98], the forward kinematics for the point-mass suspended CDPR with one redundant cable were calculated. The computational model is built based on the cable sagging equation and interval analysis. A system to measure the signals of cable lengths, cable angles and cable tensions were also built to evaluate the results of the forward kinematics with the influence of uncertainties. In [99], Fabritius and Pott built a new inverse kinematic code applied for CDPR that has more than one redundant cable. The results show that the new method for the workspace is nearly 20% larger than the other method. In [100], the authors also calculated the forward kinematics of CDPR taking into account the influence of cable sagging and guide pulleys. The calculation results show that there is a difference compared with the standard geometric model, in which the obtained WFW and stiffness are smaller than that of the standard model. These results show a significant influence of the cable sag model and pulley parameter on the calculation of forward and reverse kinematics of redundantly CDPRs. From point of view of Yuan et al. [101, 102] analyzed the relationship between cable sagging, stiffness, and dynamics for suspended CDPRs when the cable and MP vibrated during operation. These researches can be used to build vibration reduction solutions for CDPRs of large sizes or working outdoors. The authors also construct the dynamic stiffness matrix of a single cable to calculate the dynamic equations of CDPRs [103]. This computational model is tested on a spatial suspended CDPRs 6 DOFs—6 cables. The results show that there is an influence of dynamic cable on the dynamic model and the accuracy of CDPRs. Arsenault [3] has established a CDPR stiffness representation model that takes into account the sagging of the cables. The results show the influence of cable sagging on the workspace and the stiffness matrix of the robot.

Duan et al. [104] built a deployment and retrieval cable mathematical model based on the lumped mass method taking into account the cable mass. The simulation result for a suspended CDPR 6 DOFs - 6 cables (50 m scaled model) shows that the model is effective in analyzing the dynamic response of cables. Wei et al. [105] analyzed the influence of the cable's inertia on the stability of the CDPR. That was a large size and high-speed cable robot used to move the camera. The dynamic model of the CDPR was determined based on the cable catenary equation and the finite element method, from these calculation results, a camera CDPR controller was designed and simulated. Phan Gia Luan et al. [106] have introduced a new model to calculate the inverse kinematic for CDPR with the influence of cable sagging in quasistatic based on both analytical and practical methods. Experimentally, this result is only valid for CDPRs operating at low speeds and small accelerations. Tho et al. [107] built a cable sagging calculation model using ANFIS, and this model is based on the results of Irvine's catenary equation. The calculation results show that the accuracy of the model is quite good with small errors and short computation time. However, the model is only built for a given robot configuration and a specific method of cable tension distribution. The model can apply to real-time control requirements for large CDPRs.

## 6. Conclusion

This article summarized the studies, typical applications, and important issues in the research and implementation of CDPRs. The basic problems of CDPR are presented focusing on the design of the mechanical structure, analysis of workspace, distribution of cable tension, and determination of cable sag. The mathematical models for CDPRs are also presented in a general form to help readers save review time when synthesizing general knowledge about the design process and analyzing CDPRs. The special feature of CDPRs compared with parallel robots driven by rigid-link is that the position and orientation of the MP are controlled by flexible cables. This creates the outstanding advantages of CDPR such as high speed, high acceleration, and higher load-to-weight ratio. In particular, large workspaces can be achieved due to the flexibility in the storage and distribution of cables. However, a challenge when designing and modeling CDPRs is the unidirectional character of the cables, which mean that the cable only works with positive tension. This leads to a different approach in the study of CDPRs compared to rigid-link robots. The important issues of CDPRs such as kinematics, dynamics, and workspaces are different from those of rigid-link robots, and their mathematical basis is related to the tension of the cables. In recent years, many studies focusing on optimal design, kinetics, and controller systems of CDPRs, which facilitate the expansion of the applicability of CDPRs. Through the analysis of research works on CDPRs, it is shown that the structural optimization of CDPRs focuses on the constraints of the workspace, stiffness, payload, and geometric configuration. Especially studies on CDPRs are reconfigurable for more flexible applications.

Cable tension distribution studies focus on generating continuous tension distributions with constraints of dynamic stiffness, energy consumption, or safe tension. Many methods have been studied to reduce computation time, which is useful for applications requiring online control. Cable sagging studies are especially important for CDPs with large workspace because cable sagging directly affects the CDP kinematics accuracy. Most of the cable sagging calculation models are based on the famous catenary cable equation of Irvine. Based on the above analysis, further studies on CDPs can be carried out in the following directions: developing controllers and tracking the moving trajectory of MP; improving high-load capacity with optimization of structure and materials; increasing the accuracy of workspace definition methods; shortening the time to calculate the tension distribution according to the given constraints; simplify the cable sagging calculation model for specific CDP configurations. In addition, the research direction on the reconfigured form of CDPs promises to expand the applicability of CDPs.

### Data Availability

No data were used to support the findings of the study.

### Conflicts of Interest

The authors declare that there are no conflicts of interest regarding the publication of this paper.

### References

- [1] C. B. Pham, H. Y. Song, and G. Yang, "Workspace analysis and optimal design of cable-driven planar parallel manipulators," vol. 1, pp. 219–224, in *Proceedings of the IEEE Conference on Robotics, Automation and Mechatronics*, vol. 1, IEEE, Singapore, December 2004.
- [2] G. Yang, C. B. Pham, and H. Y. Song, "Workspace performance optimization of fully restrained cable-driven parallel manipulators," in *Proceedings of the 2006 IEEE/RSJ International Conference on Intelligent Robots and Systems*, pp. 85–90, IEEE, Beijing, China, October 2006.
- [3] M. Arsenault, "Workspace and stiffness analysis of a three-degree-of-freedom spatial cable-suspended parallel mechanism while considering cable mass," *Mechanism and Machine Theory*, vol. 66, pp. 1–13, 2013.
- [4] X. Tang, "An overview of the development for cable-driven parallel manipulator," *Advances in Mechanical Engineering*, vol. 6, Article ID 823028, 2014.
- [5] W. Lv, L. Tao, and Z. Ji, "Sliding mode control of cable-driven redundancy parallel robot with 6 DOF based on cable-length sensor feedback," *Mathematical Problems in Engineering*, vol. 2017, Article ID 1928673, 21 pages, 2017.
- [6] D. Q. Nguyen, M. Gouttefarde, Olivier Company, and F. Pierrot, "On the simplifications of cable model in static analysis of large-dimension cable-driven parallel robots," in *Proceedings of the 2013 IEEE/RSJ International Conference on Intelligent Robots and Systems*, pp. 928–934, IEEE, Tokyo, Japan, November 2013.
- [7] R. Yao, H. Li, and X. Zhang, "A modeling method of the cable driven parallel manipulator for FAST," in *Cable-driven Parallel Robots*, pp. 423–436, Springer, Heidelberg, Germany, 2013.
- [8] A. I. G. U. O. Ming and T. Higuchi, "Study on multiple degree-of-freedom positioning mechanism using wires. II: development of a planar completely restrained positioning mechanism," *International Journal of the Japan Society for Precision Engineering*, vol. 28, no. 3, pp. 235–242, 1994.
- [9] A. Pott, *Cable-driven parallel robots: theory and application*, Vol. 120, Springer, New York, NY, USA, 2018.
- [10] H. Hong, J. Ali, and L. Ren, "A review on topological architecture and design methods of cable-driven mechanism," *Advances in Mechanical Engineering*, vol. 10, no. 5, Article ID 168781401877418, 2018.
- [11] S. Qian, B. Zi, W.-W. Shang, and Q.-S. Xu, "A review on cable-driven parallel robots," *Chinese Journal of Mechanical Engineering*, vol. 31, no. 1, p. 66, 2018.
- [12] H. Xiong and X. Diao, "A review of cable-driven rehabilitation devices," *Disability and Rehabilitation: Assistive Technology*, vol. 15, no. 8, pp. 885–897, 2020.
- [13] E. Idà, T. Bruckmann, and M. Carricato, "Rest-to-rest trajectory planning for underactuated cable-driven parallel robots," *IEEE Transactions on Robotics*, vol. 35, no. 6, pp. 1338–1351, 2019.
- [14] Z. Zake, F. Chaumette, N. Pedemonte, and S. Caro, "Robust 2½D visual servoing of a cable-driven parallel robot thanks to trajectory tracking," *IEEE Robotics and Automation Letters*, vol. 5, no. 2, pp. 660–667, 2020.
- [15] R. Bostelman, J. Adam, N. Dagalakis, and A. James, "RCS-based RoboCrane integration," in *Proceedings of the International Conference on Intelligent Systems: A Semiotic Perspective*, NIST, Gaithersburg, MD, USA, October 1996.
- [16] A. M. Lytle and K. S. Saïdi, "NIST research in autonomous construction," *Autonomous Robots*, vol. 22, no. 3, pp. 211–221, 2007.
- [17] R. Verhoeven, M. Hiller, and S. Tadokoro, "Workspace of tendon-driven Stewart platforms: basics, classification, details on the planar 2-dof class," vol. 3, pp. 871–876, in *Proceedings of the 4th International Conference on Motion and Vibration Control*, vol. 3, pp. 871–876, ETH Zurich, Switzerland, December 1998.
- [18] R. Verhoeven, M. Hiller, and S. Tadokoro, "Workspace, stiffness, singularities and classification of tendon-driven stewart platforms," in *Advances in Robot Kinematics: Analysis and Control*, pp. 105–114, Springer, Dordrecht, Netherlands, 1998.
- [19] R. Verhoeven and M. Hiller, "Estimating the controllable workspace of tendon-based Stewart platforms," in *Advances in Robot Kinematics*, pp. 277–284, Springer, Dordrecht, Netherlands, 2000.
- [20] R. Verhoeven, *Analysis of the workspace of tendon-based Stewart platforms*, Universität Duisburg-Essen, Rhine-Westphalia, Germany, PhD Diss, 2006.
- [21] M. Gouttefarde and C. ment M. Gosselin, "On the properties and the determination of the wrench-closure workspace of planar parallel cable-driven mechanisms," in *Proceedings of the International Design Engineering Technical Conferences and Computers and Information in Engineering Conference*, vol. 46954, pp. 337–346, Salt Lake City, Utah, USA, September 2004.
- [22] M. V. K.. Reddy, *Orientability of the Moving Platform in Planar Cable Robots*, Bengaluru, India, 2019.
- [23] J. Pusey, A. Fattah, S. Agrawal, and E. Messina, "Design and workspace analysis of a 6–6 cable-suspended parallel robot,"

- Mechanism and Machine Theory*, vol. 39, no. 7, pp. 761–778, 2004.
- [24] M. Gouttefarde and C. M. Gosselin, “Analysis of the wrench-closure workspace of planar parallel cable-driven mechanisms,” *IEEE Transactions on Robotics*, vol. 22, no. 3, pp. 434–445, 2006.
- [25] A. T. Riechel and I. Ebert-Uphoff, “Force-feasible workspace analysis for underconstrained, point-mass cable robots,” vol. 5, pp. 4956–4962, in *Proceedings of the IEEE International Conference on Robotics and Automation, 2004. Proceedings. ICRA’04. 2004*, vol. 5, pp. 4956–4962, IEEE, New Orleans, LA, USA, April 2004.
- [26] X. Diao and O. Ma, “A method of verifying force-closure condition for general cable manipulators with seven cables,” *Mechanism and Machine Theory*, vol. 42, no. 12, pp. 1563–1576, 2007.
- [27] W. B. Lim, G. Yang, S. H. Yeo, and S. K. Mustafa, “A generic force-closure analysis algorithm for cable-driven parallel manipulators,” *Mechanism and Machine Theory*, vol. 46, no. 9, pp. 1265–1275, 2011.
- [28] Bo. Ouyang and W.-W. Shang, “A new computation method for the force-closure workspace of cable-driven parallel manipulators,” *Robotica*, vol. 33, no. 3, pp. 537–547, 2015.
- [29] C. B. Pham, H. Y. Song, and G. Yang, “Tension analysis of cable-driven parallel mechanisms,” in *Proceedings of the 2005 IEEE/RSJ International Conference on Intelligent Robots and Systems*, pp. 257–262, IEEE, Canada, CA, USA, August 2005.
- [30] C. B. Pham, S. H. Yeo, G. Yang, M. S. Kurbanhusen, and I.-M. Chen, “Force-closure workspace analysis of cable-driven parallel mechanisms,” *Mechanism and Machine Theory*, vol. 41, no. 1, pp. 53–69, 2006.
- [31] K. Azizian, P. Cardou, and B. Moore, *Classifying the Boundaries of the Wrench-Closure Workspace of Planar Parallel cable-driven Mechanisms by Visual Inspection*, ASME. J. Mechanisms Robotics, vol. 4, no. 2, Article ID 024503, 2012.
- [32] A. Pott, “Forward kinematics and workspace determination of a wire robot for industrial applications,” in *Advances in Robot Kinematics: Analysis and Design*, pp. 451–458, Springer, Dordrecht, Netherlands, 2008.
- [33] A. Pott, “Efficient computation of the workspace boundary, its properties and derivatives for cable-driven parallel robots,” in *Computational Kinematics*, pp. 190–197, Springer, Cham, Switzerland, 2018.
- [34] S. Perreault, P. Cardou, C. M. Gosselin, and M. J.-D. Otis, “Geometric Determination of the Interference-free Constant-Orientation Workspace of Parallel cable-driven Mechanisms,” *Journal of Mechanisms and Robotics*, vol. 2, Article ID 031016, 2010.
- [35] S. Rezazadeh and S. Behzadipour, “Workspace Analysis of Multibody cable-driven Mechanisms,” *Journal of Mechanisms and Robotics*, vol. 3, Article ID 021005, 2011.
- [36] Z. Sheng, J.-H. Park, S. Paul, and S. K. Agrawal, “Analytic determination of wrench closure workspace of spatial cable driven parallel mechanisms,” in *Proceedings of the International Design Engineering Technical Conferences and Computers and Information in Engineering Conference*, vol. 57144, August 2015, Article ID V05CT08A048.
- [37] T. Bruckmann, L. Mikelsons, M. Hiller, and D. Schramm, “Continuous workspace analysis, synthesis and optimization of wire robots,” in *Proceedings of the International Design Engineering Technical Conferences and Computers and Information in Engineering Conference*, vol. 43260, pp. 59–66, New York, NY, USA, August 2008.
- [38] M. Gouttefarde, D. Daney, and J.-P. Merlet, “Interval-analysis-based determination of the wrench-feasible workspace of parallel cable-driven robots,” *IEEE Transactions on Robotics*, vol. 27, no. 1, pp. 1–13, 2011.
- [39] S. A. Khalilpour, A. Zarif Loloie, H. D. Taghirad, and M. T. Masouleh, “Feasible kinematic sensitivity in cable robots based on interval analysis,” in *Cable-driven Parallel Robots*, pp. 233–249, Springer, Heidelberg, Germany, 2013.
- [40] A. Zarif Loloie, H. D. Taghirad, and N. N. Kouchmeshky, “Interval analysis of controllable workspace for cable robots,” *AUT Journal of Electrical Engineering*, vol. 45, no. 1, pp. 1–8, 2013.
- [41] H. Lamine, S. Bennour, and L. Romdhane, “Design of cable-driven parallel manipulators for a specific workspace using interval analysis,” *Advanced Robotics*, vol. 30, no. 9, pp. 585–594, 2016.
- [42] J.-P. Merlet, “Trajectory verification in the workspace for parallel manipulators,” *The International Journal of Robotics Research*, vol. 13, no. 4, pp. 326–333, 1994.
- [43] A. Pott and W. Kraus, “Determination of the wrench-closure translational workspace in closed-form for cable-driven parallel robots,” in *Proceedings of the 2016 IEEE International Conference on Robotics and Automation (ICRA)*, pp. 882–887, IEEE, Stockholm, Sweden, May 2016.
- [44] D. Lau, O. Denny, K. Saman, and Halgamuge, “Wrench-closure Workspace Generation for cable Driven Parallel Manipulators Using a Hybrid Analytical-Numerical Approach,” *Journal of Mechanical Design*, vol. 133, Article ID 071004, 2011.
- [45] G. Abbasnejad, J. Eden, and D. Lau, “Generalized ray-based lattice generation and graph representation of wrench-closure workspace for arbitrary cable-driven robots,” *IEEE Transactions on Robotics*, vol. 35, no. 1, pp. 147–161, 2019.
- [46] Z. Zhang, H. H. Cheng, and D. Lau, “Efficient wrench-closure and interference-free conditions verification for cable-driven parallel robot trajectories using a ray-based method,” *IEEE Robotics and Automation Letters*, vol. 5, no. 1, pp. 8–15, 2020.
- [47] G. Boschetti and A. Trevisani, “Cable robot performance evaluation by wrench exertion capability,” *Robotics*, vol. 7, p. 15, 2018.
- [48] W.-J. Shiang, D. Cannon, and J. Gorman, “Optimal force distribution applied to a robotic crane with flexible cables,” vol. 2, pp. 1948–1954, in *Proceedings of the 2000 ICRA. Millennium Conference. IEEE International Conference on Robotics and Automation. Symposia Proceedings (Cat. No. 00CH37065)*, vol. 2, pp. 1948–1954, IEEE, San Francisco, CA, USA, April 2000.
- [49] C. B. Pham, G. Yang, and H. Y. Song, “Dynamic analysis of cable-driven parallel mechanisms,” in *Proceedings of the 2005 IEEE/ASME International Conference on Advanced Intelligent Mechatronics*, pp. 612–617, IEEE, Monterey, CA, USA, August 2005.
- [50] So-R. Oh and S. K. Agrawal, “Cable suspended planar robots with redundant cables: controllers with positive tensions,” *IEEE Transactions on Robotics*, vol. 21, no. 3, pp. 457–465, 2005.
- [51] P. H. Borgstrom, B. L. Jordan, G. S. Sukhatme, M. A. Batalin, and W. J. Kaiser, “Rapid computation of optimally safe tension distributions for parallel cable-driven robots,” *IEEE Transactions on Robotics*, vol. 25, no. 6, pp. 1271–1281, 2009.
- [52] M. Agahi and L. Notash, “Redundancy resolution of wire-actuated parallel manipulators considering contact forces in machining applications,” in *Proceedings of the CCToMM*



- Symposium on Mechanisms, Machines, and Mechatronics*, Queen's University, Canada, CA, USA, June 2011.
- [53] P. Liu, Y. Qiu, Yu Su, and J. Chang, "On the minimum cable tensions for the cable-based parallel robots," *Journal of Applied Mathematics*, vol. 2014, pp. 1–8, 2014.
- [54] T. Bruckmann, "Andreas Pott, and Manfred Hiller. "Calculating force distributions for redundantly actuated tendon-based Stewart platforms," in *Advances in Robot Kinematics*, pp. 403–412, Springer, Dordrecht, Netherlands, 2006.
- [55] H. Li, X. Zhang, R. Yao, J. Sun, G. Pan, and W. Zhu, "Optimal force distribution based on slack rope model in the incompletely constrained cable-driven parallel mechanism of FAST telescope," in *Cable-Driven Parallel Robots*, pp. 87–102, Springer, Heidelberg, Germany, 2013.
- [56] T. Bruckmann, C. Sturm, and W. Lalo, *Wire Robot Suspension Systems for Wind Tunnels*, pp. 29–50, Wind tunnels and experimental fluid dynamics research, Heidelberg, Germany, 2010.
- [57] A. F. Côté, P. Cardou, and C. Gosselin, "A tension distribution algorithm for cable-driven parallel robots operating beyond their wrench-feasible workspace," in *Proceedings of the 2016 16th International Conference on Control, Automation and Systems (ICCAS)*, pp. 68–73, IEEE, Gyeongju, Republic of Korea, October 2016.
- [58] A. Pott, B. Tobias, and L. Mikelsons, "Closed-form force distribution for parallel wire robots," in *Computational Kinematics*, pp. 25–34, Springer, Berlin, Heidelberg, 2009.
- [59] C. Gosselin and M. Grenier, "On the determination of the force distribution in overconstrained cable-driven parallel mechanisms," *Meccanica*, vol. 46, no. 1, pp. 3–15, 2011.
- [60] R. G. Roberts, T. Graham, and T. Lippitt, "On the inverse kinematics, statics, and fault tolerance of cable-suspended robots," *Journal of Robotic Systems*, vol. 15, no. 10, pp. 581–597, 1998.
- [61] R. Verhoeven and M. Hiller, "Tension distribution in tendon-based stewart platforms," in *Advances in Robot Kinematics*, pp. 117–124, Springer, Dordrecht, Netherlands, 2002.
- [62] M. Hassan and A. Khajepour, "Optimization of actuator forces in cable-based parallel manipulators using convex analysis," *IEEE Transactions on Robotics*, vol. 24, no. 3, pp. 736–740, 2008.
- [63] T. Bruckmann, L. Mikelsons, M. Hiller, and D. Schramm, "A new force calculation algorithm for tendon-based parallel manipulators," in *Proceedings of the 2007 IEEE/ASME International Conference on Advanced Intelligent Mechatronics*, pp. 1–6, IEEE, Zurich, Switzerland, September 2007.
- [64] Yu. Su, Y. Qiu, and P. Liu, "The continuity and real-time performance of the cable tension determining for a suspend cable-driven parallel camera robot," *Advanced Robotics*, vol. 29, no. 12, pp. 743–752, 2015.
- [65] Z. Cui, X. Tang, S. Hou, and H. Sun, "Non-iterative geometric method for cable-tension optimization of cable-driven parallel robots with 2 redundant cables," *Mechatronics*, vol. 59, pp. 49–60, 2019.
- [66] R. Boumann and T. Bruckmann, "Real-time cable force calculation beyond the wrench-feasible workspace," *Robotics*, vol. 9, no. 2, p. 41, 2020.
- [67] A. Pott, "An improved force distribution algorithm for overconstrained cable-driven parallel robots," in *Computational Kinematics*, pp. 139–146, Springer, Dordrecht, Netherlands, 2014.
- [68] L. Mikelsons, B. Tobias, M. Hiller, and D. Schramm, "A real-time capable force calculation algorithm for redundant tendon-based parallel manipulators," in *Proceedings of the 2008 IEEE International Conference on Robotics and Automation*, pp. 3869–3874, IEEE, Pasadena, CA, USA, May 2008.
- [69] J. Lamaury and M. Gouttefarde, "A tension distribution method with improved computational efficiency," in *Cable-Driven Parallel Robots*, pp. 71–85, Springer, Heidelberg, Germany, 2013.
- [70] M. Gouttefarde, J. Lamaury, C. Reichert, and T. Bruckmann, "A versatile tension distribution algorithm for  $n$ -dof parallel robots driven by  $n+2$  cables," *IEEE Transactions on Robotics*, vol. 31, no. 6, pp. 1444–1457, 2015.
- [71] T. Rasheed, P. Long, D. Marquez-Gamez, and S. Caro, "Tension distribution algorithm for planar mobile cable-driven parallel robots," in *Cable-driven Parallel Robots*, pp. 268–279, Springer, Cham, Switzerland, 2018.
- [72] Da. Song, L. Zhang, and F. Xue, "Configuration optimization and a tension distribution algorithm for cable-driven parallel robots," *IEEE Access*, vol. 6, pp. 33928–33940, 2018.
- [73] K. Müller, C. Reichert, and B. Tobias, "Analysis of a real-time capable force computation method," in *Cable-driven Parallel Robots*, pp. 227–238, Springer, Cham, Switzerland, 2015.
- [74] A. Pott, "On the limitations on the lower and upper tensions for cable-driven parallel robots," in *Advances in Robot Kinematics*, pp. 243–251, Springer, Cham, Switzerland, 2014.
- [75] L. Notash, "Impact of perturbation on wire tension vector," in *Advances in Robot Kinematics*, pp. 41–49, Springer, Cham, Switzerland, 2014.
- [76] Yu. Su, Y. Qiu, and P. Liu, "Optimal cable tension distribution of the high-speed redundant driven camera robots considering cable sag and inertia effects," *Advances in Mechanical Engineering*, vol. 6, Article ID 729020, 2014.
- [77] A. Rodriguez-Barroso and R. Saltaren, "Tension planner for cable-driven suspended robots with unbounded upper cable tension and two degrees of redundancy," *Mechanism and Machine Theory*, vol. 144, Article ID 103675, 2020.
- [78] E. Ueland, T. Sauder, and R. Skjetne, "Optimal force allocation for overconstrained cable-driven parallel robots: continuously differentiable solutions with assessment of computational efficiency," *IEEE Transactions on Robotics*, vol. 37, no. 2, pp. 659–666, 2021.
- [79] H. Hussein, J. C. Santos, J. B. Izard, and M. Gouttefarde, "Smallest maximum cable tension determination for cable-driven parallel robots," *IEEE Transactions on Robotics*, vol. 37, no. 4, pp. 1186–1205, 2021.
- [80] H. Max Irvine, *Cable Structures*, The NTTPress, Chiyoda-ku, Tokyo, 1981.
- [81] K. Kozak, Q. Zhou, and J. Wang, "Static analysis of cable-driven manipulators with non-negligible cable mass," *IEEE Transactions on Robotics*, vol. 22, no. 3, pp. 425–433, 2006.
- [82] M. H. Korayem, M. Bamdad, and M. Saadat, "Workspace analysis of cable-suspended robots with elastic cable," in *Proceedings of the 2007 IEEE International Conference on Robotics and Biomimetics (ROBIO)*, pp. 1942–1947, IEEE, Sanya, China, December 2007.
- [83] N. Riehl, M. Gouttefarde, S. Krut, C. Baradat, and F. Pierrot, "Effects of non-negligible cable mass on the static behavior of large workspace cable-driven parallel mechanisms," in *Proceedings of the 2009 IEEE International Conference on Robotics and Automation*, pp. 2193–2198, IEEE, Kobe, Japan, May 2009.
- [84] N. Riehl, M. Gouttefarde, C. Baradat, and F. Pierrot, "On the determination of cable characteristics for large dimension

- cable-driven parallel mechanisms,” in *Proceedings of the 2010 IEEE International Conference on Robotics and Automation*, pp. 4709–4714, IEEE, Anchorage, AK, USA, May 2010.
- [85] L. I. Hui, “A giant sagging-cable-driven parallel robot of FAST telescope: its tension-feasible workspace of orientation and orientation planning,” in *Proceedings of the 14th IFToMM World Congress*, pp. 373–381, Department of Mechanical Engineering, National Taiwan University, June 2015.
- [86] M. Gouttefarde, F. C. Jean, N. Riehl, and C. Baradat, “Simplified static analysis of large-dimension parallel cable-driven robots,” in *Proceedings of the 2012 IEEE International Conference on Robotics and Automation*, pp. 2299–2305, IEEE, Saint Paul, MN, USA, May 2012.
- [87] M. Gouttefarde, D. Q. Nguyen, and C. Baradat, “Kinetostatic analysis of cable-driven parallel robots with consideration of sagging and pulleys,” in *Advances in Robot Kinematics*, pp. 213–221, Springer, Cham, Switzerland, 2014.
- [88] D. Q. Nguyen, *On the study of large-dimension reconfigurable cable-driven parallel robots*, UNIVERSITE MONTPELLIER, vol. 2, 2014 PhD diss.
- [89] T. Dallej, M. Gouttefarde, N. Andreff, P.-E. Hervé, and P. Martinet, “Modeling and Vision-Based Control of Large-Dimension cable-driven Parallel Robots Using a Multiple-Camera Setup,” vol. 61, *Mechatronics*, 2019.
- [90] D. Sridhar and R. L. Williams, “Kinematics and statics including cable sag for large cable-suspended robots,” in *Proceedings of the International Design Engineering Technical Conferences and Computers and Information in Engineering Conference*, vol. 50152, June 2016, Article ID V05AT07A075.
- [91] J.-P. Merlet and J. Alexandre-dit-Sandretto, “The forward kinematics of cable-driven parallel robots with sagging cables,” in *Cable-driven Parallel Robots*, pp. 3–15, Springer, Cham, Switzerland, 2015.
- [92] J.-P. Merlet, “The kinematics of cable-driven parallel robots with sagging cables: preliminary results,” in *Proceedings of the 2015 IEEE International Conference on Robotics and Automation (ICRA)*, pp. 1593–1598, IEEE, Seattle, WA, USA, May 2015.
- [93] J.-P. Merlet, “On the inverse kinematics of cable-driven parallel robots with up to 6 sagging cables,” in *Proceedings of the 2015 IEEE/RSJ International Conference on Intelligent Robots and Systems (IROS)*, pp. 4356–4361, IEEE, Hamburg, Germany, September 2015.
- [94] J.-P. Merlet, “On the workspace of suspended cable-driven parallel robots,” in *Proceedings of the 2016 IEEE International Conference on Robotics and Automation (ICRA)*, pp. 841–846, IEEE, Stockholm, Sweden, May 2016.
- [95] J.-P. Merlet, “An experimental investigation of extra measurements for solving the direct kinematics of cable-driven parallel robots,” in *Proceedings of the 2018 IEEE International Conference on Robotics and Automation (ICRA)*, pp. 6947–6952, IEEE, Brisbane, Australia, May 2018.
- [96] J. P. Merlet, “Some properties of the Irvine cable model and their use for the kinematic analysis of cable-driven parallel robots,” *Mechanism and Machine Theory*, vol. 135, pp. 271–280, 2019.
- [97] J.-P. Merlet, “Singularity of cable-driven parallel robot with sagging cables: preliminary investigation,” in *Proceedings of the 2019 International Conference on Robotics and Automation (ICRA)*, pp. 504–509, IEEE, Canada, CA, USA, May 2019.
- [98] J. P. Merlet, “The forward kinematics of the 4-1 cable-driven parallel robot with non elastic sagging cables,” in *International Symposium on Advances in Robot Kinematics*, pp. 98–108, Springer, Cham, Switzerland, 2020.
- [99] M. Fabritius and A. Pott, “An inverse kinematic code for cable-driven parallel robots considering cable sagging and pulleys,” in *European Conference on Mechanism Science*, pp. 423–431, Springer, Cham, Switzerland, 2020.
- [100] M. Fabritius and A. Pott, “A forward kinematic code for cable-driven parallel robots considering cable sagging and pulleys,” in *International Symposium on Advances in Robot Kinematics*, pp. 218–225, Springer, Cham, Switzerland, 2020.
- [101] H. Yuan, E. Courteille, and D. Deblaise, “Static and dynamic stiffness analyses of cable-driven parallel robots with non-negligible cable mass and elasticity,” *Mechanism and Machine Theory*, vol. 85, pp. 64–81, 2015.
- [102] H. Yuan, E. Courteille, M. Gouttefarde, and P.-E. Hervé, “Vibration analysis of cable-driven parallel robots based on the dynamic stiffness matrix method,” *Journal of Sound and Vibration*, vol. 394, pp. 527–544, 2017.
- [103] H. Yuan, E. Courteille, and D. Deblaise, “Elastodynamic analysis of cable-driven parallel manipulators considering dynamic stiffness of sagging cables,” in *Proceedings of the 2014 IEEE International Conference on Robotics and Automation (ICRA)*, pp. 4055–4060, IEEE, Hong Kong, China, May 2014.
- [104] Q. J. Duan, J. L. Du, B. Y. Duan, and A. F. Tang, “Deployment/retrieval modeling of cable-driven parallel robot,” *Mathematical Problems in Engineering*, vol. 2010, Article ID 909527, 1 page, 2010.
- [105] H. Wei, Y. Qiu, and Yu Su, “Motion control strategy and stability analysis for high-speed cable-driven camera robots with cable inertia effects,” *International Journal of Advanced Robotic Systems*, vol. 13, no. 5, Article ID 172988141666337, 2016.
- [106] P. Gia Luan and N. Truong Thinh, “Empirical quasi-static and inverse kinematics of cable-driven parallel manipulators including presence of sagging,” *Applied Sciences*, vol. 10, no. 15, p. 5318, 2020.
- [107] T. P. Tho, N. T. Thinh, and N. Truong Thinh, “Analysis and evaluation of CDPR cable sagging based on ANFIS,” *Mathematical Problems in Engineering*, vol. 2021, pp. 1–20, 2021.



## Bài báo số 3 – SCIE Q1 - IF 3.9

Tuong Phuoc Tho & Nguyen Truong Thinh (2023) Evaluating cable tension distributions of CDPR for virtual reality motion simulator, *Mechanics Based Design of Structures and Machines*, DOI: 10.1080/15397734.2023.2265452, Volume 0, page 1-19.

Link: <https://doi.org/10.1080/15397734.2023.2265452>





# Evaluating cable tension distributions of CDPR for virtual reality motion simulator

Tuong Phuoc Tho & Nguyen Truong Thinh

**To cite this article:** Tuong Phuoc Tho & Nguyen Truong Thinh (06 Oct 2023): Evaluating cable tension distributions of CDPR for virtual reality motion simulator, *Mechanics Based Design of Structures and Machines*, DOI: [10.1080/15397734.2023.2265452](https://doi.org/10.1080/15397734.2023.2265452)

**To link to this article:** <https://doi.org/10.1080/15397734.2023.2265452>



© 2023 The Author(s). Published with license by Taylor & Francis Group, LLC



Published online: 06 Oct 2023.



Submit your article to this journal [↗](#)



View related articles [↗](#)



View Crossmark data [↗](#)

# Evaluating cable tension distributions of CDPR for virtual reality motion simulator

Tuong Phuoc Tho<sup>a</sup> and Nguyen Truong Think<sup>b</sup>

<sup>a</sup>Faculty of Mechanical Engineering, Ho Chi Minh City University of Technology and Education, Ho Chi Minh City, Vietnam; <sup>b</sup>Institute of Intelligent and Interactive Technologies, University of Economics Ho Chi Minh City – UEH, Ho Chi Minh City, Vietnam

## ABSTRACT

This paper presents a study on modeling, analysis, and control of an over-constrained Cable-Driven Parallel Robot taking into account the deformation of the cable transmission system due to the elastic model of the transmission mechanism and the affection of tension distribution for cables. The Cable-Driven Parallel Robot is used for a virtual reality motion simulation system with a simulation cabin mounted on a moving platform. A nonlinear cable length controller with tension feedback is designed to control the cabin to move along a trajectory extracted from the virtual simulated environment. The tension distribution algorithm is integrated into the controller to compensate for the dynamic error caused by the two redundant cables and the elastic characteristic of the transmission mechanism. The tensions are calculated based on the constraints of the workspace, the structure of the system, and the force limits of actuators. The cable tension feedback control algorithm was tested on the concept Cable-Driven Parallel Robot, the experimental results show that the joint trajectories meet the desired moving trajectory with high accuracy, and the cable tensions are controlled in the optimal region to ensure safety and save energy, but still suitable for the control requirements of the virtual reality motion simulator system.

## ARTICLE HISTORY



Received 11 April 2023  
Accepted 25 September 2023

## KEYWORDS

Cable driven parallel robots; CDPRs; tension distribution; virtual reality; motion simulator

## 1. Introduction

A Virtual Reality Motion Simulator (VRMS) is a complex integrated system of mechanical engineering, robotics, control and information technology. This system can provide operators (users) with a realistic feeling (including vision and motion) of the real environments to be simulated. VRMS usually includes the following components: A device that displays a 3D virtual reality environment such as a virtual reality headset or a 3D display screen; Motion structure, usually in the form of parallel robots (Kljuno and Williams 2008; Cao et al. 2015), high-load serial robots (Teufel et al. 2007) and more recently Cable-Driven Parallel Robots (CDPR) (Miermeister et al. 2016; Usher et al. 2004), since these robotic systems have sufficient dexterity, degrees of freedom and loads suitable for generating simulated cabin movement. The motion controller is responsible for controlling the actuators from the signals of the virtual reality (VR) environment. In VRMSs,

**CONTACT** Nguyen Truong Think  [thinknt@ueh.edu.vn](mailto:thinknt@ueh.edu.vn)  Institute of Intelligent and Interactive Technologies, University of Economics Ho Chi Minh City – UEH, Ho Chi Minh City, Vietnam.  
Communicated by Joerg Fehr.

© 2023 The Author(s). Published with license by Taylor & Francis Group, LLC

This is an Open Access article distributed under the terms of the Creative Commons Attribution-NonCommercial-NoDerivatives License (<http://creativecommons.org/licenses/by-nc-nd/4.0/>), which permits non-commercial re-use, distribution, and reproduction in any medium, provided the original work is properly cited, and is not altered, transformed, or built upon in any way. The terms on which this article has been published allow the posting of the Accepted Manuscript in a repository by the author(s) or with their consent.

users sit in the cabin to operate virtual machines for vehicle training applications or experience the environment of virtual reality games. In this way, the operators can feel they are controlling or being as if on real devices. Freeman et al. (1995) presented the Iowa driving simulator based on a large parallel robot, the robot was a Stewart Platform configuration with a simulated cabin mounted on a moving platform, the cabin is controlled to move in 6 degrees of freedom, including 2 rotations and 3 translations, according to the signals extracted from the virtual reality simulation model. Kane et al. 2004 built a flight simulator based on the point-mass cable robot with 3 degrees of freedom and controlled by 4 cables. The authors have mentioned the cable tension feedback but did not apply it to the controller design, which could lead to cable slack causing instability of the moving platform. An experimental model to test the calculation results, the initial experimental results show the feasibility of the solution for the requirements of simulating the position in the workspace (not including the orientation). Kljuno and Williams (2008) introduced a Vehicle Simulation System using a suspended CDPR configuration. This article studied a robot suspended by over-constraint 6 DOFs with 9 cables to control the movement of the moving platform with a fuzzy logic-based controller. The tension solution is determined based on the numerical iterative method. The analysis results are simulated on Matlab to evaluate the feasibility of the mathematical model of the system. The simulating results show that the cable tension has a large change during the control process with many cable tensions reduced to the minimum value, especially in the large trajectory. This is not suitable for VR applications because cable tension can exceed maximum or minimum values, causing unsafe and instability of the system. Miermeister et al. (2016) introduced a prototype of a large-scale motion simulation system based on Cable Driven Parallel Robots. A CDPR prototype is designed to simulate motion for humans with the dynamic properties of the system. The research results were tested on the helicopter pilot training simulation process, the summary results show that there are still some problems arising in the use of cables as actuators that need to be improved such as distributing cable tension and eliminating unwanted cable excitation noise.

The existing problems of the research and development of VR motion simulators based on traditional robots (serial robots and rigid-linked parallel robots) are high cost and limited working space. Models developed based on cable robots have a great deal of potential due to their simple structure, ease of installation, and low cost, especially for configurations requiring extremely large loads and workspace (Amare et al. 2018). The advantage of a CDPR is that the actuator has a small size, resulting in a small inertia of the actuator and mechanism, this is suitable for applications where flexible motion control is required while still responding to high loads and high speeds. The problem of determining dynamic load limits is useful for variable load CDPR application studies, especially for fully or over-constrained CDPRs, where additional cables can disperse the load, thereby increasing the load carrying capacity or reducing the tension limit (actuator power for given trajectories) (Korayem and Bamdad 2009). Controllers with algorithms for determining the dynamic load carrying capacity (DLCC) have been designed and applied to the under-constrained CDPR studied (Korayem, Tourajizadeh, and Bamdad 2010; Korayem et al. 2014), the results show the relationship between dynamic load carrying capacity, the torque of actuators and the controller. This result is the foundation for the optimization problems of path control according to the parameters of dynamic load and power of the actuator. To reduce computation time in real-time controllers, Zhang et al. (2022) have developed a controller called Dual-Loop Dynamic Control, in which, the tension control loop has a tension distribution algorithm that is calculated offline using the Moore–Penrose pseudoinverse matrix, the aim is to decrease the influence of the cable tension problem on the controller response. The results are tested on point-mass CDPR 3 DOFs – 4 cables, but not applied on over-constraint CDPR 6 DOFs. Santos, Gouttefarde, and Chemori (2022) built a Nonlinear Model Predictive Control to monitor the position of the CDPR, which has a built-in tension distribution solution. Experimental research results on CDPR 6 DOFs driven by 8 cables show that the tracking



accuracy has been significantly reduced compared to previous studies. Ueland, Sauder, and Skjetne (2021) introduced a method of tension distribution for over-constrained CDPRs with the goal of continuous cable strains. A new objective function is designed to ensure continuity for cable tensions and avoid discontinuous accelerations of the actuator, however, the number of iterations of the tension distribution algorithm needs attention because only suitable for offline computing requirements. Gouttefarde et al. (2015) have developed a cable tension calculation algorithm called the “Versatile Tension Distribution Algorithm”, which is applied to 6 DOF CDPRs driven by 8 cables. With this configuration, the possible set of cable tensioning solutions is a 2D convex polygon with 2 redundant cables. The algorithm is designed based on determining the vertices of the polygon clockwise or counterclockwise. Calculation results were verified on two 8-cable CDPR 6-DOF samples in CABLAR and CoGiRo projects. This method is effective with different requirements to determine the optimal tension distribution, as well as to establish the maximum number of repetitions in the worst case.

In general, for CDPRs designed for purposes that perform tasks requiring real-time control, it is necessary to have an appropriate cable tension distribution calculation model, both to ensure the calculation time and to satisfy the constraints on tension limits, continuity, and controller response. For heavy load applications, high cable tension can distort the control trajectory, affecting controller response due to the elasticity of the cable, cable distribution, and cable tension measuring device. Based on the previous studies, this paper introduces a VRMS driven by a CDPR. This VRMS consists of an over-constrained suspended CDPR with a motion simulation cabin placed in a moving platform for the user. The signal from the VR is extracted and converted into a CDPR control signal. Position control modifier with cable tension distribution algorithm that takes into account the influence of elasticity of cable winches and cables designed to control CDPR. Compared with the implemented configurations, the proposed structure of CDPR has the advantage of reducing the capacity of the actuator, thereby reducing the manufacturing cost, as well as the system size.

The contributions of this paper are determining the compensation for cable length due to the deformation of the cable transmission system, taking into account the elastic model of the transmission mechanism. Based on the calculation results, build the cable tension distribution suitable for the high-speed controller of a VR simulator and design a controller for CDPR in the virtual reality motion simulation system. Research results are tested on a CDPR concept, the main system parameters were collected and analyzed to evaluate the system’s performance, as well as identify any remaining issues that need to be resolved in the future.

## 2. Kinematic model of CDPR

The moving platform of the CDPR is controlled by the movements of the cables, which are distributed by the winches. The control signal is calculated through the inverse kinematics problem of CDPR, the inverse kinematics determines the lengths of the cables for a given moving platform pose and must be calculated to control the position of the moving platform according to a given trajectory. In this study, the poses of the simulator’s cabin are extracted directly from the virtual simulation data and sent to the inverse kinematics calculation program to combine the corresponding control signals for the actuator. The complexity of the kinematic model of the CDPR is to satisfy the tension and equilibrium constraints of the system. The CDPR is a parallel robot structure with the actuators being cables and the moving platform is connected to the actuators through cable suspension anchor points. The cables are distributed by winches placed on the fixed frame, through controlling the length of the cables, the moving platform is moved to the given poses. The structure of CDPR easily achieves a large workspace, high payload, and low cost; these characteristics make CDPRs particularly suitable for motion simulation applications such as training or entertainment purposes. The

inverse kinematics of the CDPR is finding the control variable for the motor ( $q_i$ ,  $i=1, 2, \dots, n$ ) with tension distribution to satisfy the equilibrium equation and kinematic constraints corresponding to the desired pose of the moving platform ( $\mathbf{p}$ ,  $\mathbf{R}$ ). In the kinematic of CDPR, the structural matrix is obtained from the wrench equilibrium equation of the moving platform as the following equation.

$$\mathbf{A}\boldsymbol{\tau}=\mathbf{J}^T\boldsymbol{\tau}=-\mathbf{w} \quad (1)$$

where  $\mathbf{J}$  is the Jacobian matrix and  $\mathbf{A}=\mathbf{J}^T$  is the structure matrix of CDPR.

The kinematic model of CDPR is illustrated in Fig. 1. Assuming that pulleys are considered as the fixed anchor points attached to the fixed frame denoted by  $A_i$ , while the moving anchor point attached to the moving platform is denoted by  $B_i$ ,  $\mathbf{b}_i$  denotes vector  $PB_i$  in frame  $F_p$ ,  $\mathbf{p}$  denotes vector  $OP$  in frame  $F_b$ ,  $G$  is the center of mass of the moving platform,  $F_p$  is the local frame attached to moving platform and  $F_b$  is the main reference frame of the system. Similar to typical parallel robots, the inverse kinematics of CDPR can be obtained by the vector method. The  $L_i$  denotes the vector of the  $i^{th}$  cable calculated as follows:

$$\mathbf{L}_i=\mathbf{u}_iL_i=\mathbf{p}+\mathbf{R}\mathbf{b}_i-\mathbf{a}_i \quad (2)$$

where  $\mathbf{u}_i$  and  $L_i$  denote the unit vector and the length of the  $i^{th}$  cable:

$$\mathbf{u}_i=\frac{\mathbf{L}_i}{\|\mathbf{L}_i\|} \quad (3)$$

The  $\mathbf{R}$  denotes the rotation matrix representing the orientation of  $F_p$  in frame  $F_b$ .

$$\mathbf{R}=\begin{bmatrix} c_\beta c_\gamma & s_\alpha s_\beta c_\gamma - c_\alpha s_\gamma & c_\alpha s_\beta c_\gamma + s_\alpha s_\gamma \\ c_\beta s_\gamma & s_\alpha s_\beta s_\gamma - c_\alpha c_\gamma & c_\alpha s_\beta s_\gamma - s_\alpha c_\gamma \\ -s_\beta & s_\alpha c_\beta & c_\alpha c_\beta \end{bmatrix} \quad (4)$$

In Equation (4),  $c$  and  $s$  stand for cosine ( $\cdot$ ) and sine ( $\cdot$ ) functions,  $\alpha$ ,  $\beta$  and  $\gamma$  are respectively rotation angles around the x, y, and z-axis. Derive Equation (2), note that  $\mathbf{b}_i=\mathbf{R}\times\mathbf{b}_i$  and  $\mathbf{a}_i'=\mathbf{0}$ , the result is obtained as following equation (Chellal et al. 2013):

$$\dot{\mathbf{L}}_i=\mathbf{u}_i^T\dot{\mathbf{p}}+(\mathbf{b}_i\times\mathbf{u}_i^T)\boldsymbol{\omega} \quad (5)$$

where  $\dot{\mathbf{p}}$  and  $\boldsymbol{\omega}$  denotes the linear and rotational velocity vector of the moving platform expressed in the  $F_b$  frame.

$$\boldsymbol{\omega}=\mathbf{E}\begin{bmatrix} \dot{\alpha} \\ \dot{\beta} \\ \dot{\gamma} \end{bmatrix}^T \quad (6)$$

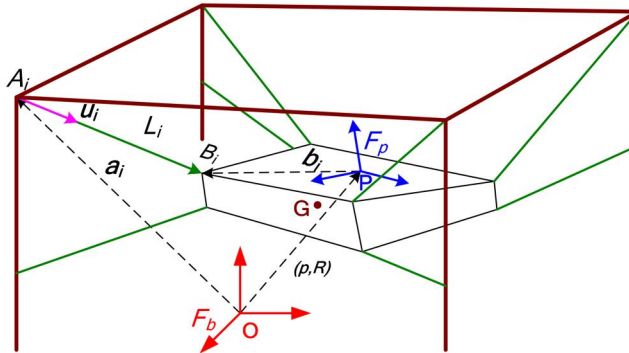


Figure 1. Kinematic model of CDPR.

$$E = \begin{bmatrix} c_\gamma c_\beta & -s_\gamma & 0 \\ s_\gamma c_\beta & c_\gamma & 0 \\ -s_\beta & 0 & 1 \end{bmatrix} \quad (7)$$

The velocity kinematic of CDPR can be obtained in the following form:

$$\dot{\mathbf{L}}_i = \mathbf{J} [\dot{\mathbf{p}} \ \boldsymbol{\omega}]^T \quad (8)$$

$$\mathbf{J} = \begin{bmatrix} \mathbf{u}_1 & \mathbf{R}(\mathbf{b}_1 \times \mathbf{u}_1) \\ \mathbf{u}_2 & \mathbf{R}(\mathbf{b}_2 \times \mathbf{u}_2) \\ \vdots & \vdots \\ \mathbf{u}_m & \mathbf{R}(\mathbf{b}_m \times \mathbf{u}_m) \end{bmatrix} \quad (9)$$

Eqs. (6) - (9) show the relationship between joint and moving platform velocity and  $\mathbf{J}$  is the Jacobian matrix of CDPR. These equations are used to calculate the dynamic model of CDPR and integrated into the motion and velocity controller of the CDPR.

### 3. Dynamic model of CDPR

Generally, the dynamic of CDPR is used for the design of the controller with the conditions of structure, velocity, acceleration, and payload. Dynamic models of rigid link robots cannot be applied to CDPR because of the constraints of the distribution of positive cable tension directly acting on the moving platform. The general dynamic model of the CDPR has the following form (Chellal et al. 2013; Gagliardini, Gouttefarde, and Caro 2018):

$$\mathbf{w}_e - \mathbf{H}\ddot{\mathbf{x}} - \mathbf{C}\dot{\mathbf{x}} + \mathbf{w}_g - \mathbf{J}^T \boldsymbol{\tau} = \mathbf{0} \quad (10)$$

where  $\mathbf{w}_e$  is the external wrench (force) acting on the moving platform;  $\mathbf{H}$  is the spatial inertia matrix of the moving platform and  $\mathbf{C}$  is the matrix of the centrifugal and Coriolis forces,  $\mathbf{w}_g$  is the gravity wrench,  $\boldsymbol{\tau}$  is the tension of driven cables.

$$\mathbf{H} = \begin{bmatrix} m_p \mathbf{I}_{3 \times 3} & -\mathbf{M}\hat{\mathbf{X}}_p \mathbf{M}\hat{\mathbf{X}}_p \end{bmatrix} \quad (11)$$

where  $m_p$  is the mass of the moving platform;  $\mathbf{I}_{3 \times 3}$  is the identity matrix;  $\mathbf{M}\hat{\mathbf{X}}_p$  is the skew-matrix associated with the first momentum  $\mathbf{M}\hat{\mathbf{X}}_p$  of the moving platform expressed in frame  $F_b$ ;  $\mathbf{X}_p = [x_g, y_g, z_g]^T$  is the coordinate of the center of mass  $G$  in the frame  $F_b$ .

$$\mathbf{M}\hat{\mathbf{X}}_p = \mathbf{R} [m_p x_g, m_p y_g, m_p z_g]^T \quad (12)$$

Based on Huygens Steiner's theorem, the inertia tensor matrix  $\mathbf{I}_p$  of the moving platform can be obtained as:

$$\frac{\mathbf{I}_p = \mathbf{R}\mathbf{I}_t\mathbf{R}^T - \mathbf{M}\hat{\mathbf{X}}_p \mathbf{M}\hat{\mathbf{X}}_p}{m_p} \quad (13)$$

$$\mathbf{I}_t = \begin{bmatrix} I_{xx} & I_{xy} & I_{xz} \\ I_{yx} & I_{yy} & I_{yz} \\ I_{zx} & I_{zy} & I_{zz} \end{bmatrix} \quad (14)$$

where  $\mathbf{I}_t$  is the moving platform inertia tensor. Coriolis and centrifugal forces acting on MP during movement are determined as follows:

$$C\dot{\mathbf{x}} = [\hat{\boldsymbol{\omega}} \hat{\boldsymbol{\omega}} M \mathbf{X}_p \hat{\boldsymbol{\omega}} I_t \boldsymbol{\omega}] \quad (15)$$

where  $\hat{\boldsymbol{\omega}}$  is the skew-matrix associated with the angular velocity  $\boldsymbol{\omega}$  of the moving platform expressed in frame  $F_b$ . Since the center of mass  $G$  and the origin  $P$  of frame  $F_p$  of the moving platform do not coincide, the gravity wrench is obtained as:

$$\mathbf{w}_g = \begin{bmatrix} m_p \mathbf{I}_{3 \times 3} \\ M \hat{\mathbf{X}}_p \end{bmatrix} \mathbf{g} \quad (16)$$

The dynamic model of the driven motor can be obtained (Picard et al. 2020):

$$\mathbf{I}_q \ddot{\boldsymbol{\phi}} + \mathbf{f}_v \dot{\boldsymbol{\phi}} + \mathbf{f}_s \text{sign}(\dot{\boldsymbol{\phi}}) - \frac{k}{r_w} \boldsymbol{\tau} = \boldsymbol{\tau}_{m0} \quad (17)$$

where  $\boldsymbol{\phi} = [\phi_1, \dots, \phi_b, \dots, \phi_m]^T$  is the matrix of the position of the motors,  $\mathbf{I}_q$  ( $m \times m$ ) is the inertia of the actuators and rotating parts of the winches,  $\mathbf{f}_v$  ( $m \times m$ ) denotes the viscous diagonal matrix,  $\mathbf{f}_s$  ( $m \times m$ ) denotes the dry friction coefficients diagonal matrix,  $k$  is the reduction ratio of the gearbox of the motor,  $r_w$  is the radius of the winch. The relationship between the motor angles and the position of cables is defined by the following equation:

$$\phi_i = \frac{\Delta L_i}{\kappa_i} r_{wi} = \frac{L_i - L_{oi}}{\kappa_i} r_{wi}; \quad \dot{\phi}_i = \frac{\dot{L}_i}{\kappa_i} r_{wi}; \quad \ddot{\phi}_i = \frac{\ddot{L}_i}{\kappa_i} r_{wi} \quad (18)$$

The CDPR dynamics problem is represented in Eqs (10)-(17). This result is used in the design of the controller for CDPR, where the cable tension will be calculated according to the given binding conditions.

## 4. Tension distribution solution

Cable tension distribution is an important problem in the design and control of CDPRs, especially for redundant CDPRs. The cable tension is calculated based on the kinematic model, the constraint conditions on the limit of the actuator, and the rigidity of the system. Tension constraints can also be used as a direct input to controllers, dynamics, and workspace definition (Tho and Think 2022). Cable tension not only keeps the balance of the system but also ensures the minimum tension and maximum tension of the driven cable, since the cables only exert pulling force, the cable tension must always be positive and not exceed the limit of the cable distribution motor.

### 4.1. Closed-form method

To expand the workspace, increase the speed and load capacity of the cable, and reduce the power of the cable distribution motors, a redundant suspended CDPR 6 DOFs driven by 8 cables is used to build the motion simulator in this paper. This configuration has two degrees of redundant, due to there being many tension distributions for each pose of the MP, the problem to solve is to determine the solution to satisfy the following dynamic constraints and optimize conditions:

$$\mathbf{A}\boldsymbol{\tau} = \mathbf{H}\ddot{\mathbf{x}} + \mathbf{C}\dot{\mathbf{x}} - \mathbf{w}_g \quad \mathbf{0} \leq \boldsymbol{\tau}_{\min} \leq \boldsymbol{\tau} \leq \boldsymbol{\tau}_{\max} \quad (19)$$

To determine a solution of cable tension satisfying the constraints of force equilibrium and dynamics in Equation (19), many methods were used to find the optimal tension distribution such as Linear Programming, Quadratic Programming, and Closed Form Method. For high-speed control requirements, the cable tensions are chosen to be preferred near the average value

of the limits of cable tensions, reason is to reduce the possible overload of the motor while ensuring the stiffness of the system. In this paper, the Closed-Form Method (Pott, Bruckmann, and Mikelsons 2009) is used to find the optimal cable tension distribution solution. The advantage of this method is the short computation time, which is suitable for real-time control for motion simulation applications. This method starts by dividing the cable tension into 2 components as follows:

$$\tau = \tau_M + \tau_A \quad (20)$$

where  $\tau_M$  is the average cable tension and  $\tau_A$  is any force vector of the  $i^{th}$  cable, Eq (19) is rewritten as:

$$\begin{aligned} A\tau_A &= H\ddot{x} + C\dot{x} - w_g - A\tau_M \\ \tau_M &= \frac{\tau_{\min} + \tau_{\max}}{2}, \quad 0 \leq \tau_{\min} \leq \tau \leq \tau_{\max} \end{aligned} \quad (21)$$

The least-square solution that satisfies Equation (19) is determined with the Euclidian norm ( $p=2$ ) by the Moore-Penrose inverse matrix.

$$A^+ = A^T(AA^T)^{-1} \quad (22)$$

Multiply both sides of Equation (21) by  $A^+$ , we get as.

$$\tau_A = A^+(H\ddot{x} + C\dot{x} - w_g - A\tau_M) \quad (23)$$

The tension distribution can be obtained by substituting Equation (23) into Equation (20).

$$\tau = \tau_M + A^+(H\ddot{x} + C\dot{x} - w_g - A\tau_M) \quad (24)$$

#### 4.2. Compensation for cable length due to the deformation of the cable transmission system

Figure 2 shows the schematic of the transmission cable transmission mechanism, the cable length is determined by the respective design parameters and the coordinates of the moving platform. The length of the cable is measured from the encoder, to determine the control cable length, a fixed posture in the CDP's workspace is taken as the standard with predefined cable lengths,

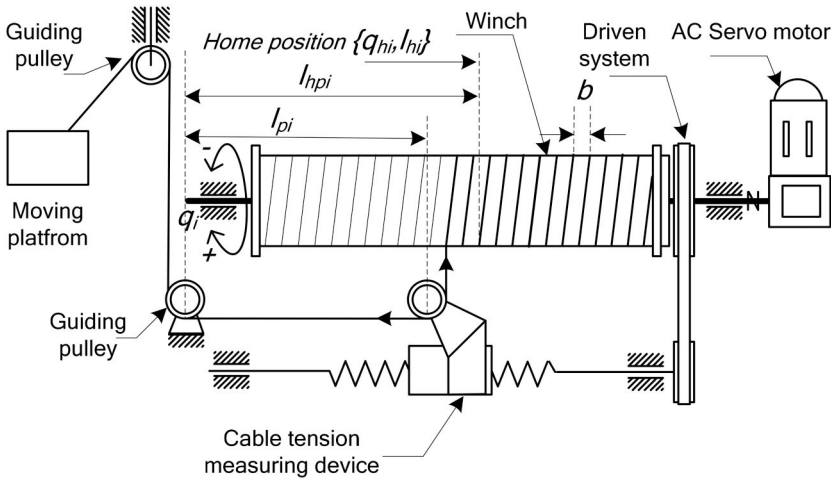


Figure 2. Schematic of cable winch of CDP.

which can be considered as the Home position with initial parameters  $\{q_{hi}, l_{hi}\}$ . From this position, the absolute length of the cables  $l_i \{i=1, \dots, n\}$  corresponding to the rotation angle of the motor  $q_i$  can be calculated by the following equation:

$$l_i = l_{hi} + (q_i - q_{hi})r + (q_i - q_{hi})\frac{b}{2\pi} \tag{25}$$

where  $b$  the width of each groove on the cable reel (mm);  $q_{hi}$  motor rotation angle at the home position;  $l_{hi}$  cable length at the home position.

In the problem of position kinematics of cable robots, the elasticity of transmission mechanisms and cables directly affects the control position of the moving platform, so it is necessary to build an elastic model based on the structure of the cable robot to increase the accuracy of the system. The elasticity of the cable transmission mechanism is concentrated on the transmission cable and the cable tension measuring device – Fig. 2. To simplify the calculation model, the elastic model of the cable and the tension measuring mechanism is represented in the form of a linear spring model in Fig. 3a. From the elastic model of the cable tension measuring device in Fig. 3b, we can obtain.

$$\Delta l_i = \Delta l_{c,i} + l_{pi} - l'_{pi} + l_{wi} - l'_{wi} \tag{26}$$

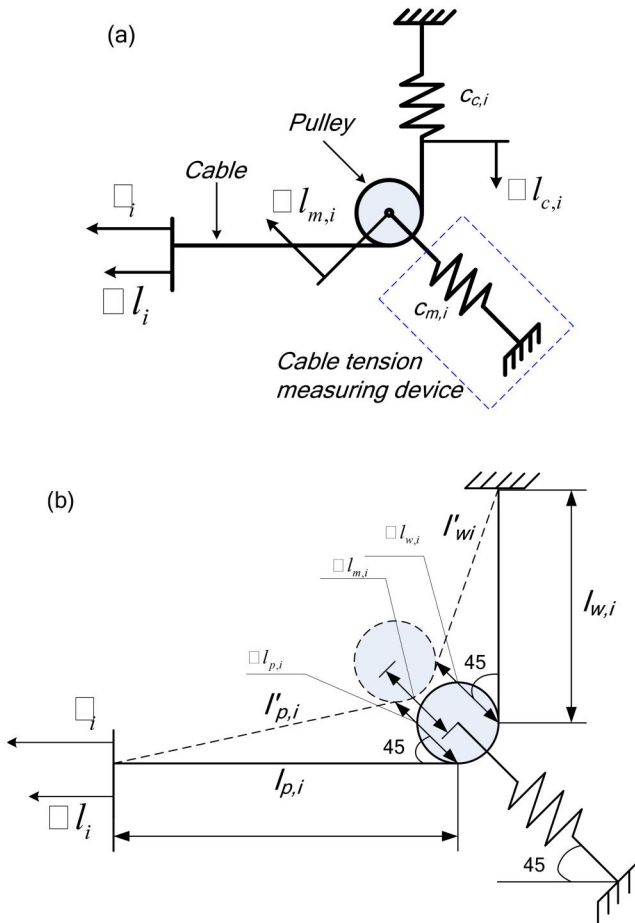


Figure 3. (a) Elastic model of cable transmission system (b) elastic model of cable tension measuring device.

$$\Delta l_{c,i} = l_i - l_{0i} = \frac{\tau_i}{c_{c,i}} \quad (27)$$

Equation (26) represents the compensating length of the cable due to the elasticity of the cable and the actuator, where  $l_{0i}$   $\{i = 1, \dots, n\}$  is the length of the cables taking to account the deformation of cable transmission mechanism,  $\Delta l_{c,i}$  is the elongation of the  $i^{th}$  cable calculated from the cable tension and the stiffness of cable  $i^{th}$  according to Equation (27).

$$c_{c,i} = \frac{EA}{l_{0i}} = \frac{EA}{l_i - \Delta l_i} = \frac{EA}{l_i}, \Delta l_i \ll l_i \quad (28)$$

Equation (28) is used to calculate the stiffness of the transmission cable, where  $E$  is Young's modulus and  $A$  is the cross-section of the cable. In this case, because of  $\Delta l_{c,i} \ll l_i$ ,  $\Delta l_{c,i}$  is ignored. From Fig. 3b, the components related to the strain of the tension measuring device  $l_{pi}$ ,  $l'_{pi}$ ,  $l_{wi}$ ,  $l'_{wi}$ , Equation (26) can be calculated, assuming that  $\Delta l_{m,i}$  is small.

$$l'_{pi} = (l_{pi}^2 + \Delta l_{m,i}^2 - 2l_{pi}\Delta l_{m,i} \cos \frac{\pi}{4})^{1/2} = (l_{pi}^2 + \Delta l_{m,i}^2 - \sqrt{2}l_{pi}\Delta l_{m,i})^{1/2} \quad (29)$$

$$l'_{wi} = (l_{wi}^2 + \Delta l_{m,i}^2 - 2l_{wi}\Delta l_{m,i} \cos \frac{\pi}{4})^{1/2} = (l_{wi}^2 + \Delta l_{m,i}^2 - \sqrt{2}l_{wi}\Delta l_{m,i})^{1/2} \quad (30)$$

$$\Delta l_{m,i} = \Delta l_{p,i} = \Delta l_{w,i} = \frac{\sqrt{2}\tau_i}{c_{m,i}} \quad (31)$$

$$l_{pi} = l_{hpi} + (q_i - q_{hi}) \frac{b}{2\pi} \quad (32)$$

where  $c_{m,i}$  is the stiffness of the cable tension mechanism that can be obtained experimentally. Thus, the elongation due to the elasticity of the cable and the cable tension measuring device can be calculated by substituting the Eqs. (27) – (32) into Equation (26).

#### 4.3. Compensation of cable length due to the pulley kinematic

In the transmission system for cable robots, the size of the guide pulley at the cable exit point affects the accuracy of the inverse kinematics problem. The anchor points at the moving platform are considered fixed, the exit point at the base frame is not fixed and depends on the size of the

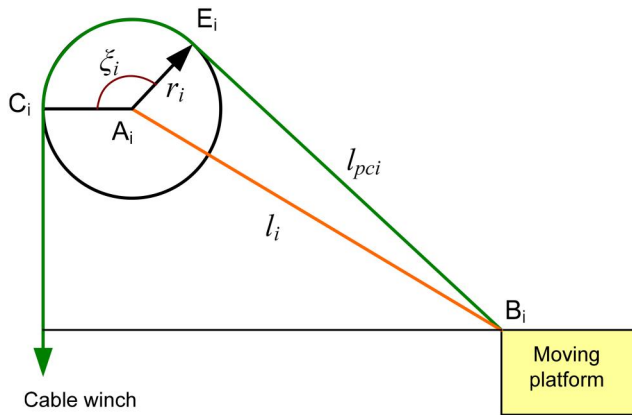


Figure 4. Pulley kinematic at the exit point.

pulley, the position of the MP, and the angle of cable contact on the pulley – Fig. 4. The calculation model of pulley kinematic for cable robots is referenced in (Kieu and Huang 2021).

$$l_{pci} = l_i + r_i \zeta_i \quad (33)$$

where  $l_{pci}$  length of cable  $i^{th}$  taking to account the pulley compensation,  $r_i$  pulley radius,  $\zeta_i$  wrap-ping angle of cable on pulley  $i^{th}$ .

## 5. Structure of simulation system

A general VR simulator is a system that helps humans immerse in a virtual reality environment for entertainment or training purposes. Figure 5 shows a structure of a VR simulator consisting of five components: software (SW), hardware (HW), interconnection network, users, and applications. In which, SW and HW are the 2 most important components, the software is always a vital aspect of any contemporary computer system. To model and simulate objects, any computer language or graphical software can be utilized. Shaping and simulation are the two primary functions of any software. After that, the software must be able to simulate the motion and behavior of the object. The hardware of a simulation system includes the computer, input devices, and output devices. The computer is responsible for recreating the real environment through the output devices, which are sensory displays and sensory feedback to bring players into the 3-D virtual environment. The sensory display is commonly used as virtual reality glasses and headsets that help players see 3D visuals and sounds, while sensory feedback (pressure feedback, vibrotactile feedback, force feedback ...) recreates tactile sensations when the user touches and holds or acts as a force on objects. Input devices help the user interact with the virtual environment, they can recognize where the user is pointing or looking, such as wire gloves, head-trackers, or other devices, thereby helping players move in the virtual environment and manipulate virtual objects.

### 5.1. Controller of VR simulator based on CDPR

The goal of a CDPR controller in a virtual reality motion simulation application is to control the moving platform to achieve the desired position and orientation in real time, which requires the controller to respond to acceleration and velocity components with nonlinear dynamic and kinetic models. It is also important that the position, velocity, and acceleration of the moving platform are designed in the Cartesian coordinate system, but the direct control variables are the cable length, in addition, the joint trajectory is designed with the complicated constraint condition such as the tension is always within a given limit, because the cables do not exert a push force, only a pull force on the moving platform. Thus, the nonlinear model of the transformation between the coordinates is designed to control the moving platform coordinates. The control

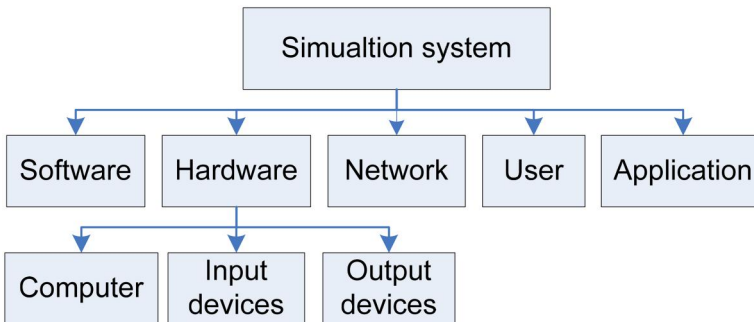


Figure 5. Simulation system block diagram.



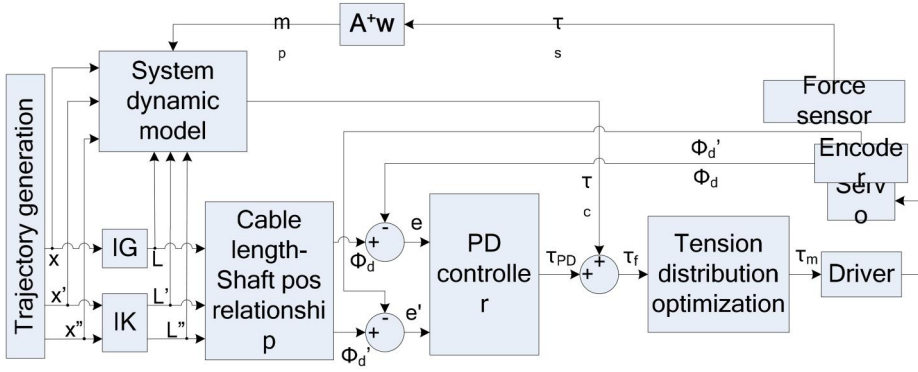


Figure 6. Controlling scheme of CDPR.

model for this system is built based on the kinematics and dynamic model that includes tension distribution, elastic model of cable transmission mechanisms, and PD controller. The objective of this section is to design a controller for CDPR that integrates cable tension control taking into account the cable elasticity and driven mechanism to improve speed, reduce errors and ensure safety for the actuator. The structure of the controller model is shown in Fig. 6. The dynamic block is used to calculate and transfer the tensile and friction force for the motor shafts from the desired control trajectory. IG and IK block denote the inverted geometry and inverse kinematics of velocity and acceleration.

In the simulator system, the characteristics of the payload depend on the player's physique, so it is necessary to estimate and update the payload characteristics for the new player to increase the robustness of the system (Picard et al. 2018). The payload estimator is designed with the following assumptions: the moving platform moves with low angular and linear velocity, and the moving platform is only affected by gravity, ignoring the effects of inertia and Coriolis. With  $\mathbf{x} = [p_x, p_y, p_z, \alpha, \beta, \gamma]^T$  denotes the poses of MP in Cartesian space including the position and orientation;  $\dot{\mathbf{x}}$  ( $6 \times 1$ ), and  $\ddot{\mathbf{x}}$  ( $6 \times 1$ ) denotes the velocity and acceleration vector of MP. The tension sensors are used to estimate payload  $\mathbf{w}$  due to gravity and  $\mathbf{m}_p$  is obtained from the following equation:

$$\mathbf{J}^T \begin{bmatrix} \tau_1 \\ \vdots \\ \tau_2 \\ \vdots \\ \tau_3 \end{bmatrix} = \begin{bmatrix} 0 \\ 0 \\ -m_p g \\ -m_p g y_g \\ m_p g x_g \\ 0 \end{bmatrix} \quad (34)$$

where  $\tau$  is the tension vector calculated by Equation (21), and vector  $\tau_c$  is the computed torque obtained by the dynamic block. The length of the cable and motor rotation angle relationship is expressed in Eqs (17)-(18). The PD motor controller is built as follows:

$$\tau_{PD} = K_d \dot{e} + K_p e \quad (35)$$

where  $K_d$  and  $K_p$  are the derivative and proportional gains of the PD controller, both factors can be calibrated so that the moving platform can reach the required precision;  $e$  and  $e'$  denote the position and velocity errors of the motor rotation angle.

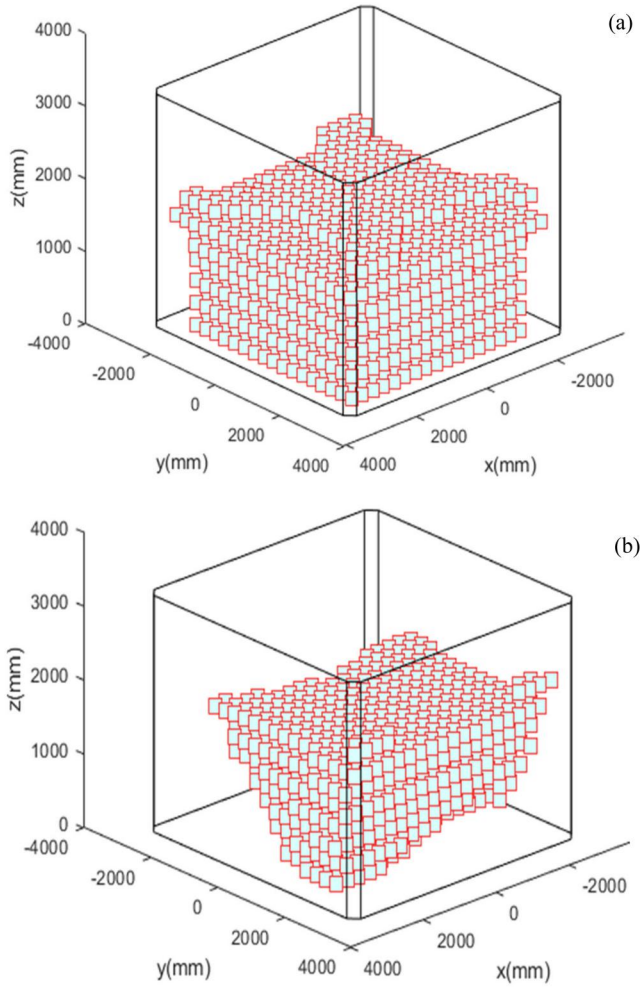


**Figure 7.** The static workspace of CDPR, (a) translation workspace; (b) rotation workspace.

## 5.2. Static workspace

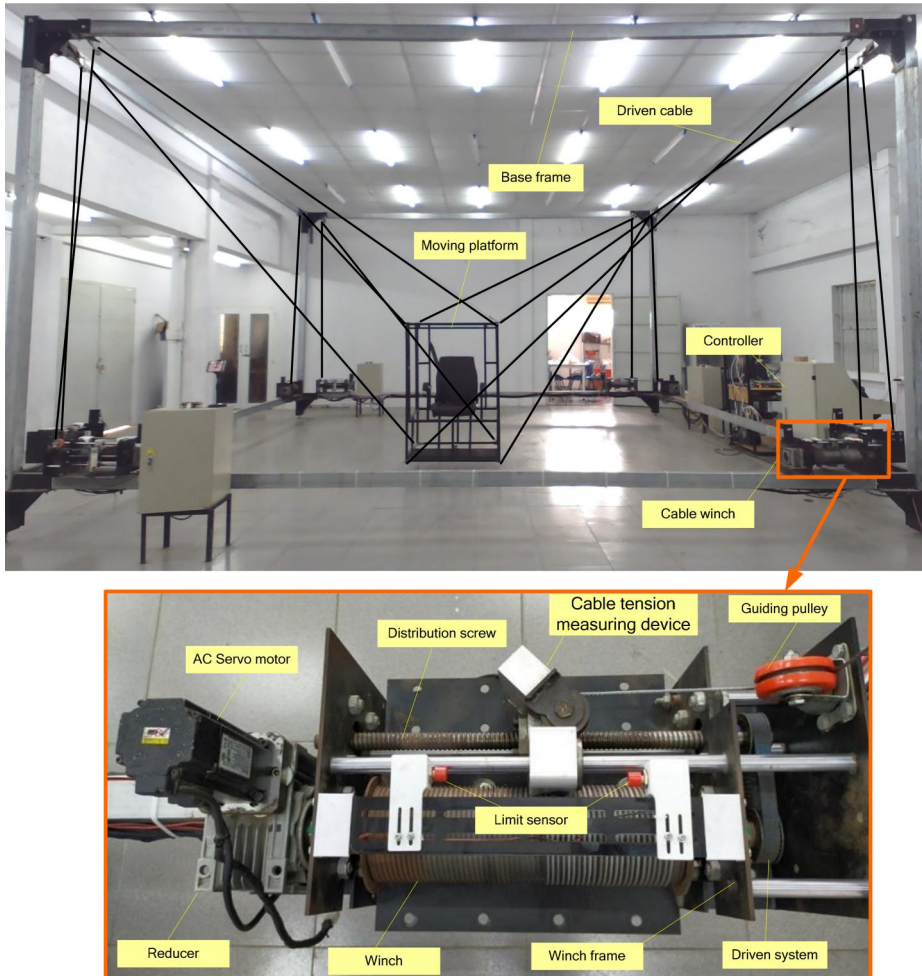
Static workspace or pseudo-static workspace of CPDR is determined by only considering static wrench. Consider Equation (11) and ignore the force of inertia and Coriolis, the problem of determining the workspace of CDPR becomes the problem of finding the existence of a cable tension solution satisfying the following system of equations:

$$\mathbf{w}_e + \mathbf{w}_g - \mathbf{J}^T \boldsymbol{\tau} = \mathbf{0} \quad \tau_{\min} \leq \tau \leq \tau_{\max} \quad (36)$$

Equation 36 can be analyzed in many ways to determine the existence of a valid tension distribution solution. Figure 7a shows the translational workspace with zero directional angles of the moving platform, Figure 7b is the workspace taking into account the directional rotation angles, with the limits given in Table 1 and the cables tensions for both cases limited to the range [50–800] N. These two results show that the workspace is significantly reduced when the rotation angles are changed within a given limit, increasing the limit of rotation angles will rapidly reduce the size of the workspace. This is very important for designing the trajectory for CDPR, ensuring the design trajectory is in the safe zone, and avoiding damage to the actuators due to excessive cable tension when the moving platform coordinates are outside the static workspace.

**Table 1.** Specification of CDPR.

Particulars	Specification
Dimension of fixed frame (LxWxH)	6180 × 6180 × 3200 mm
Dimension of moving platform (LxWxH)	985 × 935 × 1401 mm
Force feasible workspace	4000 × 4000 × 2000 mm
Rotation angle of MP	$x - y: \pm 40^\circ; z: \pm 10^\circ$
Tension	[40-800] N
Number of cables	8
Number of DOFs	6
Maximum velocity	760 m/s
Maximum acceleration	7 m/s <sup>2</sup>
Maximum load	100 kg

**Figure 8.** The CDPR prototype and cable winch for motion simulator.

## 6. Experiments and discussions

CDPR has a simple structure, with a large workspace and high acceleration due to the low inertia of the drive links. These advantages make it possible to create a VRMS with low cost, high flexibility, and easy configuration change. In particular, it is possible to expand the workspace without having to replace the actuator due to the large cable storage capacity. To give players a sense of

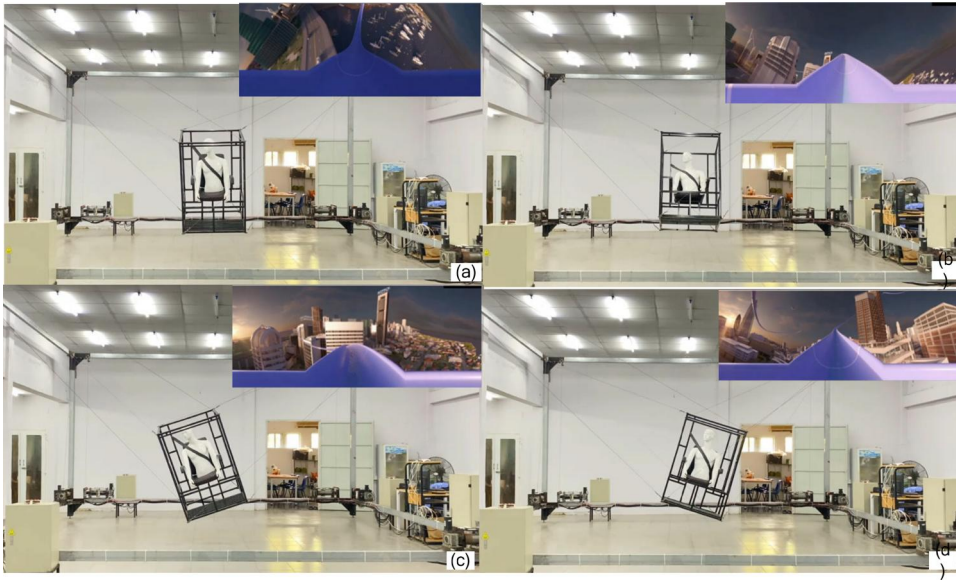


**Figure 9.** Experimental results of the VR motion simulation.

immersion in the virtual environment, the seats are placed in the moving platform finished in the same material as a car seat, and the two armrest positions are also covered with leather. In addition, the seat has a seat belt to improve the safety of the user. A virtual thrilling ride 3D game was used to test the system's ability for simulating movement, the signal of the game was extracted and changed to the poses for the moving platform, respectively. The software is designed to solve the kinematic and tension solutions, then analyzing results are transferred to the position controller to control the length of the cable.

**Figure 8** depicts the structure of the CDPR-based motion simulation system and the cable winch used to experiment. The system consists of a simulated cabin mounted in a cable-controlled moving platform. The moving platform with 6 degrees of freedom is connected to a fixed base *via* 8 cables. The Suspended Over Constrain CDPR configuration allows the cabin to perform movements in 3D space, including position and orientation according to given signals. The specifications of CDPR are shown in **Table 1**.

The experimental process is built based on signals from 3D video, players will wear virtual reality glasses and sit in a cabin equipped with seat belts, when the simulation video starts, the signals from the video are extracted in the form of the positions and orientation of the cabin, these signals are converted into the motion control signal of the CDPR, the control signals are recorded and compared with the response signal from the encoders of the drive motors for evaluating the response of the controller. Cable tension is also measured to assess the safety of the system. **Figure 9** is the experimental results of the VRMS, the position and direction response are consistent with the signal from the virtual motion video. **Figure 9a** is the response of the moving platform to the tilt angle of the sled going down low, the moving platform is controlled to tilt forward, **Fig. 9b** is the response of the moving platform to the tilt angle of the sled going up, the moving platform is controlled to tilt backward, **Fig. 9c** is the response of the moving platform to the low right slope of the sled, the controlled moving platform is tilted forward and left, **Fig. 9d** is the response of the moving platform to the tilt angle of the sled ascending to the left, the moving platform is controlled to tilt backward and to the right. The initial experimental results show that the response of the system is compatible with the signal from the virtual reality simulation.

The joint control trajectory designed for the VR trajectory of the moving platform is shown in **Fig. 10a**. **Figure 10b** shows the difference in joint trajectories when the effects of cable tension

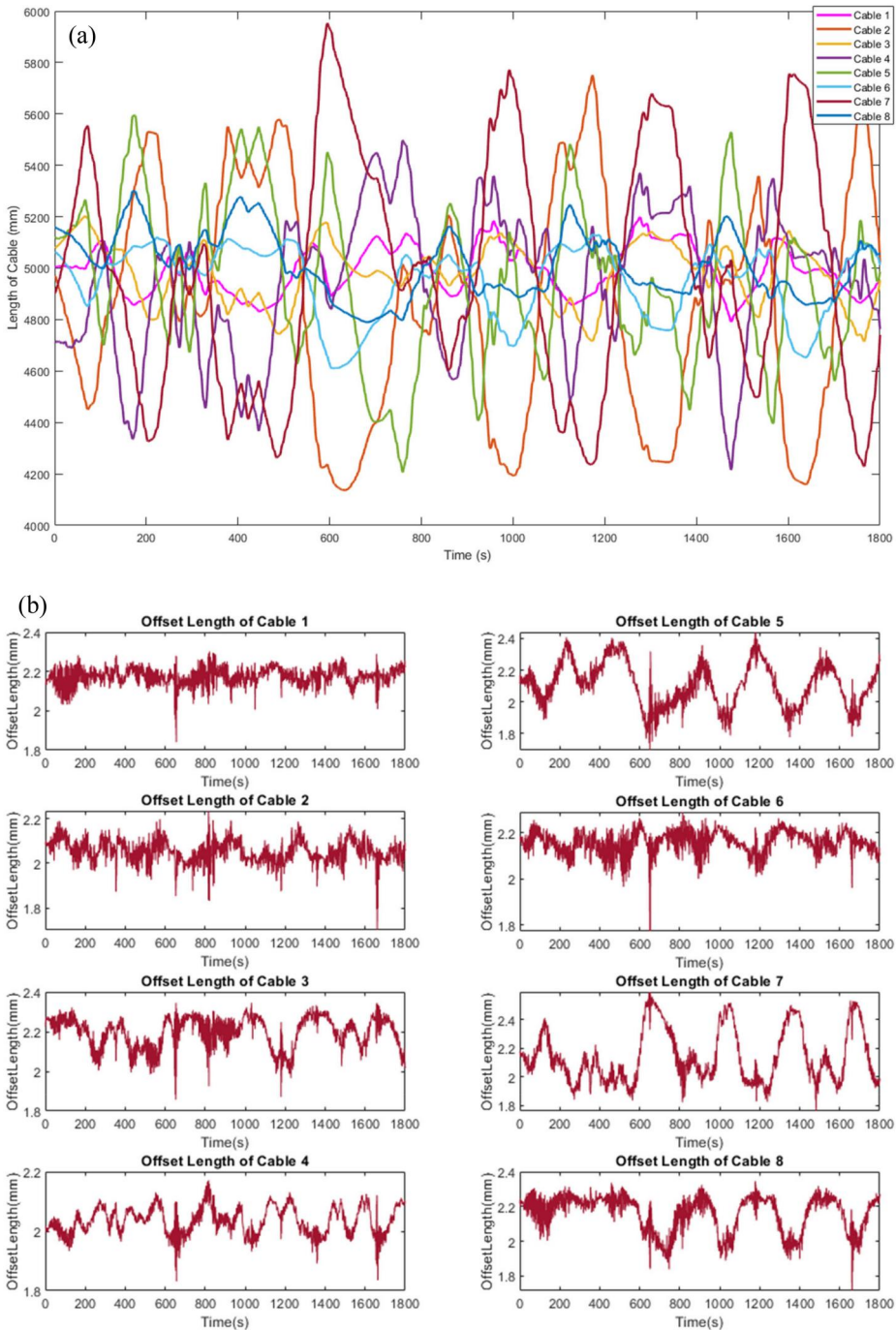


**Figure 10.** (a) Cable lengths in the experiments. (b) Offset lengths of cables in the experiments.

and the elasticity of the cable transmission mechanism were not included in the model when they should have been. To achieve this, a method of determining the joint trajectories based on the direct invert kinematic model will be used over the entire VR trajectories. The next step involves determining the length of each cable corresponding to the VR trajectory using a cable model that takes into account the effect of the feedback cable tension and the elasticity of the cable

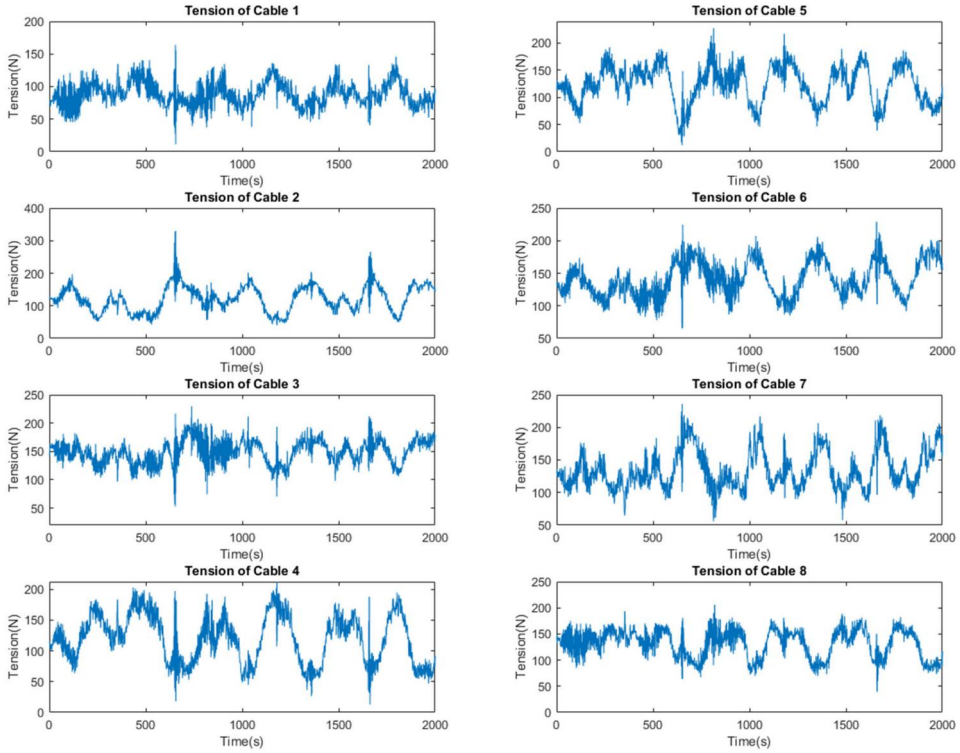


**Figure 11.** Cable tension in experiments.

transmission mechanism. It allows us to compare two joint trajectories obtained with the same moving platform trajectories. The results show that the compensated cable lengths due to the influence of cable tension and the deformation of the cable transmission mechanism have similar shapes to the feedback cable tensions as well as the length of the cables, which is consistent with the model that has been built. [Figure 11](#) is the cable tension measured during the moving platform performs a thrilling ride simulation, this experimental result shows that the integrated controller with cable tension algorithm gives non-negative cable tension control results and is always within the allowable limit. The cable tension fluctuation amplitude fluctuates in the range [50 400] N and has a continuous form according to the design trajectory. Some cable tensions approach the lower limit and have high fluctuations, this is due to tension controller hysteresis, the error of mechanical structure and measurement equipment, however, due to redundant configuration with  $DORs = 2$ , the stability of the moving platform is still guaranteed by the remaining cables. This result shows that the control model with the cable tension distribution algorithm satisfies the requirements, as well as demonstrates the effectiveness of the cable tension distribution algorithm in controlling the moving platform. The cable tension values have a continuous form according to the joint trajectory, ensuring the balance and stability of the cable system. With the total load of the moving platform and the player about 1000 N, the cable tension distribution solution and the controller came into play, evenly distributing the load with a maximum cable tension of only 400 N. This has important implications for the optimal design of transmission parameters, which can use small-size actuators to move large loads.

[Figure 12](#) depicts the real-time coordinates of the moving platform extracted from the virtual reality thrilling ride simulation video. Based on the motion properties of the object to be simulated, the coordinates in the  $z$  direction and the two rotation angles  $\alpha(Roll)$  and  $\beta(Pitch)$  around the  $x$  and  $y$  axes change, and the remaining coordinates are fixed. During operation, the rotations

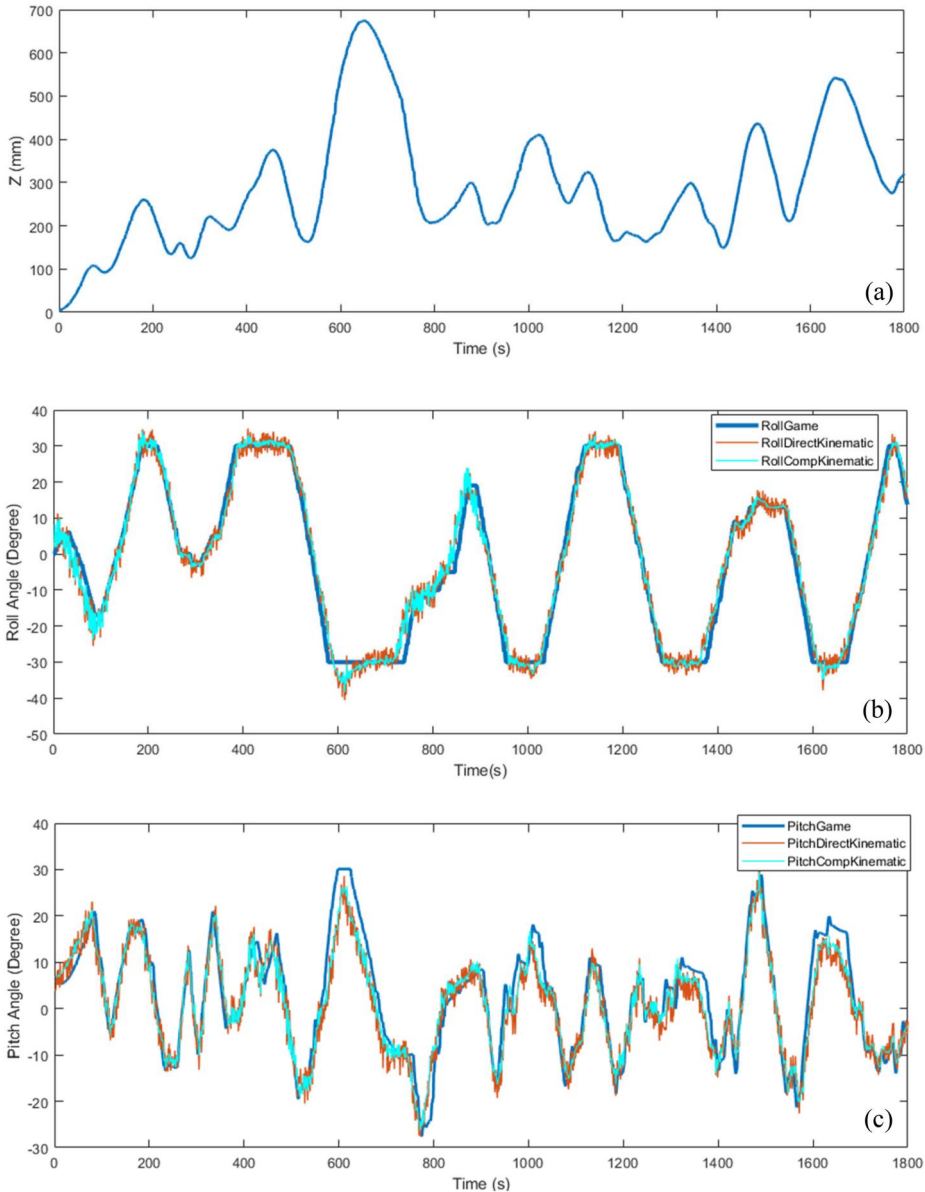


**Figure 12.** (a) Z axis coordinates from Game; (b) Roll angles from Game and Experiment; (c) Pitch angles from Game and experiment.

around the  $x$  and  $y$  axes are limited to  $[-40^\circ, 40^\circ]$ , and the rotation around the  $z$ -axis is limited to  $[-10^\circ, 10^\circ]$ , the  $z$  coordinate is controlled within  $[200, 1800]$  (mm) (Fig. 12a) to ensure that the positions of the moving platform are not outside the pre-calculated workspace. The 6-axis Motion Tracking device includes a 3-axis gyroscope, and a 3-axis accelerometer used to measure the rotation angles of the simulation cabin. Figures 12b and 12c show that, the angular response of the elastic-compensated kinematic model has a better response than the direct kinematics model, and the rotation angles amplitude compared to the desired signal is also significantly improved. This shows that the cable tension feedback control model that takes into account the deformation of the cable transmission mechanism has an impact on the system stability, the amplitude and frequency of the feedback rotations show the vibration is significantly reduced.

## 7. Conclusions

The paper described a complete VR motion simulator system based on a type of cable-driven parallel robot (CDPR). The key components of this system were modeled, calculated, fabricated, and tested on 6 DOFs suspended CDPR driven by 8 cables. To design a controller for a virtual reality simulation system, the kinematics, dynamics, workspace, cable tension distribution algorithm, and deformation of cable transmission mechanism are integrated into the CDPR controller. The cable tension distribution algorithm is applied to calculate the tension for the controller to ensure the stability of the simulated cabin as well as the safety of the cable transmission mechanism. Moreover, the noise caused by the cable tension acting on the elastic mechanisms of the cable transmission system has also been calculated. The PD torque controller is designed to control the movement of the cabin based on the kinematics, tension distribution, and workspace models. A real-time model for estimating the mass change of the moving platform is also built through the cable tension measurements, which allows the controller to be continuously updated with the load value. The controller can control the robot according to the signals collected from the virtual reality motion simulation video, experiment results show that the controller works with high stability, and the speed and position of the simulated cabin are precisely controlled according to the signal received from VR Game. The tension values obtained from the tension measuring devices are all within the limits and have a continuous form according to the control trajectory, the compensated value of joint variables (cable lengths) due to the deformation of the cable transmission mechanism is suitable with the calculated model, these ensure the rigidity and stability of the VR system. Based on these results, the main objectives in the future will be to design and improve control algorithms for high-dynamic simulation scenarios taking into account the sagging of cable. Combining virtual reality with a CDPR system to create a simulated environment makes users immerse themselves in the experience of simulating the internal environment. Instead of viewing a screen in front of them, the immersed user can interact with the 3D world through the assistive device. When any simulation motion is simulated, it brings many practical experiences for users. It has the potential to be developed into a support system for practicing flying military aircraft.

## Acknowledgments

This research is funded by University of Economics Ho Chi Minh City – UEH, Vietnam.

## Disclosure statement

The authors have no conflicts of interest to declare that are relevant to the content of this article

## References

- Amare, Z., B. Zi, S. Qian, J. Du, and Q. J. Ge. 2018. Three-dimensional static and dynamic stiffness analyses of the cable driven parallel robot with non-negligible cable mass and elasticity. *Mechanics Based Design of Structures and Machines* 46 (4):455–82. doi: [10.1080/15397734.2017.1358094](https://doi.org/10.1080/15397734.2017.1358094).
- Cao, R., F. Gao, Y. Zhang, D. Pan, and W. Chen. 2015. A new parameter design method of a 6-DOF parallel motion simulator for a given workspace. *Mechanics Based Design of Structures and Machines* 43 (1):1–18. doi: [10.1080/15397734.2014.904234](https://doi.org/10.1080/15397734.2014.904234).
- Chellal, R., E. Laroche, L. Cu villon, and J. Gangloff. 2013. An identification methodology for 6-dof cable-driven parallel robots parameters application to the inca 6d robot. cable-driven parallel robots, 301–17.
- Freeman, J. S., G. Watson, Y. E. Papelis, T. C. Lin, A. Tayyab, R. A. Romano, and J. G. Kuhl. 1995. The Iowa driving simulator: An implementation and application overview (No. 950174). SAE Technical Paper.
- Gagliardini, L., M. Gouttefarde, and S. Caro. 2018. Determination of a dynamic feasible workspace for cable-driven parallel robots. *Advances in Robot Kinematics* 2016, 361–70.



- Gouttefarde, M., J. Lamaury, C. Reichert, and T. Bruckmann. 2015. A versatile tension distribution algorithm for  $n$ -DOF parallel robots driven by  $n + 2$  cables. *IEEE Transactions on Robotics* 31 (6):1444–57. doi: [10.1109/TRO.2015.2495005](https://doi.org/10.1109/TRO.2015.2495005).
- Kieu, V. N., and S. C. Huang. 2021. Dynamic and wrench-feasible workspace analysis of a cable-driven parallel robot considering a nonlinear cable tension model. *Applied Sciences* 12 (1):244. doi: [10.3390/app12010244](https://doi.org/10.3390/app12010244).
- Kljuno, E., and R. L. Williams. 2008. Vehicle simulation system: Controls and virtual-reality-based dynamics simulation. *Journal of Intelligent and Robotic Systems* 52 (1):79–99. doi: [10.1007/s10846-008-9204-y](https://doi.org/10.1007/s10846-008-9204-y).
- Korayem, M. H., and M. Bamdad. 2009. Dynamic load-carrying capacity of cable-suspended parallel manipulators. *The International Journal of Advanced Manufacturing Technology* 44 (7-8):829–40. doi: [10.1007/s00170-008-1890-x](https://doi.org/10.1007/s00170-008-1890-x).
- Korayem, M. H., H. Tourajizadeh, and M. Bamdad. 2010. Dynamic load carrying capacity of flexible cable suspended robot: Robust feedback linearization control approach. *Journal of Intelligent & Robotic Systems* 60 (3-4): 341–63. doi: [10.1007/s10846-010-9423-x](https://doi.org/10.1007/s10846-010-9423-x).
- Korayem, M. H., A. Zehfroosh, H. Tourajizadeh, and S. Manteghi. 2014. Optimal motion planning of non-linear dynamic systems in the presence of obstacles and moving boundaries using SDRE: Application on cable-suspended robot. *Nonlinear Dynamics* 76 (2):1423–41. doi: [10.1007/s11071-013-1219-7](https://doi.org/10.1007/s11071-013-1219-7).
- Miermeister, P., M. Lächele, R. Boss, C. Masone, C. Schenk, J. Tesch, M. Kerger, H. Teufel, A. Pott, and H. H. Bühlhoff. 2016. October. The cablerobot simulator large scale motion platform based on cable robot technology. In 2016 IEEE/RSJ International Conference on Intelligent Robots and Systems (IROS) (pp. 3024–3029). IEEE. doi: [10.1109/IROS.2016.7759468](https://doi.org/10.1109/IROS.2016.7759468).
- Picard, E., S. Caro, F. Plestan, and F. Claveau. 2018. August. Control solution for a cable-driven parallel robot with highly variable payload. In International Design Engineering Technical Conferences and Computers and Information in Engineering Conference (Vol. 51814, p. V05BT07A013). American Society of Mechanical Engineers. doi: [10.1115/DETC2018-85304](https://doi.org/10.1115/DETC2018-85304).
- Picard, E., E. Tahoumi, F. Plestan, S. Caro, and F. Claveau. 2020. A new control scheme of cable-driven parallel robot balancing between sliding mode and linear feedback. *IFAC-PapersOnLine* 53 (2):9936–43. doi: [10.1016/j.ifacol.2020.12.2708](https://doi.org/10.1016/j.ifacol.2020.12.2708).
- Pott, A., T. Bruckmann, and L. Mikelsons. 2009. Closed-form force distribution for parallel wire robots. In *Computational Kinematics: Proceedings of the 5th International Workshop on Computational Kinematics* (25–34). Springer Berlin Heidelberg.
- Santos, J. C., M. Gouttefarde, and A. Chemori. 2022. A nonlinear model predictive control for the position tracking of cable-driven parallel robots. *IEEE Transactions on Robotics* 38 (4):2597–616. doi: [10.1109/TRO.2022.3152705](https://doi.org/10.1109/TRO.2022.3152705).
- Teufel, H., H. G. Nusseck, K. Beykirch, J. Butler, M. Kerger, and H. Bühlhoff. 2007. August. MPI motion simulator: Development and analysis of a novel motion simulator. In AIAA Modeling and Simulation Technologies Conference and Exhibit (p 6476). doi: [10.2514/6.2007-6476](https://doi.org/10.2514/6.2007-6476).
- Tho, T. P., and N. T. Thinh. 2022. An Overview of Cable-Driven Parallel Robots: Workspace, Tension Distribution, and Cable Sagging. *Mathematical Problems in Engineering* 2022:1–15. doi: [10.1155/2022/2199748](https://doi.org/10.1155/2022/2199748).
- Ueland, E., T. Sauder, and R. Skjetne. 2021. Optimal force allocation for overconstrained cable-driven parallel robots: Continuously differentiable solutions with assessment of computational efficiency. *IEEE Transactions on Robotics* 37 (2):659–66. doi: [10.1109/TRO.2020.3020747](https://doi.org/10.1109/TRO.2020.3020747).
- Usher, K., G. Winstanley, P. Corke, D. Stauffacher, and R. Carnie. 2004. December. A cable-array robot for air vehicle simulation. In *Proceedings of the 2004 Australasian Conference on Robotics & Automation, December* (6–8).
- Zhang, B., W. Shang, S. Cong, and Z. Li. 2022. Dual-Loop Dynamic Control of Cable-Driven Parallel Robots Without Online Tension Distribution. *IEEE Transactions on Systems, Man, and Cybernetics: Systems* 52 (10): 6555–68. doi: [10.1109/TSMC.2022.3146919](https://doi.org/10.1109/TSMC.2022.3146919).

## Bài báo số 4 – SCOPUS - IF 1.012

Tho, Tuong Phuoc, and Nguyen Truong Thinh. "Sagging Cable Analysis and Evaluation of 4-degree-of-freedom Cable Robot Using Adaptive Neural Fuzzy Algorithm." International Journal of Mechanical Engineering and Robotics Research (2022) - IJMERR 2022 Vol.11(2): 73-78

Link:

<http://www.ijmerr.com/index.php?m=content&c=index&a=show&catid=212&id=1762>



# Sagging Cable Analysis and Evaluation of 4-degree-of- freedom Cable Robot Using Adaptive Neural Fuzzy Algorithm

Tuong Phuoc Tho and Nguyen Truong Think

Department of Mechatronics, Ho Chi Minh City University of Technology and Education, Thu Duc City, Ho Chi Minh City, Viet Nam

Email: thotp@hcmute.edu.vn, thinknt@hcmute.edu.vn

**Abstract**—One of the most important problems in robot modeling and control of cable robots is the problem of inverse kinematics, that is, using the coordinate data of the end effector to calculate the corresponding joint variables. Especially with regard to the kinematics of the cable robot, the sagging of the driven cable can have a significant effect on the calculation of the cable length, and this is more evident when the cable length is large, for example in construction or agriculture applications, where needs a large workspace. The determination of cable deflection considers modeling the cable as a chain model rather than calculating the cable length as a straight-line model. Furthermore, due to the structure and constraints of cable robots or Cable Driven Parallel robots (CDPRs), the system modeling and simulation becomes complicated, thereby increasing the computation time. In this paper, we propose an algorithm of Adaptive Neural Fuzzy Inference System (ANFIS) that is used to solve the cable sag problem for the 4-cable robots. This model was applied to estimate the cable sag for medium-sized cable robots with low travel speed and does not take into account the impact of cable elasticity. A simulation model was conducted and the results showed the advantages of this method in increasing the probability of convergence with small errors. The results of computation and experiment are analyzed to evaluate the effectiveness of the proposed model

**Index Terms**—Cable robots, forward kinematics, inverse kinematics, cable sagging, ANFIS

## I. INTRODUCTION

In recent times, there are many large-sized cable robots was built and applied due to their advantages [1-3]. Cable Robots or Cable driven parallel robots (CDPRs) are a special type of robots with parallel structure, they are formed by replacing all of the hard links supported by cables, compared to traditional robots, these robots are well-suited to a variety of potential applications [4-5].

One of the complicated issues when designing and calculating the precise control of cable robots is the influence of cable sag, especially for large sized robots. P. Merlet [6] develops a mathematical model to analyze the singularity of the forward and reverse kinematics problem

of cable robots taking into account cable sag of cable, based on Irvine's elastic catenary. The results show that both kinematic problems have singularities and these points are usually located at the boundary of the active space. The "elastic catenary" was developed by Irvine [7] used to simulate the cable lengths and then handle the inverse pose kinematics problem in this study. They also offered experimental validation, demonstrating that the elastic catenary equations and experimental results are in good accord. The difference between theoretical and experimental cable tension is also provided by Russell and Lardner [8] based on an experimental model of elastic catenary models. Dheerendra Sridhar and Robert L. Williams II [9] propose a method to investigate the differences in cable length errors and computation, comparing the straight - line cables assumption vs. a cable - sag model, the study and analysis of the effects of cable sag on the calculation of cable length in CDPRs has been conducted the primary goal of the research. The study also looked into the consequences of cable density, cable diameter, robot footprint size, and computational requirements. Yu Su, Yuanying Qiu, and Peng Liu [10] employ the proposed dynamic model and the sag-to-span ratio as constraint requirements to find the best model for distributing cable tensions of CDPR used for moving camera and driven by 4 cables. An optimization method is developed based on the ideal model to find the optimal solution satisfying the constrained conditions in an infinite number of possible solutions. M. Gouttefarde, J. Collard, N. Riehl and C. Baradat [11] presents a method to determine cable deflection based on parabolic and linearized Irvin models. From there, the cable length with sag was calculated by the linear relationship between the components to decrease the computation time. The model is only valid for cable robots with the same number of cables as degrees of freedom.

The cable can only work unilaterally under tension and without compression, which is a key feature of cable controllers. The CDPRs have many different classification methods. Robot cable can be classified according to the following requirements:  $m$  is the number of cables, while  $n$  is the number of degrees of freedom. Ming and Higuchi [12] proposed this kinematic categorization to distinguish between cable robots. In this

paper, we modeled a CDRP has 3 DOF and driven by 4 cables that are fully constrained with  $m=4, n=3$  and present the structure and inverse kinematic problem (IKP) of this robot. The sagging of cables base on tension force distribution was compute by algorithm method to create train data for configuring the ANFIS model, the ANFIS model is used to predict cable sag in its workspace that is only deflected by its own weight.

II. INVERSE KINEMATIC OF THE 4 CABLE ROBOTS TAKING INTO ACCOUNT SAGGING OF CABLES

Fig. 1 illustrates the kinematic structure of the four cables CDRP, where  $P$  and  $A_i, i = 1, 2, 3, 4$ , are connecting points of the  $i^{th}$  cable attached to the moving point and four columns of the robot frame, respectively. Variable vectors  $l_1, l_2, l_3, l_4$  denote the straight length of cables. Unlike the inverse kinematics problem (IPK) of rigid-linked robots, the IPK of cable robots consists of finding the theoretical cable lengths corresponding to a given moving point  $P$  simultaneous with solving the force distribution problem to find the cable tensions corresponding to static equilibrium, then calculate the length of the cable with sag with the cable tension and the length of cables respectively [8-11], straight -line cable length can be presented in vector form

$$\vec{l}_i = \vec{OP} - \vec{OA}_i \tag{1}$$

where  $i = 1, 2, 3, 4$

The static equilibrium equation of this system can be present in  $Oxyz$  as

$$\vec{F} + \sum_{i=1}^4 \vec{\tau}_i = 0 \tag{2}$$

where  $F$  is the sum of external force acting on moving point,  $\tau_i > 0$  are tension of cables.

In this case, the cable robot has 3 DOFs driven by 4 cables so redundant of system is 1, equation (2) becomes

$$\mathbf{F} + \mathbf{A}\boldsymbol{\tau} = \mathbf{0} \tag{3}$$

where  $A$  is structure matrix of robot,  $\boldsymbol{\tau} = [\tau_1 \ \tau_2 \ \tau_3 \ \tau_4]^T$  is tension matrix. The structure matrix is given by

$$\mathbf{A} = [\mathbf{u}_1 \ \mathbf{u}_2 \ \mathbf{u}_3 \ \mathbf{u}_4] \tag{4}$$

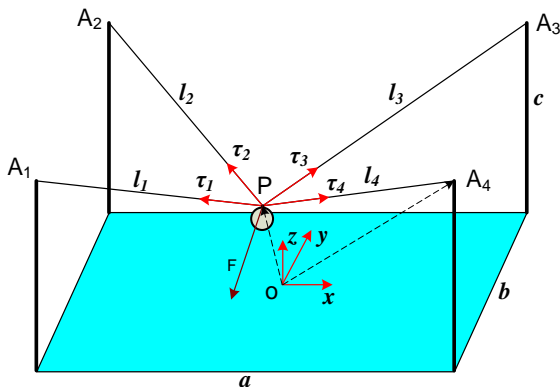


Figure 1. Cable robots with 4 sagging cables

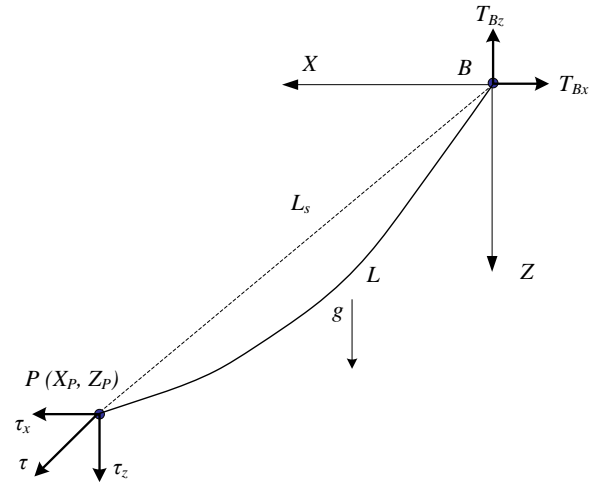


Figure 2. The cable model with sagging

where  $\mathbf{u}_{i=1} = \left[ \frac{l_{ix}}{\|l_i\|} \ \frac{l_{iy}}{\|l_i\|} \ \frac{l_{iz}}{\|l_i\|} \right]^T$  is unit vector of cable  $i$ .

To calculate the corresponding sag cable length, Irvine's famous chain cable formula is applied [7-11], with the cable model between two points given in Fig.2, where  $A$  and  $P$  is connecting point of cables on base frame and end-effector of robot,  $L_s$  is the distance between  $A$  and  $P$  or the length of straight cable,  $L$  is the cable length from  $A$  to  $P$  taking into account the cable sagging,  $\tau_x$  and  $\tau_z$  are the components of tension  $\tau$  on  $X$  and  $Z$  axis act on  $P$ , and  $(x_p, z_p)$  are the coordinates of the moving point,  $g$  is the gravity acceleration. The relationship between cable length with sagging, straight cable length and cable tension are simplified by the equation represented as follows.

$$x_p = \frac{|\tau_x|}{\rho_L g} \left[ \sinh^{-1} \left( \frac{\tau_z}{\tau_x} \right) - \sinh^{-1} \left( \frac{\tau_z - \rho_L g L}{\tau_x} \right) \right] \tag{5}$$

$$z_p = \frac{1}{\rho_L g} \left[ \sqrt{\tau_x^2 + \tau_z^2} - \sqrt{\tau_x^2 + (\tau_z - \rho_L g L)^2} \right] \tag{6}$$

Thus, to find the cable length taking into account the cable sagging, equations (1-6) must be solved simultaneously, this is a nonlinear system, which can be solved by numerical method. However, the long computation time is a problem that needs to be considered for cable robot control applications. Some studies have linearized the relationship of the components in this system to reduce computation time [11][13], however the results only apply to specific configurations.

In the next section, we use numerical methods to calculate the sag cable length in the entire workspace of robot, then combine the data to establish the ANFIS models used to predict the sag cable lengths for the configuration of cable robot above, then evaluate the accuracy of the results from the built model with numerical methods.

### III. ANFIS MODEL FOR PREDICTING SAGGING OF CABLE

ANFIS - Adaptive neuro-fuzzy inference system - is a combination algorithm between Fuzzy Inference system and artificial neural network, this combination takes advantage of two models: fuzzy logic allows easy system design, in then the neural network allows to learn what we ask of the controller [14-15]. It modifies functions dependent on shape, position and combination completely automatically. This reduces the time as well as the cost of system development. The ANFIS function creates a fuzzy inference system (FIS) utilizing the provided input/output data set, and its membership function parameters are changed using neural network training procedures such backpropagation or combine propagation with the least squares approach. As a result, our fuzzy system can "learn" from the data set. With the nonlinear relationship between input – moving point coordinates - and output - cable deflection shown in equations 1-6, the input-output nonlinear relationship in the fuzzy model needs to be built depends heavily on the fuzzy partitions of the input-output space. Therefore, determining the membership function in fuzzy models becomes very important. In fuzzy neural networks, this tuning can be considered as an optimization problem using learning algorithms to solve. By assuming the membership functions have a certain shape, then proceed to change the parameters of that shape through the process of learning by neural network. Thus, we need a data set in the form of desired input-output pairs for the neural network to learn and also need a table of initial rules based on those dependent functions.

In this study, a ANFIS model was developed for predicting cables sag of CDPR with 3DOF driven by 4 cables, the static workspace of robot was show in Fig.3. All training data for were collected on workspace of robot, i.e points that satisfy the equilibrium equation [8-11]. The Dual simplex Algorithm was used to calculate the cable tension for these locations under the condition that the sum of the cable strains is minimal, then the Trust-Region-Dogleg algorithm was used to determine the lengths of cables with the corresponding cable sagging [16].

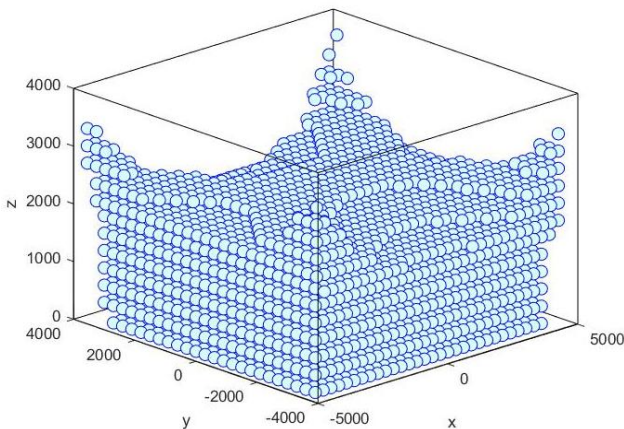


Figure 3. The workspace of 4 cables CDPR

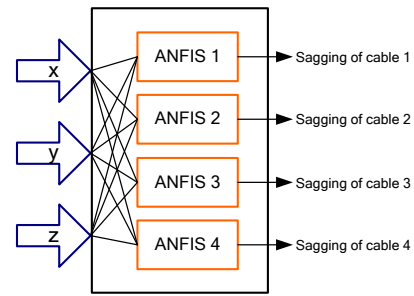


Figure 4. Proposed ANFIS architecture for cable sagging prediction

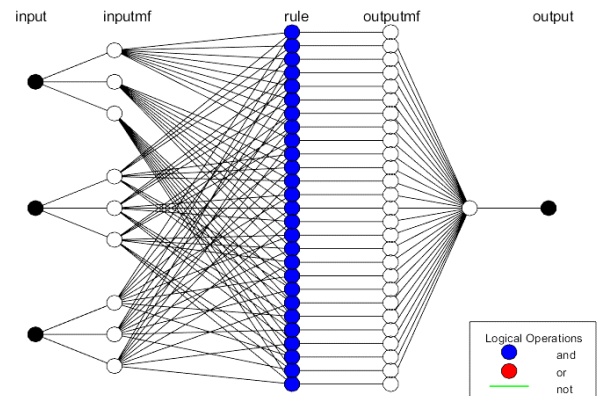


Figure 5. ANFIS structure for a cable

CDPR parameters are given in Table I and data of the IKP taking into account cable sagging are used for training ANFIS model, and also used to evaluate the accuracy of the model over the entire operating space. In the model with 3 inputs being the coordinates of the moving point and 4 outputs being the sagging of the 4 cables respectively, to predict the cable sags reported in this paper, a parallel ANFIS system is created. Fig.4 depicts a system made up of four parallel ANFIS models, each of which receives the moving point's location as input. A first-order Sugeno model with 27 rules and three generalized Gaussian membership functions is used to generate the ANFIS. The number of membership functions for each ANFIS was calculated through experimentation. The multi-layer feedforward adaptive network ANFIS structure phase  $i(i=1, \dots, 4)$  is depicted in Fig.5. The CDPRs' position coordinates are described in the first layer, which has three inputs. The rule layer is the second layer, which calculates the firing strengths of each rule using the Product t-norm. After that, a layer of normalization is performed. The training rule option is the Levenberg–Marquard variation of the gradient backpropagation method. A single output layer reflects the sinking value of cable  $i$  in the final layer. Three hidden layers are involved in inverse kinematics of CDPRs that account for cable sag.

The first is the fuzzification layer, which uses Gaussian transfer functions to convert inputs to linguistic variables. When compared to normal back-propagation, this option provides for a significantly faster learning process with fewer iterations. ANFIS network with three Gaussian membership function and hybrid learning method is trained using the coordinates and sag of cables as training

data. On the whole wrench feasible workspace of the CDPR, the training data of four ANFIS networks for sags of four cables were gathered. The ANFIS receives the coordinates as input and outputs the sag. Through a process known as training.

The membership functions will be changed during the training phase to decrease the error reach to the preset error or use up the preset epoch. ANFIS model will be fully established at the end of the training process, and it will be tested using the deduced inverse kinematics. Fig.6 show the response surface of 4 ANFIS model for predicting sagging of 4 cables of CDPR, ANFIS models were built with 3998 training data pairs and checked by 1001 data pairs, the result show that 4 surfaces have nearly the same shape, deviated at an angle of 90 degrees according to the wiring structure of the robot in the Fig.1. The correlation coefficients of four ANFIS models are greater than 0.9 and 0.934 for train data and test data respectively.

The histogram in Fig.7 shows the distribution of the calculation errors of the ANFIS model compared with the TRDA model, the errors vary between -20 mm to 20 mm, but the number of errors greater than 10(mm) is very small, the error mainly focuses from -5 to 2mm for all cables. Compared with cable lengths from 4700mm to 8700mm, this error is suitable for large-sized cable robots that are applied in tasks that do not require rigorous precision such as moving materials, controlling camera position in halls, stadiums. To evaluate the accuracy of this model, the following section will experiment on specific trajectories to analyze poses that cause large errors and propose options to improve the accuracy of the ANFIS model.

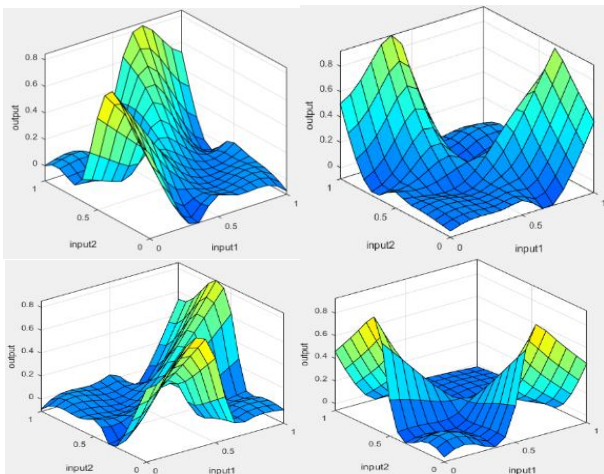


Figure 6. Response surface of ANFIS prediction system

TABLE I. SPECIFICATION OF CDPR

Input Variable	Symbol	Value
Frame Length	a (m)	8
Frame Width	b (m)	8
Frame Height	c (m)	4
End-effector mass	Me (kg)	100
Cable Diameter	Dc (mm)	8

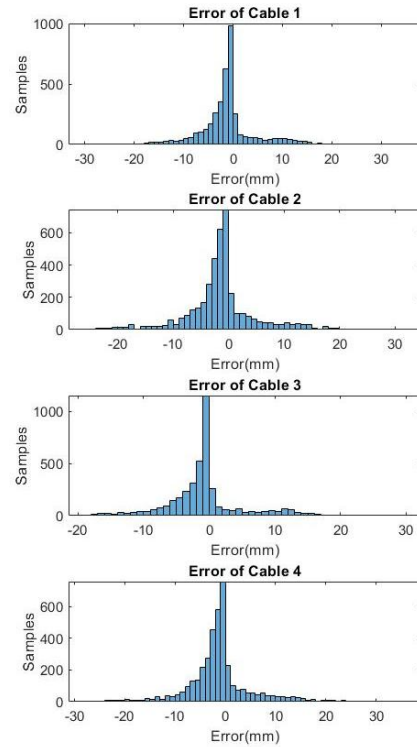


Figure 7. Response surface of ANFIS prediction system

#### IV. EXPERIMENTS AND DISCUSSIONS

To evaluate the responses of ANFIS models built for predicting sag of cables for CDPR with configuration as in Fig.1 and Table I, from the given trajectories, a computational program divides the trajectory into multi nodes for the robot to move, the nodes are checked to see if they belong to the robot's workspace, then calculate the distribution cable tension, cable sagging are calculated by two methods, which are TRDA and ANFIS, in which the input of the TRDA calculation method is the node positions and the corresponding cable tensions, while the ANFIS model only need information about the coordinates of the nodes, the cable sagging calculation results of the ANFIS models and the calculation method are performed on the same designed trajectory in the feasible workspace.

Fig.8 show the result of sagging, lengths and tensions of cables predicted by ANFIS and computation method – TRDA when robot moves along the closed curve path, the trajectory was calculated along a curve path following the equation (7), with the tension distribution method was used, the cable sagging depend on the cable length and cable tension respectively. Cable sagging is inversely proportional to cable tension and proportional to cable length, the cable sagging reaches to its maximum value about 60mm when cable length is about 8000 mm and cable tension is about 80N. cable sagging approaches its minimum values when cable tension is greater than 500N. The comparison results between the cable deflection obtained from the ANFIS model and the TRDA calculation method show that the error is very small, close to zero in the locations with high cable tension and

small deflection and the cable tension and cable deflection changes continuously.

The maximum error of the prediction model occurs at the point where there is a sudden change of cable tension and cable deflection, the maximum error is about 40mm in this position.

$$\begin{cases} x = 2800.\sin t \\ y = 1500.\cos t \\ z = 1000 \end{cases} \quad (7)$$

Table II lists 11 node points randomly taken in the robot's workspace, the point-to-point trajectories are designed as linear motion between the nodes, the trajectory starts at point P1 and ends at P11 coincides with P1. The corresponding joint trajectory is depicted in Fig.9, the length of the driven cables is calculated along the moving trajectory of the nodes, respectively, the cable sagging is calculated by the two methods TRDA and ANFIS is illustrated in Fig.10, similar to the curve path, the errors predicted by the ANFIS model occur at locations where there is a sudden change in the magnitude of the cable tension, resulting in the nature continuity of the ANFIS model, so to improve the accuracy of the prediction model, it is necessary to make the cable tension change continuously using a suitable cable tension distribution model.

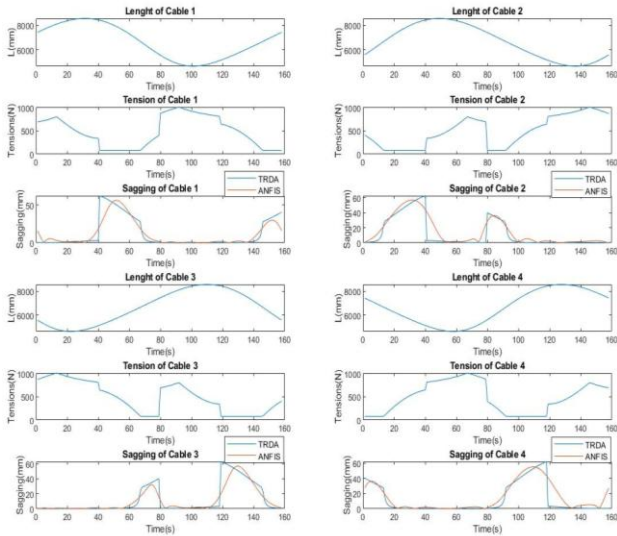


Figure 8. Sag of 4 cables along close-curve path

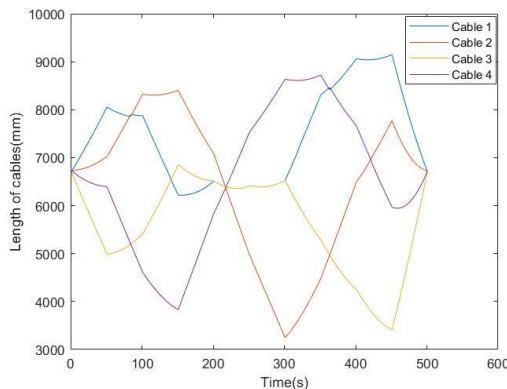


Figure 9. Length of 4 cables along linear path

TABLE II. COORDINATE OF NODE POINTS

Node points	Node points
P1(0, 0, 400)	P7(-2000, 2000, 2400)
P2(1500, 1000, 900)	P8(-500, 3000, 1400)
P2(2500, -500, 1400)	P9(1500, 2500, 900)
P4(1500, -2000, 1900)	P10(3000, 1500, 1900)
P5(500, -500, 900)	P11(0, 0, 400)
P6(-1000, 1000, 1400)	

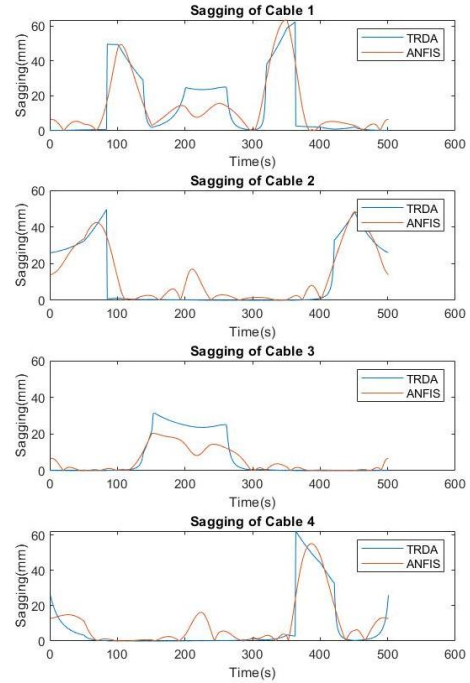


Figure 10. Sag of 4 cables along linear path

## V. CONCLUSION

The results of this study show that the efficiency of using ANFIS model to estimate the cable sag of the large size cable robot. This result can be used to build a simple estimation model for specific cable robots, simplify the calculation process, with appropriate response for cable robot applications. The results of this paper are interesting because they solve a problem that no closed-form solution is known. Therefore, ANFIS can improve the accuracy of cable robots and explore high nonlinear functions and has been successfully applied to approximate complex mapping between robot positions and cable lengths. The results of the computation of this paper have demonstrated the advantages of this method in increasing the convergence with model accuracy which is superior to the corresponding methods for parallel cable robots. In the future works, a new method of cable tension distribution will be studied to generate continuous cable tensions along the operating trajectory, which may increase the accuracy of the ANFIS prediction model. The calculated results will be tested on CDP (Fig.11) to evaluate the accuracy. The ANFIS model will also be designed and tested on different CDP configurations,



thereby having a more accurate assessment of the ability to use the ANFIS model in predicting the nonlinear noise components affecting the accuracy of CDRPs.



Figure 11. Cable robotic system in experiments.

#### CONFLICT OF INTEREST

The authors declare no conflict of interest.

#### AUTHOR CONTRIBUTIONS

All authors contributed to conceptualization and design of the study structure and content. [Tuong Phuoc Tho] performed the document preparation, data collection; [Nguyen Truong Thinh] analyzed the results; the first draft of the manuscript was written by [Tuong Phuoc Tho]; all authors commented on previous versions of the manuscript; all authors had approved the final version.

#### ACKNOWLEDGMENT

This work belongs to the project grant No: B2021-SPK-05. funded by Ministry of Education and Training, and hosted by Ho Chi Minh City University of Technology and Education, Vietnam.

#### REFERENCE

- [1] P. Miermeister *et al.*, "The CableRobot simulator large scale motion platform based on cable robot technology," in *Proc. 2016 IEEE/RSJ International Conference on Intelligent Robots and Systems (IROS)*, 2016, pp. 3024-3029.
- [2] R. Buswell, W. R. Lear de Silva, S. Jones, and J. Dirrenberger, "3D printing using concrete extrusion: A roadmap for research," *Cement and Concrete Research*, vol. 112, pp. 37-49, 2018
- [3] P. Chesser *et al.*, "Fieldable platform for large-scale deposition of concrete structures," in *Proc. Solid Freeform Fabrication Symposium*, Austin, TX, 2018.
- [4] S. Qian, B. Zi, W. W. Shang, *et al.* "A review on cable-driven parallel robots," *Chin. J. Mech. Eng.*, vol. 31, no. 66, 2018.
- [5] H. Hong, J. Ali, and I. Ren, "A review on topological architecture and design methods of cable-driven mechanism," *Advances in Mechanical Engineering*, vol. 10, no. 5, pp. 1-14, 2018.
- [6] J. P. Merlet, "Singularity of cable-driven parallel robot with sagging cables: Preliminary investigation," in *Proc. 2019 International Conference on Robotics and Automation (ICRA)*, 2019, pp. 504-509.

- [7] H. Irvine, *Cable Structures*, Cambridge, MA, USA: MIT Press, 1981.
- [8] J. C. Russell and T. J. Lardner, "Statics experiments on an elastic catenary," *J. Eng. Mech.*, vol. 123, no. 12, pp. 1322-1324, 1997.
- [9] D. Sridhar and Robert L. Williams II, "Kinematics and statics including cable sag for large cable suspended robots," *Global Journal of Researches in Engineering: H Robotics & Nano-Tech*, vol. 17, no. 1 Version 1.0 Year 2017 Publisher: Global Journals Inc. USA.
- [10] Y. Su, Y. Y. Qiu, and P. Liu, "Optimal cable tension distribution of the high-speed redundant driven camera robots considering cable sag and inertia effects," *Hindawi Publishing Corporation Advances in Mechanical Engineering*, vol. 2014, p. 11.
- [11] M. Gouttefarde, J. Collard, N. Riehl, and C. Baradat, "Simplified static analysis of large-dimension parallel cable-driven robots," in *Proc. 2012 IEEE International Conference on Robotics and Automation*, 2012, pp. 2299-2305.
- [12] A. Ming and T. Higuchi, "Study on multiple degree-of-freedom positioning mechanism using wires (Part 1) – Concept, design and control," *International Journal of the Japanese Society for Precision Engineering*, vol. 28, no. 2, pp. 131-138, 1994.
- [13] D. Q. Nguyen, M. Gouttefarde, O. Company, and F. Pierrot, "On the simplifications of cable model in static analysis of large-dimension cable-driven parallel robots," in *Proc. 2013 IEEE/RSJ International Conference on Intelligent Robots and Systems*, 2013, pp. 928-934.
- [14] M. Abdel-Nasser and O. Salah, "The inverse kinematics analysis for tendon-driven robot based on an adaptive neuro-fuzzy inference system," in *Proc. 2020 16th International Computer Engineering Conference (ICENCO)*, 2020, pp. 118-123.
- [15] M. R. A. Refaai, "Using multiple adaptive neuro-fuzzy inference system to solve inverse kinematics of SCARA robot," in *Proc. 2021 18th International Multi-Conference on Systems, Signals & Devices (SSD)*, 2021, pp. 154-159.
- [16] T. P. Tho, N. T. Thinh, "Using a cable-driven parallel robot with applications in 3D concrete printing," *Appl. Sci.* 2021, vol. 11, p. 563.

Copyright © 2022 by the authors. This is an open access article distributed under the Creative Commons Attribution License (CC BYNC-ND 4.0), which permits use, distribution and reproduction in any medium, provided that the article is properly cited, the use is noncommercial and no modifications or adaptations are made



**Tuong Phuoc Tho** is a Lecturer of Faculty of Mechanical Engineering at Ho Chi Minh City University of Technology and Education, Viet Nam. He received M.E degree in Manufacturing Technology from Ho Chi Minh University of Technology, Ho Chi Minh, Vietnam, in 2011. His work focuses on Robotics and Mechatronics system.



**Nguyen Truong Thinh** is Dean of Faculty of Mechanical Engineering at Ho Chi Minh City University of Technology and Education, VietNam. He is also Associate Professor of Mechatronics. He obtained his PhD. In 2010 in Mechanical Engineering from Chonnam National University. His work focuses on Robotics and Mechatronic system. Projects include: Service robots, Industrial Robots, Mechatronic system, AI applying to robot and machines, Agriculture smart machines.

## Bài báo số 5 – SCOPUS - IF 1.012

Tho, Tuong Phuoc, and Nguyen Truong Thinh. "A Study of Tension Distribution for Control of Planar Cable Driven Parallel Robot Using Quadratic Programming Algorithm." International Journal of Mechanical Engineering and Robotics Research - IJMERR 2022 Vol.11(7): 479-485.

Link:

<http://www.ijmerr.com/index.php?m=content&c=index&a=show&catid=212&id=1762>



# A Study of Tension Distribution for Control of Planar Cable Driven Parallel Robot Using Quadratic Programming Algorithm

Tuong Phuoc Tho and Nguyen Truong Think

Department of Mechatronics, Ho Chi Minh City University of Technology and Education

Thu Duc City, Ho Chi Minh City, Vietnam

Email: thotp@hcmute.edu.vn, thinknt@hcmute.edu

**Abstract**—The kinematic problem of Cable Driven Parallel Robots is not like that of other conventional robots due to the transmission mechanisms are the cables that can only exert the pulling force on the moving frame because the cable cannot be used to push. Therefore, the robot can only perform the task if the tensions in all cables are positive. The calculation of the kinematics and control for these types of robots as well as calculating the tension distribution to ensure the equilibrium for the moving frame at the nodes have to be done simultaneously. This paper described analysis and experiments of a planar cable driven parallel robot, in which, the inverse kinematics of the robot is solved based on a cable tension distribution model with a quadratic cost function, the values of tensions of cables are preferred to follow the mean value of the cable tension limit. A force feedback controller is also designed to control the robot based on calculated data, then the experimental results are analyzed to evaluate the effectiveness of this model.

**Index Terms**—planar cable robot, tension distribution, static kinematics

## I. INTRODUCTION

Cable Driven Parallel Robots (CDPRs) have been researched and developed in many applications due to their advantages in structure and workspace [1-2]. CDPRs are a kind of parallel structure robot with cables are used as the driving mechanism. Each cable is stored and distributed by a cable winch and connected to the moving frame or end effector after passing through the diverter pulleys. The cable is lighter in weight and smaller in volume than the rigid link of a traditional or parallel robot, which enables the development of very long drive cables without the need for an overly large cable distribution mechanism. With this structure, the moving frame of cable robot has high acceleration and speed, large workspace and be widely applied in the fields of agriculture, construction, ... [3- 4].

Kinematic analysis of the CDPRs is not like other types of parallel robots because the cables can only pull a force to the end effector and they cannot push. Therefore, the robot only performs the task if the tensions in all cables is positive [5-7]. In contrast to the large operating space, the mass and elasticity of the cable will cause

sagging [5]. The workspace CDPRs is defined as the area in space where the moving frame reaches equilibrium status under the action of external forces and positive cable tensions. The workspace and performance of CDPRs can be expanded and improved by adding drive cables, but this will complicate the kinematics and dynamics problem and increase the cost of the controller and expand the mechanical structure. When the number of driven cables is larger than the number of degrees of freedom (D.O.F) of end effector, it is necessary to find the cable tension systems satisfying the constraint conditions, which affects the design of the controller and the application of the cable robot. Hassan Bayani et al. [6] developed a planar CDPR with camera position feedback controller several controllers (sliding, adaptive sliding) used to design the controller for the robot, the experimental results are compared to evaluate the response of each controller, the pseudo-inverse matrix is used to calculate the cable tension distribution solution, the calculation results can be used as reference for the design controllers for other cable robot configurations. Javad Bolboli [7] et al. analyzed the operation space based on the stiffness matrix of the planar cable robot structure, the study showed the relationship between the internal force and the stiffness of the structure, which can be used as a standard when determining the tension distribution of other cable-driven robot configurations, in order to ensure the robot's rigidity in the operating space.

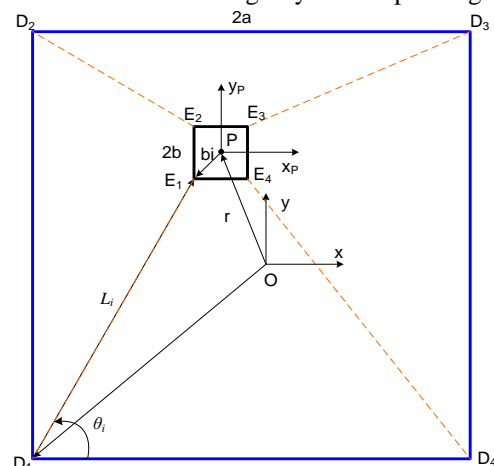


Figure 1. Kinematic structure of Planar CDPR

Min-Cheol Kim et al. [8] developed a sensor-based capsule endoscope monitoring device based on the motion of a planar CDPR. A permanent magnet is placed in the capsule endoscope, the position of the capsule endoscope is determined based on measurements of the semi-static magnetic field of the HALL effect sensor array and the forward kinematics problem of the planar cable robot. Some other studies [9][10] also used linear programming and quadratic programming to calculate the distribution of cable tension. Most of the above studies have not specifically mentioned the design of the trajectory, the calculation of the joint trajectory and the tension for the control experiment, or the monitoring of the tension value when controlling the working head according to the points given button. In order to evaluate the response and feasibility of designing and controlling a planar cable robot, this study presents a kinematic model of a planar CDPR driven by 4 cables and builds a kinematic simulation program for that model. Based on the quadratic programming algorithm for determining the combinations of tension forces, it is possible to determine the distribution of cable tension according to the joint trajectory, avoiding large changes of cable tension during the operation, otherwise, the tension values of cables are taken close to the average value to avoid cable stagnation when the tension is small or the motor overload when the tension is high due to the response of the controller. A cable tension feedback controller is designed to control the CDPR to execute the design trajectories to evaluate the accuracy of the calculated model.

II. KINEMATICS OF PLANAR CABLE ROBOT

Planar CDPRs consist of a moving frame driven by  $m$  cables distributed from cable dispensing mechanisms. The analyzed configuration in this paper includes four cables, which generate two degrees of freedom shown in Fig. 1. Each cable is connected to the fixed frame at  $D_i$  points and to the moving frame at  $E_i$  points. The length of cable  $i$  is denoted by  $L_i$  and the cable angle to the  $x_i$  axis is  $\theta_i$  ( $i = 1, 2, \dots, m$ ).

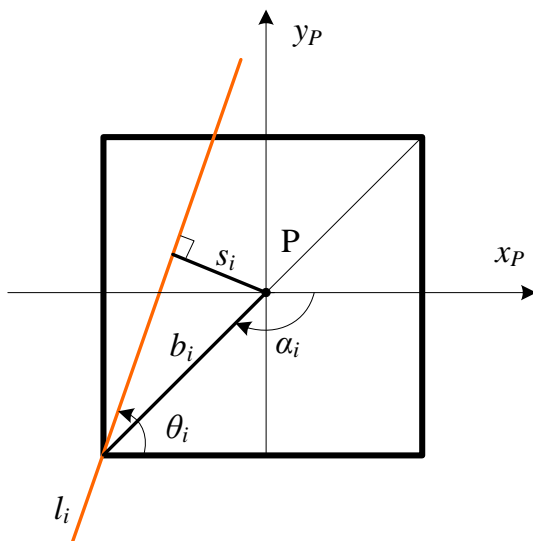


Figure 2. Diagram showing the relationship between parameters

The inverse position kinematics assumes as follows: known position  $P$  to determine the cable lengths  $L_i$ . From the position of end-effector  $P$  and each vertex  $D_i$  of the base link, we have the below equation.

$$L_i = \sqrt{(E_{ix} - D_{ix})^2 + (E_{iy} - D_{iy})^2} \quad i=1, \dots, m \quad (1)$$

According to the kinetic structure in Fig. 1, we have like as.

$$[E_1 \ E_2 \ E_3 \ E_4]^T = \begin{bmatrix} 1 & 0 & P_x \\ 0 & 1 & P_y \end{bmatrix} \begin{bmatrix} -b & -b & b & b \\ -b & b & b & -b \\ 1 & 1 & 1 & 1 \end{bmatrix} \quad (2)$$

$$[D_1 \ D_2 \ D_3 \ D_4]^T = \begin{bmatrix} -a & -a & a & a \\ -a & a & a & -a \end{bmatrix} \quad (3)$$

Cable tension is the force on the cable starting from the winch to end-effector. In moving, the robot can be considered to be in equilibrium status due to slow motion. However, the effect of cable sag needs to be taken into account because of the resulting length of the cable (in the case of a long cable). The balancing problem of a CDPRs is to determine the orientation and position of the end-effector when the length of each cable is known, and the position and direction that can keep the robot in a state balance. The problem of robot kinematics is not enough to control the CDPRs because the cable cannot provide thrust but only pull forces. Cable tension greatly affects the determination of the workspace. From the structural diagram in Fig. 1, the total forces and moments acting on the end effector of CDPRs can be represented by following system of equations:

$$\sum F = \begin{bmatrix} F_x \\ F_y \end{bmatrix} + \sum_{i=1}^m \tau_i \quad (4)$$

$$\sum M = M_z + \sum_{i=1}^m s_i \tau_i \quad (5)$$

With  $s_i$  being the actuation distance of the moment caused by the cable tension  $i$  on  $P$  (center of end effector, from the diagrams of Fig. 1 and Fig. 2, we can obtain.

$$s_i = b_i \sin(\alpha_i - \theta_i) \quad (6)$$

$$\cos \theta_i = \frac{l_{xi}}{\|L_i\|}, \sin \theta_i = \frac{l_{yi}}{\|L_i\|}, \quad i = 1, \dots, m \quad (7)$$

Where  $F$  and  $M$  are vectors of the external forces and the external torques acting on the end effector, respectively (in this case, zero);  $\tau_i$  is tension force of cable  $l_i$ ;  $b_i$  is the distance from attaching points  $B_i$  to the center of end effector  $P$ . Form the direction of driven cable, the unit vector  $u_i$  and tension vector  $\tau_i$  can be obtained.

$$\tau_i = \tau_i \times u_i \quad (8)$$

$$\mathbf{u}_i = \frac{\mathbf{L}_i}{\|\mathbf{L}_i\|} = \begin{bmatrix} \frac{L_{xi}}{\|\mathbf{L}_i\|} \\ \frac{L_{yi}}{\|\mathbf{L}_i\|} \end{bmatrix} = \begin{bmatrix} \cos \theta_i \\ \sin \theta_i \end{bmatrix} \quad (9)$$

The equilibrium equation can be described as follow.

$$\begin{bmatrix} \mathbf{u}_1 & \dots & \mathbf{u}_m \\ s_1 & \dots & s_m \end{bmatrix} \begin{bmatrix} \tau_1 \\ \vdots \\ \tau_m \end{bmatrix} + \begin{bmatrix} F_x \\ F_y \\ M_z \end{bmatrix} = 0 \quad (10)$$

By defining

$$\mathbf{A} = \begin{bmatrix} \mathbf{u}_1 & \dots & \mathbf{u}_m \\ s_1 & \dots & s_m \end{bmatrix} \quad (11)$$

$$\mathbf{w}_p = \begin{bmatrix} F_x \\ F_y \\ M_z \end{bmatrix} \quad (12)$$

Equation (10) can be written like below equation.

$$\mathbf{A}\boldsymbol{\tau} + \mathbf{w}_p = \mathbf{0} \quad (13)$$

where  $\boldsymbol{\tau} = [\tau_1 \ \tau_2 \ \dots \ \tau_m]^T$  is a cable tension vector;  $\mathbf{A}^T$  is a structure matrix of the cable robot ( $n \times m$ );  $\mathbf{w}_p$  is a vector of the external force act on the moving frame.

Therefore, a tension distribution is calculated for satisfying the system of equations (13) with the specific constraints depending on the design of the system [9-11] in a given pose of the moving frame. In this case, the static equilibrium equation and the positive tension constraints as well as the magnitude limit of the cable tension ensure that the cable does not sag nor exceed the load of the motor of cable distribution mechanism. System constraint is shown in below equation.

$$\mathbf{0} < \tau_{\min} \leq \boldsymbol{\tau} \leq \tau_{\max} \quad (14)$$

where  $\tau_{\min}$  is lower limit and  $\tau_{\max}$  is the upper limit of cable tensions.

There are many methods of tension distribution for cable robots to calculate tension of cables like as linear programming, pseudo-inverse matrix, and quadratic programming. Linear programming [9] is a method to search the best (most optimal) solution from an infinite number of solutions decided in a mathematical model with requirements are expressed in terms of equations in linear relationship, where the cost function value is the sum of the tension minimized. The advantage of this method is saving energy, the optimal solution is the one that satisfies the stated objectives of the problem depending on the constraints. The disadvantage of this method is that some of the tension tends to reach the boundary value, the tension values have a large change at the trajectory transition points, causing the actuator to be overloaded or causing slack on the driven cables, thereby reducing the accuracy of the system. The second alternative is to use a pseudo-inverse matrix [6] with the goal of finding continuous string tensions along a changing trajectory of joint variable, this method can

cause some cases with points located near the spatial boundary workspace, the cable tension may be negative. The quadratic programming algorithm was used to calculate the sets of cable tensions with the criterion that the value of the cable tensions is continuous and the preferred value clings to the average value of the cable tension limits [10]. The model of the problem of minimizing the relative tension is shown as follows.

$$\min \sum_1^m (\tau_i - \bar{\tau}_i)^2 \quad i = 1, \dots, m \quad (15)$$

$$\bar{\tau}_i = \frac{\tau_{i\max} + \tau_{i\min}}{2} \quad (16)$$

where  $\bar{\tau}_i$  is the average of  $i^{th}$  cables tension with following constrains.

$$\mathbf{A}\boldsymbol{\tau} = -\mathbf{w}_p \quad (17)$$

$$\mathbf{0} < \tau_{\min} \leq \boldsymbol{\tau} \leq \tau_{\max} \quad (18)$$

Therefore, the objective function (15) is a quadratic form of first-order constraints, the sequential quadratic programming algorithm [11][12] can be used to solve this issue. The results show that the cable tension follows the average values and the corresponding starting trajectory, which is convenient for feedback control of the driven cable, avoiding the condition of the cable being slack or the tension being too large to cause motor overload. Calculation results of cable tension along with moving trajectories and joint trajectories will be performed in the next section.

### III. SIMULATIONS, EXPERIMENTS AND EVALUATIONS

A prototype of planar cable robot was used to carry out several experiments, then experimental results also compared simulating ones to evaluate robot's performances. Fig. 3 shows the designed and developed planar cable robot with cable distribution mechanism, which is used to conduct the experiment. The structure of robot consists of 4 cable distributors indexed (1) put below to drive end-effector (3) moving on the horizontal plane through the pulleys (4) mounted on the frame (2) and the cable (6) with the force-feedback control (5). The cable distributor is driven by the motor (8) through the coupling attached to the winding roller (7) which also rotates. When the roller (7) rotates, the toothed belt drive transmits the motion that rotates the lead screw. Lead screw mechanism makes nut (9) reciprocating with a specified pitch to distribute the driven cable. A cable distribution mechanism is placed on the nut (9), which helps the wire to be fixed at the specified position. The lead screw mechanism helps to keep the wire parallel to the roller in a defined step. The cable after being distributed by the roller and the lead screw, is guided through the pulley (10) placed on the loadcell (11), this loadcell is mounted on the cable distribution mechanism frame (12) to measure the cable tension, combined with the roller placed on the robot frame to ensure the fixed direction of the tension on the loadcell.

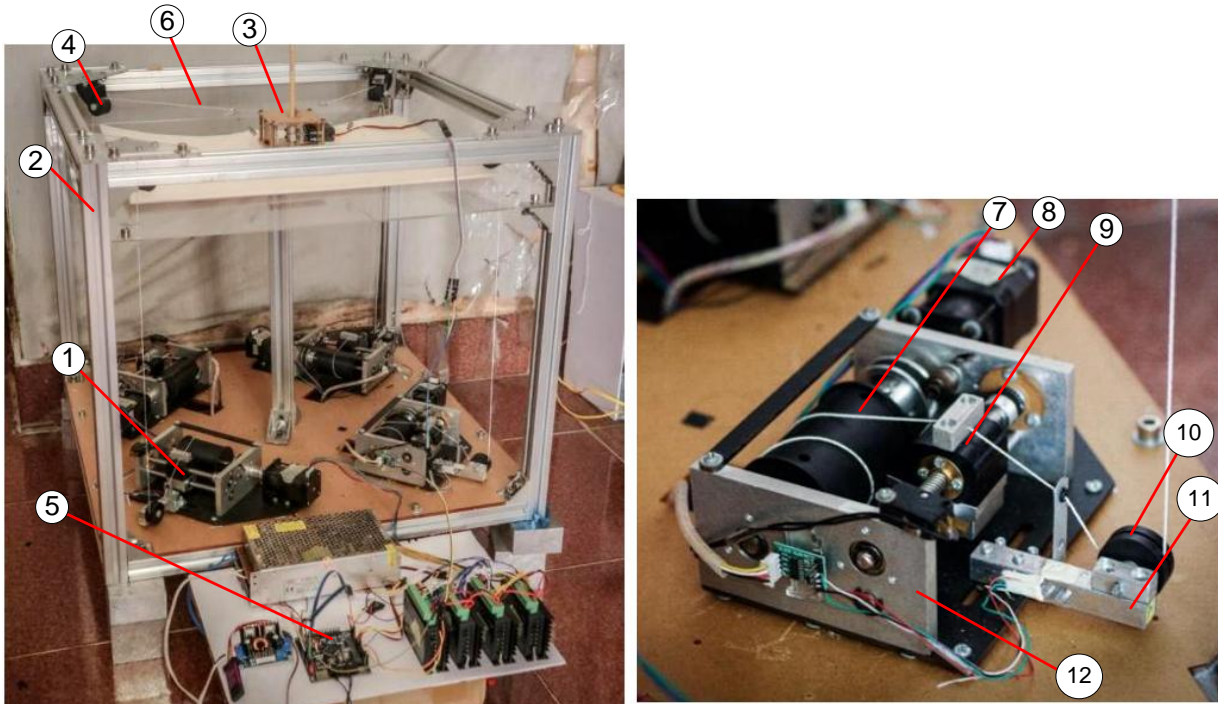


Figure 3. Planar cable robot (left) and cable distribution mechanism (right).

TABLE I. SPECIFICATION OF PLANAR CABLE ROBOT.

a	175mm
b	45mm
$\tau_{min}$	50N
$\tau_{max}$	200N

With the configuration and specifications as shown in Table I, a null space of structure matrix analysis algorithm is applied to determine the static workspace of the planar CDPR with linear constraints [13]. Static workspace is defined as the set of moving frame positions where at least one combination of cable tension exists satisfying the equilibrium equation (13) with the constraints of cable tension limit and different external forces, the workspace in this case is defined with different tension limits with external force vector is zero. After comparison between Fig. 4(a) and Fig. 4(b), the static workspace corresponding to the force limit cable tension of  $[\tau_{min}, \tau_{max}]$  in range  $[50N, 200N]$  is smaller than corresponding to a larger cable tension  $[\tau_{min}, \tau_{max}]$  in range  $[50N, 300N]$ . This result shows that the size of robot's workspace increases when the limits of tensions are extended, so it is possible to expand the workspace by increasing the motor power, which is also an important property as a design criterion and calculate the robot structure as well as choose the appropriate actuator power. The structure of the controller for cable robot is shown as the diagram in Fig. 5. There are 3 layers in this controller, the first layer is the main controller designed to calculate the value of joints, velocity and tension distribution of cables from the motion trajectory of MP through synthesis of kinematics and force balance problems.

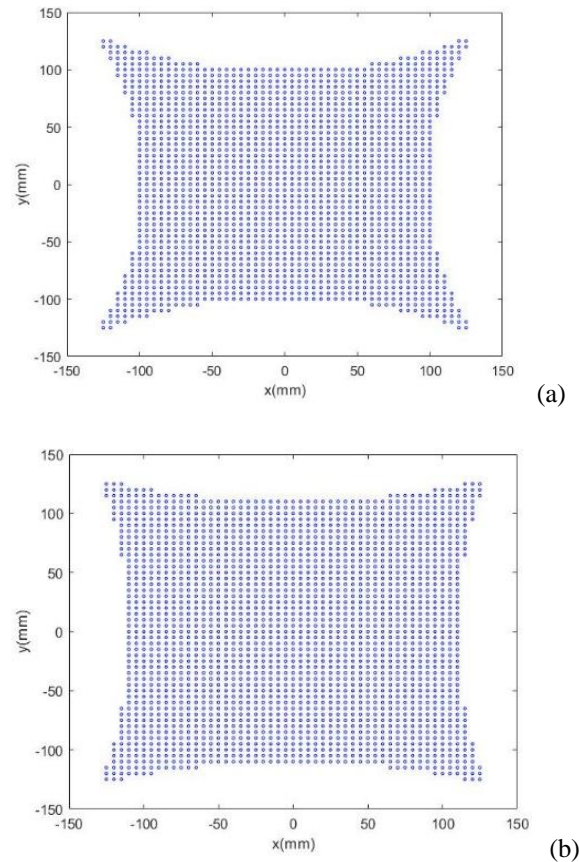


Figure 4. Static workspace of planar CDPR with different limits of cable tension  $\tau_{min} = 50N, \tau_{max} = 200N$ , and  $\tau_{min} = 50N, \tau_{max} = 300N$

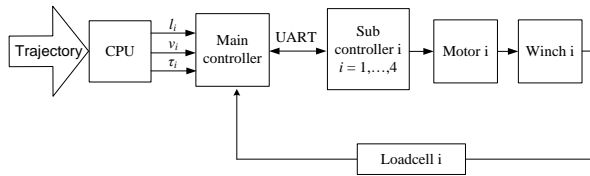


Figure 5. Diagram of cable robot control system

The second layer is the sub-controller or the position controller, which receives signals from the main controller and is responsible for outputting control signals to the servos through the drivers. The third layer controls the position, velocity and cable tension of the motor that drives the cable distributor through signals received from the sub-controller and feedback from the corresponding coded values. To evaluate the suitability of the computational model, the basic trajectories (triangle, rectangle, ...) will be designed and tested on this robot model, with the workspace being the XY plane. The robot will perform trajectories through the pen holder on the moving frame. The trajectory obtained during the experiment will be compared with the designed trajectory to measure errors in order to evaluate the model and the robot's performance. Fig. 6 shows the simulation results of rectangle trajectory (a) and experimental results (b) with dimension 55mmx70mm. The experimental results on the robot model shown in Fig. 7 show that the robot's trajectory has a continuous profile, follows the given trajectory with an error of less than 2mm, the trajectory has no fracture phenomenon due to slack phenomenon of cable during movement, the results of cable tension measured at the nodes show good response of the controller.

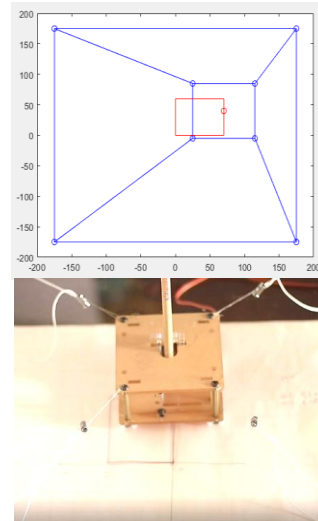


Figure 6. Simulated trajectory (a) and experimental trajectory (b) of the rectangle

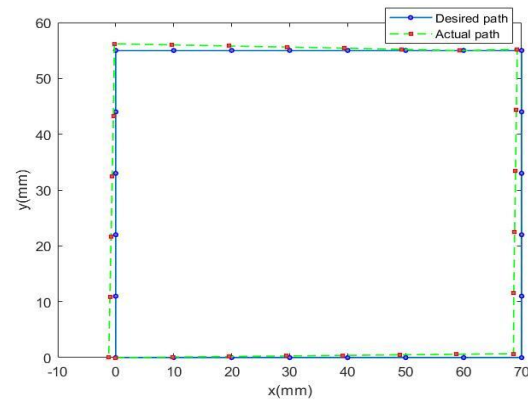


Figure 7. Rectangular path according to design and experiment

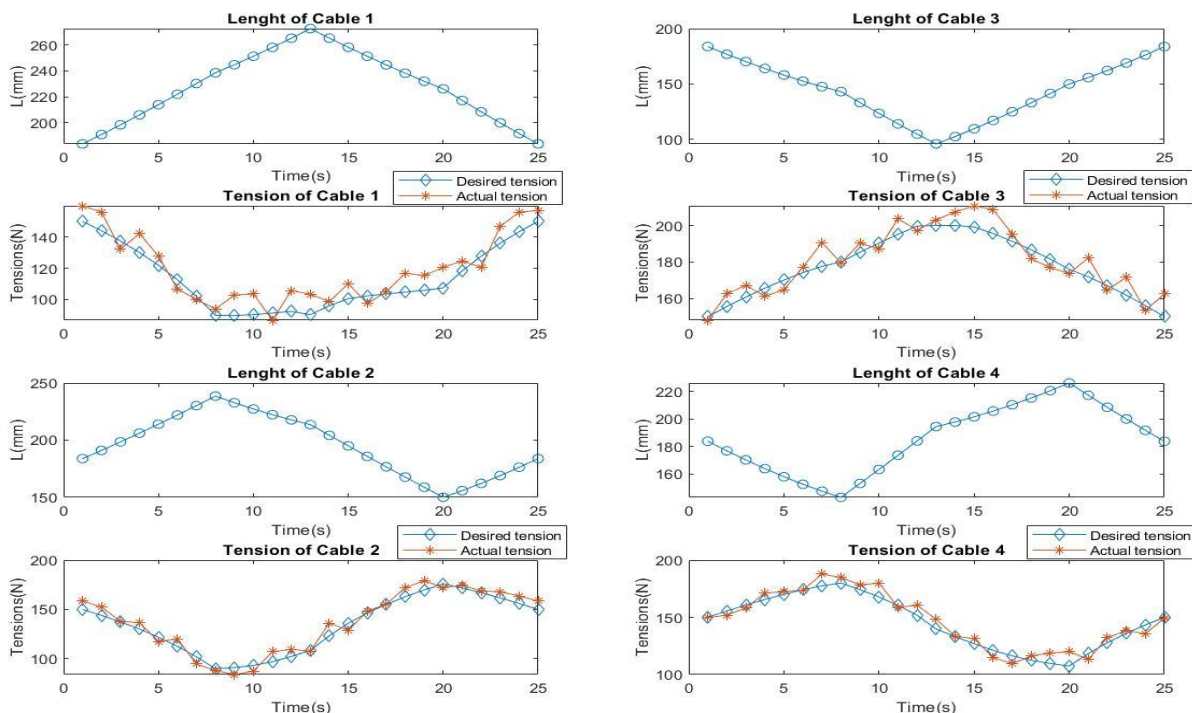


Figure 8. Diagram of joint trajectories and tension of cables according to calculations and experiments when interpolating rectangle



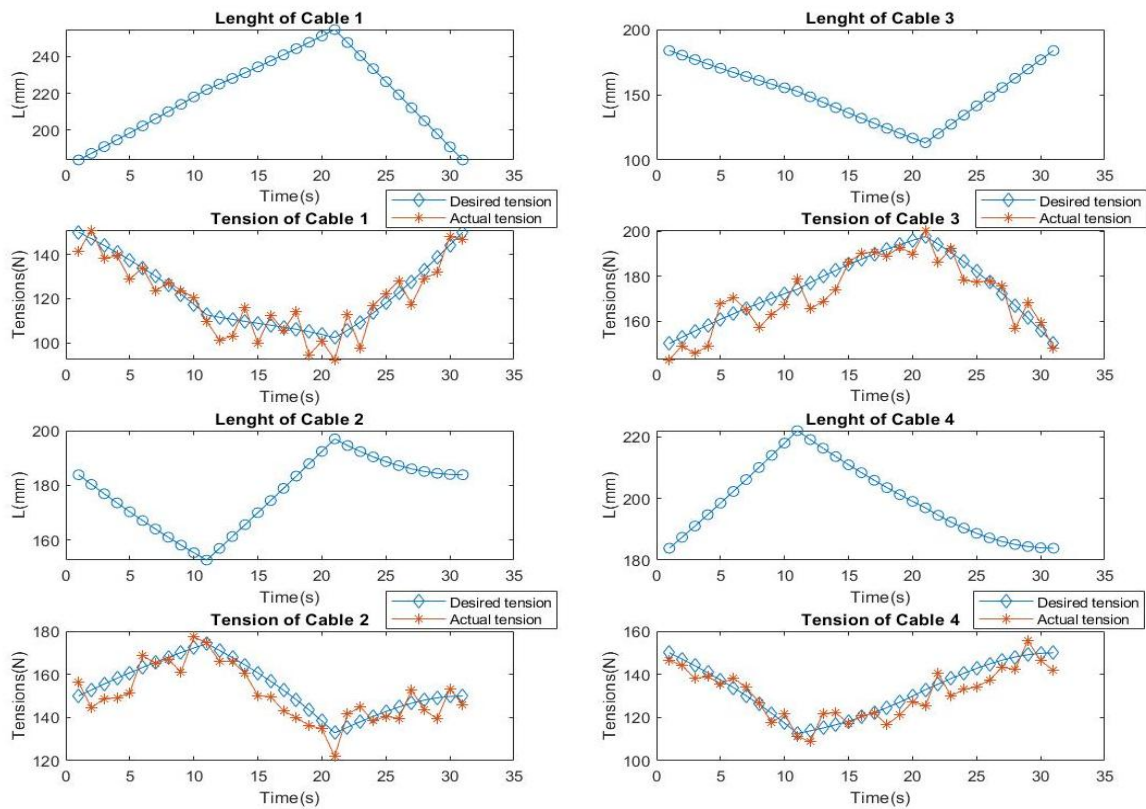


Figure 9. Diagram of joint trajectories and tension of cables according to calculations and experiments when interpolating triangle

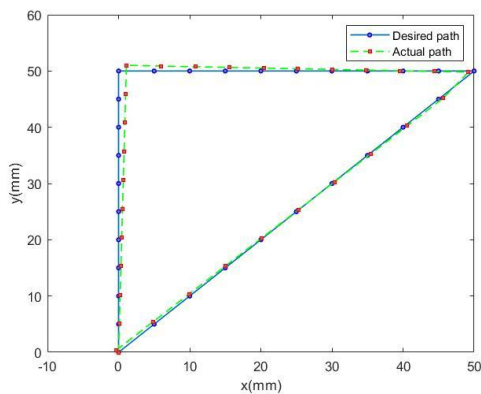


Figure 10. Triangle path according to design and experiment

The corresponding joint trajectory response for rectangle path is showed in Fig. 8 with the calculated and experimental cable tension values, this graph shows that the tension values satisfy the equilibrium equation (13), these cable tensions change continuously, following a trajectory that matches values close to the mean within the range of cable tension. This is very convenient for control based on cable tension, limiting cable slack when the control cable tension is less than the lower limit of cable tension or overloading the motor when the tension exceeds the upper limit due to the response of the controller. Similar to the above experimental results, Fig. 9 and Fig. 10 also are simulating results in joint space, cable tension for triangle-perimeter path and experimental results. The values of cable tensions corresponding to the joint trajectories have a continuous change, therefore there

is no sudden change in cable tension, causing difficulties for the control process. The cable tension values are always within the tension range based on the equilibrium equation. When the MP moves to a point, the 4 cables are stretched reaching positive cable tensions, and the cable tensions also eliminate at nodes of the moving-path. Through the simulating results based on the sequential quadratic programming method, it shows that the cable tension satisfies the constraints of the balanced equation and has values that change relatively continuously according to the nodes, thereby showing that the results of the problem have a suitable response for the tension feedback controller. The tension errors at the nodal points are set at suitable thresholds for the trajectory to move continuously.

#### IV. CONCLUSION

This paper presents a complete design, calculation and experimental procedure for a planar cable robot with 3 D.O.F, driven by 4 inelastic cables. In which, the calculation of the kinematic problem with the number of D.O.F less than the number of driven cables is performed based on the nonlinear programming method. The cable robot configuration and the null space analysis of the structure matrix method was used to determined static workspace of the CDPRs, the cable tension distribution is selected based on the given trajectories determined and the sequential quadratic programming algorithm with a quadratic objective function designed for the purpose of determining the value of tension systems along the joint trajectory calculate and follow the average value of the

upper and the lower limit of the cables tensions, a tension feedback controller is designed for a prototype planar CDPR with a tension feedback unit placed on a cable distributor, the experimental results show the agreement of the design model with the experimental strain response and trajectories according to the given trajectories. This model can be used to design and control redundant CDPRs of larger sizes with different configurations. The future work of this research direction is to apply a model for large sizes redundant CDPRs that take into account the influence of cable sags with different cabling configurations and degrees of freedom.

#### ACKNOWLEDGEMENTS

This work belongs to the project grant No: B2021-SPK-05. funded by Ministry of Education and Training, and hosted by Ho Chi Minh City University of Technology and Education, Vietnam.

#### REFERENCE

- [1] S. Qian, B. Zi, W. W. Shang, et al. "A review on cable-driven parallel robots," *Chin. J. Mech. Eng.* vol. 31, no. 66, 2018.
- [2] H. Hong, J. Ali, and I. Ren, "A review on topological architecture and design methods of cable-driven mechanism," *Advances in Mechanical Engineering*, vol.10, no. 5, pp. 1-14, 2018.
- [3] R. Buswell, W. R. Lear de Silva, S. Jones, and J. Dirrenberger, "3D printing using concrete extrusion: A roadmap for research," *Cement and Concrete Research*, vol. 112, pp. 37-49, 2018.
- [4] P. Chesser et al., "Fieldable platform for large-scale deposition of concrete structures," in *Proc. Solid Freeform Fabrication Symposium*, Austin, TX, 2018.
- [5] J. P. Merlet, "Singularity of cable-driven parallel robot with sagging cables: Preliminary investigation," in *Proc. 2019 International Conference on Robotics and Automation (ICRA)*, 2019, pp. 504-509.
- [6] H. Bayani, M. T. Masouleh, A. Kalhor, "An experimental study on the vision-based control and identification of planar cable-driven parallel robots," *Robotics and Autonomous Systems*, vol. 75, Part B, 2016, pp. 187-202.
- [7] J. Bolboli, M. A. Khosravi, F. Abdollahi, "Stiffness feasible workspace of cable-driven parallel robots with application to optimal design of a planar cable robot," *Robotics and Autonomous Systems*, vol. 114, pp. 19-28, 2019.

- [8] M. C. Kim, E. S. Kim, J. O. Park, E. Choi, C. S. Kim, "Robotic localization based on planar cable robot and hall sensor array applied to magnetic capsule endoscope," *Sensors*, vol. 20, no. 20, p. 5728, 2020.
- [9] B. Giovanni and A. Trevisani, "Cable robot performance evaluation by wrench exertion capability," *Robotics*, vol. 7, no. 2, p. 15, 2018.
- [10] S. R. Oh and S. K. Agrawal, "Cable suspended planar robots with redundant cables: controllers with positive tensions," *IEEE Transactions on Robotics*, vol. 21, no. 3, pp. 457-465, June 2005.
- [11] Schittkowski, K. Nlpql, "A fortran subroutine solving constrained nonlinear programming problems," *Annals of Operations Research*, vol. 5, pp. 485-500, 1986.
- [12] A. Pott, T. Bruckmann, and L. Mikelsons, "Closed-form force distribution for parallel wire robots," in *Proc. 2009 Computational Kinematics Conference*, Duisburg, Germany, May 6-8, 2009
- [13] B. Ouyang and W. Shang, "A new computation method for the force-closure workspace of cable-driven parallel manipulators," *Robotica*, vol. 33, no. 3, pp. 537-547, 2015

Copyright © 2022 by the authors. This is an open access article distributed under the Creative Commons Attribution License (CC BY-NC-ND 4.0), which permits use, distribution and reproduction in any medium, provided that the article is properly cited, the use is noncommercial and no modifications or adaptations are made



**Tuong Phuoc Tho** is a Lecturer of Faculty of Mechanical Engineering at Ho Chi Minh City University of Technology and Education, Viet Nam. He received M.E degree in Manufacturing Technology from Ho Chi Minh University of Technology, Ho Chi Minh, Vietnam, in 2011. His work focuses on Robotics and Mechatronics system.



**Nguyen Truong Thinh** is Dean of Faculty of Mechanical Engineering at Ho Chi Minh City University of Technology and Education, VietNam. He is also Associate Professor of Mechatronics. He obtained his PhD. In 2010 in Mechanical Engineering from Chonnam National University. His work focuses on Robotics and Mechatronic system. Projects include: Service robots, Industrial Robots, Mechatronic system, AI applying to robot and machines, Agriculture smart machines.



## Bài báo số 6 – Hội nghị quốc tế có ISBN

Xuan, Hoang Tran, Tho Tuong Phuoc, Chien Do Manh, and Nghia Vo Luong Nhon. "Design and Modeling Camera Cable Robot." In Computational Intelligence Methods for Green Technology and Sustainable Development: Proceedings of the International Conference GTSD2022, pp. 271-281. Cham: Springer International Publishing, 2022.

Link: [https://link.springer.com/chapter/10.1007/978-3-031-19694-2\\_24](https://link.springer.com/chapter/10.1007/978-3-031-19694-2_24)



# Design and modeling Camera Cable Robot

Hoang Tran Xuan<sup>1</sup>, Tho Tuong Phuoc<sup>1</sup>, Chien Do Manh<sup>1</sup> and Nghia Vo Luong Nhon<sup>1</sup>

<sup>1</sup> Ho Chi Minh City University of Technology and Education,  
No.1 Vo Van Ngan Street, Linh Chieu Ward, Thu Duc City, Ho Chi Minh City, Vietnam

thotp@hcmute.edu.vn

**Abstract.** Camera Cable Robot is a robot with a camera that can move in a predefined 3D space where the poses of the camera are determined by cables fixed to the camera. By changing the lengths of the cables, the movement of the camera can be changed. In this paper, a cable-driven parallel robot (CDPR) is designed for filming in a large space with dimensions (20m x 20m x 10m), this robot has 3 degrees of freedom, an allowable payload from 20 kg to 50 kg. The kinematic equations, algorithms and suitable matrices are given to solve the problem of controlling the position and velocity of the robot. Besides, the equilibrium equation helps to ensure the stability of the robot, and the linear programming algorithm is used to determine the tensions of the cables during the trajectory. The calculation results are simulated by Matlab software, the results show that the model has many advantages such as safety and low construction cost. In particular, it is easy to change the configuration and size of the robot with low calibration costs. The next development direction of this research is to fabricate and test the robot in a real environment, thereby evaluating the accuracy and influencing parameters such as cable sagging and the method of cable tension distribution.

**Keywords.** Cable robot, cable driven parallel robot, filming robot, camera robot

## 1 Introduction

The Camera cable robot is a type of cable-driven parallel robot (CDPR) with 3 degrees of freedoms, 4 cables and 4 tensioning mechanisms [1, 2] which are controlled by a computer or via a controller. The system is controlled through 3 dimensions in a limited open space in a stadium, an arena or a large hall... by a cable control system [3]. It is responsible for transmitting images with a new and unique angle to the audience realistically and with a better view through television waves. The camera cable robot was first invented in 1980 by a filmmaker for their filming [4, 6]. Initially, this camcorder was rarely used due to the undeveloped technology and software. In 1984, this technology was used for the first time at an American football game and received many positive comments and contributions,

which made the filming cable robot more widely used afterward [5, 7]. Up to now, all major sports events and tournaments around the world have applied this technology.

This paper introduced a cable driving structure designed for moving a camera in a large space. The main issues of cable robots such as kinematic, tension distribution and trajectory planning were studied in order to build a dynamic simulation program for the cable structure [8]. Creating a suitable model for research as well as practical application. Furthermore, it shows the feasibility and reliability of cable robots when applied in other applications such as moving heavy objects over long distances. In this research, a CDPR is designed with dimensions (20m) x (20m) x (10m) (see Fig.1), 3 degrees of freedom and an allowable load of 20kg ~ 50kg.

## **2 Design of CDPR**

### **2.1 Structure of cable driven parallel robot (CDPR)**

The CDPR consists of a rigid frame and a moving platform. The length of a cable is controlled by the four winches. One of four sets of winches is designed in Fig. 2. A winch consists of the main components such as a DC servo motor, which is connected to a moving platform through several guide rollers, and a reversing lead screw with a winch [10]. The main shaft cable reel is supported by two bearings at both ends to reduce misalignment. The difference between the pitch of the lead screw and the winding winch is adjusted by choosing the gear ratio of 1:3. The principle of the cable drive is similar to the winding element in the lifting mechanism, which converts rotational motion into reciprocating motion so that the moving cable lifts and lowers the camera.

### **2.2 Kinetic model of CDPR**

In this section, the position kinetic analysis and velocity of the spatial CDPRs are presented [11]. Inverse kinematics is required for control and simulated via monitoring [12]. Position kinematics is concerned with the relationships of the fitting, proportionality variables to the Cartesian position and the scale variables of the end-effector motion [13]. Assuming that all cables are always kept taut, the corresponding joint space CDPR is constrained to be spatial Cartesian.

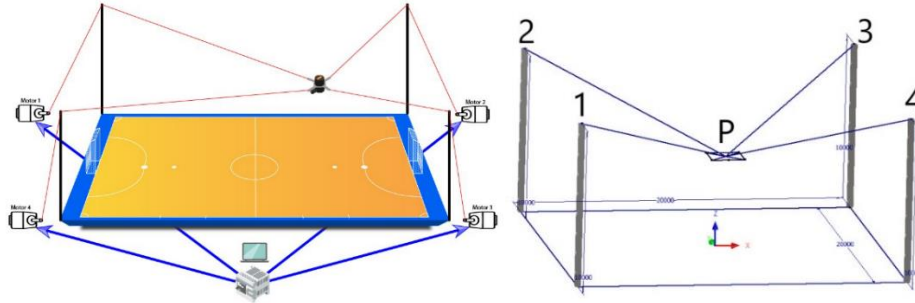


**Fig. 1.** Automatic video recording cable driven parallel robot and kinematic model

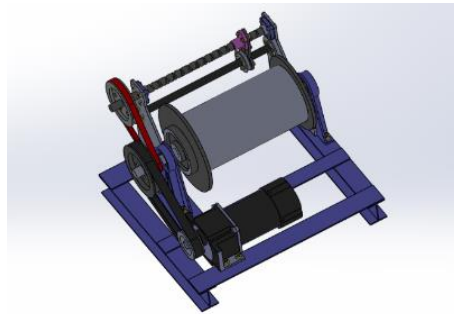


**Fig. 2.** Design of winch

### Position kinematics

The inverse position kinematics problem is posed as follows: Given the position of  $P = \{x \ y \ z\}$  and the requirement is to calculate the lengths of the cables  $L_i$  [14]. We have the following:

$$L_i = \sqrt{(x - A_{ix})^2 + (y - A_{iy})^2 + (z - A_{iz})^2} \quad (1)$$

And to apply velocity kinematics, we need to find the velocity origin P:

$$\theta_i = \tan^{-1} \left( \frac{P_y - A_{iy}}{P_x - A_{ix}} \right) \quad (2)$$

### Velocity kinematics

In order to find the velocity kinematics equations [15], we consider the vector direction of the  $i$ (th) cable:



$$\begin{cases} x \\ y \end{cases} = \begin{cases} A_{ix} + L_i \cos(\theta_i) \\ A_{iy} + L_i \sin(\theta_i) \end{cases} \quad (3)$$

Derivative to time we get:

$$\begin{cases} x' \\ y' \end{cases} = \begin{bmatrix} \cos(\theta_i) & -L_i \sin(\theta_i) \\ \sin(\theta_i) & L_i \cos(\theta_i) \end{bmatrix} \begin{cases} L'_i \\ \theta'_i \end{cases} \quad (4)$$

Inverse the Jacobian matrix of the i(th) cable, we get:

$$\begin{cases} L'_i \\ \theta'_i \end{cases} = \begin{bmatrix} \cos(\theta_i) & \sin(\theta_i) \\ -\sin(\theta_i)/L_i & \cos(\theta_i)/L_i \end{bmatrix} \begin{cases} x' \\ y' \end{cases} \quad (5)$$

Since we consider the cable length variations according to the Cartesian scale [16, 17], we can extract the first line of (5) to construct a velocity solution for a 4 cables CDPR.

$$\begin{cases} L'_1 \\ L'_2 \\ L'_3 \\ L'_4 \end{cases} = \begin{bmatrix} \cos(\theta_1) & \sin(\theta_1) \\ \cos(\theta_2) & \sin(\theta_2) \\ \cos(\theta_3) & \sin(\theta_3) \\ \cos(\theta_4) & \sin(\theta_4) \end{bmatrix} \begin{cases} x' \\ y' \end{cases} \quad (6)$$

Notice that we have omitted  $\theta'_i$  the velocity equations. The general form of the velocity kinematics equation is:

$$L' = MX' \quad (7)$$

Where:

+  $L'$  is the rate vector of variation of the lengths of n cables.

+  $M$  is the inverse Jacobian matrix CDPR.

+  $X' = \{x' \ y'\}^T$  is the velocity vector of the end-effector.

To solve the forward velocity kinematics we have to calculate the inverse equation.

$$X' = M^{-1}L' \quad (8)$$

### Calculation of tension

Cable tension distribution is an important problem in the design and control of the CDPR, with the CDPR having a larger number of cables than the number of degrees of freedom,

the cable tension is calculated to satisfy the equilibrium equation and the conditions. constraints on the positive tension or stiffness of the robot [15, 17]. We have the following system of equations:

$$F + \sum_{i=1}^4 \tau_i = 0 \quad (9)$$

$$M + \sum_{i=1}^4 (\tau_i \times b_i) = 0 \quad (10)$$

F and M are vectors of the external force (zero in this case) and the torque acting on the terminal feedback set, respectively:

+  $\tau_i$  is the force vector applied by each cable.

+ Vector  $b_i$  is the position of the moving point relative to the origin with the unit vector  $u_i$ , the force vector  $\tau_i$  can be obtained

$$\tau_i = \tau_i \times u_i \quad (11)$$

From (9) and (10) we have:

$$\begin{bmatrix} u_1 & \cdots & u_4 \\ b_1 \times u_1 & \cdots & b_4 \times u_4 \end{bmatrix} \begin{bmatrix} \tau \\ \cdots \\ \tau_m \end{bmatrix} + \begin{bmatrix} F_\rho \\ M_\rho \end{bmatrix} = 0 \quad (12)$$

We have:

$$A = \begin{bmatrix} u_1 & \cdots & u_4 \\ b_1 \times u_1 & \cdots & b_4 \times u_4 \end{bmatrix} \quad (13)$$

$$W_\rho = \begin{bmatrix} F_\rho \\ M_\rho \end{bmatrix} \quad (14)$$

Where

$$\tau = [\tau_1 \quad \tau_2 \quad \tau_3 \quad \tau_4] \quad (15)$$

$$A\tau + W_\rho = 0 \quad (16)$$

Where:

+  $\tau$  : vector of cable tension (4x1)

+  $A^T$  : CDPR Jacobian Matrix (n x m4)

+  $W_\rho$  : Vector of external force impacting on the center of the body (n x 1)

$$A\tau = -W_\rho \quad (17)$$

With constraints

$$0 < \tau_{\min} < \tau < \tau_{\max} \quad (18)$$

There are many distribution solutions of tension for cable robots such as linear programming, and a pseudo-inverse matrix is used to calculate cable tension [18-20]. Linear programming is a method for finding the best (most optimal) solution from an endless number of solutions decided in a mathematical model whose requirements are expressed by relationships of a computational system, in which the objective function value is the sum of the minimum cable tension [21].

### 3 Simulation and Discussion

**Fig. 3** shows the simulation results of the workspace, the results show that the operating range of the camera increases with the mass it carries. The above results show that this configuration is suitable for filming purposes when the load of the camera mounted on it is large enough but does not exceed the limit of the wire tension. Above we see the most suitable operating space from 30kg to 70kg. Specifications of the camera cable robot for simulation was shown in **Table 1**. **Fig.4** shows the simulating circular trajectory, the values of velocity and the cable length can be determined as in **Fig.5** and the tension of the cables is shown in **Fig. 6**. The simulation results show that the tension force and cable length satisfy the equilibrium and kinetic equations. However, between cables there is a change in tension due to the dynamics of the position as well as the length of the cable.

**Table 1.** Specification of design CDPR

Parameter	Value	Unit
Degrees of freedom	3	
Number of cables	4	
Size of fixed frame	20 x 20 x 10	m x m x m
Limit of load	[30-70]	kg
Limit of tension	[30-500]	N
Speed	0.7	m/s

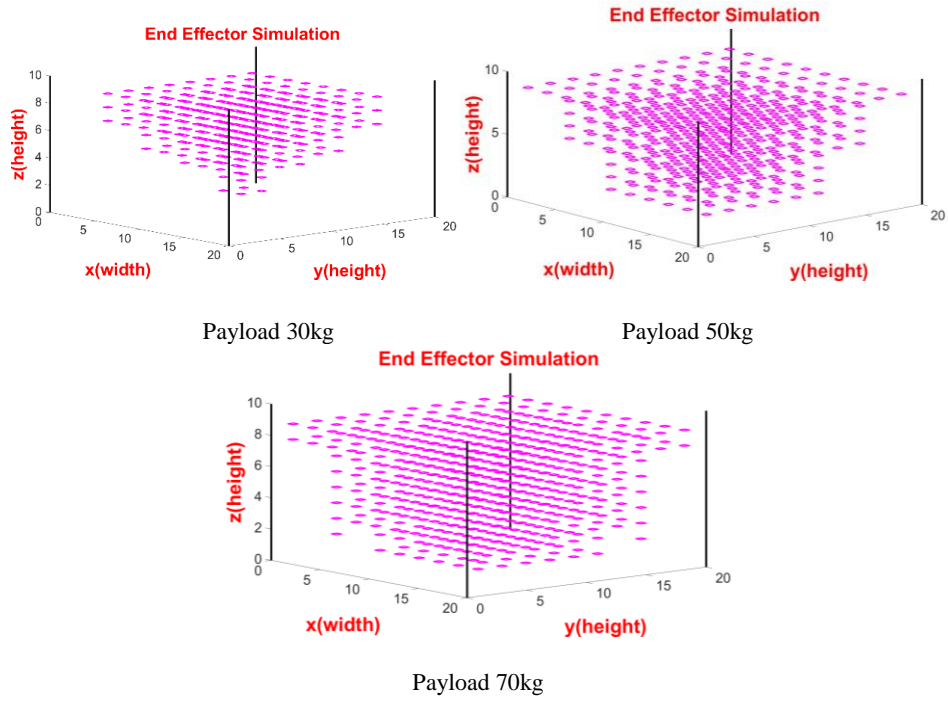


Fig. 3. Workspace of design CDPR for difference payload

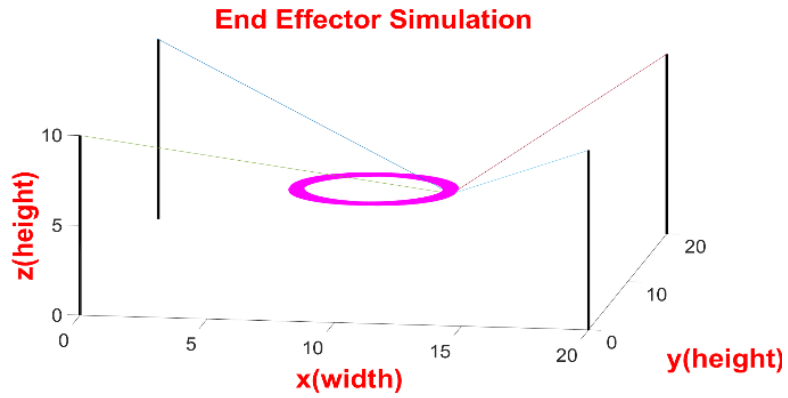
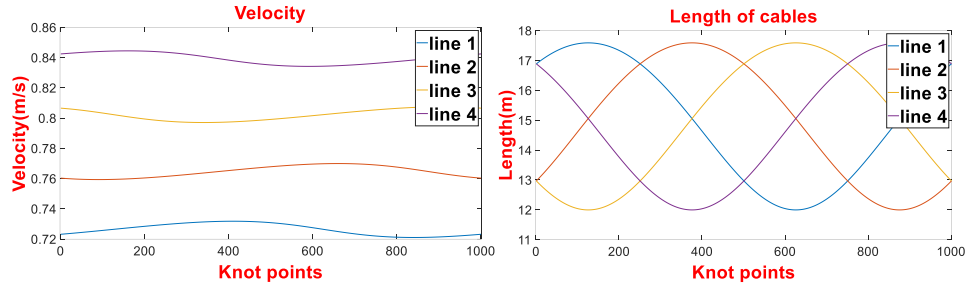
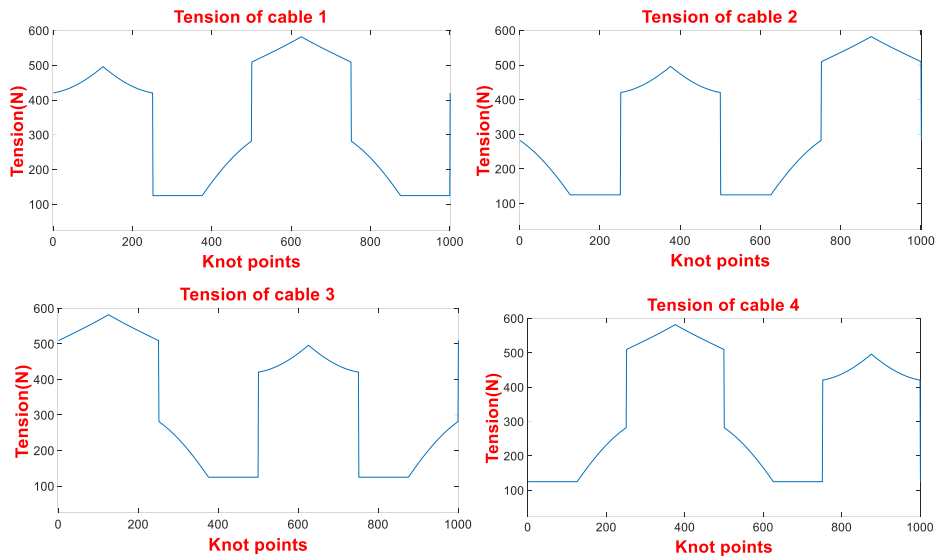


Fig. 4. Simulation of circular trajectory



**Fig. 5.** Cable velocities and cable lengths for circular path



**Fig. 6.** Cable tension in circular orbital motion

The second simulation is a trajectory with several random points in the workspace (see **Fig. 7**). The joint velocity and cable lengths are shown in **Fig. 8** and the tension distribution of the cables in **Fig. 9**. The simulation results show that, the joint velocity and cable lengths are not continuous at node points. The cable tension still tends to change suddenly with a large value like in the case of circular interpolation because the solution of cable tension distribution is performed with the optimal condition of minimum total tension. This can be improved with other tension distribution solutions such as safety tension or pseudo inverse-matrix.

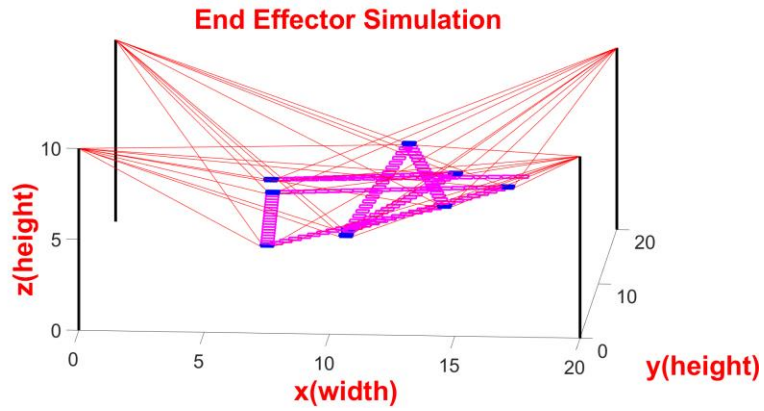


Fig. 7. Simulation of moving several points

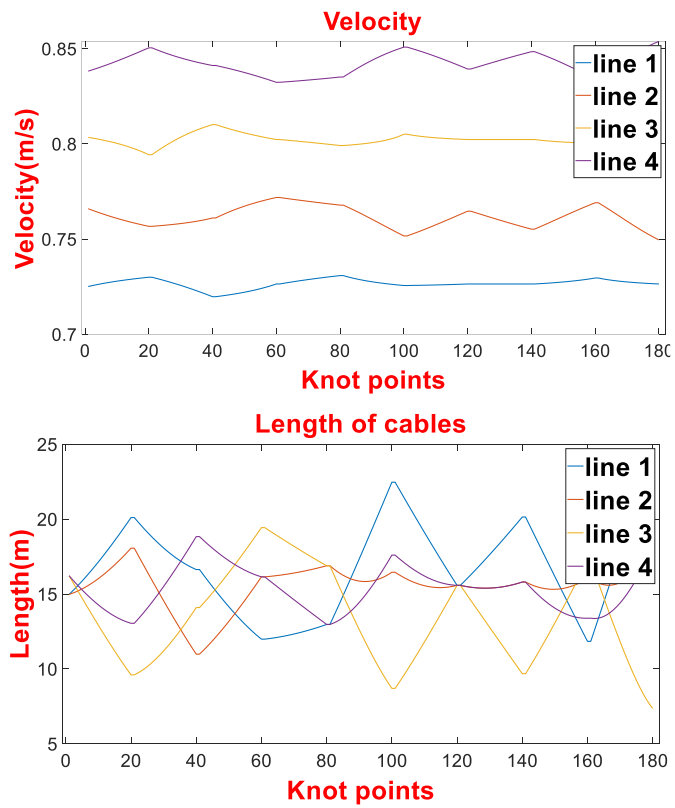


Fig. 8. Simulation of velocity and cable length in any movement

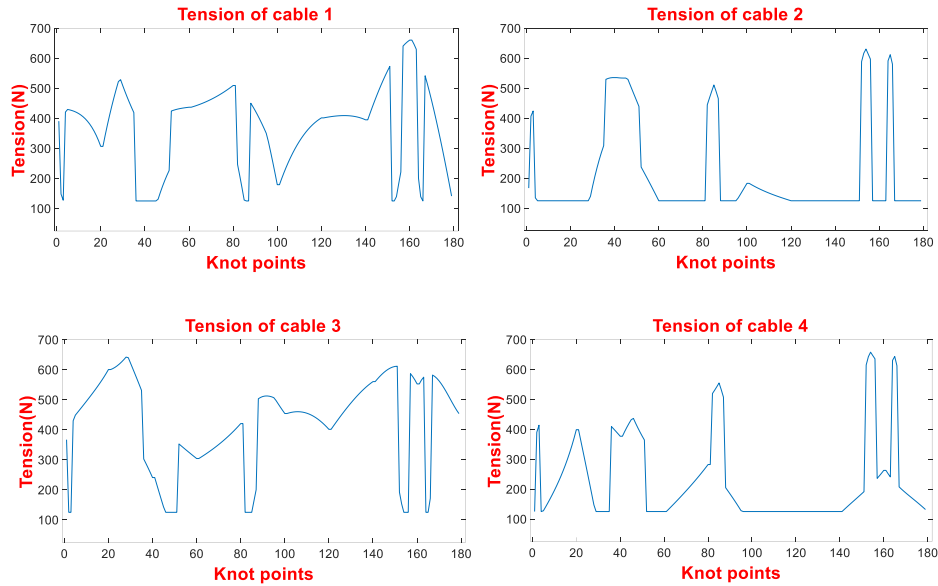


Fig. 9. Cable tension in any movement

## 4 Conclusion

This paper has introduced an overview of automatic video recording cable systems. The system includes a CDPR 3 DOFs and 4 cables to easily move the camera to get the most realistic images. Two optimal algorithms are developed to calculate the cable tension and cable length for the different trajectories based on forward and reverse kinematics problems. The results from simulating complex motions in space have shown us that, in different motion trajectories if the tension and the length of the cables can be precisely controlled, the motion of the camera can be controlled according to the position of the points you desire. This system is modeled with the assumption that the cable tensions are exerted by the gravity of the camera and the mobile platform. But in real applications, the CDPR system is also affected by other external forces such as wind, or cable sagging caused by the mass or elasticity of the cable. Therefore, to increase the feasibility of the system when applying the calculation results to the fabrication and control of CDPR, models representing the effects of interferences need to be integrated into the construction of the controller to improve position accuracy. Two PAN-TILT joints can be integrated into the moving frame to change camera orientation. By developing two optimal kinematic algorithms, we can build a cable robot that works with high precision.

## References

1. S. Kawamura, H. Kino, and C. Won, "High-speed manipulation by using parallel wire-driven robots." *Robotica* 18, no. 1, pp. 13–21, 2000.
2. L. Mikelsons, T. Bruckmann, M. Hiller, and Dieter Schramm, "A realtime capable force calculation algorithm for redundant tendon-based parallel manipulators." In *Robotics and Automation, 2008. ICRA 2008. IEEE International Conference on*, pp. 3869–3874, May 2008.
3. J.S. Albus, R. Bostelman, and N.G. Dagalakis, 1993, "The NIST ROBOCRANE", *Journal of Robotic Systems*, 10(5): 709-724.
4. Bruckmann, T., Pott, A. and Hiller, M., Calculating force distributions for redundantly actuated tendon-based Stewart platforms. In *Advances in Robot Kinematics*, Ljubljana, Slovenia, pp. 403–412, Springer (2006).
5. Baoyan, D., Qiu, Y., Fushun, Z., Zi, B., 2008. Analysis and experiment of the feed cable suspended structure for super antenna. In: *Proceedings of the IEEE/ASME International Conference on Advanced Intelligent Mechatronics*, 2 July to 5 July 2008, Xi'an, China, 329–334.
6. F. Tajdari, N.F. Rad, K. Erfan. "Robust Control of a 3-DOF Parallel Cable Robot using an Adaptive-neuro Fuzzy Interface System". April 2017.
7. Robert L.W II. *Planer Cable-Direct-Driven Robots, Part I: Kinematics and Statics*. Sep 9, 2001 Pittsburgh, PA.
8. K.G.B. Gamagedara. *Mathematical Modeling, Simulation and control of a Spider Cam System*. Galaha Rd, 20400, Sri Lanka. September. 2013.
9. P. Gholami, M.M. Aref, and H.D. Taghirad, "On the control of the KNTU CDRPM: A cable driven redundant parallel manipulator." In *2008 IEEE/RSJ International Conference on Intelligent Robots and Systems*, pp. 2404-2409. IEEE, 2008.
10. P. O. Jong, A. Pott, P. Sukho, S. Y. Ko. "Four – Cable Driven Parallel robot", School of Mechanical Engineering, Chonnam National University, Gwangju, 500-757, Korea.
11. Gouttefarde, M.; Collard, J.-F.; Riehl, N.; Baradat, C. Geometry Selection of a Redundantly Actuated Cable-Suspended Parallel Robot. *IEEE Trans. Robot.* 2015, 31, 501–510.
12. Qian, S.; Zi, B.; Shang, W.-W.; Xu, Q.-S. A Review on Cable-driven Parallel Robots. *Chin. J. Mech. Eng.* 2018, 31, 66.
13. Pusey, J.; Fattah, A.; Agrawal, S.K.; Messina, E. Design and workspace analysis of a 6–6 cable-suspended parallel robot. *Mech. Mach. Theory* 2004, 39, 761–778.
14. Sheng, Z.; Park, J.-H.; Stegall, P.; Agrawal, S.K. Analytic Determination of Wrench Closure Workspace of Spatial Cable Driven Parallel Mechanisms. In *Proceedings of the ASME 2015 International Design Engineering Technical Conferences and Computers and Information in Engineering Conference*, Boston, MA, USA, 2–5 August 2015; Volume 5C.
15. Gouttefarde, M.; Merlet, J.-P.; Daney, D. Determination of the wrench-closure workspace of 6-DOF parallel cable-driven mechanisms. In *Advances in Robot Kinematics*; Springer: Dordrecht, The Netherlands, 2006.
16. Kozak, K.; Zhou, Q.; Wang, J. Static analysis of cable-driven manipulators with non-negligible cable mass. *IEEE Trans. Robot.* **2006**, 22, 425–433.
17. Luan, P.G.; Thinh, N.T. Empirical Quasi-Static and Inverse Kinematics of Cable-Driven Parallel Manipulators Including Presence of Sagging. *Appl. Sci.* 2020, 10, 5318.



18. Bertsimas, D.; Tsitsiklis, J. *Introduction to Linear Optimization*, 1st ed.; Athena Scientific: Belmont, MA, USA, 1997.
17. Murty, K.G. *Linear Programming*, 1st ed.; Wiley: New York, NY, USA, 1983.
19. Irvine, H. *Cable Structures*; MIT Press: Cambridge, MA, USA, 1981.
20. Yingliang, Z.; Chengxian, X. A new trust region dogleg method for unconstrained optimization. *Appl. Math.* **2000**, *15*, 83–92
20. Tho, T.P.; Thinh, N.T. Using a Cable-Driven Parallel Robot with Application in 3D Concrete Printing. *Appl. Sci.* **2021**, *11*, 563

## Bài báo số 7 – Hội nghị quốc tế có ISBN

Quan, Chu Nhat Minh, Tuong Phuoc Tho, and Nguyen Truong Thinh. "Implementation of the Racing Game with the Virtual Reality and Cable Suspended Parallel Robot (CSPR)." In 2022 22nd International Conference on Control, Automation and Systems (ICCAS), pp. 288-291. IEEE, 2022.



## Implementation of the Racing Game with the Virtual Reality and Cable Suspended Parallel Robot (CSPR)

Chu Nhat Minh Quan<sup>1</sup>, Tuong Phuoc Tho<sup>1</sup> and Nguyen Truong Think<sup>2\*</sup>

<sup>1</sup> Department of Mechatronics, Ho Chi Minh City University of Technology and Education,  
Ho Chi Minh City, 70000, Vietnam

<sup>2</sup> College of Technology and Design, University of Economics Ho Chi Minh City – UEH,  
Ho Chi Minh City, 70000, Vietnam (thinknt@ueh.edu.vn)\* Corresponding author

**Abstract:** The paper aims to describe the implementation of racing game named “Arena of Speed” based a Virtual Reality (VR) utilizing a Cable Suspended Parallel Robot (CSPR), a VR headset, and a hand controller. The game “Arena of Speed” is utilized as a special kind of graphical user interface, displaying a computer-generated immersive which can be accessed utilizing hand controller. CSPR can freely manipulate objects in a large workspace with up to 6 degrees of freedom using 8 cables, which activates the proprioceptive sensation of and provides the user with a realistic and exhilarating racing experience. The method of synchronizing the movement of the virtual car with the CSPR is proposed, which includes analyzing and sending data between devices as well as calculating and operating the robot based on game data. The biggest hurdle in replicating the racing experience in real time is that the entire system must work well together and meet the specified deadline. The results of the experiments indicate that the system can provide players playing "Arena of Speed" with the realistic sensation of racing on a racetrack; however, the system occasionally misses its deadline with an acceptably low chance. Besides the entertainment purpose, it may also be ideal for individuals who want to experience driving or racing but do not have the opportunity or condition to do so in real life.

**Keywords:** Cable Parallel Suspended Robot, CSPR, Virtual Reality, Racing game, Cable robot

### 1. INTRODUCTION

It is not disputable that VR technology is revolutionizing the entire gaming industry, resulting in more immersive and engaging gaming experiences. Reinventing experiences is one of the significant aspects of the game culture, as is conquering challenges and conditions that a user would rarely or never face in real life. The ability to activate more than two sensations of the user in a VR game would provide the player with a more immersive experience. In recent years, several VR systems have been proposed to improve this gaming experience[1]. The most widely used system is the handheld controller with the VR headset, which allows users to interact with virtual environments using their hands. Whenever the user touches or triggers objects within the virtual world, these handheld controllers will collect data from built-in buttons or detect hand gestures with multiple sensors and transmit it to the system while the VR headset displays a computer-generated immersive world. This simple VR system was demonstrated in several papers dealing with virtual reality games. The limitation of this system is that it only interacts with the user through the VR headset. In this paper, the VR system utilizing CSPR, VR headset and hand controller is proposed to simulate the gaming experience in “Arena of Speed”. CSPR (Figure 1) is the robot using 8 cables as alternative linkages to manipulate an object (moving platform) in a large workspace. Each cable has one end wrapped around a rotor that is connected to a motor, and the remaining end is linked to the moving platform. The cable is much lighter than other type of linkages that use mechanical structures, therefore the long cables that are sufficiently stiff can be utilized without the employment of a complicated rigid mechanism.



Fig.2. Cable Suspended Parallel Robot employs 8 cables to manipulate the object.

As a result, the moving platform could achieve high accelerations and velocity while working in a large space, which is essential in real-time applications like virtual reality. In the VR field, CSPR can be used to simulate virtual environment experiences based on precise control. The CSPR in the system to generate the real feelings for the user and to improve sensory immersion in VR games. The VR headset is a head-mounted device that can activate the visual and auditory sensations of the user. By displaying a computer-generated immersive and providing the stereo sound, it can improve audiovisual experience of racing the in the arena. The activation of the proprioceptive sensation via the CSPR, in combination with the activation of the visual and auditory sensations via the VR headset, allows the user to experience interactions with the VR car that are identical to those experienced with the real one. The most vital thing is that the entire system must work well together in order to achieve a realistic racing experience.

In order to effectively address this real-time issue, it is critical to optimize both the data transmission process and the computation, operation of CSPR. The game used to simulate with this system must be constructed to work well with the system's hardware. Besides, the game should include two requirements: the first is the capacity to connect and transfer required data between devices in the system, and the second is the ability to display a computer-generated, three-dimensional racing track. And "Arena of Speed" is a VR game specifically developed for CSPR simulation. The game also provides users with an exhilarating gaming experience. It can display a 3D arena racing where users can race against many autonomous cars with different levels of difficulty. The game also has a mixed class racing track with realistic dynamics, as well as an excellent graphic and a vibration, immersive sound environment, making "Arena of speed" suitable for VR experience.

## 2. METHODOLOGY

The system consists of four main components: a hand controller, a virtual reality game, a data receiving and computing application, and a CSPR. The controlling system is shown in **Figure 2**. The system is designed to interface with its hand controller via Bluetooth. When the user presses the built-in button on the keypad, this data is transmitted to the VR game, which updates the car movement in the virtual world. VR headsets, in combination with VR games, play a role in displaying computer-generated immersive, three-dimensional racetracks and providing immersive sound, allowing users to thoroughly immerse themselves in the virtual racetrack[2]. An application for receiving and analyzing data is constructed in LabView and used to calculate the data used to drive the robot once the data has been transmitted to the application. The CSPR is the last component which has a big workspace, a large payload, and a quick movement speed. In the prototype, the platform is positioned and oriented using eight cables.

The CSPR's workspace restrictions hinder it from precisely imitating the movement of the car, hence restricting its mobility is important. Inverse kinematic difficulties for parallel robots are easier to solve than those for series robots.

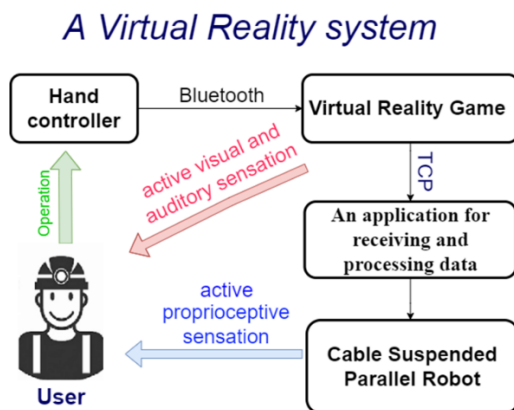


Fig.2. A virtual Reality system in racing game.

Inversely, parallel robots' forward kinematic issues become more complicated. Thus, the inverse kinematic model will be the ideal way for replicating the car's movement, including prismatic and rotation translation, as well as its velocity. The inverse kinematic issue of the CSPR can be described as follows: Given the required load placement and orientation, determine the motor position that fulfills the static and geometric equilibrium conditions. The platform requires three coordinates to establish its position in 3-D space. As a result, there are three unknowns in each joint. Furthermore, the tension of each cable varies. As a result, the 8-cable will have up to 32 unknowns.

## 3. DATA TRANSMISSION

Data transfer protocols play the pivotal role in the real time system like VR. If an inappropriate protocol is used, the simulation may fail or have a significant lag due to the data loss or the speed of the transferring process. Thus the optimum protocol for simulation is one that can transport data quickly while yet ensuring that data loss during transfer is minimized. In this system, two protocols are used: Bluetooth and UDP. Bluetooth is a wireless technology for transmitting data between hand controller and the VR game using UHF radio waves. In the reality test, the data transferred from the hand controller to the VR game was small and simple enough that the transmission speed met the system's requirements. The User Datagram Protocol, which is used to transfer data from a VR game to an application for receiving and processing data, is the second protocol. The UDP has a wide range of installed and used applications, particularly real-time applications like this VR system. The programming of this protocol is challenging despite the fact that it is quite simple because it must account for how to set, assign port numbers, and execute addresses. LabView makes the setup process for VR systems a little easier. On the other hand, the data transferred from the VR game to the receiving and computing application is more complex and large. It has 12 parameters, which are updated once every millisecond and are divided into six for translation and six for rotation. UDP is the best protocol for this because it can transfer this large amount of data quickly. Although UDP occasionally loses some data packages in the reality test, the rate is still acceptable.

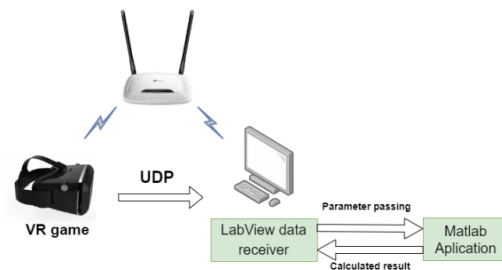


Fig.3. Schematic of data transmission.

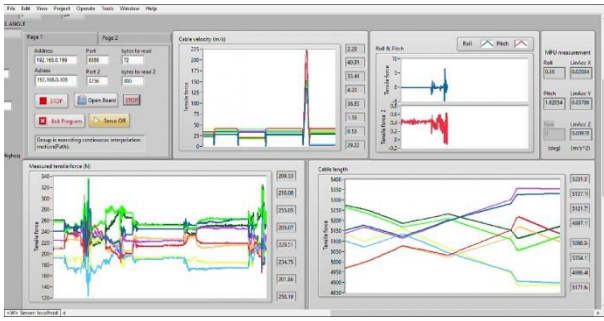


Fig.4. Application interface based on Labview.

And finally, the data transmitted to the calculating application constructed in Lab-VIEW and Matlab [3]. In the reality test the proposed transfer method has little latency in simulation. Since the data is transferred one direction from the game to the robot instead of being transferred from robot to the game. The biggest advantage of this transfer method is that it easy to simulation because Unity engine can export the enough parameters used for simulation. On the other hand, collecting data from the cage and then simulate it in the Unity will be much more complicated.

### 3. GAME SYSTEM DESIGN

The left and right joysticks of the controller can be used by the player to control the car in Arena of Speed. Translation of the moving forward and reversing car is controlled by the left joystick. On the other hand, the car's rotation, including turning left and right, is controlled by the right joystick. In addition, pressing button L1 Shoulder will take you back to the Main Menu screen while pressing button R1 Shoulder will restart the game. Each waypoint in the waypoint system is a coordinate in 3D space that designates a significant location on the racetrack. Due to this system's efficiency and simplicity, many early racing video games utilized car. In Arena Of Speed, way-points are stored as a sorted list of positions in 3D space using the List generic class. This list of way-points is read into the game's software system, which iterates through the list until the computer-controlled car has passed each waypoint. When the game-controlled car is found to be within a certain distance of its current waypoint, the game system only moves on to the next waypoint in the list. The game system conducts a series of vector calculations to determine how much steering is required to turn the car in the direction of its current waypoint. These calculations are based on an initial vector created by both the position of the current waypoint and the current position of the car itself. This series of calculations produces an output vector, which provides the bases for the steering and braking output levels of the car. However, during development of the game, it was found that using only the method of waypoints with vector calculations was ineffective in controlling the car. Before sending data to Labview, must processing data for simulation shown in Figure 4. There are five parameters needing to be processed. The difference distance and velocity in the horizontal dimension of the road, the angle and the angular velocity

of vertical axis, and the acceleration to the forward

## 4. EXPERIMENTS AND DISCUSSIONS

The structure of CSPR for VR game has dimensions of length 5 meters, wide 3 meters, and height 3 meters. Eight passive pulleys direct the cables from the winches to the cable departure point when they are wound on 100mm motorized winches [4]. The game must meet a number of requirements in order for the system to operate stably, guarantee user safety, and provide users with the most realistic experience possible. The robot may cause serious injury to the user during the experience, therefore the requirements of CSRR systems, which are used or work directly with humans, are always required to ensure human safety. Experimentally with its configuration, the robot can operate with a large range (Shown in **Table 1**). Determining the "safe workspace" for robots is extremely necessary, especially for robots with parallel kinematic structures; Because during operation, the tension in all 8 cables is extremely large, so if the robot is unstable and there is a problem, it is likely to cause injury to the user. A lot of experiments on robots have been conducted to determine this "safe workspace". The game "Arena of Speed" is implemented based on this "safe workspace", and the speed of the virtual car with "safe workspace".

Table 1. Technical parameters of CSPR

Characteristic	Values
Maximum velocity	760m/s
Maximum acceleration	7m/s <sup>2</sup>
Maximum load	100 kg
Workspace	4000x4000x2000mm
Degree of Freedom	6

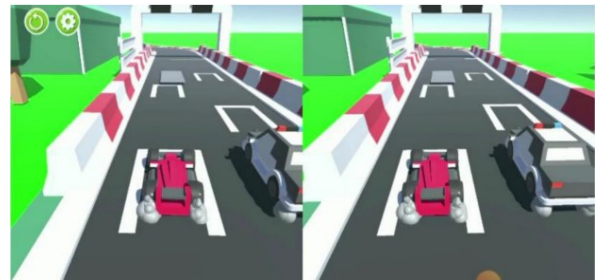


Fig. 5. Arena of Speed.



Fig.6. Experiments for VR Racing game.

Accuracy is one of the most important variables to consider for building and implementing a CSPR. The cable's vibrations and sagging limit positioning accuracy in large workspace[5]. Therefore, the dynamic modeling of CDSP should be consider in applications using VR. CSPR's accuracy can be limited by design tolerance, manufacturing error, thermodynamic inaccuracy, control responsiveness, and other parameters. Suppose, we set the coordinate axis of the car as shown below. The virtual reality system is for simulating 2 degrees of freedom (DOFs) of the car including translation along the x-axis and rotation around the z-axis. In addition, a DOF of rotation in y axis is used to create an additional feeling of acceleration or deceleration for user. Because in reality, when the car starts to accelerate, the driver tends to fall backwards and vice versa when the car brakes hard, it will tend to fall forward, this phenomenon is caused by the force of inertia. It can be seen quite clearly in high-acceleration vehicles. First to simulate the x-axis of the car, it is necessary to determine the center of the track. The robot use this center line as a landmark to determine whether the current car is going to the left or right and how much distance is going. By convention, when the robot goes to the left, the output parameter will bring a negative sign and vice versa to the right will output a positive number, the parameter of magnitude is the distance from the center line to the left or right side. In the game "Arena of Speed" (**Figure 5**), the car will go through a lot of road segments with different shapes and sizes, so to determine the center line, we need to follow two steps: One is to determine the vehicle is entering the segment. What is the shape of the road, the second is to determine the centerline of each road segment and calculate the required distance. On the robot side, it also uses the system center as a landmark and uses the same sign convention as the virtual car. Experimental results show that the robot can simulate the horizontal movement of the vehicle well like **Figure 6**. On the other hand, when reversing direction to the left and to the right, the car rotates in the z axis. To simulate the z axis, we will use vector, whose direction is along the track and the direction from the starting position to the destination position. By scalar multiplication of the vehicle's current z unit vector and the unit vector used as a reference, the vehicle's current rotation angle can be deduced. Experimental results show that the robot can simulate the rotation of the vehicle well. The controlling signals are sent to the cable robot through a program written on LabView. To be able to operate the CSPR, it is necessary to solve the problem of inverse kinematics of the CSPR in order to convert the car's coordinate and velocity into controlling signals, which are sent to 8 motors to execute the work of CSPR. After the signal from the game is sent, the system check signals within the CSPR's "safe workspace" to ensure user's safety. Experiments show that using games can provide useful data to players in the virtual world that is not as easy to obtain as playing in the real world. We can absolutely say that playing games in the virtual world gives players a real feeling that when playing normally does not have.

## 5. CONCLUSIONS

In general, the results of the experiments show that the system can provide "Arena of Speed" players a genuine sense of racing on a racetrack; yet, the algorithm occasionally misses its deadline with an acceptably low probability. In this study, some conclusions were drawn as follows:

- The result gives me a pretty good interaction between CSPR and users in the virtual environment.
- The CSPR system has provided users with a real feelings when playing the game "Arena of Speed".
- The CSPR system and the game "Arena of Speed" have worked together to create interactive tasks.

## REFERENCES

- [1] Katzourin, Michael, et al. "Swordplay: Innovating game development through VR." *IEEE Computer Graphics and Applications* 26.6 (2006): 15-19.
- [2] Makarov, Ilya, et al. "First-person shooter game for virtual reality headset with advanced multi-agent intelligent system." *Proceedings of the 24th ACM international conference on Multimedia*. 2016.
- [3] Liu, Wenjing, Zhi Li, and Jianguo Wang. "Real-time data analysis and processing based on UDP communication platform based on LabVIEW." *Journal of Physics: Conference Series*. Vol. 1213. No. 2. IOP Publishing, 2019.
- [4] Duy, Le Duc, and Nguyen Truong Thinh. "A Thoroughly Approach: Pulley Kinematic, Actuator Dynamic and Stiffness on Cable Suspended Parallel Robots." *Regional Conference in Mechanical Manufacturing Engineering*. Springer, Singapore, 2022.
- [5] Tho, Tuong Phuoc, and Nguyen Truong Thinh. "Analysis and Evaluation of CDPR Cable Sagging Based on ANFIS." *Mathematical Problems in Engineering* 2021 (2021).

Bài báo số 8 – Bài báo đăng trên tạp chí khoa học chuyên ngành trong nước (Trong danh mục được tính điểm của HĐCDGSNN)

Dao, Cong Hoang Kha, Phuoc Tho Tuong, Ngoc Duc Vu, and Minh Nhat Nguyen. "On Research of Cable Tension Distribution Algorithm for Four Cables-Three DOF Planar Cable-Driven Parallel Robot." Journal of Technical Education Science 78B (2023): 8-17.

Link: <https://jte.edu.vn/index.php/jte/article/view/1312>





## On Research of Cable Tension Distribution Algorithm for Four Cables - Three DOF Planar Cable-Driven Parallel Robot

Cong Hoang Kha Dao, Phuoc Tho Tuong\*, Ngoc Duc Vu, Minh Nhat Nguyen

Ho Chi Minh City University of Technology and Education, Vietnam

\*Corresponding author. Email: [thotp@hcmute.edu.vn](mailto:thotp@hcmute.edu.vn)

### ARTICLE INFO

Received: 21/11/2022  
Revised: 13/01/2023  
Accepted: 23/02/2023  
Published: 28/08/2023

### KEYWORDS

Tension distribution algorithm;  
Cable-driven parallel robot;  
Quadratic programming;  
Over-constraint CDPR;  
3 DOF parallel robot.

### ABSTRACT

One of the main concerns in controlling the cable-driven parallel robot (CDPR) mechanism is dealing with the distribution of tension on each cable, which is critical to the operation of the entire cable system. It can be said that adjusting the cable tension will determine the power consumption of the motors and the stiffness of the structure. Therefore, the problem that needs to be solved is how to handle the cable tension when the end-effector moves throughout the entire workspace. The tension of each cable needs to be adjusted properly to ensure it remains the same. Moment and force act in a static state, keeping the kinematic position of the end moving platform from being deflected and the main purpose is to ensure that the robot achieves a rigid state and eliminates vibration when moving. Because of that essential demand, this article will refer to the Quadratic programming algorithm to solve the problem of tension distribution for the Planar Cable-Driven Parallel Robot consisting of 4 cables with 3 degrees of freedom. This article will be the foundation for applying this algorithm to an 8-cable robot with 6 degrees of freedom (Spatial Cable-Driven Parallel Robot for example). At the same time, in this article, the simulation results for the algorithm will also be presented in this paper.

Doi: <https://doi.org/10.54644/jte.78B.2023.1312>

Copyright © JTE. This is an open access article distributed under the terms and conditions of the [Creative Commons Attribution-NonCommercial 4.0 International License](https://creativecommons.org/licenses/by-nc/4.0/) which permits unrestricted use, distribution, and reproduction in any medium for non-commercial purpose, provided the original work is properly cited.

## 1. Introduction

Cable-driven parallel robot (CDPR) is a type of parallel robot that uses the cable to control the end effector (E-E) instead of using rigid joints. One of the main advantages of CDPR is the ability to create a large workspace while maintaining high stiffness and low inertness. Low cost for large workspaces is also a notable advantage [1]. Thanks to the advantages of CDPR, it can be used in many research fields like rehabilitation, haptic, movement simulation, and 3D printing..... The feature of tension distribution for CDPRs is one of the most considerations in designing, and controlling the problem of CDPRs. Tension involves issues such as system balancing, feasible workspace determination, actuator power, mechanism stiffness, trajectory movement, and controller design [2]. Many proposed methods of tension distribution have been conveyed in the research of CDPR, Tuong Phuoc Tho and Nguyen Truong Thinh [3] used linear optimization to find the solution of tension distribution for the CDPR used for 3D concrete printing, under high-load working conditions and long working hours, reducing power consumption is paramount to save energy, because printing velocity is slow, dynamic effects are ignored. Besides, Cong Bang Pham et al [4] also used the “Linear Optimization” algorithm to build the calculation of cable tension. So-Ryeok Oh and Sunil K. Agrawal [5] applied the proposed “Linear Optimization” method to find cable tension for PM-CDPR form, the results were simulated successfully. Based on these models, all authors also develop an algorithm to control the robot by providing negative tension. Soon after, Per Henrik Borgstrom et al. [6] made improvements to the “Linear Programming” algorithm to simplify the calculation process applied for tension distribution. In the specific case where the positive tension aggregation method has been selected to finalize the optimal solutions and the optimal criterion.

Similar to the Linear Programming algorithm, the Non-linear Programming algorithm has been applied to find the tension distribution of the cables. The disadvantage of Linear Programming is the discontinuous tension distribution along the joint trajectory. A new Quadratic Programming method has



each formula. The origin is at point O, and applying geometric knowledge we can deduce the general formula to calculate the length of each cable:

$$\begin{cases} l_1^2 = x_A^2 + (y_{\max} - y_A)^2 \\ l_2^2 = (x_{\max} - x_B)^2 + (y_{\max} - y_B)^2 \\ l_3^2 = (x_{\max} - x_C)^2 + x_C^2 \\ l_4^2 = x_D^2 + y_D^2 \end{cases} \quad (1)$$

For solving the (1) using parameter  $\theta$  and coordinate of G ( $x_G, y_G$ ) which is the E-E position, we have to find the relation between points A ( $x_A, y_A$ ), B ( $x_B, y_B$ ), C ( $x_C, y_C$ ), D ( $x_D, y_D$ ) and pose  $\theta, x_G, y_G$

Finally, the set of equations that express inverse kinematic:

$$\begin{cases} l_1^2 = (x_G - l_{56} \cos(\theta - \alpha))^2 + (y_{\max} - y_G + l_{56} \sin(\theta - \alpha))^2 \\ l_2^2 = (x_{\max} - x_G - l_{56} \cos(\theta + \alpha))^2 + (y_{\max} - y_G - l_{56} \sin(\theta + \alpha))^2 \\ l_3^2 = (x_{\max} - x_G - l_{56} \cos(\theta - \alpha))^2 + (y_G + l_{56} \sin(\theta - \alpha))^2 \\ l_4^2 = (x_G - l_{56} \cos(\theta + \alpha))^2 + (y_G - l_{56} \sin(\theta + \alpha))^2 \end{cases} \quad (2)$$

where  $\alpha = \arctan\left(\frac{l_6}{l_5}\right)$  and  $l_{56} = \frac{\sqrt{l_5^2 + l_6^2}}{2}$

## 2.2. Forward kinematic

Forward kinematics is the process of calculating the position and orientation of the E-E knowing all the matching joint's variables, namely the lengths of the cables for the configuration of the CDPR type [12].

To calculate the position and orientation of E-E from the set of matching joint's values, for the method proposed in this article, we need to deduce from the system of inverse kinematics equations, based on the existing system of inverse kinematic equation (2), we will obtain a new system of equations that satisfies the requirements of forward kinematics.

Using the set of inverse kinematic equations (2), we can solve the forward kinematics. After withdrawing  $\theta, x_G$  and  $y_G$ , which are a set of parameters defining the position and orientation of E-E, from equations (2), we can deduce the new set of equations. (Notably, sometimes a symbol of  $\sin(x)$  and  $\cos(x)$  will be short as  $s_x$  and  $c_x$ )

After solving, a set of forward kinematic equations can be expressed as

$$\theta = \text{atan} \frac{s_\theta}{\sqrt{1 - s_\theta^2}}; x_G = \frac{\sigma_1 - \sigma_2}{\sigma_3}; y_G = \frac{\sigma_4 - \sigma_5}{\sigma_6} \quad (3)$$

where  $s_\theta = \frac{l_1^2 + l_3^2 - (l_2^2 + l_4^2)}{-4l_{56}(x_{\max} s_\alpha - y_{\max} c_\alpha)}$ . The symbols  $\sigma_1, \sigma_2, \sigma_3, \sigma_4, \sigma_5$  and  $\sigma_6$  are used as substitutes. The values of these are expressed as

$$\begin{aligned}\sigma_1 &= (l_1^2 - l_3^2 + x_{\max}^2 - y_{\max}^2 - 2x_{\max}l_{56}c_{(\theta-\alpha)} - 2y_{\max}l_{56}s_{(\theta-\alpha)})(-2y_{\max} + 4l_{56}s_{(\theta+\alpha)}) \\ \sigma_2 &= (-2y_{\max} - 4l_{56}s_{(\theta-\alpha)})(l_2^2 - l_4^2 - x_{\max}^2 - y_{\max}^2 + 2y_{\max}l_{56}s_{(\theta+\alpha)} + 2x_{\max}l_{56}c_{(\theta+\alpha)}) \\ \sigma_3 &= (2x_{\max} - 4l_{56}c_{(\theta-\alpha)})(-2y_{\max} + 4l_{56}s_{(\theta+\alpha)}) - (-2y_{\max} - 4l_{56}s_{(\theta-\alpha)})(4l_{56}c_{(\theta+\alpha)} - 2x_{\max}) \\ \sigma_4 &= (2x_{\max} - 4l_{56}c_{(\theta-\alpha)})(l_2^2 - l_4^2 - x_{\max}^2 - y_{\max}^2 + 2y_{\max}l_{56}s_{(\theta+\alpha)} + 2x_{\max}l_{56}c_{(\theta+\alpha)}) \\ \sigma_5 &= (4l_{56}c_{(\theta+\alpha)} - 2x_{\max})(l_1^2 - l_3^2 + x_{\max}^2 - y_{\max}^2 - 2x_{\max}l_{56}c_{(\theta-\alpha)} - 2y_{\max}l_{56}s_{(\theta-\alpha)}) \\ \sigma_6 &= (2x_{\max} - 4l_{56}c_{(\theta-\alpha)})(-2y_{\max} + 4l_{56}s_{(\theta+\alpha)}) - (-2y_{\max} - 4l_{56}s_{(\theta-\alpha)})(4l_{56}c_{(\theta+\alpha)} - 2x_{\max})\end{aligned}$$

### 3. Limitation for the orientation of end-effector

At each position of E-E, the angle  $\theta$  will pose different minimum and maximum limitation values. These limit values will never be fixed during the E-E movement in the robot's workspace. When examining in the simulation all the positions that the robot can reach, we can illustrate the concept of orientation limitation.

The limiting angle  $\theta$  is calculated when we examine each cable length or each joint's value of the robot during operation. Each cable exists  $\gamma$ , which is the angle that was formed in Figure 2. For this robot's configuration, it will consist of 4 angles  $\gamma$  (known as  $\gamma_1, \gamma_2, \gamma_3$  and  $\gamma_4$ ). We can assume that  $\theta_{lim}$  the angle  $\theta$  limitation appeared when  $\gamma$  reach  $180^\circ$ .  $\theta_{lim}$  can be considered as maxima limitation angle or minima limitation angle or none of them. For this assumption, calculation  $\theta_{lim}$  required some comparisons to choose angles  $\theta_{lim}$  to set  $\theta$  as maxima ( $\theta_{max}$ ) and minima ( $\theta_{min}$ ).

With a random position of E-E on the workspace of the robot, based on this theory, there will be four angles  $\theta_{lim}$  ( $\theta_{lim1}, \theta_{lim2}, \theta_{lim3}$  and  $\theta_{lim4}$ ) for this robot's configuration.

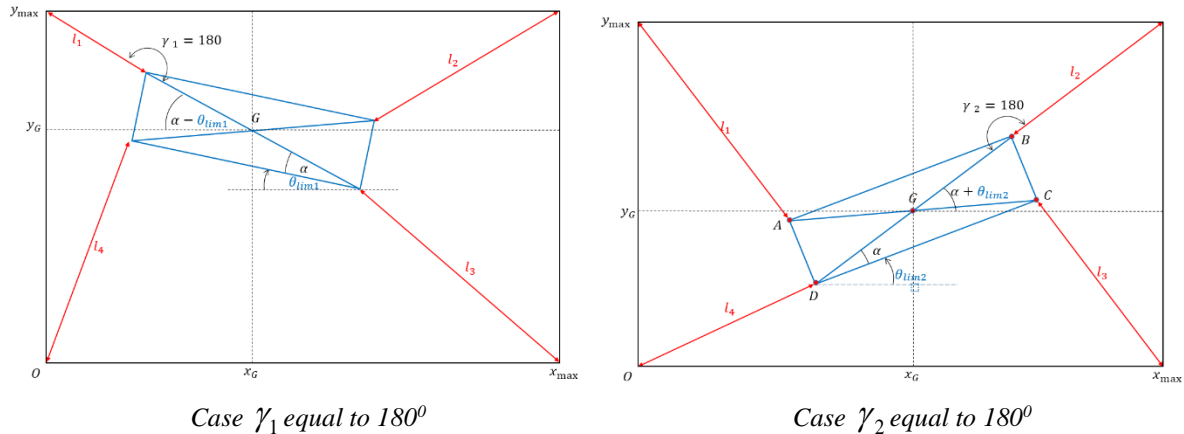


**Figure 2.** Rotational limitation

From the above pose, examples are shown in Figure 2, there are four cases where respectively angles  $\gamma$  equal to  $180^\circ$ . For each case, we can be obtained a formula for the rotational limitations as

$$\begin{cases} \theta_{lim1} = \alpha - \tan^{-1} \frac{y_{\max} - y_G}{x_G}; \theta_{lim2} = \tan^{-1} \frac{y_{\max} - y_G}{x_G} - \alpha \\ \theta_{lim3} = \alpha - \tan^{-1} \frac{y_G}{x_{\max} - x_G}; \theta_{lim4} = \tan^{-1} \frac{y_G}{x_G} - \alpha \end{cases} \quad (4)$$

Maxima and minima rotational angles  $\theta$  that E-E can be created by choosing the values which have been compared of  $\theta_{lim1}, \theta_{lim2}, \theta_{lim3}$  and  $\theta_{lim4}$ . By eliminating the maximum and minimum values of

this set, select two values  $\theta_{lim}$  that remain to set as  $\theta_{max}$  and  $\theta_{min}$ . Therefore, at each position of E-E, the value  $\theta$  after calculation must satisfy the condition.

$$\theta \in [\theta_{min}, \theta_{max}] \quad (5)$$

The comparison between all  $\theta_{lim}$  values will always change during operation. Due to this calculation, verification, and selection of the limitations  $\theta$  should depend on the position of E-E.

#### 4. Cable tension distribution algorithm

##### 4.1. Problem in cable tension distribution

Forces act on the E-E shown in Figure 3. The problem of cable tension distribution is to determine the value  $T_i$  with  $i = 1, 2, 3, 4$  corresponding to the number of cables. The net of forces created by the tension of each cable can be described in the following form.

$$\mathbf{A}\boldsymbol{\tau} = \mathbf{w}_p \quad (6)$$

where  $\mathbf{A} \in \mathbf{R}^{3 \times 4}$  is the structure matrix  $\mathbf{A} = \begin{bmatrix} \mathbf{u}_1 & \mathbf{u}_2 & \mathbf{u}_3 & \mathbf{u}_4 \\ \mathbf{d}_1 \times \mathbf{u}_1 & \mathbf{d}_2 \times \mathbf{u}_2 & \mathbf{d}_3 \times \mathbf{u}_3 & \mathbf{d}_4 \times \mathbf{u}_4 \end{bmatrix}$ , the vector

$\boldsymbol{\tau} = [T_1 \ T_2 \ T_3 \ T_4]^T \in \mathbf{R}^{4 \times 1}$  contains values of the tension force of all cables, and  $\mathbf{w}_p = [\mathbf{F} \ \boldsymbol{\eta}]^T \in \mathbf{R}^{3 \times 1}$  is the matrix which describes the net force created by the tension force of all cables affect to E-E at point G,  $\mathbf{F} = [\mathbf{F}_x \ \mathbf{F}_y]^T \in \mathbf{R}^{2 \times 1}$  is external force, and  $\boldsymbol{\eta} = M_z \in \mathbf{R}^{1 \times 1}$  is the momentum about Oz direction. From this robot's configuration, cables could only cause the tensile force which leads to the vector  $\boldsymbol{\tau}$  as a non-negative vector.

Note that the vector  $\vec{u}_i$  in Figure 3 is the unit vector of cable  $i$  presented  $[u_i^x \ u_i^y]^T \in \mathbf{R}^{2 \times 1}$  and the vector  $\vec{d}_i$  is the relative position vector from G to  $A_i$  can be presented as  $[d_i^x \ d_i^y]^T \in \mathbf{R}^{2 \times 1}$ . Equation (6) is more detail presented as:

$$\begin{bmatrix} u_1^x & u_2^x & u_3^x & u_4^x \\ u_1^y & u_2^y & u_3^y & u_4^y \\ d_1^x u_1^y + d_1^y u_1^x & -d_2^x u_2^y + d_2^y u_2^x & -d_3^x u_3^y - d_3^y u_3^x & d_4^x u_4^y - d_4^y u_4^x \end{bmatrix} \begin{bmatrix} T_1 \\ T_2 \\ T_3 \\ T_4 \end{bmatrix} = \begin{bmatrix} F_x \\ F_y \\ M_z \end{bmatrix} \quad (7)$$

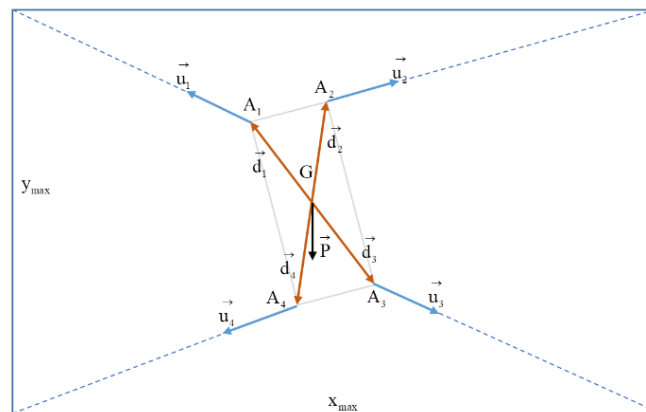


**Figure 3.** Force analysis

The tension force of each cable will be limited by two values of minimum tension force  $\underline{\tau} \in \mathbf{R}^{4 \times 1}$  and maximum  $\bar{\tau} \in \mathbf{R}^{4 \times 1}$ , these binding conditions can be expressed as:

$$0_m \leq \underline{\tau} \leq \tau \leq \bar{\tau} \quad (8)$$

where  $0_m \in \mathbf{R}^{4 \times 1}$  is a vector with the value 0.

The problem posed in this paper is to determine how the tension forces of each cable are distributed but still satisfy both (8) and (7).

For this problem, a solution proposed is to select some constraints that can be relaxed. Specifically, for the constraint on the tension limit (8), we can hardly interfere as this shall not be violated to make sure all tensile forces are always positive. But the constraint on the balance of external force (6) is relaxable. A matrix containing the slack variables is proposed to interfere with this constraint, then equation (6) converts to

$$\mathbf{A}\boldsymbol{\tau} + \mathbf{s} = \mathbf{w}_p \quad (9)$$

where  $\mathbf{s} = [s_1 \quad s_2 \quad s_3] \in \mathbf{R}^{3 \times 1}$  is the matrix containing the slack variables  $s_1$ ,  $s_2$  and  $s_3$  to be added. To ensure the constraint at (9) is always satisfied, it is necessary to calculate to optimize the values  $\mathbf{s}$  in the objective function of the optimization problem. Based on available tension distribution algorithms, the problem of Linear Programming and Quadratic Programming is the most suitable and adaptive model to solve this problem.

#### 4.2. Quadratic programming – cable tension distribution algorithm

A basic Quadratic Programming problem is proposed and applied to solve the problem of cable tension distribution for the Planar-CDPR robot. There have been many studies and experiments to compare the efficiency between linear programming and quadratic programming for this problem [13-15]. The calculation results of quadratic programming are preferred because of ensuring the continuity of the whole system. The optimal equation containing slack variables and cable tension distribution quantities has the following form.

$$\text{Minimize: } \mathbf{s}^T \mathbf{D}_1 \mathbf{s} + (\boldsymbol{\tau} - \boldsymbol{\tau}^*)^T \mathbf{D}_2 (\boldsymbol{\tau} - \boldsymbol{\tau}^*) \quad (10)$$

$$\text{Subject to: } \mathbf{A}\boldsymbol{\tau} + \mathbf{s} = \mathbf{w}_p \text{ and } 0_m \leq \underline{\tau} \leq \tau \leq \bar{\tau}$$

$$\text{Where } \mathbf{D}_1 = \begin{bmatrix} d_{11} & 0 & 0 \\ 0 & d_{12} & 0 \\ 0 & 0 & d_{13} \end{bmatrix}, \mathbf{D}_2 = \begin{bmatrix} d_{21} & 0 & 0 & 0 \\ 0 & d_{22} & 0 & 0 \\ 0 & 0 & d_{23} & 0 \\ 0 & 0 & 0 & d_{24} \end{bmatrix}, \boldsymbol{\tau}^* = [\mathbf{T}^* \quad \mathbf{T}^* \quad \mathbf{T}^* \quad \mathbf{T}^*]^T$$

With  $\mathbf{D}_1 \in \mathbf{R}^{3 \times 3}$  and  $\mathbf{D}_2 \in \mathbf{R}^{4 \times 4}$  are weight matrices, which were expressed in the form of diagonal matrices ( $d_{11}$ ,  $d_{12}$ ,  $d_{13}$ ,  $d_{21}$ ,  $d_{22}$ ,  $d_{23}$  and  $d_{24}$  are weight values). Vector  $\boldsymbol{\tau}^* \in \mathbf{R}^{4 \times 1}$  contains the target values for tension force  $\mathbf{T}^*$ , this value decides the high or low level of tension distribution for each cable.

By selecting  $\boldsymbol{\tau}^* \leq \underline{\tau}$ , the desired tension force with minimum stiffness and power is reached. By selecting  $\boldsymbol{\tau}^* = \frac{\underline{\tau} + \bar{\tau}}{2}$ , the ideal tension force with relative stiffness and power is obtained. Selecting  $\boldsymbol{\tau}^* \geq \bar{\tau}$ , the solution will lead to the highest tension distribution as well the highest stiffness.

The magnitude of every value  $\mathbf{D}_1$  should be chosen higher than values in  $\mathbf{D}_2$ . For each time compute the optimal distribution force, we will able to determine values of slack variables, the aim that

they will asymptote to zero. However, we can easily set those slack variables by selecting suitable weight matrices  $D_1$  and  $D_2$ . The final quadratic optimization problem can be expressed as:

$$f_{\min} = \begin{bmatrix} s_1 \\ s_2 \\ s_3 \end{bmatrix}^T \begin{bmatrix} d_{11} & 0 & 0 \\ 0 & d_{12} & 0 \\ 0 & 0 & d_{13} \end{bmatrix} \begin{bmatrix} s_1 \\ s_2 \\ s_3 \end{bmatrix} + \begin{bmatrix} T_1 - T^* \\ T_2 - T^* \\ T_3 - T^* \\ T_4 - T^* \end{bmatrix}^T \begin{bmatrix} d_{21} & 0 & 0 & 0 \\ 0 & d_{22} & 0 & 0 \\ 0 & 0 & d_{23} & 0 \\ 0 & 0 & 0 & d_{24} \end{bmatrix} \begin{bmatrix} T_1 - T^* \\ T_2 - T^* \\ T_3 - T^* \\ T_4 - T^* \end{bmatrix} \quad (11)$$

From this quadratic programming equation, we will expand and transform it into a general form, by following the steps. First, assume that

$$\mathbf{X} = [x_1 \ x_2 \ x_3 \ x_4 \ x_5 \ x_6 \ x_7 \ x_8]^T = [s_1 \ s_2 \ s_3 \ T_1 \ T_2 \ T_3 \ T_4 \ 1]^T$$

Finally, the general quadratic optimization form can be written as.

$$f_{\min}(\mathbf{X}) = \mathbf{X}^T \begin{bmatrix} d_{11} & 0 & 0 & 0 & 0 & 0 & 0 & 0 \\ 0 & d_{12} & 0 & 0 & 0 & 0 & 0 & 0 \\ 0 & 0 & d_{13} & 0 & 0 & 0 & 0 & 0 \\ 0 & 0 & 0 & d_{21} & 0 & 0 & 0 & 0 \\ 0 & 0 & 0 & 0 & d_{22} & 0 & 0 & 0 \\ 0 & 0 & 0 & 0 & 0 & d_{23} & 0 & 0 \\ 0 & 0 & 0 & 0 & 0 & 0 & d_{24} & 0 \\ 0 & 0 & 0 & 0 & 0 & 0 & 0 & 4T^{*2} \end{bmatrix} \mathbf{X} + \begin{bmatrix} 0 \\ 0 \\ 0 \\ -2T^* \\ -2T^* \\ -2T^* \\ -2T^* \\ 0 \end{bmatrix} \mathbf{X} \quad (12)$$

Subject to

$$\begin{bmatrix} 1 & 0 & 0 & u_1^x & u_2^x & u_3^x & u_4^x & 0 \\ 0 & 1 & 0 & u_1^y & u_2^y & u_3^y & u_4^y & 0 \\ 0 & 0 & 1 & d_1^x u_1^y + d_1^y u_1^x & d_1^x u_1^y + d_1^y u_1^x & -d_3^x u_3^y - d_3^y u_3^x & d_4^x u_4^y - d_4^y u_4^x & 0 \\ 0 & 0 & 0 & 0 & 0 & 0 & 0 & 1 \end{bmatrix} \mathbf{X} = \begin{bmatrix} F_x \\ F_y + P \\ M_z \\ 1 \end{bmatrix} \quad (13)$$

And

$$\begin{bmatrix} 0 & 0 & 0 & -1 & 0 & 0 & 0 & 0 \\ 0 & 0 & 0 & 0 & -1 & 0 & 0 & 0 \\ 0 & 0 & 0 & 0 & 0 & -1 & 0 & 0 \\ 0 & 0 & 0 & 0 & 0 & 0 & -1 & 0 \\ 0 & 0 & 0 & 1 & 0 & 0 & 0 & 0 \\ 0 & 0 & 0 & 0 & 1 & 0 & 0 & 0 \\ 0 & 0 & 0 & 0 & 0 & 1 & 0 & 0 \\ 0 & 0 & 0 & 0 & 0 & 0 & 1 & 0 \end{bmatrix} \mathbf{X} \leq \begin{bmatrix} -\bar{\tau} \\ -\bar{\tau} \\ -\bar{\tau} \\ -\bar{\tau} \\ \bar{\tau} \\ \bar{\tau} \\ \bar{\tau} \\ \bar{\tau} \end{bmatrix} \quad (14)$$

## 5. Offline simulation

Offline simulation is a crucial process that contributes to evaluating the performance of the operations and concepts in this article. As for the problem of tension distribution, many experiments have been carried out to verify more precisely. However, this article is only presented in the form of an offline simulation because it is not eligible to equip the necessary equipment.

To simulate how the Quadratic programming algorithm (12) works, we perform the following steps.



- Selecting the characteristics of the frame:  $x_{\max} = 1$  (m),  $y_{\max} = 1$  (m)
- Selecting the characteristics of end-effector:  $l_5 = 0.05$  (m),  $l_6 = 0.2$  (m)
- Selecting the limitation of tension force:  $T_{\max} = 20$ (N),  $T_{\min} = 1$  (N)
- Selecting the desired tension parameter in turn at the level of the mechanism reaching:
  1. Case with high stiffness:  $T^* = T_{\max}$
  2. Case with moderate stiffness:  $T^* = \frac{T_{\max} - T_{\min}}{2}$
  3. Case with low stiffness:  $T^* = T_{\min}$
- Selecting the start point of E-E:  $x_G = 0.5$  m,  $y_G = 0.5$  m,  $\theta = 0^0$
- Assume the external forces that affect E-E with:  $F_x = 0$  (N),  $F_y = 0$  (N),  $M_z = 0$ (Nm) - (\*\*)  
(These parameters will be used to verify the result after the simulation)
- Selecting the mass of E-E platform:  $m = 1$  (kg), then  $P = mg = 9.81$  N ( $g = 9.81$  m/s<sup>2</sup>)
- Establish the computational parameters for Quadratic Programming:  $D_{11}=10^{10}$ ,  $D_{12}=10^{10}$ ,  $D_{13}=10^{10}$ ,  $D_{21}=1$ ,  $D_{22}=1$ ,  $D_{23}=1$ ,  $D_{24}=1$

After choosing the necessary parameters for the algorithm, we use the MATLAB support tool to solve the Quadratic Programming problem, the results are as follows:

The desired inverse kinematics will produce the path of E-E in the form of a helical loop with the starting point from the center going away (Figure 4). Along with each step of E-E, the cable tension is also modeled according to Figure 5. In addition, to check the accuracy of the algorithm, we will also output the values of the external forces (Figure 6) according to the position of E-E. After observation of the result generated from simulations, the desired tension force  $\tau^* \in \mathbf{R}^{4 \times 1}$  is obtained from the maximum stiffness solution (Figure 5-a), each cable will create the tension force which tends to reach the maximum value (20 N). Similar to the case when the desired tension force tend to reach the minimum stiffness solution (Figure 5-c), cable number 2 and 3 sequentially reach the minimum value (1 N) while cable number 1 and 2 tend to keep a moderate force. In Figure 5-b, the desired tension force is set at a medium stiffness level which leads to all cables tending to stand at moderate tension force but also none of them will reach the maximum or minimum like in previous cases. The result gained from the simulation is clear and we can confirm that desired values of tension force affect the stiffness of the mechanism, and also affect the energy consumption and power for the controlling robot. Depending on the usage purpose, carefully choose the desired tension force to ensure power efficiency.

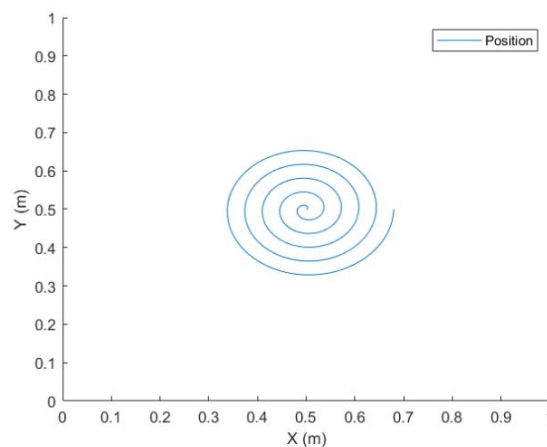


**Figure 4.** Positional record

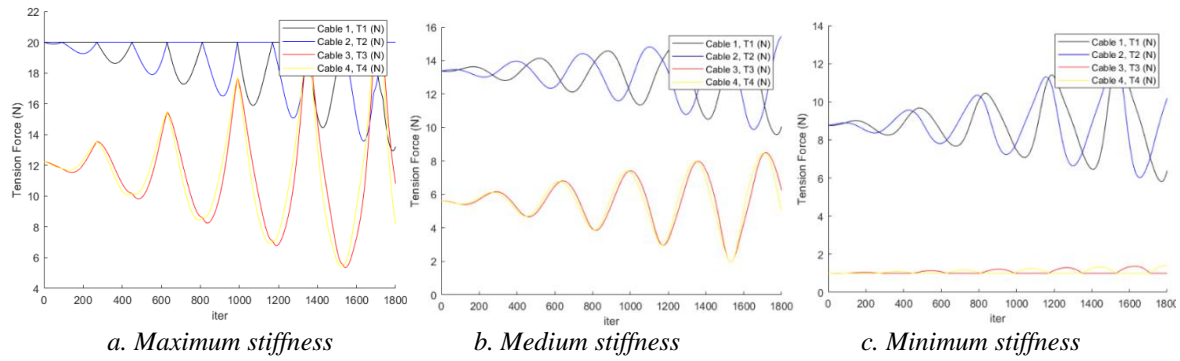


**Figure 5.** Tensional force record

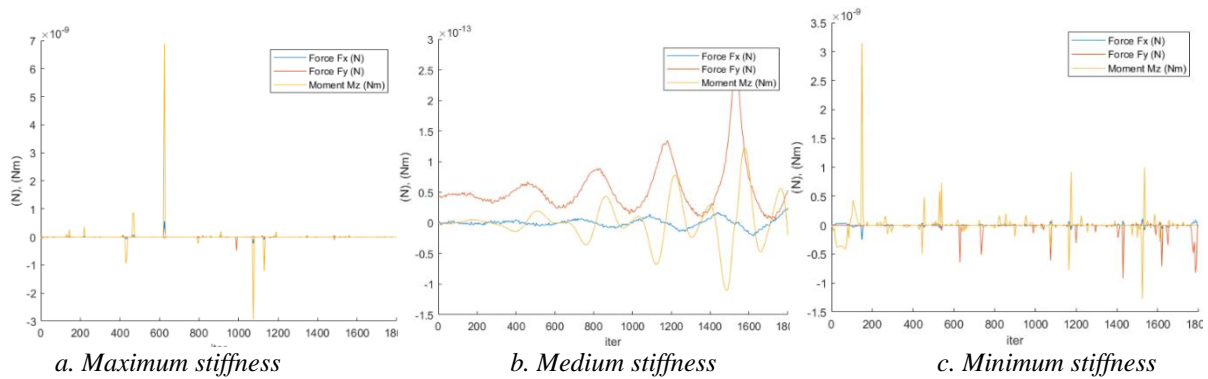


**Figure 6.** External wrench record

We can see that during E-E spiral moving (Figure 4) simulated for three cases with different desired stiffness, all values of external force always fluctuate around value 0 with an extremely small amplitude (observations can be seen in Figure 6), compared to the initial set value of the external force acting at (\*\*), it is possible to see that the results are completely different from expectations, the reason is that the existence of the slack variables shall create this unnecessary fluctuation. In addition, the noise of the calculation tool has not been taken into account. However, with this extremely small error margin, we can accept the results, in general, the fluctuation value is not significant, but to draw more accurate conclusions, it is necessary to verify the deviation of external forces acting in the entire workspace of the robot.

## 6. Conclusions

In general, the Quadratic Programming algorithm for calculating the cable tension distribution for the CDPR form has been specifically analyzed to solve the problem of adjusting the stiffness of the robot mechanism. The calculation process is successfully simulated on the MATLAB simulation, the results for the cable tension and the values related to this algorithm are relatively positive, and accurate based on the analysis theory platform. In the process, the article also presented the analysis process and specify solutions to the problem of inverse and forward kinematics for the Planar CDPR form, results were also verified in detail, which is transparent through the above simulation. With this result, it is possible to apply the tension distribution algorithm by Quadratic Programming to the Spatial Cable Driven Parallel robot by changing the parameter matrices optimization problem and the structure matrix in the optimization problem in kinematics. However, there is a disadvantage that the amount of computation will increase significantly, consuming resources of the control device, this suffering later can be overcome by upgrading the control device, but in return, the Spatial form will bring much flexibility, and higher performance than the planar form, and more economic efficiency also. This paper serves as an essential step forward for our further in-depth studies of other complex issues related to our Planar CDPR and Spatial CDPR types in the future.

## Acknowledgments

This work was funded by the Ministry of Education and Training of Vietnam, under grant no. B2021-SPK-05, and hosted by Ho Chi Minh City University of Technology and Education, Vietnam.

## REFERENCES

- [1] Sen Qian, Bin Zi, Wei-Wei Shang and Qing-Song Xu – “A Review on Cable-driven Parallel Robots.” - Chinese Journal of Mechanical Engineering - volume 31, number 66 – 2018.
- [2] Tho, Tuong Phuoc, and Nguyen Truong Thinh – “An Overview of Cable-Driven Parallel Robots: Workspace, Tension Distribution, and Cable Sagging.” - Mathematical Problems in Engineering 2022 – 2022.
- [3] Tho, Tuong Phuoc, and Nguyen Truong Thinh. "Using a cable-driven parallel robot with applications in 3D concrete printing." *Applied Sciences* 11, no. 2 (2021): 563.
- [4] Pham, Cong Bang, Guilin Yang and Song Huat Yeo – “Dynamic analysis of cable-driven parallel mechanisms.” - In Proceedings, 2005 IEEE/ASME International Conference on Advanced Intelligent Mechatronics - pp. 612-617. IEEE - 2005.
- [5] Oh, So-Ryeok, and Sunil Kumar Agrawal – “Cable suspended planar robots with redundant cables: Controllers with positive tensions.” - IEEE Transactions on Robotics - 21, no. 3, pp.457-465 – 2005.
- [6] Borgstrom, Per Henrik, Brett L. Jordan, Gaurav S. Sukhatme, Maxim A. Batalin, and William J. Kaiser – “Rapid computation of optimally safe tension distributions for parallel cable-driven robots.” - IEEE Transactions on Robotics 25 - no. 6, pp.1271-1281 – 2009.
- [7] Liu, Peng, Yuanyang Qiu, Yu Su, and Jiantao Chang. "On the minimum cable tensions for the cable-based parallel robots." - Journal of Applied Mathematics 2014 – 2014.
- [8] Bruckmann, Tobias, Andreas Pott, and Manfred Hiller - "Calculating force distributions for redundantly actuated tendon-based Stewart platforms." - In Advances in Robot Kinematics, pp.403-412. Springer, Dordrecht - 2006.
- [9] Li, Hui, Xinyu Zhang, Rui Yao, Jinghai Sun, Gaofeng Pan, and Wenbai Zhu. "Optimal force distribution based on slack rope model in the incompletely constrained cable-driven parallel mechanism of FAST telescope." - In Cable-driven parallel robots - pp. 87-102. Springer, Berlin, Heidelberg - 2013.
- [10] Bruckmann, Tobias, Christian Sturm, and Wildan Lalo - "Wire robot suspension systems for wind tunnels." - Wind tunnels and experimental fluid dynamics research (2010) – pp.29-50 – 2010.
- [11] Côté, Alexis Fortin, Philippe Cardou, and Clément Gosselin - "A tension distribution algorithm for cable-driven parallel robots operating beyond their wrench-feasible workspace." - In 2016 16th International Conference on Control, Automation and Systems (ICCAS) - pp. 68-73. IEEE - 2016.
- [12] J.-P. Merlet INRIA Sophia-Antipolis, France – “Solving the Forward Kinematics of a Gough-Type Parallel Manipulator with Interval Analysis.” - The International Journal of Robotics Research 2004 – 23, pp.221 – 2004.
- [13] Philip Wolfe - “The Simplex Method For Quadratic Programming.” - The Econometric Society - Vol. 27, No. 3 (Jul., 1959), pp.382-398 – 1959.
- [14] Alexis Fortin Côté, Philippe Cardou, Clément Gosselin - “A Tension Distribution Algorithm for Cable-Driven Parallel Robots Operating Beyond their Wrench-Feasible Workspace.” - IEEE – 2016.
- [15] Etienne Picard, Stéphane Caro, Franck Plestan, Fabien Claveau – “Stiffness Oriented Tension Distribution Algorithm for Cable-Driven Parallel Robots.” - Advances in Robot Kinematics 2020, ARK 2020, Springer Proceedings in Advanced Robotics - 15, pp.209-217 – 2020.

### First Author.



**Dao Cong Hoang Kha** is a student at Ho Chi Minh City University of Technology and Education, in the academic year 2018 - 2022. He is in the process of completing his graduation thesis at the university. His specialty is Mechatronic in Engineering Technology.

### Second Author.



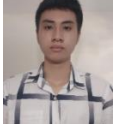
**Tuong Phuoc Tho** is a Lecturer at the Faculty of Mechanical Engineering at Ho Chi Minh City University of Technology and Education, Viet Nam. He received M.E degree in Manufacturing Technology from Ho Chi Minh University of Technology, Ho Chi Minh, Vietnam, in 2011. His work focuses on Robotics and Mechatronics systems.

### Third Author.



**Vu Ngoc Duc** is a student at Ho Chi Minh City University of Technology and Education, the academic year 2018 - 2022. He is in the process of completing his graduation thesis at the university. His specialty is Mechatronics in Engineering Technology.

### Fourth Author.



**Nguyen Minh Nhat** is a student at Ho Chi Minh City University of Technology and Education, the academic year 2018 - 2022. He is in the process of completing his graduation thesis at the university. His specialty is Mechatronic in Engineering Technology.

Bài báo số 9 – Bài báo đăng trên tạp chí khoa học chuyên ngành trong nước (Trong danh mục được tính điểm của HĐCDGSNN)

Tuong, Phuoc Tho, and Nguyen Luan Vu Truong. "Thiết Kế và Tính Toán Hệ Thống Phân Phối Cấp cho CDPR." *Journal of Technical Education Science* 19, no. SI01 (2024): 64-71.

Link: <https://jte.edu.vn/index.php/jte/article/view/1486>



## Design and Calculation of Cable Distribution System for CDRP

Phuoc Tho Tuong\*, Nguyen Luan Vu Truong  
HCMC University of Technology and Education, Vietnam

\*Corresponding author. Email: [thotp@hcmute.edu.vn](mailto:thotp@hcmute.edu.vn)

### ARTICLE INFO

Received: 18/10/2023  
Revised: 13/11/2023  
Accepted: 29/11/2023  
Published: 28/02/2024

### KEYWORDS

Cable winch;  
Cable robot;  
Tension measurement;  
Cable parallel robot;  
Cable robot simulation.

### ABSTRACT

This article presents the design and calculation of a cable distribution system used for large-sized cable robots. The main function of the cable distribution system is to convert the rotational motion of the motor shaft into the translational motion of the cable with constraints on position, velocity and cable tension. With a clear relationship between cable length and motor angle, the cable distribution system is designed to guarantee that cables are fully distributed and oriented. The main contributions of the research are as follows: Designing a cable distribution system with a built-in mechanism for measuring cable tension; Building cable distribution system mathematical models, incorporating the results into a mathematical model of a 6-degree-of-freedom CDRP configuration powered by 8 cables and simulating the computational results. The analysis findings suggest that the structure of the cable distribution system meets the design specifications and is suitable for developing actuators in cable robot applications that involve heavy loads and large sizes.

## Thiết Kế và Tính Toán Hệ Thống Phân Phối Cáp cho CDRP

Tuởng Phước Thọ\*, Trương Nguyễn Luân Vũ  
Đại học Sư phạm Kỹ thuật Thành phố Hồ Chí Minh, Việt Nam

\* Tác giả liên hệ. Email: [thotp@hcmute.edu.vn](mailto:thotp@hcmute.edu.vn)

### THÔNG TIN BÀI BÁO

Ngày nhận bài: 18/10/2023  
Ngày hoàn thiện: 13/11/2023  
Ngày chấp nhận đăng: 29/11/2023  
Ngày đăng: 28/02/2024

### TỪ KHÓA

Tời phân phối cáp;  
Robot cáp;  
Đo lực căng cáp;  
Robot cáp song song;  
Mô phỏng robot cáp.

### TÓM TẮT

Bài báo này trình bày thiết kế, tính toán hệ thống phân phối cáp sử dụng cho robot cáp kích thước lớn. Hệ thống phân phối cáp của robot cáp có chức năng biến chuyển động quay từ trục động cơ thành chuyển động tịnh tiến của dây cáp với các điều kiện ràng buộc về vị trí, vận tốc và lực căng cáp. Hệ thống phân phối cáp được thiết kế đảm bảo dây cáp được phân phối và định hướng hoàn toàn với mỗi liên hệ rõ ràng giữa chiều dài cáp và góc quay động cơ truyền động. Các đóng góp chính của nghiên cứu bao gồm: Thiết kế hệ thống phân phối cáp có tích hợp cơ cấu đo lực căng cáp; Xây dựng các mô hình tính toán hệ thống phân phối cáp, tích hợp kết quả tính toán vào mô hình toán của một cấu hình CDRP 6 bậc tự do được truyền động bởi 8 dây cáp, mô phỏng kết quả tính toán và đánh giá. Kết quả phân tích cho thấy kết cấu của hệ thống phân phối cáp phù hợp với các yêu cầu thiết kế, có thể ứng dụng triển khai làm bộ truyền động cho các Robot cáp có kích thước và tải trọng lớn.

Doi: <https://doi.org/10.54644/jte.2024.1486>

Copyright © JTE. This is an open access article distributed under the terms and conditions of the [Creative Commons Attribution-NonCommercial 4.0 International License](https://creativecommons.org/licenses/by-nc/4.0/) which permits unrestricted use, distribution, and reproduction in any medium for non-commercial purpose, provided the original work is properly cited.

### 1. Giới thiệu

Robot song song điều khiển bằng cáp (Cable driven parallel robot - CDRP) là một loại robot cấu trúc song song có cấu hình đặc biệt, trong đó các cơ cấu truyền động cơ khí như bánh răng, vít me, khâu kết nối cứng được thay thế bằng các dây cáp có thể thay đổi chiều dài. Cáp truyền động được quấn và nhả bằng các bộ truyền động tuyến tính hoặc quay (được gọi là tời hoặc cơ cấu phân phối cáp) và được định hướng bằng cách sử dụng các thiết bị dẫn hướng như pulley tới một bệ di động (Moving platform - MP),

trên đó các đầu dây cáp được bố trí theo cấu hình song song [1]. Ưu điểm lớn nhất của các CDPR là có khả năng cho một không gian làm việc rất lớn và có thể cấu hình lại dễ dàng. Đặc tính này đến từ việc cơ cấu chấp hành là những sợi cáp rất dài, có thể được trữ và phân phối trên các bộ tời và các dây cáp hoạt động hiệu quả về mặt kết cấu, chỉ chịu tải trọng kéo. Ngoài ra, các bộ truyền động và hệ thống dẫn hướng có thể được bố trí lại dễ dàng, cho phép thay đổi nhanh chóng về kích thước và hình dạng không gian làm việc. Một vấn đề khó khăn trong việc triển khai các CDPR là việc đảm bảo cho các dây cáp truyền động hoạt động ở trạng thái căng và các lực căng cáp nằm trong giới hạn cho trước ứng với các tải trọng khác nhau [2]-[3]. Một ưu điểm khác của CDPR so với các robot nối tiếp là các cơ cấu chấp hành có thể lắp đặt trên bệ cố định, không ảnh hưởng đến tải trọng thiết kế hoặc dễ dàng bố trí đối trọng để cân bằng lực tác động [4]. Tuy có nhiều ưu điểm trong thiết kế và khả năng ứng dụng, việc sử dụng CDPR trong thực tế vẫn còn hạn chế do những thách thức về các vấn đề thiết kế, điều khiển và an toàn. Khả năng điều khiển và an toàn có thể được cải thiện bằng cách sử dụng nhiều dây cáp hơn số bậc tự do của MP (Cấu hình thừa ràng buộc). Tuy nhiên, điều này dẫn đến sự phức tạp của các bài toán động học – cân bằng lực và có thể khiến các dây cáp va chạm với nhau hoặc va chạm với môi trường xung quanh, làm hạn chế không gian làm việc của robot, do đó đòi hỏi phải sử dụng các kỹ thuật thiết kế phức tạp để giải quyết các vấn đề nêu trên [5]. Trong trường hợp này, khả năng mở rộng không gian làm việc có thể được cải thiện bằng cấu hình treo cáp (Cấu hình mắc cáp có bộ di động nằm phía dưới các điểm mắc cáp cố định theo hướng lực trọng trường) và sử dụng nhiều cáp dự phòng (số lượng cáp lớn hơn số bậc tự do của MP) [6]-[7], mặc dù vậy, khả năng va chạm giữa cáp với cáp có thể tăng lên và mô hình toán cũng phức tạp hơn. Do đó, để đơn giản hóa thiết kế và hợp lý hóa chi phí của việc phát triển CDPR, các cấu hình CDPR dạng treo đơn giản hơn đã được đề xuất, với số lượng dây cáp truyền động ít hơn số bậc tự do của MP, điều này dẫn đến một bộ điều khiển đơn giản hơn vì MP không bị thừa ràng buộc [8]-[9]. Trong các nghiên cứu về CDPR, để có thể điều khiển được dây cáp đáp ứng các yêu cầu động học, cần phải xác định rõ mối liên hệ giữa độ dịch chuyển của bộ truyền động  $\Delta q$  (động cơ) và độ dịch chuyển của cáp  $\Delta l$  (chiều dài cáp). Do đó, việc đảm bảo tính toán được tỷ số truyền của bộ truyền động cơ cấu phân phối cáp  $K = \Delta l / \Delta q$  là một điều kiện tiên quyết khi các nhà nghiên cứu thiết kế các bộ tời phân phối cáp mới cho mục đích truyền động cho các loại robot nói chung và CDPR nói riêng [10].

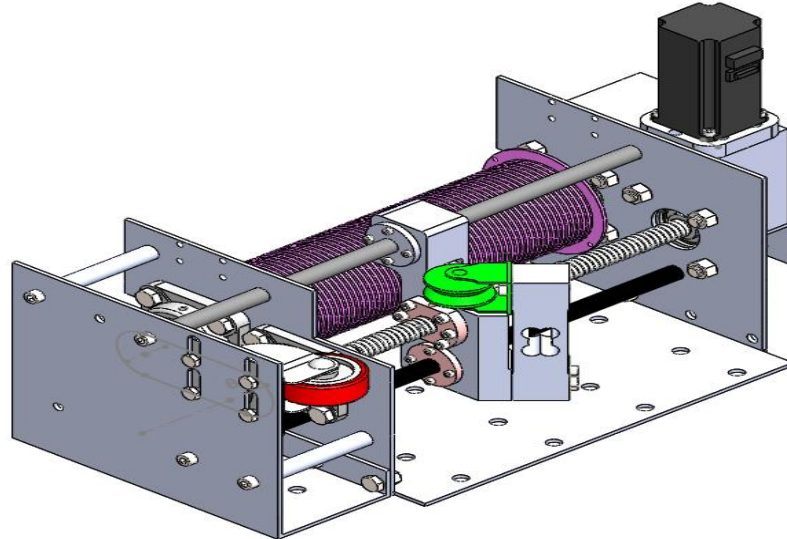
Về mặt giải pháp, cách đơn giản nhất để trữ cáp là sử dụng một tang trống quấn cáp nối với động cơ, như phân tích ở trên. Tuy nhiên, việc thiết kế các phương pháp quấn cáp trên tang là không đơn giản, do chiều dài dây cáp phụ thuộc vào bán kính và vị trí vòng dây trên tang không phải là một hàm của góc quay động cơ. Để tăng chiều dài cáp được dự trữ, dây cáp có thể được quấn trên các trống tròn hoặc có rãnh và đảo chiều bằng vít tự đảo chiều hoặc sử dụng các trống có bán kính thay đổi được [11], [12]. Ngoài ra, dây cáp cũng có thể được quấn chồng lên nhau trên các trống ngăn [13]; tất cả những giải pháp này là để thu được mối tương quan chính xác giữa chuyển vị của cáp và góc quay động cơ. Tuy nhiên, tỷ số truyền  $K$  là một hàm của góc tuyệt đối của động cơ, có thể không xác định được tại thời điểm bắt đầu nếu không có chế độ lưu vị trí khi ngắt điện, hay khi bán kính tang  $r$  thay đổi do quấn nhiều lớp sẽ làm thay đổi các giới hạn lực căng khác nhau đối với công suất định mức động cơ nhất định. Giải pháp có thể đơn giản hơn và có sẵn trên thị trường đối với hằng số  $K$  đã biết là sử dụng một tời nâng dạng hệ ròng rọc và một bộ truyền động tuyến tính để điều khiển nó [14], tuy nhiên, giải pháp này làm tăng kích thước, tăng độ mòn cáp do ma sát khi lưu trữ cáp dài.

Qua các khảo sát cho thấy, CDPR có tiềm năng phát triển lớn, tuy nhiên vẫn chưa có một nghiên cứu chi tiết về việc thiết kế và tính toán bộ tời phân phối cáp hoàn chỉnh theo các yêu cầu cụ thể, cũng như tích hợp cơ cấu đo lực căng cáp phục vụ quá trình điều khiển. Do đó, nghiên cứu này tập trung vào việc thiết kế, tính toán và mô phỏng bộ tời phân phối cáp sử dụng cho các cấu hình robot cáp khác nhau với tải trọng tối đa là 500N, chiều dài lưu trữ cáp là 20m. Đóng góp chính của nghiên cứu là thiết kế cấu trúc bộ tời phân phối cáp tích hợp thiết bị đo lực căng cáp, xây dựng mô hình toán biểu diễn mối liên hệ giữa chiều dài cáp và góc quay động cơ truyền động, kết quả này được áp dụng để xây dựng bộ điều khiển và mô phỏng trên một cấu hình CDPR để đánh giá sự phù hợp của mô hình nghiên cứu.

## 2. Thiết kế hệ thống phân phối cáp

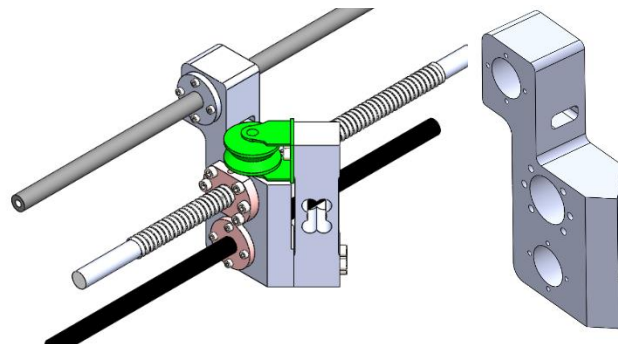
Cơ cấu phân phối cáp cho các CDPR có nguyên lý tương tự như các bộ tời nâng hạ vật, biến chuyển động quay ở trục động cơ thành chuyển động tịnh tiến của dây cáp. Khác với các bộ tời chuyên dụng,

chiều dài dây cáp nâng hạ được điều chỉnh trực tiếp từ người vận hành, cơ cấu phân phối cáp phải được điều khiển chiều dài và vận tốc của cáp truyền động một cách chính xác theo các bài toán quy hoạch quỹ đạo cho trước. Do đó, việc thiết kế và tính toán hệ thống phân phối cáp phải thỏa mãn các yêu cầu sau: thứ nhất, có khả năng phân phối cáp với độ chính xác về vị trí, vận tốc và đáp ứng tải trọng cho trước; thứ 2, có thể lưu trữ số lượng cáp nhất định, tùy theo kích thước của C DPR; thứ 3, có cơ cấu đo lực căng cáp phục vụ quá trình điều khiển.



**Hình 1.** Thiết kế bộ tời phân phối cáp

Trong nghiên cứu này, bộ tang cuốn phân phối dây cáp bằng thép được thiết kế như trên **hình 1**. Để các dây cáp không bị rơi trong khi quán và xả dây, một cơ cấu phân phối hỗ trợ dẫn hướng dây cáp được thiết kế như **hình 2**, trên đó có tích hợp một cảm biến lực (loadcell) dùng để đo lực căng của dây cáp. Bộ dẫn hướng bao gồm: Một thanh vít me đường kính 20mm, bước 5mm; Hai thanh dẫn hướng đường kính 16mm; Bộ gá đai ốc vít me, đai ốc thanh dẫn; Loadcell (100kg) để đo lực căng dây cáp do tải trên đầu công tác tác động về bộ điều khiển. Bộ dẫn hướng được truyền động thông qua bộ truyền đai răng được đặt ở cuối trục tang. Để dây cáp cuốn vào và xả ra không bị chùng, tang cuốn cáp được thiết kế các rãnh định hướng cáp với bước rãnh phù hợp với sự dịch chuyển của bộ dẫn hướng bằng vít me và bộ truyền đai. Với tải trọng yêu cầu 50kg và trữ được 20m dây cáp, so sánh với bảng thông số cáp **theo tiêu chuẩn** thì chọn cáp 4mm là phù hợp. Do bộ phân phối cáp và tang cuốn cáp hoạt động đồng bộ với nhau, vít me có bước răng  $p_1 = 5$ , bước trên tang cuốn cáp  $p_2 = 5$  nên ta chọn tỉ số truyền cho tang và vít me  $k = 1$ .



**Hình 2.** Thiết kế bộ dẫn hướng cáp và chi tiết gá đai ốc và cảm biến lực

Chu vi một vòng tang cuốn dây cáp:

$$C_T = \pi(D + d) = \pi(100 + 4) = 104\pi(\text{mm}) \quad (1)$$



Trong đó,  $C_T$  là chu vi tang quấn cáp (mm),  $D$  là đường kính tang quấn cáp (mm),  $d$  là đường kính cáp (mm)

Số vòng dây cần quấn được đề đạt được 20m:

$$N = \frac{L}{C_T} = \frac{20 \times 10^3}{104\pi} = 61.21 \text{ (Vòng)} \quad (2)$$

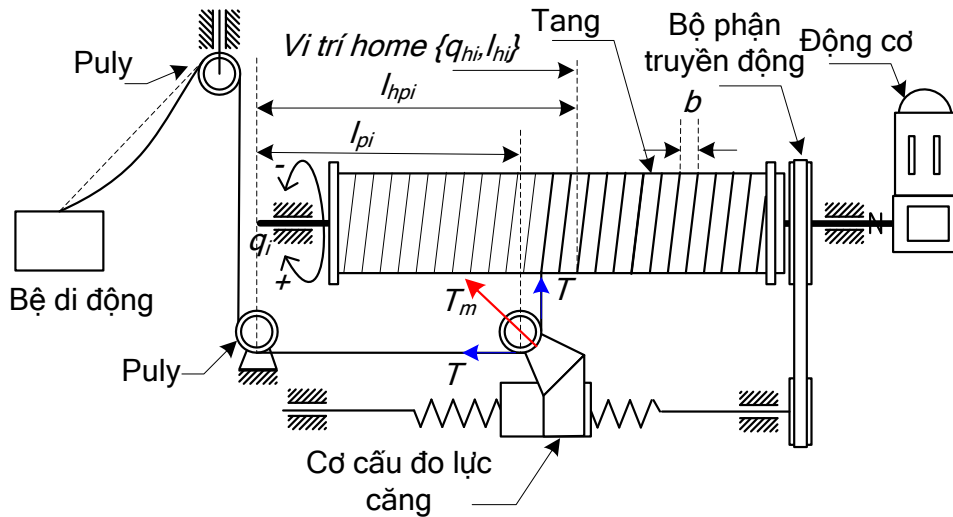
Với  $L$  là chiều dài tối đa tang có thể trữ được (m)

Chiều dài cần thiết của tang cuốn cáp:

$$L_T = N \times b = 61.21 \times 5 = 306 \text{ (mm)} \quad (3)$$

Trong đó,  $L_T$  là chiều dài tang cuốn cáp (mm),  $b$  là bề rộng mỗi bước răng trên tang cuốn cáp (mm).

### 3. Mô hình truyền động CDPR



Hình 3. Sơ đồ truyền động của Robot cáp và hệ thống phân phối cáp

Hình 3 cho thấy sơ đồ truyền động của cơ cấu phân phối cáp CDPR, chiều dài cáp là biến đầu vào điều khiển được xác định bởi các tham số thiết kế tương ứng và quỹ đạo của bộ di động, mô hình toán liên quan được trình bày trong các nghiên cứu [7], [15], chiều dài thực tế của cáp phản hồi về bộ điều khiển khi hoạt động được đo từ encoder. Để xác định mối liên hệ giữa chiều dài cáp và góc quay động cơ, một vị trí cố định trong không gian làm việc CDPR được lấy làm chuẩn với các chiều dài cáp được xác định trước, có thể coi đây là vị trí Home với các tham số ban đầu  $\{q_{hi}, l_{hi}\}$ . Từ vị trí này, chiều dài tuyệt đối của  $l_i$  cáp  $\{i=1, \dots, n\}$  tương ứng với góc quay của động cơ  $q_i$  (độ) có thể được tính theo các công thức sau:

$$l_i - l_{hi} = (q_i - q_{hi}) \left( \frac{\sqrt{\pi^2 d_{bi}^2 + b^2} + b}{360 k_{mi}} \right) = (q_i - q_{hi}) k_{ci} \quad (4)$$

$$k_{ci} = \frac{\sqrt{\pi^2 d_{bi}^2 + b^2} + b}{360 k_{mi}} \quad (5)$$

$$q_i - q_{hi} = \frac{(l_i - l_{hi})}{k_{ci}} = \frac{(l_i - l_{hi}) 360 k_{mi}}{\sqrt{\pi^2 d_{bi}^2 + b^2} + b} \quad (6)$$

trong đó:

$l_i$ : chiều dài không quấn trên tang của cáp thứ  $i$  (mm)

$l_{hi}$ : chiều dài cáp tại vị trí Home (mm)

$k_{mi}$ : tỷ số truyền hộp giảm tốc từ động cơ đến trang trống

$d_{bi}$ : đường kính bước trống của tời thứ  $i$  (mm)

$q_i$ : góc quay của động cơ, với  $i = 1, \dots, m$  (độ)

$q_{hi}$ : góc quay động cơ tại vị trí ban đầu (độ)

$b_i$ : chiều rộng của mỗi rãnh trên tang cuộn cáp (mm)

Để kiểm tra lực căng trên dây cáp, một cảm biến lực được thiết kế đặt trên bộ dẫn hướng cáp, khi đầu công tác có tải trọng sẽ gây ra một lực căng nhất định lên dây cáp. Lực căng dây được giữ nguyên giá trị thông qua các ròng rọc định hướng dây cáp. Theo sơ đồ **hình 3**, lực căng của dây cáp được tính bằng công thức:

$$T = \frac{T_m}{\sqrt{2}} \quad (9)$$

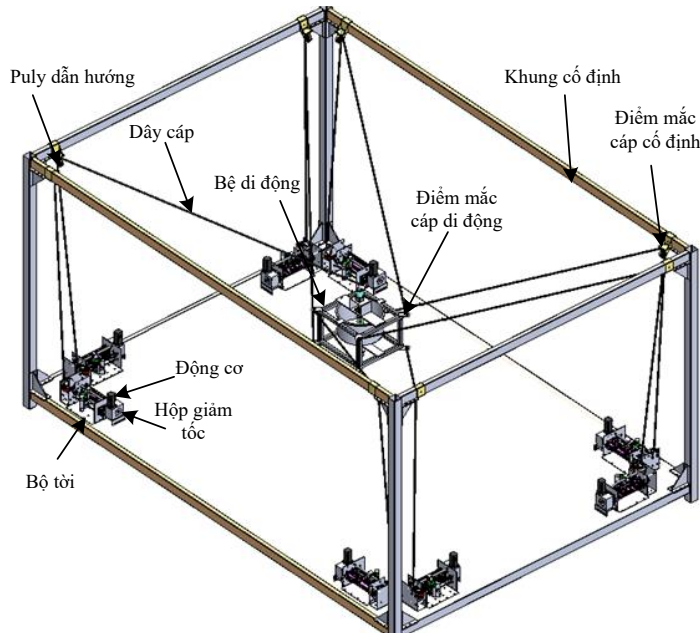
Trong đó,  $T$  là lực căng cáp,  $T_m$  là lực căng cáp đo được từ cảm biến lực.

Từ bài toán động lực học được phân tích trong [15]-[16], mô hình động lực học của động cơ truyền động cơ cấu phân phối cáp được biểu diễn theo công thức sau:

$$\Gamma_m = \mathbf{I}_m \ddot{q} + \mathbf{f}_v \dot{q} + \mathbf{f}_s \text{sign}(\dot{q}) + \mathbf{K}_C \tau \quad (10)$$

Trong đó  $\mathbf{I}_m \in \mathbb{R}^{m \times m}$  là ma trận biểu diễn quán tính của động cơ, tang quán cáp và các bộ phận quay khác,  $\mathbf{f}_v \in \mathbb{R}^{m \times m}$  và  $\mathbf{f}_s \in \mathbb{R}^{m \times m}$  là ma trận đường chéo của hệ số ma sát nhớt và ma sát khô tương ứng,  $\mathbf{K}_C = \text{diag}(k_{c1}, \dots, k_{cm}) \in \mathbb{R}^{m \times m}$  là ma trận hệ số truyền động bao gồm tỷ số truyền hộp giảm tốc, đường kính tang và bước trống, và  $\Gamma_m \in \mathbb{R}^m$  là véc tơ mômen của động cơ truyền động. Từ công thức (10) với các điều kiện biên về tải trọng, gia tốc và vận tốc dây cáp, công suất động cơ và hộp giảm tốc được tính toán và lựa chọn.

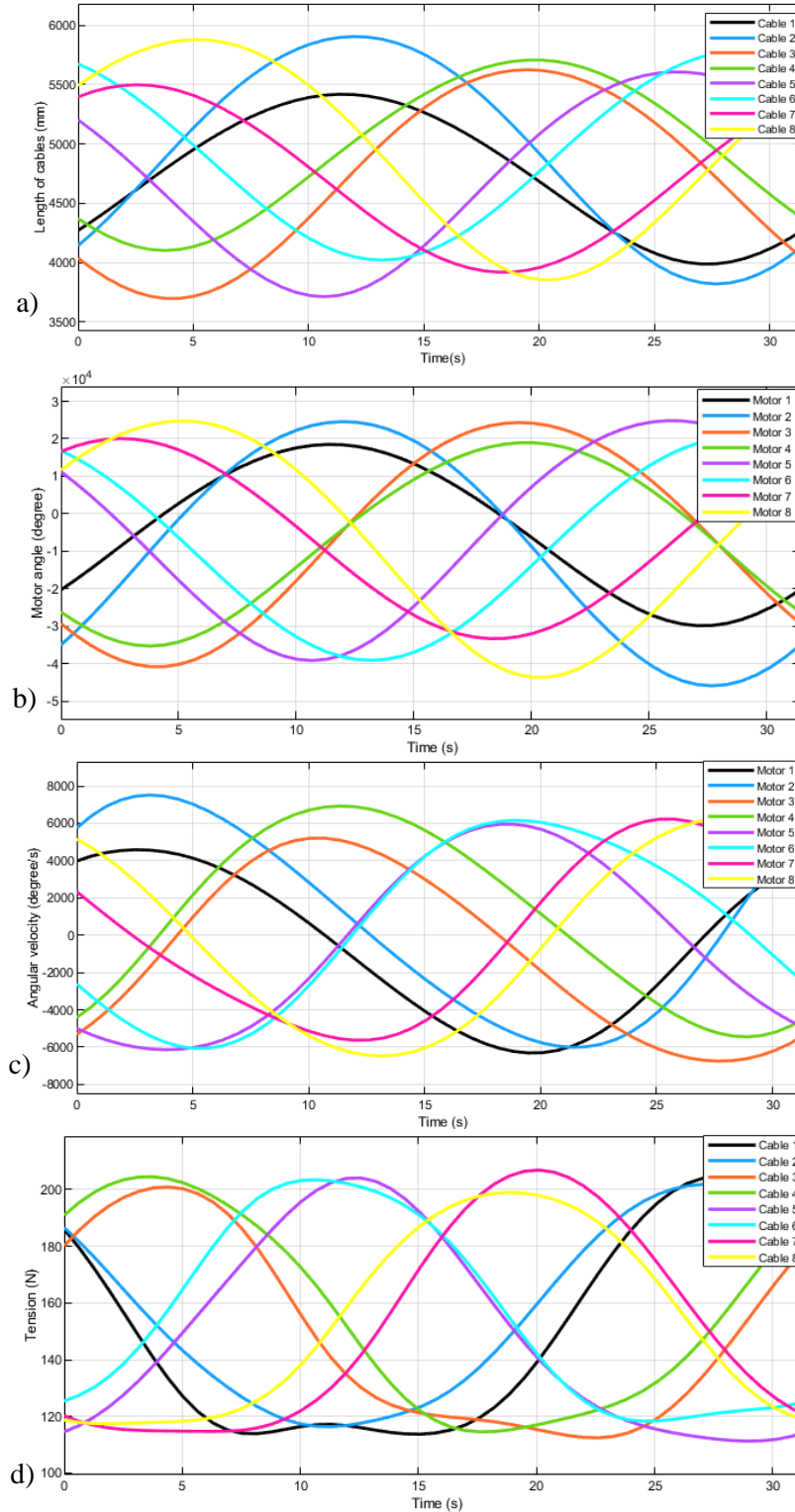
#### 4. Mô phỏng và đánh giá



**Hình 4.** Robot cáp cấu hình song song

Mô hình thiết kế của bộ tời phân phối cáp được mô phỏng trên một CDPR 6 bậc tự do truyền động bởi 8 dây cáp (8 bộ tời) được thiết kế để di chuyển vật nặng. **Hình 4** mô tả cấu trúc của CDPR trong ứng dụng này và các mô hình toán của hệ thống được xây dựng trong các công thức từ (4-7), (10) và trong nghiên cứu [15]. Với quỹ đạo mô phỏng đường tròn bán kính  $r = 1$  (m); đường tròn nằm trên mặt phẳng XY với  $z = 1000$  mm, và được chia thành nhiều điểm nút. Một thuật toán được thiết kế để kiểm

tra xem các tọa độ này có nằm trong vùng làm việc của CDRP hay không (thỏa mãn phương trình cân bằng lực). Nếu quỹ đạo là có thể thực hiện được, dữ liệu tọa độ này sẽ được đưa vào thuật toán để tìm các giải pháp phân bố lực căng cáp tương ứng, quỹ đạo và vận tốc khớp cũng được tính toán theo cấu hình CDRP.



**Hình 5.** Đáp ứng mô phỏng 8 bộ tời cho nội suy đường tròn bán kính  $r = 1m$

**Hình 5** biểu diễn kết quả mô phỏng tương ứng quỹ đạo nội suy đường tròn với bán kính  $r = 1m$ . **Hình 5a** là chiều dài của 8 sợi cáp hay quỹ đạo khớp tính toán tương ứng với quỹ đạo điều khiển, các biến khớp có dạng liên tục dọc theo quỹ đạo điều khiển, cho thấy tất cả các điểm nút đều nằm trong không gian hoạt động khả thi (WFW) [1]. Chiều dài cáp thay đổi từ 3600mm đến 6000mm nằm trong thông số thiết kế của tang trữ cáp. **Hình 5b** là đáp ứng các góc quay động cơ theo các biến chiều dài cáp tương ứng, một số góc quay có giá trị âm do quỹ đạo hoàn toàn nằm phía trên vị trí Home, giá trị của góc quay của các động cơ phù hợp với quỹ đạo khớp tương ứng, các đáp ứng góc quay động cơ cũng có dạng liên tục và thay đổi trong khoảng từ  $-5 \times 10^4$  đến  $3 \times 10^4$  (độ). **Hình 5c** là vận tốc của các động cơ tương ứng, kết quả tính toán cho thấy các vận tốc động cơ dao động trong khoảng  $\pm 8000^0/s$  tương ứng  $\pm 1333$  vòng/phút, các giá trị này nằm trong khoảng vận tốc thiết kế của các động cơ AC Servo, dấu của vận tốc thể hiện chiều quay của động cơ trong quá trình quán cáp hoặc xả cáp. **Hình 5d** là biểu đồ biểu diễn các lực căng cáp tương ứng dọc quỹ đạo thiết kế, đây là bài toán quan trọng trong quá trình điều khiển CDP, đối với cấu hình có 2 cấp dự phòng, một giải thuật tính toán phù hợp để tối ưu các giải pháp phân bố lực căng cho quỹ đạo điều khiển [3], [15] đã được tích hợp vào trong bài toán thiết kế quỹ đạo, kết quả tính toán cho thấy tất cả các lực căng được tính toán đều nằm trong vùng giới hạn cho trước và lớn hơn 0, điều này cho thấy tất cả các dây cáp đều hoạt động ở trạng thái căng với lực căng dương và không vượt quá giới hạn tải trọng của động cơ thiết kế.

Thông qua kết quả mô phỏng tính toán ở **hình 5** cho thấy, thiết kế và mô hình tính toán của cơ cấu phân phối cáp đáp ứng được yêu cầu thiết kế ban đầu về tải trọng, khả năng lưu trữ cáp, tốc độ kéo thả cáp. Trong đó đáp ứng góc quay và vận tốc gốc của động cơ truyền động đã được tính toán trực tiếp từ quỹ đạo khớp (chiều dài và vận tốc dài cáp truyền động). Đặc biệt lực căng cáp luôn nằm trong giới hạn cho phép với tải trọng 500N, trong đó, các giá trị các lực căng cáp lớn nhất đều không vượt quá 220N, điều này cho thấy ưu điểm của các CDP trong việc phân tán tải trọng của các dây cáp truyền động, qua đó có thể giảm công suất cơ cấu chấp hành bằng cách tối ưu giải thuật phân phối lực căng cáp, trong khi vẫn đảm bảo được tải trọng yêu cầu.

## 5. Kết luận

Bài báo đã trình bày kết quả thiết kế và tính toán bộ tời phân phối cáp tích hợp cơ cấu đo lực căng cáp sử dụng cho CDP, bộ tời có khả năng phân phối dây cáp chính xác với tốc độ cao cho yêu cầu điều khiển vị trí và quỹ đạo với tải trọng cho trước. Kết quả mô phỏng trên mô hình CDP 6 bậc tự do truyền động bởi 8 dây cáp cho thấy thiết kế và tính toán bộ tời phân phối cáp là phù hợp với yêu cầu điều khiển của các CDP, mô hình tính toán cho thấy quỹ đạo góc quay và vận tốc của động cơ phù hợp với quỹ đạo khớp thiết kế, các giá trị hoạt động của động cơ đều nằm trong vùng cho phép. Đặc biệt là các giá trị lực căng tính toán đều dương và nằm trong giới hạn hoạt động của động cơ. Kết quả này có thể làm cơ sở tham khảo cho việc thiết kế tính toán bộ tời phân phối cáp, triển khai chế tạo, thử nghiệm và ứng dụng truyền động cho các CDP. Các công việc tiếp theo bao gồm chế tạo và thực nghiệm các bộ tời phân phối cáp trên CDP, đánh giá độ chính xác và khả năng kết hợp của nhiều bộ tời cho các cấu hình CDP phức tạp, nghiên cứu ảnh hưởng của độ đàn hồi của các cơ cấu truyền động và độ võng cáp đến độ chính xác của CDP có kích thước và tải trọng lớn.

## Lời cảm ơn

Công trình này thuộc đề án năm 2023 được tài trợ kinh phí bởi Trường Đại học Sư phạm Kỹ thuật Thành phố Hồ Chí Minh.

## Xung đột lợi ích

Các tác giả tuyên bố không có xung đột lợi ích trong bài báo này.

## TÀI LIỆU THAM KHẢO

- [1] T. P. Tho and N. T. Thinh, "An Overview of Cable-Driven Parallel Robots: Workspace, Tension Distribution, and Cable Sagging," *Mathematical Problems in Engineering*, vol. 2022, pp. 1-15, 2022.
- [2] V. Mattioni, E. Idà, and M. Carricato, "Force-distribution sensitivity to cable-tension errors in overconstrained cable-driven parallel robots," *Mech. Mach. Theory*, vol. 175, p. 104940, 2022.
- [3] C. H. K. Dao, T. P. Tho, N. D. Vu, and M. N. Nguyen, "On Research of Cable Tension Distribution Algorithm for Four Cables-Three DOF Planar Cable-Driven Parallel Robot," *Journal of Technical Education Science*, vol. 78B, pp. 8-17, 2023.

- [4] T. Bruckmann *et al.*, "An energy-efficient wire-based storage and retrieval system," in *Proceedings of the 2013 IEEE/ASME International Conference on Advanced Intelligent Mechatronics*, Wollongong, Australia, 9–12 July 2013, pp. 631–636.
- [5] K. Iturralde *et al.*, "Cable-driven parallel robot for curtain wall module installation," *Autom. Constr.*, vol. 138, p. 104235, 2022.
- [6] D. Lin *et al.*, "Dynamically-Feasible Trajectories for a Cable-Suspended Robot Performing Throwing Operations," in *ROMANSY 23—Robot Design, Dynamics and Control*, G. Venture *et al.*, Eds. Springer International Publishing, 2021, pp. 547–555.
- [7] T. P. Tho and N. T. Thinh, "Using a cable-driven parallel robot with applications in 3D concrete printing," *Applied Sciences*, vol. 11, no. 2, p. 563, 2021.
- [8] E. Idà, S. Briot, and M. Carricato, "Robust Trajectory Planning of Under-Actuated Cable-Driven Parallel Robot with 3 Cables," in *Advances in Robot Kinematics 2020*, J. Lenarcic and B. Siciliano, Eds. Springer International Publishing, 2021, pp. 65–72.
- [9] E. Idà and M. Carricato, "A New Performance Index for Underactuated Cable-Driven Parallel Robots," in *Cable-Driven Parallel Robots*, M. Gouttefarde *et al.*, Eds. Springer International Publishing, 2021, pp. 24–36.
- [10] J. P. Merlet, "Comparison of Actuation Schemes for Wire-Driven Parallel Robots," in *New Trends in Mechanism and Machine Science*, F. Viadero and M. Ceccarelli, Eds. Springer, 2013, pp. 245–254.
- [11] L. Scalera *et al.*, "Cable-Based Robotic Crane (CBRC): Design and Implementation of Overhead Traveling Cranes Based on Variable Radius Drums," *IEEE Trans. Robot.*, vol. 34, pp. 474–485, 2018.
- [12] S. Seriani and P. Gallina, "Variable Radius Drum Mechanisms," *J. Mech. Robot.*, vol. 8, p. 021016, 2015.
- [13] M. S. Varziri and L. Notash, "Kinematic calibration of a wire-actuated parallel robot," *Mech. Mach. Theory*, vol. 42, pp. 960–976, 2007.
- [14] J. P. Merlet, "Kinematics of the wire-driven parallel robot MARIONET using linear actuators," in *Proceedings of the 2008 IEEE International Conference on Robotics and Automation*, Pasadena, CA, USA, 19–23 May 2008, pp. 3857–3862.
- [15] T. P. Tho and N. T. Thinh, "Evaluating cable tension distributions of CDPR for virtual reality motion simulator," *Mechanics Based Design of Structures and Machines*, vol. 0, pp. 1-19, 2023, doi: 10.1080/15397734.2023.2265452.
- [16] J. Lamaury and M. Gouttefarde, "Control of a large redundantly actuated cable-suspended parallel robot," in *2013 IEEE International Conference on Robotics and Automation*, 2013, pp. 4659-4664.



**Tuong Phuoc Tho** is a Lecturer of the Faculty of Mechanical Engineering at Ho Chi Minh City University of Technology and Education, Viet Nam. He received his B.S. degree from Ho Chi Minh City University of Technology and Education in 2006, and his master's degree in Manufacturing Technology from Ho Chi Minh University of Technology in 2011. His work focuses on Robotics and Mechatronics systems. Email: [hotp@hcmute.edu.vn](mailto:hotp@hcmute.edu.vn).

ORCID:  <https://orcid.org/0000-0002-5688-6096>



**Truong Nguyen Luan Vu** is currently an Associate Professor of Mechanical Engineering at Ho Chi Minh City University of Technology and Education, Viet Nam. He received his B.S. degree from Ho Chi Minh City University of Technology, Ho Chi Minh City National University in 2000, and his master's and Ph.D. degrees from Yeungnam University, the Republic of Korea in 2005 and 2009, respectively. He has also taught at Yeungnam University for two years in terms of being an International Professor. His research interests include multivariable control, fractional control, PID control, process control, automatic control, and control hardware. Email: [vuluantn@hcmute.edu.vn](mailto:vuluantn@hcmute.edu.vn)